Sliding Mode Control of Mechatronic Systems

From robust control towards self-tuning control with experimental investigations on hydraulic valves

DISSERTATION

submitted in partial fulfillment
of the requirements for the degree

Doktor Ingenieur
(Doctor of Engineering)

in the

Faculty of Electrical Engineering and Information Technology
at TU Dortmund University

by

Christoph Krimpmann, M.Sc.
Dortmund, Germany

Date of submission: October 6, 2017

First examiner: Univ.-Prof. Dr.-Ing. Prof. h.c. Dr. h.c. Torsten Bertram
Second examiner: Univ.-Prof. Dr.-Ing. Stephan Rinderknecht

Date of approval: July 20, 2018

Preface

When I started electrical engineering, I was fascinated by mechanisms letting systems act like automated machines. A few semesters later, I realized that these fascinating mechanisms are controllers and I found my passion for control theory. With this work, I drove the passion to its extent; however, this work would not have come to completion without the guidance and support of my academic peers and friends.

I thank Univ.-Prof. Dr.-Ing. Prof. h.c. Dr. h.c. Torsten Bertram for giving me the opportunity to work at the Institute of Control Theory and Systems Engineering (RST). Especially, I am thankful for his confidence and the freedom of developing my work in the direction I wanted.

Additionally, I would like to thank Univ.-Prof. Dr.-Ing. Stephan Rinderknecht for his work as the second reviewer of my thesis.

Many thanks go to my former colleagues Jan Braun and Jörn Malzahn who introduced me to the work of a research assistant; especially how to publish my work and to set up experimental test benches. A wholehearted thank you to all the other colleagues at the RST for their close amicable comradeship during all the years. In particular, I want to say thank you to Christoph Rösmann for the discussions and his comments on my work, Frank Hoffmann for controversy but always fair discussions, Jürgen Limhoff and Rainer Müller-Burtscheid for their quick and comprehensive support with the laboratory soft- and hardware infrastructure, and Gabriele Rebbe for her kind assistance with administrative issues.

Many parts of this work have been developed in a research cooperation with the Bosch Rexroth AG. Thank you very much for the productive partnership and the provision of hydraulic devices. Many thanks to Dr.-Ing. Georg Schoppel for his contributions and especially to Ingo Glowatzky, who became a real colleague of mine, for his technical support.

It was a pleasure to supervise my students, who investigated parts of my work during their theses. Dear Mustafa, Timo, Fabian, Faiza, Bernd, Daniel, Oliver, Carla, and Caroline, thank you for your work, and I wish you all the best for your future.

Wrapping up, I would like to thank my whole family for all your support and encouragement throughout the past years. Finally, I want to say thank you to my girlfriend Maren. Thank you for all of your loving support and patience during the last years. Without you, this work wouldn't have been successful.

Christoph Krimpmann, August 16, 2018

Contents

Nomenclature

The following list explains all abbreviations and symbols used throughout this work. In general scalar symbols are represented by normal font letters. Vectors are expressed as bold lower case letters, matrices are indicated by bold upper case letters and sets are notated as upper case caligraphic letters.

Abbreviations and acronyms

ALS	**A**nalytic **L**inear **S**ystem
AOSM	**A**rbitrary **O**rder **S**liding **M**ode
CCF	**C**ontrol **C**anonical **F**orm
CI	**C**omputational **I**ntelligence
CMA	**C**ovariance **M**atrix **A**daption
ES	**E**volutionary **S**trategy
FD	**F**inite **D**ifference
FIR	**F**inite **I**nput **R**esponse
HiL	**H**ardware **i**n the **L**oop
HOSM	**H**iger **O**rder **S**liding **M**ode
HPU	**H**ydraulic **P**ower **U**nit
IAE	**I**ntegral of **A**bsolute **E**rror
IATE	**I**ntegral of **A**bsolute **T**imeweighted **E**rror
MOEA	**M**ulti-**O**bjective **E**volutionary **A**lgorithm
NSGA	**N**ondominated **S**orting **G**enetic **A**lgorithm
OEM	**O**riginal **E**quipment Manufacturer
PF	**P**olynomial **F**ilter
PID	**P**roportional **I**ntegral **D**erivative
PWM	**P**ulse **W**idth **M**odulation
RED	**R**obust **E**xact **D**ifferentiator
SiL	**S**oftware **i**n the **L**oop
SMC	**S**liding **M**ode **C**ontrol
SOSM	**S**econd **O**rder **S**liding **M**ode
SPA	**S**uccessive **P**ole **A**adjustment
STA	**S**uper **T**wisting **A**lgorithm
TA	**T**wisting **A**lgorithm

TO	**T**ime **O**ptimal
TOS	**T**ime **O**ptimal **S**urface
TS	**T**akagi-**S**ugeno, a type of fuzzy system
VDI	**V**erein **D**eutscher **I**ngenieure
VSC	**V**ariable **S**tructure **C**ontrol

Greek symbols

α, α_0, α_1	control gains
β	control gain proportionality factor
Δ_λ	SPA design parameter
δ_σ	SMC adaption threshold
Δt, Δu	finite differences of t and u
δ_x	surface adaption threshold
ϵ	boundary layer thickness
η	inequality factor
γ	SMC adaption rate
κ	surface adaption rate
λ	eigenvalue, or offspring population size
μ	parent population size
Ω	solution space
ω	angular frequency
Φ	landing surface
ϕ	boundary width
Ψ	HOSM control law
ρ	stability design parameter
Σ	HOSM sliding function
σ	sliding function
ς	transformed sliding variable
τ	inequality factor
$\boldsymbol{\theta}$	solution parameter set
ζ	perturbation function, auxiliary variable

Mathematical expressions

x	scalar
$\mathbf{x}$	vector
$\mathbf{X}$	matrix
$\mathcal{X}$	set, a well-defined collection of distinct objects
$f(\cdot)$	scalar function
$\mathbf{f}(\cdot)$	vectorized function
$\nabla f(\cdot)$	gradient of the function $f(\cdot)$
$\mathcal{L}_f g(\mathbf{x})$	Lie derivative, $\nabla g(\mathbf{x}) f(\cdot)$
$x \in (0 \quad 1)$	$0 < x < 1$

$x \in (0 \quad 1]$	$0 < x \leq 1$
$x \in [0 \quad 1]$	$0 \leq x \leq 1$
$\lfloor x \rceil$	rounding to next integer value
$\lfloor x \rceil^{\alpha}$	sign dependent root, $\mid x \mid^{\alpha} \operatorname{sign}(x)$ with $\alpha \in [0\ 1)$

Roman symbols

$\mathbf{a}$	transformed state function
a	acceleration
A, B, P, T	hydraulic connection ports
a_k	polynomial coefficient
$\mathbf{b}$	transformed input function
c_i	eigenvalue proportionality factor
c_Φ	separation curve
e	control error
$\mathbf{f}$	state function
F	force
f_c	cutoff frequency
G	linear transfer function
g	input function
i	solenoid current
j	imaginary number, $\sqrt{-1}$
J	objective function
j_c	constant jerk
K	discontinuous control gain
k	relative degree
L	Lipschitz-constant
$\mathcal{L}_f$, $\mathcal{L}_g$	Lie derivatives
$\mathcal{L}_r$	r^{th} order sliding set
$\mathcal{L}_s$	solution set
M	half-sided filter length
m	polynomial sample
Mo	maximum overshoot
n	system order
p	hydraulic pressure
Q	flow rate
r	sliding order
r_i	sliding function coefficients
$\mathcal{S}$	sliding set
$\mathcal{S}_B$	boundary set
T	time interval, period duration
t	Time
T_r	rise time
T_s	settling time

$\mathbf{u}$, u	control input
v	velocity
V, V_λ	candidate Lyapunov function
$\mathbf{x}$	state vector
x	piston stroke
$\hat{x}$	estimated value of a variable x
$\mathcal{X}$	feasible state space
y	system output
z	transformed state variable

1 Introduction

1.1. Motivation

Hydraulic actuators are common choices for industrial applications when high actuating forces and/or torques are required while only small assembly space is given. The hydraulics is a wide-spread principle, e.g., in automotive manufacturing processes, industrial robotics, large-scale handling systems and mobile construction machinery. In the last decades, hydraulic systems evolved from mainly mechanical devices to highly automated systems. These mechatronically developed electro-hydraulic systems offer huge strength combined with high accuracy and fast response times provided by sophisticated algorithms as well as integration into a superordinate infrastructure by networking capabilities.

To obtain this high performance and accuracy, the design of the control strategies is the crucial point. The fundamental task of the control algorithms is to force the hydraulic or from a broader perspective the mechanical system to follow a predefined trajectory to obtain a desired behavior. For these systems, the control algorithms have to calculate precisely the demanded actuating force or torque such that technical and/or economic objectives are fulfilled. It is a challenging task to determine an algorithm that fulfills the imposed objectives and provides the desired performance.

The performance of linear controllers such as classic and well-known PID controllers are comparably poor or even unstable for typical systems if a wide operational range is demanded. Such systems comprise nonlinear effects like friction, saturations or turbulent flow effects that are difficult to handle because they cannot be linearized easily. By linearizing the nonlinear differential equations, linear controllers can be designed for particular working points in the state space, but their validity is restricted to certain regions in the state space. By superposition and interpolation between different parameterizations for linear controllers, a nonlinear gain scheduling strategy is realized. This is a simple approach to achieve improved control quality compared to conventional linear algorithms. However, stability cannot always be guaranteed since the controller only is valid at certain working points while for the interpolated control gains in between the working points, nothing can be guaranteed.

Among the nonlinear control design methods, the direct deduction of a set law by using Lyapunov's direct method provides a general way to obtain a nonlinear con-

troller with strong stability properties in a guided process. However, this theoretically elegant method leads to strong impediments even for systems of medium complexity. The difficulty rests upon the conditions that the subordinate Lyapunov candidate functions need to fulfill. Consequently, a suitable candidate function is rather difficult to obtain.

Feedback linearization also is a well-known method to convert a nonlinear system description into a linear one such that classical linear control approaches are applicable. While this method performs well for linearizing motion equations of automotive systems, e.g., the one-track or bicycle model, it is not able to handle discontinuous nonlinearities like Stribeck friction curves. The nonlinearities are compensated by large control inputs that are practically not applicable due to input limitations. Due to its model based design approach, the feedback linearization additionally is sensitive to any model inaccuracies or parameter changes as well as to external perturbations.

To manage the discontinuous nonlinear effects and slowly changing parameters, adaptive control is a method to obtain optimal closed loop performance as long as the structure of the system does not change. By using gradient-based estimations or Lyapunov approaches, optimal parameterizations and/or set laws are realized. In general, the adaptive control has difficulties to distinguish between parameter drifts to adapt to and disturbances to compensate. Therefore, the quantification of robustness of the controller is comparably small for the sake of an optimal adaption.

For the control of mechatronic systems, strategies are demanded that take the nonlinearities, modeling uncertainties as well as the disturbances into account. The concept of sliding mode control (SMC) provides means to overcome these issues. The SMC theory provides algorithms that ensure that the system dynamics becomes identical to a predefined one and that the dynamics is insensitive against parameter variations or external perturbations.

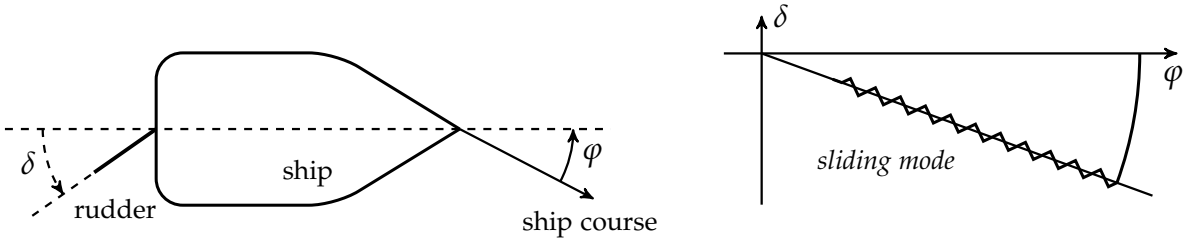

Figure 1.1.: Sliding mode control of a ship course. Left: top view of a simplified ship, right: corresponding phase diagram of the ship course φ and the rudder angle δ.

In 1934, Nikol'skii outlined one of the earliest relay control examples considering the course control of a ship by discrete actuation of the ship's rudder as illustrated in figure 1.1. He already used modern control theoretical phrases like *phase plane*, *switching line* or even *sliding mode* to describe the properties of the given path controller (cf. Utkin, Guldner, and Shi 2009). This publication is one of the earliest that investigates the system behavior in the phase plane instead of solving a time-continuous mathematical description. The ease of design as well as its guaranteed robustness paved the way for the relay control or later known as sliding mode control for various applications to combine high closed loop dynamics with superior disturbance rejection.

1.2. Related work

The research interest in hydraulics dates back to approximately 400 to 300 B.C. with the usage of the first water wheels (cf. Oleson 1984). With the invention of the hydraulic press by Pascal in 1663, the first industrial application was in sight. However, it still took over 100 years until in 1795 the first water-actuated hydraulic press assembled by Josef Bramah in London was used for pre-industrial applications. With the dawn of the servo-hydraulics in the 1950s and 1960s especially driven by Blackburn, Reethof, and Shearer (1960), a significant step towards automation was done and opened a wide range of new application fields. From that time, the large forces and torques provided by the hydraulics are precisely adjustable such that accurate control of heavy-duty applications like automated mining machines or aircraft controls are feasible. Due to the approximately linear dynamics of servo valves, the control design of servo-hydraulic systems can be realized by using conventional linear control theoretical methods. However, by the end of the 1980s, the performance requirements increased such that the already old-fashioned servo-hydraulics was the limiting bottleneck. The use of directional control spool valves resolved this bottleneck but also introduced new challenges. Because of the nonlinear valve dynamics, the control design became rather complex. The well-known and wide spread linear PID-controller now was equipped by nonlinear gain curves to compensate the nonlinear valve dynamics (cf. Gamble and Vaughan 1996). By supplementary gain curves and further increases in complexity, the originally linear PID controller was extended to fulfill the still growing performance requirements within the further three decades until its complexity reached such an extent that the conventional process expert is not able to achieve a suitable parameterization. By now, the use of computational intelligence, e.g., the evolutionary optimization is one of the few approaches to obtain high valve or system performance in short time (cf. Krettek et al. 2009; Ritelli and Vacca 2014).

Since the emergence of sliding mode control in the early 1960s, the portfolio of different SMC methods grew continuously. The textbook by Slotine and Li published in 1991 conveys the basic approaches of classical SMC and its application to real world use cases very comprehensively. Due to its eminence, until now a significant amount of new application-focused publications rests upon the approaches outlined in this textbook. However, by the development of higher order sliding modes (HOSM) at the beginning of the 1990s new and extended methods have been introduced that solve many problems like chattering that occur by using conventional SMC. Their dissemination towards practical applications still is limited; perhaps due to the mathematical complexity of HOSM solution. The following literature survey yields a solid overview of the development in hydraulics as well as in the sliding mode community. Surrounding influences of computational intelligence, as well as adaptive systems, are also incorporated.

Sliding mode control

From the 1950s, SMC, as well as its superordinate concept of Variable Structure Control (VSC), have been developed by the Institute of Control Problems as a solution for the

automatic control of an aircraft with dynamics varying in a wide range (Emel'yanov 2007). From the early sixties, first publications regarding the SMC are published in Russian by Emel'yanov and Taran (1962) and Emel'yanov et al. (1970). However, these concepts were not known outside of the Soviet Union until Itkis (1976) published the first monograph in English on SMC and followed by Utkin (1977) who initially presented the first survey paper. In the 1980s, the publications by Slotine and Sastry (1983) as well as Slotine and Coetsee (1986) gave a significant impetus towards the practical application of SM controllers since they focused on the chattering compensation using boundary layers and soft switching instead of discrete switching strategies. Based on this success, the textbook by Slotine and Li (1991) became one of the most cited references in this topic. However, by using boundary strategies, the robustness properties of the SMC are weakened such that a convergence into the steady state is not given (cf. e.g. Bessa 2009). With the invention of second order sliding modes (SOSM) by Levantovskii (1985), the theoretical solution for the chattering problem was invented. Consequentially, the initial English publication by Levant (1993) gained significant importance. It outlines different approaches to establish SOSM and to alleviate the harmful chattering from a theoretical perspective. Compared to Slotine and Sastry (1983) and Slotine and Coetsee (1986) the robustness and convergence properties of the controllers are not weakened to compensate the chattering.

Within the following years, SOSM gained importance in research, e.g. Davila, Fridman, and Levant (2005) and Levant (1998) highlighted SOSM observer structures. Parallel to this, Levant (1997, 2001, 2002, 2003, 2005a) focused on the generalization of HOSM with the development of HOSM or arbitrary order sliding mode (AOSM) control laws. A detailed overview of the development of SMC and current state-of-the-art control approaches is given in the book chapter by Fridman (2012).

One major drawback of SOSM respectively HOSM was its difficult stability analysis. Originally, the stability was proven geometrically for each control law (cf. e.g. Levant 1993). However, Moreno and Osorio (2008) introduced a suitable Lyapunov function by which the stability of the super-twisting algorithm (STA) – a prominent member of the SOSM algorithms (Fridman 2012) – is proven by the use of Lyapunov's direct method. In 2012, Moreno and Osorio extended the outlined approach for systems with less restricted uncertainties and Sanchez and Moreno (2014) published a constructive method to design Lyapunov functions for a broader class of SOSM controllers.

The introduction of Lyapunov-based stability analysis for SOSM enabled the deduction of adaptive STA controllers that automatically determine their parameterization to establish optimal sliding motion. The initial idea by Shtessel et al. (2010) only is on the theoretical properties while Shtessel, Taleb, and Plestan (2012) and Taleb, Levant, and Plestan (2013) or Barth et al. (2015) focused on more application-oriented designs. Parallel to the adaptive SOSM, Plestan et al. (2010) and Plestan et al. (2013) investigated the adaptive parameter estimation of conventional first order SMC. The adaptive first order SMC, though, is not a novelty. Slotine and Coetsee (1986) and Slotine and Li (1991) already outlined the adaption of the boundary layer width three decades before. The boundary adaption, however, is not directly comparable to the newly introduced adaptive first order SMC.

Basic principle of sliding modes

Consider the class of nonlinear and time variant systems with affine control inputs

$$\dot{\mathbf{x}} = \mathbf{f}\,(t,\,\mathbf{x}) + \mathbf{g}\,(t,\,\mathbf{x})\;\mathbf{u}(t) + \boldsymbol{\zeta}(t,\,\mathbf{x}), \tag{1.1}$$

where $\mathbf{x} \in \mathbb{R}^n$ is the n-dimensional state vector and $\mathbf{u} \in \mathbb{R}^m$ denotes the m-dimensional control input. The nonlinear state function is given by $\mathbf{f}\colon \mathbb{R}_{\geq 0} \times \mathbb{R}^n \mapsto \mathbb{R}^n$ as well as the nonlinear input function by $\mathbf{g}\colon \mathbb{R}_{\geq 0} \times \mathbb{R}^n \mapsto \mathbb{R}^{n\times m}$. Both, the state and input functions are assumed continuously differentiable vector fields. The vector function $\boldsymbol{\zeta}\colon \mathbb{R}_{\geq 0} \times \mathbb{R}^n \mapsto \mathbb{R}^n$ summarizes the unknown parameter uncertainties and external disturbances. The design task in sliding mode control is to find a suitable control function $\mathbf{u}(\mathbf{x})$ as a function of the system state

$$u_i(\mathbf{x}) = \begin{cases} u_i^+(t,\,\mathbf{x}) & \text{if } \sigma_i(\mathbf{x}) > 0 \\ 0 & \text{if } \sigma_i(\mathbf{x}) = 0 \\ u_i^-(t,\,\mathbf{x}) & \text{if } \sigma_i(\mathbf{x}) < 0 \end{cases} \quad i \in \{1,\,2,\ldots,\,m\} \tag{1.2}$$

$$u_i(\mathbf{x}) = -K\;\mathrm{sign}\,(\sigma_i\,(\mathbf{x})) \tag{1.3}$$

with u_i^+ denoting the i^{th} control input for a positive switching action and u_i^- as the control input for a negative switching action while equation (1.3) is a practical realization of equation (1.2) with the control gain $K > 0$. The different switching actions shall force the system onto the switching function. The user-defined switching function $\boldsymbol{\sigma}\colon \mathbb{R}^n \mapsto \mathbb{R}^m$ is a continuous differentiable function and represents the sliding manifold within the state space. A detailed discussion of the properties of switching functions along with their linear and nonlinear definitions is given in chapter 3. Further, the control function exhibits the discontinuity

$$\lim_{\sigma_i(\mathbf{x})\to 0^+} u_i^+(\mathbf{x}) \neq \lim_{\sigma_i(\mathbf{x})\to 0^-} u_i^-(\mathbf{x}). \tag{1.4}$$

Sliding mode is the solution of the controlled system (1.1) for $\sigma\,(\mathbf{x}) = 0$. However, system (1.1) is not differentiable at the point of discontinuity $\sigma\,(\mathbf{x}) = 0$ using a discrete switching law. The missing Lipschitz-continuity prevents the application of standard methods for deriving unique solutions for (1.1). Hence, methods for solving differential inclusions in the form of $\dot{\mathbf{x}} \in \mathbf{F}\,(t,\,\mathbf{x}) + \mathbf{g}(t,\,\mathbf{x})\;\mathbf{u}$ have to be applied, where

$$\mathbf{F}\,(t,\,\mathbf{x}) = \left\{ f(t,\,\mathbf{x}) \middle| \mathbf{x} \in \mathcal{X} \subset \mathbb{R}^n \right\} \tag{1.5}$$

is a multi-valued map than rather a function providing a single point in the state space.

One easily understandable approach to obtain a unique solution of (1.1) was presented by A. Filippov in the early 1960's. An English transcription of the formerly in Russian published works is given by Filippov and Arscott (1988). An illustration of Filippov's method is shown in figure 1.2. It is assumed that the sliding manifold $\sigma\,(\mathbf{x}) = 0$ is attractive and can be reached by the state point for a given control input

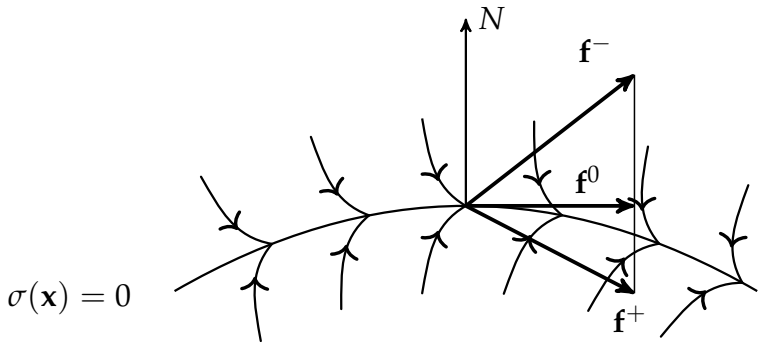

Figure 1.2.: Illustration of Filippov's method.

$u\,(t,\,\mathbf{x})$. The reachability conditions for establishing a sliding mode will be introduced in the latter discussion.

By examining the closed loop system description of system (1.1) with control law (1.2) and figure 1.2, we can conclude that two different behaviors occur for the two different control strategies $u^+(t,\,\mathbf{x})$ and $u^-(t,\,\mathbf{x})$. In the given illustration, the control action $u^-(t,\,\mathbf{x})$ causes a strong repelling behavior $\mathbf{f}^-(t,\,\mathbf{x})$ while the control action $u^+(t,\,\mathbf{x})$ causes a rather weak behavior $\mathbf{f}^+(t,\,\mathbf{x})$. However, both behaviors $\mathbf{f}^\pm(t,\,\mathbf{x})$ do not describe the system's motion in sliding mode $\mathbf{f}^0(t,\,\mathbf{x})$ which is perpendicular to the normal N of the sliding manifold $\mathcal{S}$. The vector is the desired state velocity for motion in sliding mode. As introduced by Filippov, the vector $\mathbf{f}^0(t,\,\mathbf{x})$ may be obtained by geometrical superposition of $\mathbf{f}^+(t,\,\mathbf{x})$ and $\mathbf{f}^-(t,\,\mathbf{x})$:

$$\mathbf{f}^0(t,\,\mathbf{x}) = \alpha\,\mathbf{f}^-(t,\,\mathbf{x}) + (1-\alpha)\;\mathbf{f}^+(t,\,\mathbf{x}), \quad 0 \leq \alpha \leq 1. \tag{1.6}$$

The value of the scaling factor α may be obtained from the condition $\dot{\sigma}\,(\mathbf{x}) = 0$. This condition restricts the system onto the sliding manifold and prevents a subsequent deviation. The detailed introduction of reaching conditions for a first order sliding motion and a general design of a model-based SM controller using Lyapunov's direct method is outlined in appendix A.

Control of hydraulic systems

The hydraulics predominantly follows the concept of *quality by design* to achieve desired system accuracy, e.g., by using servo-valves with almost linear system dynamics. However, for high-performance applications, their use is no longer feasible, and directional valves are equipped. The control of such valves is rather challenging as Blumendeller et al. (2000) stated. They propose that the control structure is always tailored to the nonlinear characteristics like actuator-force performance or friction effects. This experience is analog to Gamble and Vaughan (1996), who discuss, i.e., the application of an analog PI controller with a nonlinear proportional gain curve to compensate the nonlinear effects of the valve. The controller is stated to be an industry standard approach.

With the price decline of micro controllers in the late 1980s, the use digital control systems enabled several new control approaches for the hydraulics. Preliminary, the

digital controllers are used for the control of hydraulic drives like cylinders. One of the new enabled concepts was the adaptive control using on-line parameter identification like recursive least square methods. Köckemann (1989) outlined the application of digital adaptive drive control as an example. However, he still utilized open-loop servo-valves as actuators and only focused on the control of the superordinate system. Parallel to the application-oriented development of new controllers also the actuation mechanism of the directional valve's solenoids was reinvented. By using discrete switching actions like pulse-width modulations (PWM) instead of continuous analog signals, the reactions of the valves could be increased significantly so that the formerly as strong but slow postmarked directional valves became direct competitors of the servo-valves. The investigations of Lausch (1990) outline the advantages of PWM controlled directional valves.

In the following years, the digital control emerged and became industrial standard. The continuous increase of computational performance enabled more complex control approaches, e.g., basing on fuzzy control; see Albadawi (2010) as a contemporary example. The more control theoretical field of Lyapunov-based soft structure variable control without sliding modes also was highlighted by the application example of a control valve given by Adamy (1991) or the control of a cylinder by Niewels (2002). The variable structure control with siding modes spread wider into the hydraulics by the end of the 1990s. While the first applications of SMC by Gamble (1992) and Gamble and Vaughan (1996) strictly rely on discrete switching controllers, the use of boundary layer techniques was the first common solution to the disadvantageous chattering. Bonchis et al. (2001) or Chen, Renn, and Su (2005) e.g. outline the successful boundary layer control of hydraulic cylinders being used for robotic manipulators or positioning systems. However, Bartolini, Ferrara, and Usani (1998) outlined comparably early the necessity of higher order sliding mode control for mechatronic systems and Bartolini et al. (2003) gave a comprehensive survey of several mechanical examples that are reasonable to control by second order sliding modes. Nevertheless, it still lasted several years until Reichhartinger and Horn (2009) outlined the application of second order sliding modes for the observer as well as the controller design of a throttle valve. Within the last years, the work by Komsta (2013) can be understood as state-of-the-art of robust cylinder control while again open loop servo-valves are used as actuators. The presented integral SMC disturbance compensation effectively canceled out the bounded perturbations like load changes (cf. Komsta, Adamy, and Antoszkiewicz 2010). Braun, Reuter, and Rudolph (2017) proceeded the work of Komsta and focused on the subordinate control of the directional valve. They propose a trajectory reference controller based on an inverted linear valve model in conjunction with a sensor-less piston position observer.

In the current decade, the adaptive SMC is investigated repeatedly by Shtessel, Taleb, and Plestan (2012) or by Plestan et al. (2013) and Taleb, Levant, and Plestan (2013). They are all in common to investigate the properties of the controller on pneumatic cylinder drives, which are rather comparable in their settings to hydraulic cylinder drives.

Computational intelligence in hydraulics

The computational intelligence (CI) as has always been used by engineers to solve difficult engineering tasks by means of heuristic and data based methods instead of using analytic approaches. Kiendl (2012) highlights insightful the evolution of the CI from a contemporary witness' perspective. For a detailed overview of the different fields of CI, the interested reader is referred to the comprehensive textbook by Kruse et al. (2015).

Finding a set of suitable controller parameters is often a challenging task for real world applications. While the theoretical deduction of control structures like SMC guarantees certain robustness properties in case of suitable parameterization, the parameterization itself is not discussed sufficiently. Thus, Li et al. (1996) highlighted the genetic parameter optimization of SMC controller for practical applications through the minimization of the tracking error. Parallel to the work of Li et al., the Chair of Electrical Control Engineering at the University of Dortmund developed approaches for Hardware-in-the-Loop (HiL) parameter optimization of directional valve controllers; to quantify the control quality a fuzzy-based ranking of step responses is used (cf. Blumendeller et al. 2000; Nicolaus et al. 2001). The HiL optimization of control parameters is successfully continued by the work of Krettek et al. (2007) for hybrid SiL-HiL settings. The use of multi-objective optimization algorithms (MOEA) simplifies the design of optimization problems since no longer several conflicting objectives need to be concentrated into one quality measure. The application of MOEA for parameterizing a directional valves controller is successfully investigated by Krettek (2013) and Krettek et al. (2009) who expanded the commonly known MOEA NSGA-II by Deb et al. (2002) to incorporate the expert's preferences interactively into the optimization process.

The CI methods are not only used for parameterization of given controllers. The data-based black box modeling of hydraulic devices is extensively discussed in the textbook by Jelali and Kroll (2003). They outline a detailed overview of different identification techniques as well as their application to hydraulics. A circumstance of black box modeling is the absence of structural information of the system and thus, a focused control design is difficult. To compensate the lack of information Braun et al. (2011a,b) introduce an evolutionary optimization-based approach to identify the parameter and structure of a system at a time to obtain a white-box model. The idea resting upon this approach is to use the structural information for a targeted control design. A different commonly used approach is the use of fuzzy models to describe the dynamics of hydraulic systems. An example is given by Schauten (2008) where the hydraulic flow forces are modeled using fuzzy sets. Kroll and Schulte (2014) discuss a set of application benchmarks whereas several hydraulic applications are motivated. The one example illustrates the fuzzy-based gain scheduling control of a cylinder (Schulte and Hahn 2004) while the other one discusses either the control of a hydrostatic drive train using an adaptive fuzzy SMC strategy (Do and Ahn 2013) or the Takagi-Sugeno-fuzzy (TS-fuzzy, Takagi and Sugeno 1985) based modeling of the drive train (Schulte 2007).

1.3. Contribution and outline

This thesis is primarily driven by the idea that the absence of precise system models is not an ultimate problem for the high-performance control design. The experiences that are collected at the Institute of Control Theory and Systems Engineering at the TU Dortmund University during several cooperate research projects concerning the parameterization of industrial controllers for hydraulic valves lead to insight that existing control structures within the field of hydraulics rest upon empirical modifications of simple PI-like controllers. However, to meet the industrial requirements, e.g., defined by tracking accuracy, the number of design parameters rose such that the process expert has difficulties to parameterize the controller within an acceptable time. Thus, the given thesis investigates new methods for robust control of hydraulic valves. The control design is oriented such that no plant models are required for the design process to achieve a simple and fast adaption of the control structure to different systems of the same class and hence, to have an ease of application.

Chapter 2: This thesis discusses the control of three different hydraulic valves with different structures, actuation mechanisms, and working principles as examples of mechatronic systems. This chapter introduces the idea of mechatronics and mechatronic systems, motivates the necessity of a holistic design philosophy and briefly introduces a design methodology known as the V-model. In the second part, the direct actuated directional control valve is introduced as an example of a mechatronic system, and its properties are investigated towards the control design. The introduction of additional valves can be found in appendix B.

Chapter 3: The design of sliding manifolds is a crucial task in the design process since they directly define the closed loop dynamics. Thus, this chapter introduces the basic linear approaches and discusses their practical relevance. To increase the closed loop performance for practical applications, the use of nonlinear sliding functions is motivated, and several methods from the literature are discussed. Due to their restrictions, a new nonlinear sliding function is introduced that rests upon the idea to adjust the eigenvalues of the system at run time. Since the choice of the parameters of a sliding function is as crucial as its structure, a Lyapunov-based parameter adaption process is deduced that offers self-tuning capabilities for either linear sliding functions or the newly introduced nonlinear sliding function.

Chapter 4: The chattering phenomenon is one of the dominant difficulties of the practical application of discrete switching SMC. By outlining the properties of first order SMC boundary control approaches, the necessity of higher order sliding motions is motivated. Higher order sliding motion is an effective concept to compensate the chattering and to provide robustness against known and unknown perturbations. The chapter briefly introduces the HOSM and different control laws that establish second order sliding motion. Additionally, the properties of the super-twisting algorithm are investigated towards its application to adaptive sliding surfaces, and an assessment of possible control structures is given.

Chapter 5: SMC is implemented by means of nonlinear state feedback controllers. However, the hydraulic valves only offer output measurements, and thus, the state vector needs to be observed. For this, model-free observers are introduced that are implemented either as FIR-filters or as auxiliary control loops. Both observer structures realize a robust differentiator such that no model-knowledge is mandatory for their design. The state estimation is benchmarked for different parameterizations and scenarios.

Chapter 6: This chapter deals with the derandomized evolutionary optimization and its extension to multi-objective optimization problems. Initially, the derandomized covariance matrix adaptation evolutionary strategy is briefly introduced and its multi-objective equivalent deduced. With regard to the HiL parameterization of the valve controllers, expedient objective functions for the evaluation of sliding mode controllers are outlined.

Chapter 7: The SMC set laws are evaluated in practical experiments to investigate their applicability. The first of two chapters about the practical investigation focuses on the robust control of the valves. To achieve a high-performant robust motion, the control gains are optimized by using the outlined optimization algorithms. Initially, the resulting Pareto-sets are analyzed while latter; the properties of different linear and nonlinear sliding functions are compared. The results clearly indicate good dynamics by using nonlinear sliding functions compared to linear ones. As an additional example, the cascades SOSM control of a directional main stage valve is analyzed in time and frequency domain.

Chapter 8: The second chapter on the practical evaluation of the hydraulic valve control is about the self-tuning features. While initially the sole adaption of the linear or nonlinear sliding function is investigated, the latter part of this chapter focuses on a novel adaptive sliding mode controller. By combining the surface adaption with the self-tuning of the set law, both parts of the controller can be self-tuned within a fraction of the time that is used for an evolutionary HiL optimization.

Chapter 9: This thesis comes to an end with a concluding discussion about the accomplished results and suggests possible directions for further work.

2

Development of Mechatronic Systems

The theoretical control concepts that are investigated in this work are evaluated for the control of electro-hydraulic valves. As one particular example, the piston position control of a direct actuated directional control valve is investigated. Additionally, the cascade control of a directional main stage valve and the pressure control of a relief valve are discussed. However, the developed approaches are not restricted to hydraulics and can be applied to a wide range of mechatronic systems. To provide a shared comprehension of *mechatronics*, this chapter initially characterizes the mechatronics, and a commonly accepted design methodology is highlighted. In the latter part, examples of mechatronic systems are introduced, and their requirements concerning the control are discussed.

2.1. Characterization and design methodology of mechatronics

The word *mechatronics* was introduced by an engineer of the Yaskawa Electric Corporation in 1969 (Kyura and Oho 1996). The term was defined to provide a framework for technical and practical considerations for the design of systems with mechanical and electrical parts. The initial definition of a synergistic design of mechanical and

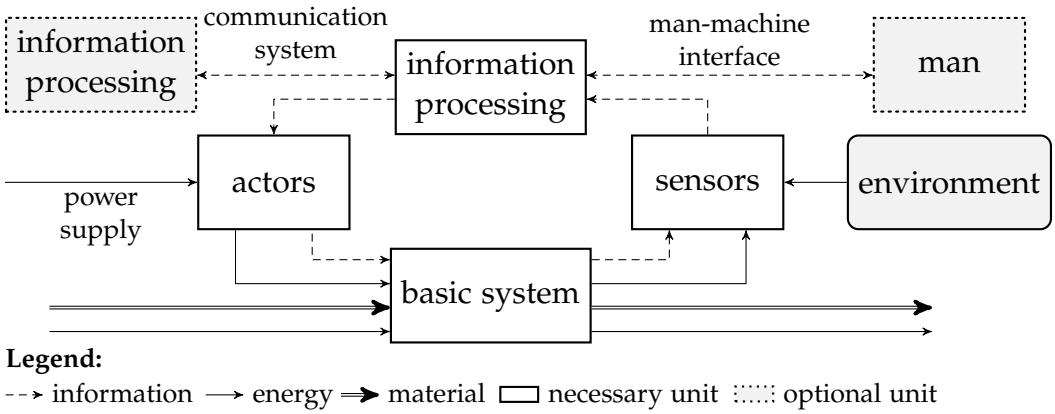

Figure 2.1.: Basic structure of a mechatronic system.

electronic components evolved in the following decades and the information technology incorporating the automation and control theory became an equivalent third domain. Later, the communication technology, which formerly stands alone among mechatronic products, became a further fully balanced domain. Following Harashima, Tomizuka, and Fukuda (1996), a well-established definition of mechatronics is *"the synergetic integration of mechanical engineering with electronic and intelligent computer control in the design and manufacturing of industrial products and processes."* A more holistic definition is given by Tomizuka (2002), who focuses on physical systems instead of mechanical ones. However, this imprecisiation is a drawback since now; almost any system can be understood as mechatronic. Kaynak (2017) states that the general definition of mechatronics did not change and still is valid. However, he also mentions the influences of big data and disruptive developments in electronics that may lead to a reformulation of existing definitions.

The guideline VDI 2206 by the Association of German Engineers (Verein Deutscher Ingenieure 2004), which also relies on the definition by Harashima, Tomizuka, and Fukuda (1996), describes a mechatronic system as a functional and spatial integration of a basic system, actors, sensors and an information processing (see figure 2.1). The basic system consumes energy and material from the surrounding and processes them mechanically, hydraulically, pneumatically, optically, and/or electrically before emitting them again. Thereby, the relevant state information of the basic system is directly measurable via sensors or are determinable by adequate observer structures. The information processing supervises the basic system upon the gathered state information. In case of deviations from the desired operation point, the information processing influences the basic system via suitable actuators that transfer further energy into the system to stimulate the inner processes.

The complexity of such mechatronic systems and their interactions between subsystems or with other systems demands an interdisciplinary way of thinking and engineering. Thus, a sequential design process focusing on single engineering domains is not goal leading so that only an iterative domain-spanning design process is successful.

Among others, the Association of German Engineers published a renowned design procedure as the guideline VDI 2206 (Verein Deutscher Ingenieure 2004). This guideline bases on the V-model that originally was published by Bröhl and Dröschel (1995) as a methodology for structured and effective software development. The VDI guideline 2206 adapted the V-model to the design of mechatronic systems. The main design procedure for mechatronic systems can be composed into following major parts:

- Adapted V-model as a macro cycle to describe the formal procedure between requirements and the solution.
- Problem solving as micro-cycles at which alternative solutions for particular engineering problems are determined and evaluated.
- Repeated tasks are formulated as predefined process steps.
- Modeling and analysis support the entire macro cycle

Figure 2.2 depicts the problem-specific V-model. The diagram shows the general macroscopic design cycle for mechatronic systems that starts with assessing the re-

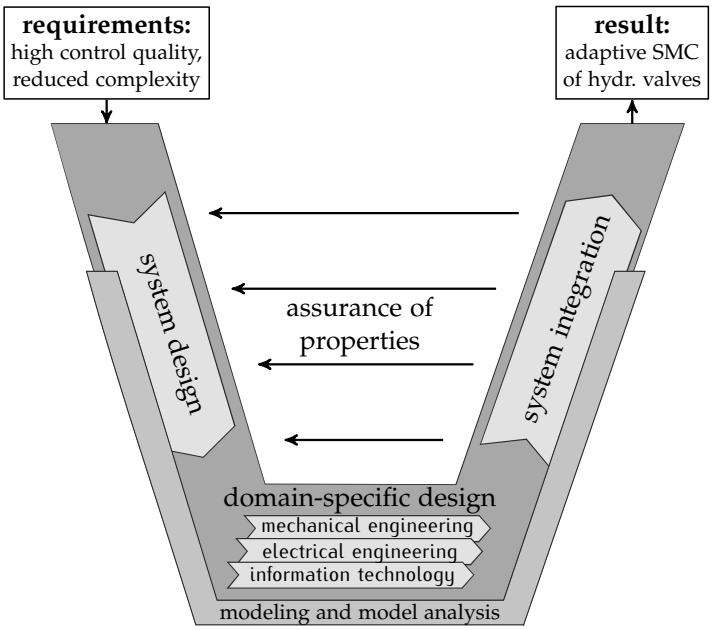

Figure 2.2.: V-model as a macro cycle (Verein Deutscher Ingenieure 2004).

quirements for the latter solution or product. A crisp and complete set of requirements is mandatory for a successful development. In case of an incomplete formulation, the design process is not sufficiently focused, and the resulting product is not compliant with the customers' demands or does not offer the intended functionality. For the given work, the requirements are formulated as follows:

- high control quality of the hydraulic valve with fast and aperiodic responses,
- fast and intuitive parameterization of the controller,
- reduced complexity compared to the current industrial solutions.

The left part of the V-model focuses on the system design at which a general structure of the system is created. The focus of this section is to identify or design the different subsystems and their interconnections on an abstract level that is neutral regarding a solution. Deducing the working-mechanism block set diagrams of the mechatronic system is obligatory, and its practical realization for different hydraulic valves is shown in the latter part of this chapter. A supplementary simple modeling of each component is also common to obtain a basic simulation model for further system analyses. After setting up the general architecture, the domain-specific engineering of each component is carried out in parallel. This is, e.g., the mechanical construction of an actuator or the design of power electronics. For this particular work, only the information technology, which also incorporates the control theory, is considered because only the redesign of the control structure for the hydraulic valve is intended. A requirement is to use the physical system as it is given. The right part of the V-model describes the system integration. Starting with the integration of single software components into the system model, first integrability tests can be performed using SiL experiments. Specific integrability tests for mechanical or electrical components are performed using HiL setups. These investigations are supported by a continuously performed modeling and simulation process. After successful partial integration, a first prototype test is

the next possible step. The tests are used to validate the system properties that are formulated on the left side of the V-model. In case of unsuccessful tests, a detail-engineering needs to be carried out again. Thus, the V-model shall not be understood as a one-directional process without fallbacks to prior sections. If all properties are validated, the design process ends with the specified result. The result should not be understood as the final mechatronic product. Rather, the result can be a detailed, pure simulation model or a prototype of the system. Basing on these intermediate results, new passes of the V-model are performed whereby the previous result is the starting point of the new development cycle.

2.2. The directional control valve as a mechatronic example

If giving examples of mechatronic systems, often devices or components in the field of automotive are taken. A popular system is the anti-lock braking system (ABS) that prevents the vehicle's wheels from being locked in braking maneuvers such that hazardous situations are prevented. Only by following the mechatronic design principle, the realization of the ABS with its wheel speed sensors, electro-hydraulic actuation unit and sophisticated digital control design was possible (see e.g. Isermann 2008; Verein Deutscher Ingenieure 2004). In contrast to this renowned mechatronic example, the hydraulics oftentimes still is understood as the purely mechanical system being designed without following the mechatronic way of thinking. In the past decades, especially the hydraulic valves were designed such that their properties only rely on an advanced mechanical design while the control was implemented using comparably simple approaches. However, due to increased requirements, this design philosophy is replaced in the last decade, and more mechatronically-influenced designs have risen.

To provide a deep and detailed understanding of the experimental systems that are used to validate the control concepts that are discussed in this work, an introductory example of the application fields of the hydraulic valves is given, and in the latter part, the directional control valve itself is introduced as a mechatronic system.

An introductory example:

The electro-hydraulics are wide spread in industrial applications due to their high power-density and flexibility in spatial design. This is also the reason, why there are many settings for mobile and industrial applications. One dedicated example is shown in figure 2.3. The lower layer constitutes the hydraulic supply unit consisting of an electrically actuated pump with variable displacement providing the system's pressure (also known as hydraulic power unit, HPU) and the oil flow for the hydraulic actuators. A gas accumulator is attached to the pump to compensate small changes of the oil flow by absorbing or relieving oil volumes. To provide a more sophisticated control of the system's pressure, an electrically actuated pressure relief valve is placed in parallel to the hydraulic pump. By actuating the pressure relief valve, a bypass to the further application layers is adjusted. Hence, a certain amount of fluid flows directly back to the fluid tank such that the overall system's pressure is reduced. By closing the bypass, the pressure is increased. Thus, by controlling the system's pressure via adjusting

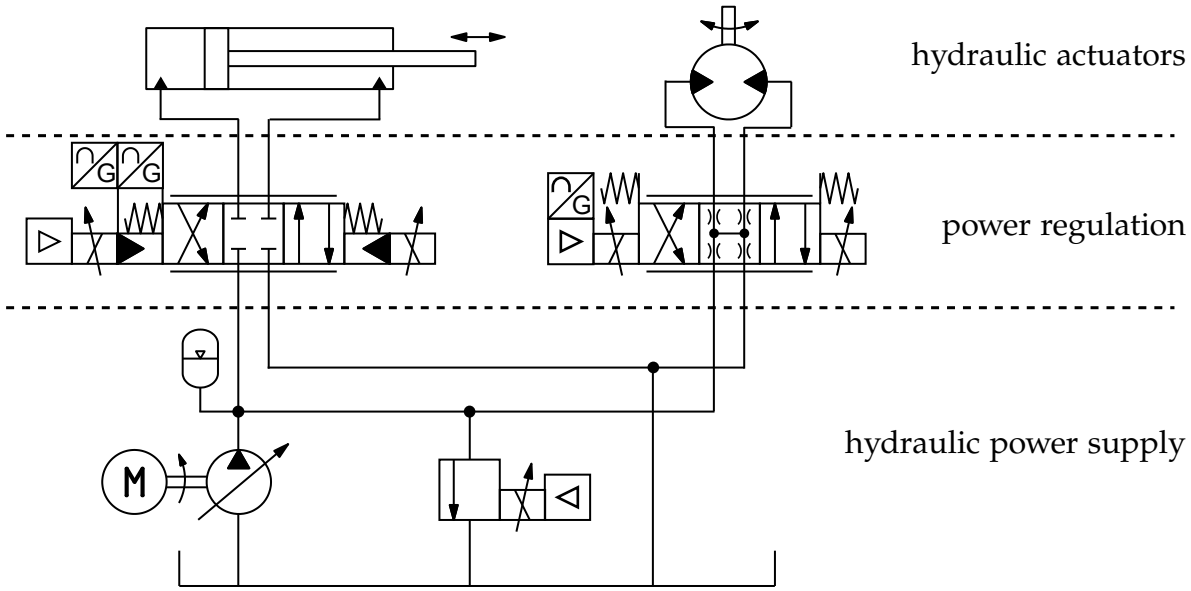

Figure 2.3.: Example of a schematic structure of a valve-controlled electro-hydraulic system.

the pressure relief valve, the pressure can be kept constant within the whole system even though there are pressure or flow disturbances caused by varying load of the hydraulic actuators. See section B.1 for a further introduction of the valve. For this example, the hydraulic power is dynamically shared by two different actuators. The first actuator is a differential hydraulic cylinder that may be used as a press actuator. The cylinder can be moved in and out in depending on the oil flow applied to the connecting ports. To regulate the oil flow and its direction, a cascaded directional control valve is used. Depending on the position of the main stage valve's piston, either the oil flows into the cylinder and pushes the cylinder piston out, or the oil flows into the second chamber pushing the piston back into the cylinder. The behavior of the cylinder strongly depends on the movement of the directional valve's piston since small movements of it change the oil flow into the cylinder. Thus, the valve has to offer a high control quality. If having a high-quality controller for the directional valve, superimposed control structures may provide different behaviors of the cylinder. See section B.2 for a further introduction of the valve. The second hydraulic actuator being shown in figure 2.3 is a hydraulic motor providing a torque, e.g. to accelerate a drive train. Compared to electrical motors, a hydraulic motor provides a higher power density while having the same construction space. The torque or the rotational speed is regulated by a subordinate direct actuated directional control valve that again adjusts the actuating oil flow in dependence on its piston position.

The behavior of the hydraulic actuators strongly rests upon the subordinate systems. To obtain the best feasible performance on the actuator level, the overall system's design cannot be successful if the control strategies for the intermediate actuators like the hydraulic valves are not ideal. Therefore, using standard control structures like simple PID controllers while having an advanced mechanical design of the system is not constructive. In fact, the synergistic system development as illustrated before is necessary for a high-performance system.

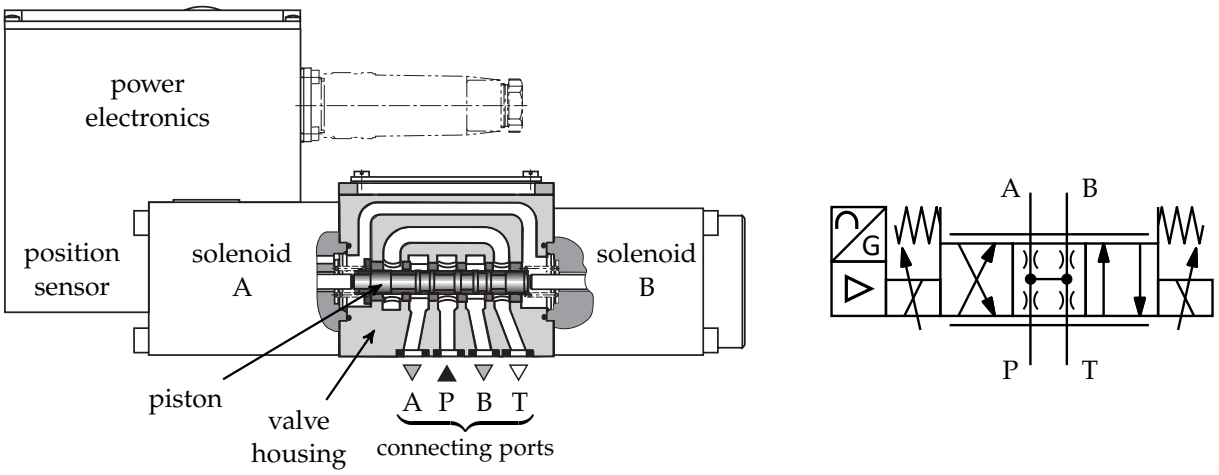

Figure 2.4.: Cross sectional view and hydraulic symbol of a directional control valve with two counteracting solenoids.

The direct actuated directional control valve:

Directional control valves e.g. as shown in figure 2.4 are multi-polar hydraulic switches that are used to regulate the oil flow in a hydraulic system by adjusting the position of the valve's piston by using either one solenoid and a counteracting control spring or two counteracting solenoids. Historically seen, the directional control valves rest upon the proportional valve technology being developed almost a century ago (Jelali and Kroll 2003). Due to the utilized proportional solenoids, the proportional valves emerged as one of the default switches to regulate the oil flows and thus the behavior of the subsequent hydraulic actuators, e.g., cylinders or hydrodynamic motors. These valves adjust the piston's position proportional to the applied input signal. This is achieved by a certain construction of the solenoids. The air gap of the solenoid is constructed in a way such that the generated force becomes rather independent of the piston's position. Further constructive details of solenoids can be found in Kallenbach (2012). Figure 2.5 illustrates the progress of the solenoid force F_{sol} according to varying positions. Within the operational range of approximately $x/x_{max} \in [0.6 \quad 0.8]$ the force is comparably independent of the position. Because of this, the typical stroke of a piston is limited to a maximum of $|\Delta x| \leq \pm 0.1\, x_{\max}$. Therefore, the valve provides a proportional positioning of the piston. Since the solenoids have a non-negligible hysteresis and the valve's piston also sustains a friction-induced hysteresis, the accuracy

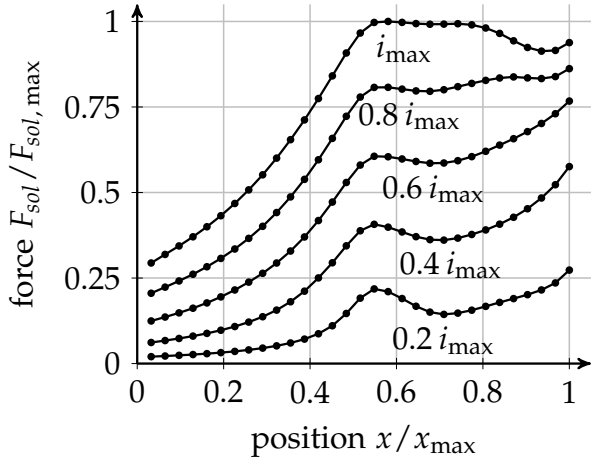

Figure 2.5.: Force measurement of a typical proportional solenoid in dependence on the position x and the current i. The operational position range is $x/x_{max} \in [0.6 \quad 0.8]$.

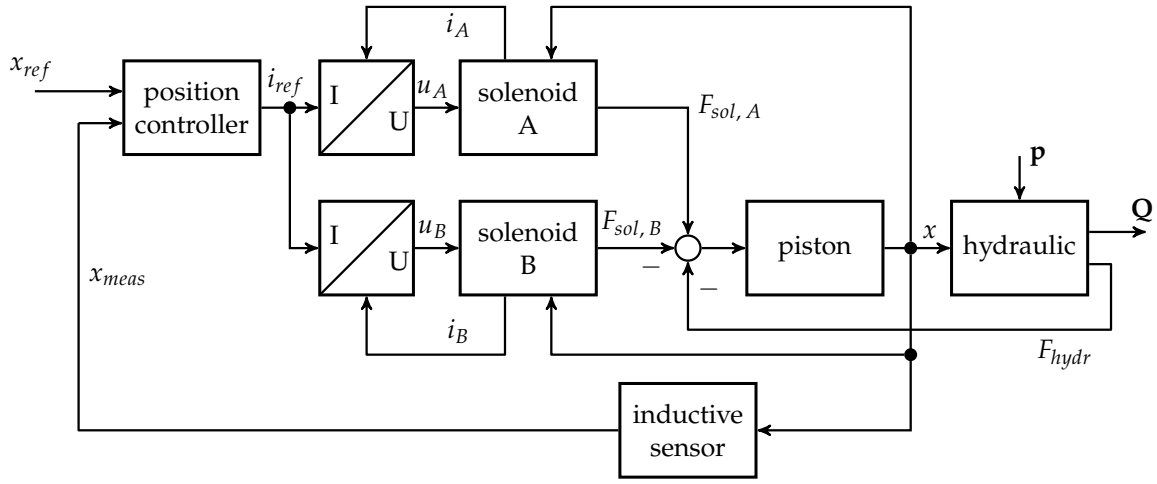

Figure 2.6.: Working principle of a double actuated directional control valve.

of open-loop control proportional valves is limited. Thus, their application is restricted to velocity regulations of subsequent actors (Jelali and Kroll 2003). Further tasks such as, e.g., force/torque or position/angle control are not to be fulfilled due to the lacking performance so that a different kind of valve with increased precision is applied. By adding position control to proportional valves, the inaccuracies are compensated, and high-bandwidth positioning of the piston is achieved. In the early 1970s, the first PID controllers emerged and until PID controllers with nonlinear gain characteristics became state of the art (see e.g. Gamble and Vaughan 1996; Krettek et al. 2007 for controller examples).

A *4WRSEH 6 V24LD* type valve manufactured by the Bosch Rexroth company is used for this work and is comparable to the valve shown in figure 2.4 while the working principle of this valve is depicted in figure 2.6. The valve contains an analog PID controller and a position and velocity feedback to calculate a reference current i_{ref}. The power electronics of the valve contains two independent pulse width modulators providing the binary switching voltages u_A and u_B for the solenoids A and B. The resulting currents i_A and i_B are controlled by P-controllers to reach the desired values. The solenoids are counteracting so that the force $F_{sol,B}$ is counted negative. The solenoid A pushes in the positive direction of the piston's position x.

Further, a hydraulic force F_{hydr} caused by the oil flowing through the valve acts against the piston's movement. Friction-induced forces are also present, but due to brevity not depicted in figure 2.6. To compensate the stick-slip friction (see e.g. Armstrong-Hélouvry 1991; Ruderman 2012) the power electronics keeps the piston in slight oscillation by superimposing a dither signal onto the control inputs. In case of disabled power electronics, two counteracting control springs center the piston so that an oil flow is prevented. The oil flows through the connecting ports $\mathbf{Q} = [Q_\mathrm{A},\, Q_\mathrm{B}]^\mathrm{T}$ depend on the differential pressure Δp between the outlet port and the pressure port P or the tank port T. This dependency switches with the piston position. If the position is positive $x > 0$, the oil flows from port P to A and B is connected to T. This connection is inverted for $x < 0$.

A detailed simulation model of the directional valve can be obtained by applying a

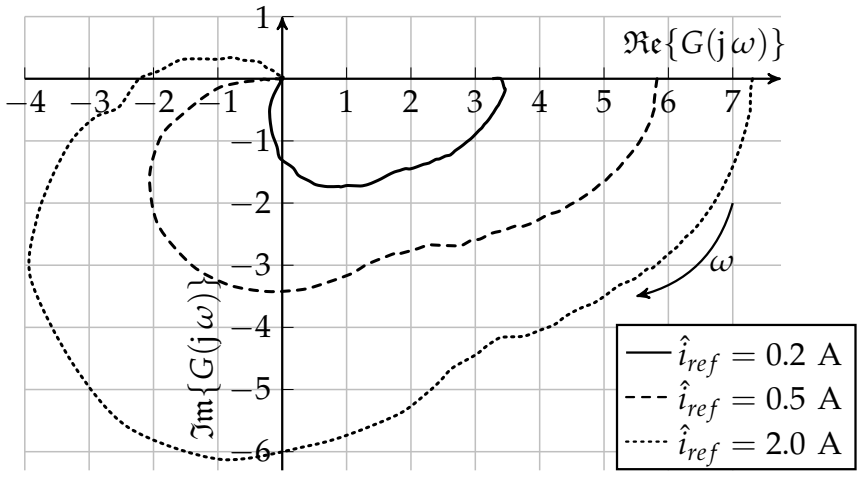

Figure 2.7.: Measured open-loop Nyquist diagrams of the directional control valve for varying input amplitudes $\hat{i}_{ref}$.

cascaded identification process as presented by Makarow (October 2014) and Makarow et al. (2015a,b). However, this modeling approach demands detailed prior knowledge of the solenoid force characteristics given in the form of measured lookup tables providing the solenoid $F_{sol}\,(i,\,x)$ in dependence on the current i and the position x. These relations are not available for the current valve. Thus a simulation-based analysis as shown for the pressure relief valve is not applicable to evaluate the effective system order.

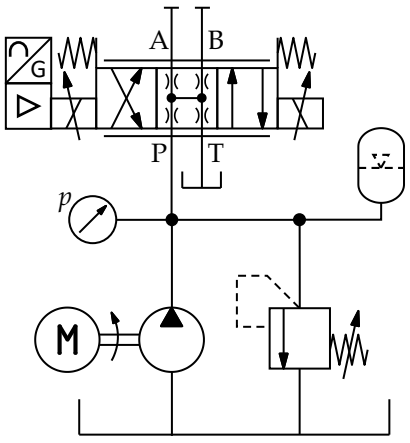

Figure 2.8.: Simplified diagram of the hydraulic experimental setup of the directional control valve. Bottom to top: HPU with passive overpressure relief valve, pressure accumulator and pressure indicator, directional valve with locked connection ports A and B.

To evaluate the effective system order, frequency response measurements are carried out; the resulting Nyquist diagrams are shown in figure 2.7. For this and for all further experiments considering this valve, the hydraulic setup as depicted in figure 2.8 is used where the HPU provides an oil flow with a constant pressure p that is connected to the P-port. The ports A and B are closed such that no oil flows through the valve. The port T is directly relieved back to the tank. This setup is identical to the ones being used in industry. The valve is excited with sinusoidal reference current signals with different amplitudes $\hat{i}_{ref}$. The frequency dependent gain $|G\,(\mathrm{j}\,\omega)|$ is the ratio of the effective values of the input i and output x while the phase shift $\angle G\,(\mathrm{j}\,\omega)$ is calculated by a cross correlation of both signals. The Nyquist diagram clearly indicates the nonlinear properties of the directional valve. As can be seen, the steady state gain depends on the input amplitude $\hat{i}_{ref}$. While the influence for small values is rather high, the gain is not comparably increased for higher solenoid currents. Additionally, the system has a strong damping

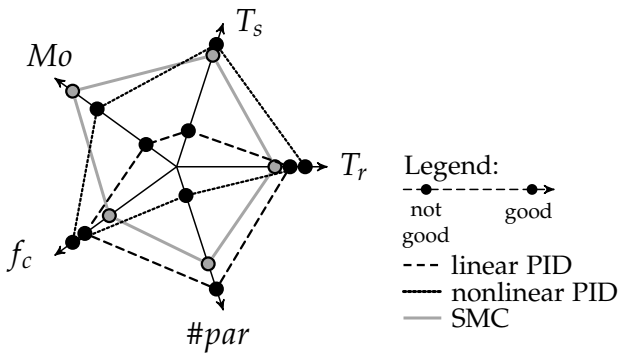

Figure 2.9.: Qualitative comparison of control algorithms.

for higher frequencies and small input amplitudes. The resulting behavior indicates a second order behavior since the visible phase shift is lower than $\angle G(\mathrm{j}\omega) < \pi$ before the output entirely is damped. Only for higher amplitudes, the valve shows third order behavior because now the phase shift $\angle G(\mathrm{j}\omega)$ is between π and $\frac{3\pi}{2}$. Based on the frequency response evaluation the directional control valve is considered as a third order system $(n = 3)$ with the states $\mathbf{x} = [x,\, v,\, a]^{\mathrm{T}}$, where v and a denote the velocity and acceleration of the piston. The piston position controller that is to be designed for the direction valve has to comply with several requirements irregardless of the selected control concept. On the one hand, the control structure itself is assessed and on the other hand, the control quality needs to fulfill certain performance indexes:

- No model-based design
- Limited system knowledge mandatory
- Small number of design parameters (#*par*)
- Ease of parameterization
- Fast step responses/rise times (T_r)
- Short settling times (T_s)
- Only small or no maximum overshoots (*Mo*)
- High cutoff frequencies (f_c)

In figure 2.9, an empiric comparison of three different control approaches is given. The scoring, however, may be understood as subjective. The points located further outside of the arrow indicate better performance than the ones at the origin. If assessing the linear PID controller, the comparison is mixed. While having only a few parameters, either the rise times or the settling times are good since the controller is not able to provide means to all requirements. A nonlinear gain-scheduled PID controller as introduced in section B.3 achieves good results in all considered objectives. However, this result is achieved by many design parameters that increase the controller's complexity extensively. SMC as an alternate approach offers competing performances in all objectives. It cannot be understood as the best solution, however, in contrast to the PID-based solutions, it does not have any requirement that is not fulfilled adequately. For the introduction of further experimental systems, the reader is referred to section B.2 for the directional main stage valve and to section B.1 for the pressure relief valve. In the following, for all introduced valves, control approaches based on sliding modes are designed.

3
Design of Sliding Functions

In the given chapter, the terminology and properties of sliding manifolds or also known as sliding surfaces are discussed. Although linear sliding functions are prevalent in literature, nonlinear sliding functions offer several advantages for practical applications. However, most publications concerning sliding mode control discuss the suitable selection of a control law; the sliding function only is chosen in a simple fashion. Parts of this chapter have been previously published by Krimpmann et al. (2015a,b, 2016b).

As a remark, only sliding functions with a relative degree of $k = 1$ are considered in this section since these sliding functions are compatible with the presented control laws. For arbitrary relative degrees of sliding functions, the author is pleased to refer to section 4.4.

3.1. Linear sliding functions

While the control laws discussed in the previous chapter solely influence the robustness or the smoothness of the system's motion, the sliding manifold $\sigma(\mathbf{x}) = 0$ constitutes the dynamics of the closed loop system. An adequate choice of a sliding function is indispensable to achieve the ideal system performance. However, this may lead to an increased complexity for nonlinear or partially unknown systems. To maintain the simplicity of the design process, the usage of linear sliding functions is the first choice to achieve a fully functional sliding mode controller.

The linear sliding function can be defined as the linear combination of the control states with strictly positive weighting factors r_i:

$$\sigma(\mathbf{x}) = \sum_{i=1}^{n} r_i \, x_i, \quad r_i > 0 \wedge \mathbf{r}, \mathbf{x} \in \mathbb{R}^n. \tag{3.1}$$

Considering the sliding function from a geometrical perspective, the sliding condition $\sigma(\mathbf{x}) = 0$ constitutes an $(n-1)$-dimensional surface passing through the origin of the n-dimensional state space. Due to this geometrical interpretation, the sliding function $\sigma(\mathbf{x})$ also is known as *sliding surface*.

By considering the properties of a sliding function in regard of the system that is supposed to be controlled, the sliding function exhibits further properties. Oftentimes,

the state space differential equation of the system is given in a control canonical form (CCF), in general given as

$$\begin{aligned} \dot{x}_i &= x_{i+1}, \quad i \in \{1, 2, \ldots, n-1\} \\ \dot{x}_n &= f(t, \mathbf{x}) + g(t, \mathbf{x})\ u \\ y &= x_1 \end{aligned} \tag{3.2}$$

where the control input only acts on the n^{th} state while the other states are obtained by integrating x_n. The system output y is equal to the first state x_1. To obtain the dynamics of the sliding motion $\sigma(\mathbf{x}) = 0$, the equation of the sliding surface $\sigma(\mathbf{x})$

$$\sigma(\mathbf{x}) = r_1\, x_1 + r_2\, x_2 + \cdots + r_{n-1}\, x_{n-1} + r_n\, x_n = 0 \tag{3.3}$$

is solved for x_n:

$$x_n = -r_1\, x_1 - r_2\, x_2 - \cdots - r_{n-1}\, x_{n-1}. \tag{3.4}$$

Without the loss of generality and as a practical simplification it is common to choose $r_n = 1$. This reduces the number of independent design parameters. By substitution of the state x_n in the system description of equation (3.2) by equation (3.4), one obtains the differential equations

$$\begin{aligned} \dot{x}_i &= x_{i+1}, \quad i \in \{1, 2, \ldots, n-2\} \\ \dot{x}_{n-1} &= -r_1\, x_1 - r_2\, x_2 - \cdots - r_{n-1}\, x_{n-1} \end{aligned} \tag{3.5}$$

that describe the dynamics of the closed loop system in sliding motion. It should be noted that the state x_n now is expressed by the algebraic equation (3.4) instead of using a differential equation for $\dot{x}_n$ that therefore is omitted. The resulting differential equation does not longer depend on the system's state dynamics given by $f(t, \mathbf{x})$. Thus, the dynamics in sliding motion is robust against parameter variations and model inaccuracies of the system. A notable aspect of equation (3.5) is the reduced order dynamics. The dynamics in sliding motion are of reduced order $n-1$ compared to the system's dynamics of the order n, a detailed discussion of the invariance conditions for linear systems is given by Draženović (1969) while the robustness properties for arbitrary systems are discussed by Gao and Hung (1993). In addition, the parameters r_i of the sliding surface are equal to those of the characteristic polynomial for the closed loop system in sliding motion. Hence, the roots of the characteristic polynomial are equal to those of the sliding function for $\sigma(\mathbf{x}) = 0$. This indicates that the sliding function defines the poles of the closed loop system. For this, the sliding function can be written as

$$\sigma(\mathbf{x}) = \prod_{i=1}^{n-1} \left(\frac{\mathrm{d}}{\mathrm{d}\, t} - \lambda_i \right) x_1, \quad \lambda_i < 0 \wedge \boldsymbol{\lambda} \in \mathbb{R}^{n-1} \tag{3.6}$$

if the system description is given as shown in equation (3.2) and the further states x_i, $i \in \{2, 3, \ldots, n\}$ are derivatives of x_1. The differential operator $\frac{\mathrm{d}}{\mathrm{d}\, t}$ only acts on x_1; products of the differential operator describe higher derivatives of x_1. The time-independent design parameters λ_i are equivalent to the poles or rather the eigenvalues of the closed loop system in sliding motion $\mathcal{S}$.

The invariance against parameter variations and the fact that the sliding surface parameters are identical to the coefficients of the characteristic polynomial allow the sliding mode control to be used as pole placement technique for systems whose order n is the only known information while the dynamics are not modeled. For this, the only restriction is given by the control input u. The control input u has to be sufficiently large so that the system is transferred to arbitrary points in the state space and is not restricted due to input limitations.

3.2. Nonlinear sliding surfaces

Linear sliding functions are studied well, and their usage is the first choice if the properties of sliding mode control laws are discussed or deduced. From a theoretical perspective, this approach is straightforward since, for instance, the convergence properties of the Lyapunov function (A.2) are not effected quantitatively by the shape sliding function. Independent of the shape of the sliding surface, the control law (A.9) still provides finite time convergence into sliding mode from arbitrary initial conditions.

For practical applications, however, the main objective is to achieve a certain closed loop behavior for the desired control task. The sliding mode control is only one purpose for achieving this goal by providing a set of properties of the closed loop system. Hence, the shape of the sliding surface is a major design factor.

Time-varying surfaces

Starting with the work of Harashima, Hashimoto, and Kondo (1985), the application-driven development of time-variant sliding surfaces initially was introduced. The main idea of time-variant sliding surfaces is to combine the two conflicting sliding-mode properties of high robustness and fast convergence. To achieve a fast convergence, the eigenvalues of the closed loop system are to be selected to be rather small. This leads to a sliding surface of a steep slope. By considering equation (3.6) for an example in which a second order system and a linear sliding function $\sigma(\mathbf{x}) = r_1 x_1 + x_2$ is discussed, the eigenvalue of the closed loop dynamics is given by $\lambda_1 = -r_1$. To increase the convergence rate, the slope of the surface has to be increased by adjusting r_1. However, this leads to an extended time in which the system remains in the reaching phase. During this time, the system does not offer the robustness properties of the sliding motion, and the disturbance rejection is not guaranteed. In addition to that, the system does not operate with the desired dynamics.

As a solution to this issue, Harashima, Hashimoto, and Kondo (1985) presented an extension to the linear surfaces so that the reaching phase is eliminated and the robustness and desired dynamics are established form the initial condition $\mathbf{x}_0$ until reaching the final state $\mathbf{x}_e$. For this, the sliding function is selected to intersect with the initial condition $\mathbf{x}_0$ and for $t > t_0$ the slope of the surface is varied to increase the velocity of the system. A comparable approach by Choi, Park, and Jayasuriya (1994) also considers an additional translational motion of the surface through the state space.

However, as Bartoszewicz (1995) reveals, these approaches prevent the system to enter sliding motion at all. Due to the movement of the surface, the system is pulled away from it, and thus, the sliding motion is not preserved. Generally speaking, the system is kept in a continuous reaching phase in the vicinity of the sliding surface. This may lead to improved dynamics but the robustness of the motion is not given. By incorporating a precise plant model into the adaption process of the sliding function Bartoszewicz (1995) additionally presented an approach that established ideal motion for a time-variant sliding surface. This approach has been extended to third order systems with state and input constraints by Bartoszewicz and Nowacka (2006) and Bartoszewicz and Nowacka-Leverton (2010) to introduce a design procedure that optimizes a given objective function. In the particular case, the IAE or ITAE minimization is illustrated. However, all approaches presented by Bartoszewicz et al. are in common that the resulting sliding function directly incorporates the initial state vector $\mathbf{x}_0$ and the initial time t_0. The resulting controller only is applicable for one predefined scenario consisting of $\mathbf{x}_0$ and t_0. For different initial conditions or continuous reference trajectories, the resulting controller is not applicable since its design assumptions are not valid.

The time-varying sliding functions offer increased closed loop performance for specific selective scenarios of well-known initial conditions and precise system models. However, for uncertain systems and continuously changing reference signals, this approach does not show any benefits due to its parameterization that compensates the initial values. Nevertheless, the adjustment of the sliding surface and hence, its resulting nonlinear shape illustrates the need for a more sophisticated design of sliding functions as a simple selection of eigenvalues for linear ones.

Quasi time-optimal sliding surfaces

As shown in the previous section, the dynamics of the closed loop system in sliding motion cannot be increased beyond the dynamics of linear sliding functions if arbitrary initial conditions and imprecise plant models are given. As a solution to this, the formulation of nonlinear sliding surfaces constituting nonlinear closed loop dynamics in sliding motion are a major design influence.

While the time-variant sliding function approaches rest upon the optimization of an IAE or ITAE objective, a different objective that often is used for control design is the time-optimality that quantifies the time delay between the initial time instance t_0 and the time t^* at which the system is transferred from the initial condition $\mathbf{x}_0$ into the steady state $\mathbf{x}_e = \mathbf{0}$:

$$J_{TO} = \int_{t_0}^{t^*-t_0} 1 \, \mathrm{d}\, t. \tag{3.7}$$

In case of an accurate system description without any perturbations, Pontryagin's theorem can be applied to obtain the solution for the optimal control problem with constraint input. For this, the reader may refer to Föllinger (1985). The resulting controller is sensitive to any inaccuracy of the underlying system model or any perturbations so that no robustness of the closed loop system is guaranteed.

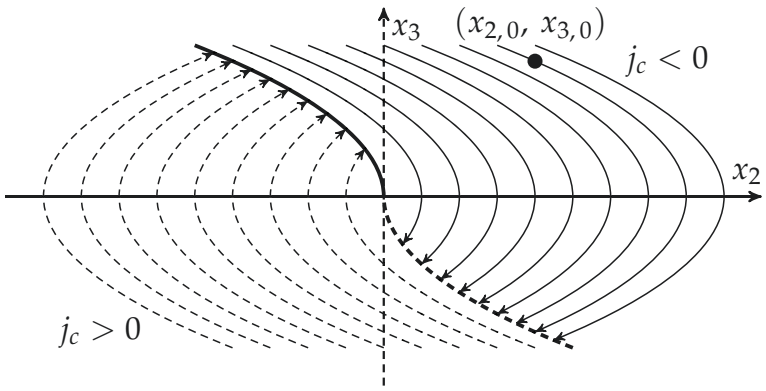

Figure 3.1.: Positive and negative landing domain of a 3rd order system. A positive jerk j_c causes upward directed trajectories while trajectories heading downward are caused by a negative jerk j_c.

If only the system's order n is known precisely, the solution for equation (3.7) cannot be derived. Nevertheless, a quasi time-optimal sliding motion can be established for systems in CCF using a certain nonlinear sliding surface. The motion indeed is not optimal in the classical sense because the sliding mode controller needs to keep a margin to the optimal solution to cope with inaccuracies and disturbances to provide the robustness properties. While the system is kept on the surface, the motion is characterized by discrete values of $\dot{x}_n \in \{\dot{x}_n^-,\ \dot{x}_n^+\}$ where $\dot{x}_n^-$ are $\dot{x}_n^+$ are of the same absolute value and of different sign. This can be understood as a motion of constant acceleration for a second order system.

To derive the so-called *quasi-time-optimal* sliding surface, the system is assumed to be an n^{th} integrator system. This can be understood as a special case of the control canonical description of equation (3.2) if the system dynamics $f(t,\ \mathbf{x})$ are equal to zero or are assumed to be a parametric perturbation of a pure integrator chain. Now, for the n^{th} order system the general solution for the time-optimal objective function (3.7) can be calculated. For system orders of $n \leq 3$ this can be done directly by the application of Pontryagin's theorem but if the system's order is arbitrary, the solution may be derived recursively using the approaches by Gulko and Kogan (1963) or Fuller (1973).

In the following, the system order is selected to be $n = 3$, hence the order coincides with the system order of the directional valve shown in section 2.2. Based on the general solution of the time-optimal control problem for given initial conditions $\mathbf{x}_0$, the so called landing surface $x_{1,d} = \Phi_s(j_c,\ x_2,\ x_3)$ can be defined as shown by Koh, Aum, and Cho (1999) for a different context than sliding mode control. The landing surface $\Phi_s(x_2,\ x_3)$ calculates a desired position $x_{1,d}$ in accordance of the speed x_2 and the acceleration x_3 from which the system moves into the origin in minimal time if the derivative of the acceleration $\dot{x}_3$ – the jerk j_c – is constant and only changes its sign. The evaluation of the two-dimensional $(x_2,\ x_3)$-projection of $\Phi_s(\cdot)$ as shown in figure 3.1 reveals the typical trajectories of the time-optimal solution for a second order integrator system as e.g. described by Föllinger (1985). Further can be seen that the

landing surface can be separated along the curvature

$$c_\Phi\left(x_2,\, x_3\right) = 0 = x_2 + \frac{x_3^2}{2\, j_c}\,\mathrm{sign}\left(x_3\right). \tag{3.8}$$

If a sub-state point $(x_2,\, x_3)$ lies above the separation curve $c_{\Phi(x_2,\, x_3)} > 0$, the system is exposed with the negative jerk to be moved towards the target $\mathbf{x}_e = \mathbf{0}$. When reaching the curve, the jerk is altered to a positive value. For a sub-state point below the separation curve, the sign of the jerk is reversed. By combining these properties, the sign-dependent jerk is defined as

$$j_c^* = j_c\ \mathrm{sign}\left(x_2 + \frac{x_3^2}{2\, j_c}\,\mathrm{sign}\left(x_3\right)\right). \tag{3.9}$$

The detailed derivation of $\Phi_s\left(\cdot\right)$ is omitted at this point; the full deduction is shown by Koh, Aum, and Cho (1999). The resulting description of the landing surface is given as follows with ξ as an auxiliary variable:

$$\begin{aligned}\Phi_s\left(j_c,\, x_2,\, x_3\right) &= -\frac{x_3^3}{3\, j_c^2} - \frac{x_2\, x_3}{j_c^*} + \frac{\xi^3}{j_c^2}\\ \xi &= -\,\mathrm{sign}\left(j_c^*\right)\left(x_2\, j_c^* + \frac{x_3^2}{2}\right)^{1/2}.\end{aligned} \tag{3.10}$$

As previously discussed by Krimpmann et al. (2015a), the landing surface $\Phi_s\left(\cdot\right)$ can be used to define a sliding surface that provides a near time-optimal sliding motion for an unperturbed system. Since for many third order systems the jerk cannot be controlled directly, the direct optimal control using a constant jerk j_c^* is not applicable. Hence, the jerk needs to be controlled implicitly by the following sliding surface. Let

$$\sigma\left(\mathbf{x}\right) = \Phi_s^{-1}\left(j_c,\, x_1,\, x_2\right) - x_3 = 0 \tag{3.11}$$

be a sliding surface on which the point in the state space remains due to an appropriate discontinuous control law, then the system approaches into the steady state $\mathbf{x}_e = \mathbf{0}$ with a predefined constant jerk j_c providing a *quasi-time-optimal* sliding motion. The function $\Phi_s^{-1}(j_c,\, x_1,\, x_2)$ is the inverse function of equation (3.10) in regard of the state x_3. The inverted landing surface $\Phi_s^{-1}(\cdot)$ calculates the desired acceleration $x_{3,\,d}$ of the system. If the true acceleration x_3 is equal to $x_{3,\,d}$, the system acts with the desired dynamics. Due to the numerous sign functions used in $\Phi_s\left(\cdot\right)$, the analytic inverse function $x_{3,\,d} = \Phi_s^{-1}\left(j_c,\, x_1,\, x_2\right)$ does not exist. However, by using numerical methods the inverse function is approximated. For this, the objective function

$$J_\Phi = \Big(\Phi_s\left(j_c,\, x_2,\, x_3\right) - x_1\Big)^2 \tag{3.12}$$

is defined that quantifies the quadratic error between desired state $x_{1,\,d}$ and the given one x_1. By solving the optimization problem

$$x_3^* = \arg\min_{x_3} J_\Phi \tag{3.13}$$

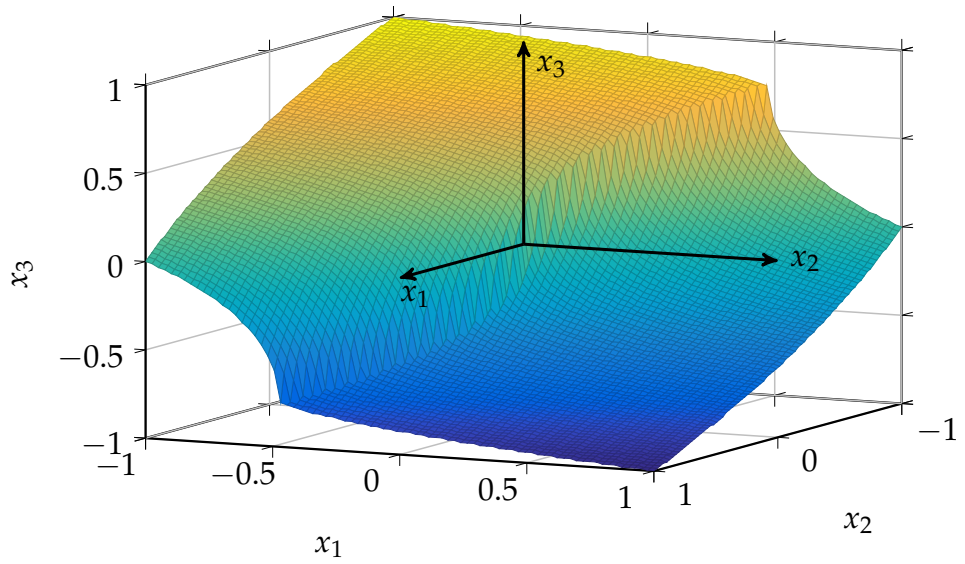

Figure 3.2.: Numerical approximation of the inverse function of a landing surface $\Phi_s(j_c,\, x_2,\, x_3)$ using a discretization of 80 samples per dimension with intervals of $-1 \leq x_1 \leq 1$ and $-1 \leq x_2 \leq 1$.

for a discrete set of $(x_1,\, x_2)$ tuples, the inverted landing surface $\Phi_s^{-1}(\cdot)$ is approximated by a two-dimensional nonlinear surface $\mathcal{I}_\Phi(j_c,\, x_1,\, x_2)$. An illustrative approximation of an inverted landing surface is shown in figure 3.2.

By replacing the analytic inverse $\Phi_s^{-1}(\cdot)$ that is incorporated in the sliding function shown in equation (3.11) by its numerical approximation, an approximate *time-optimal* sliding surface (TOS)

$$\sigma(\mathbf{x}) = J_\Phi(j_c,\, x_1,\, x_2) - x_3 \tag{3.14}$$

is created for a third order system providing a motion of constant jerk and hence, time-optimality for a triple-integrator system if ideal conditions are given. However, as can be seen in figure 3.2 the sliding surface contains a line of discontinuity at which the surface has an infinite slope. This discontinuity is caused by the separation curve $c_\Phi(x_2,\, x_3)$ that separates the landing surface into two domains by switching the jerk j_c^*. As shown in the latter experimental evaluation of the sliding surface in section 7.3, the discontinuity comprises a serious issue for sliding motion. If the system reaches the discontinuity, the velocity vector $\dot{\mathbf{x}}$ has to change its direction instantaneously. This is a serious issue for real systems in CCF because only $\dot{x}_n$ can be changed immediately by switching u. Hence, the control law compensates any deviations of the system from the sliding surface directly, but for practical applications, this direction change is not feasible straight away.

3.3. Successive pole adjustment sliding surfaces

While the linear sliding functions lead to linear closed loop dynamics of sliding motion by using a purely mathematical design, the quasi time-optimal sliding surface rests upon a numerical approximation of the solution of the time-optimal control design resulting in a data-driven lookup table. Hence, the effort of designing an increased closed loop dynamics for sliding modes is rather high due to the numerical inversion. To reduce the effort, an analytically describable nonlinear sliding function is reasonable to use. For instance as shown by Reichhartinger and Horn (2009) for a second order system, the linear sliding function can be extended by a cubic nonlinear damping term $\sigma(\mathbf{x}) = r_1\, x_1 + x_2 + \hat{r}_1\, x_1^3$. Using a cubic damping increases the slope of the surface for increased values of x_1 and hence, the convergence rate of large deviations from the origin becomes high while the convergence rate for comparable small deviations is low. From a practical perspective, this sliding function increases the reaching phase for large deviations since the system needs to achieve a high speed to reach the sliding manifold. However, at this point, the discontinuous control law has to expose a comparable high control input amplitude u to stabilize the system on the manifold $\mathcal{S}$ while the compensation of small deviations is slow using only a fraction of the control input amplitude. By examining figure 3.3, this fact is evident to see. The figure illustrates different sliding functions intersecting at the edges of the constrained state space $\mathbf{x} \subset \mathcal{X} \in \mathbb{R}^2$. As discussed in section 3.1, the linear sliding surface leads to a linear closed loop dynamics in sliding motion. The time-optimal switching function can be understood as a natural border for any sliding function. On the switching function, the control input reaches its limits to stabilize the system on a given manifold to reach the origin with a non-oscillatory motion. Hence, any sliding function has to be located in the sector between the x_1 axis and the time-optimal switching line for this two-dimensional example.

Now, considering the cubical damped sliding function by Reichhartinger and Horn (2009), it is evident to see that the closed loop system in sliding motion only has a

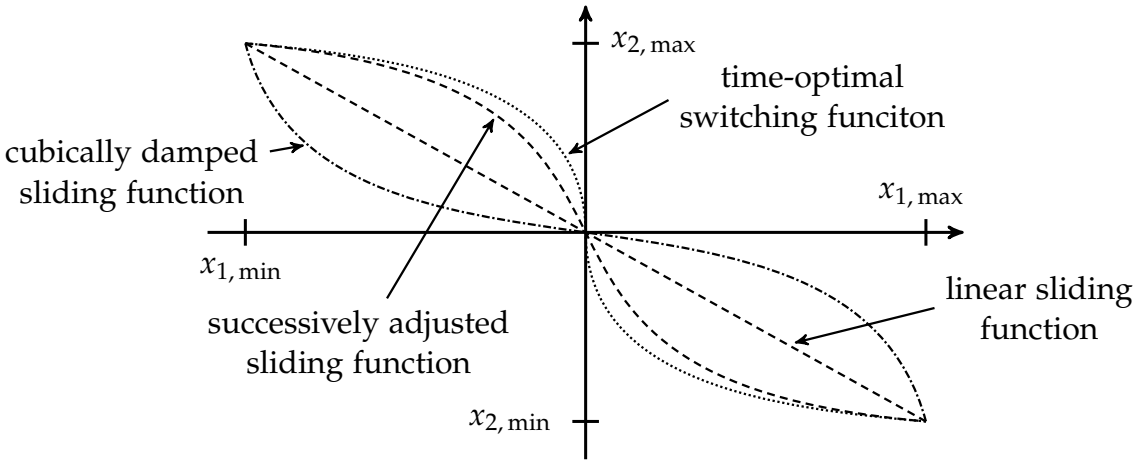

Figure 3.3.: Comparison of different sliding functions for a two-dimensional constrained state space.

minimum speed for a small deviation resulting in a creepage into the origin. Thus, a clockwise bending of the linear surface results in an increased speed compared to the linear surface. This shape is given by the second nonlinear sliding function offering a steep slope at the origin that decreases to the edges of the state space. This sliding function is inspired by the idea to compensate small deviations with higher dynamics as it would be possible for significant deviations from the origin.

As Krimpmann et al. (2015a,b, 2016c) discussed priory, this sliding surface applies a successive adjustment of the eigenvalues of the closed loop system in sliding motion. For this, the linear sliding function as shown in equation (3.6) is investigated further:

- **Second order system** $(n = 2)$: For a system of two states the sliding function is given as

$$\sigma(\mathbf{x}) = \left(\frac{\mathrm{d}}{\mathrm{d}\,t} - \lambda_1\right) x_1 = \dot{x}_1 - \lambda_1 x_1 = x_2 - \lambda_1 x_1 \tag{3.15}$$

  where λ_1 defines the slope of the surface or rather its inverse amount is equal to the time constant of the first order closed loop system. To increase the system dynamics, the eigenvalue of the system and thus the root of the characteristic polynomial is to be decreased by reducing λ_1. Consequently, the slope of the sliding function (3.15) is increased. The idea of increasing the dynamics for small deviations from the origin now is incorporated as a linear adjustment of λ_1 in dependence on x_1 using a linear equation:

$$\lambda_1(x_1) = \Delta_\lambda |x_1| + \lambda_0, \quad \Delta_\lambda,\, \lambda_0 \in \mathbb{R},\, \Delta_\lambda > 0 \wedge \lambda_0 < 0 \tag{3.16}$$

  The ordinate intercept λ_0 is the eigenvalue of the system in sliding motion for $x_1 = 0$ and defines the fastest possible dynamics. To limit the system's reaction for increased deviations, the slope Δ_λ reduces the dynamics by increasing the eigenvalue $\lambda_1(x_1)$. However, to maintain the stability of the sliding motion the value of λ_1 has to remain negative. Otherwise, the eigenvalue of the system in sliding motion becomes positive and therefore, the system in sliding motion diverges. To determine the largest possible slope $\Delta_{\lambda,\max}$, the stability limit

$$\lambda_1(x_{1,\max}) = \lambda_{1,\max} = \Delta_{\lambda,\max} |x_{1,\max}| + \lambda_0 < 0 \tag{3.17}$$

  is considered, where the state $|x_1| \leq x_{1,\max}$ is assumed to be symmetrically bounded. By solving inequality (3.17) for $\Delta_{\lambda,\max}$, one obtains the largest possible value for

$$\Delta_{\lambda,\max} < -\frac{\lambda_0}{|x_{1,\max}|}. \tag{3.18}$$

- **Third and higher order system** $(n \geq 3)$: For systems of higher order than two, $n-1$ eigenvalues are to be adjusted. Expanding the depicted approach for $n = 2$ by an independent adjustment for every single eigenvalue would lead to a precise adjustability of the resulting nonlinear sliding surface. Due to the large number of $2 \cdot (n-1)$ design parameters, the surface design is not easy to be carried out by a process expert. In addition, oftentimes the limits of the states are not known if the states represent velocities or accelerations of motions.

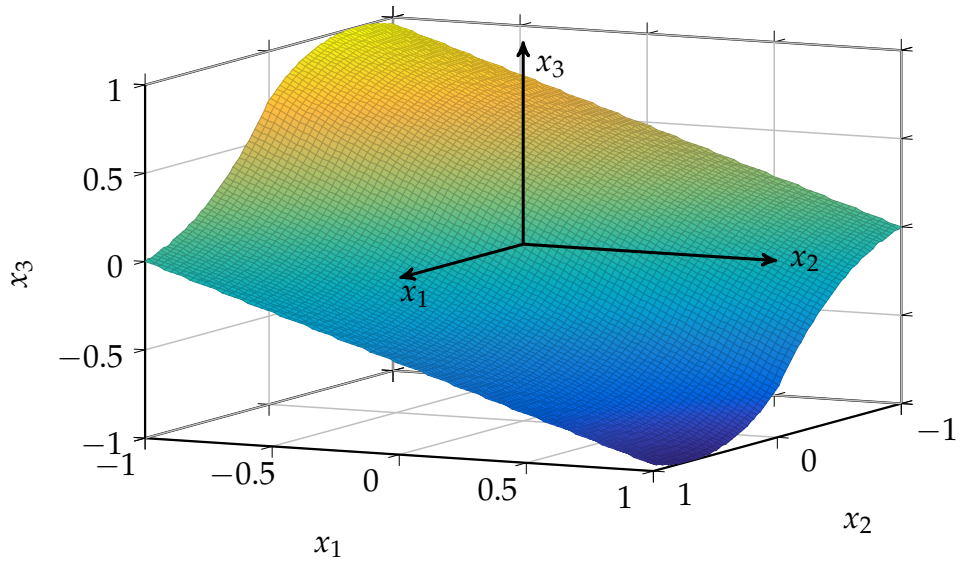

Figure 3.4.: Nonlinear sliding surface for a third order system using the successive pole adjustment approach.

To constrain the influence of the dimension n on the complexity, the eigenvalues λ_i, $i \in \{2, 3, \ldots, n-1\}$ are adjusted proportional to $\lambda_i \propto \lambda_1(x_1)$. The eigenvalue λ_1 is considered dominant concerning the further ones. Especially mechatronic systems comprised of mechanical and electrical subsystems, the dominance of single eigenvalues is given (see appendix C.2). Ergo, the nonlinear sliding function for a n^{th} oder system is given as follows:

$$\begin{aligned} \sigma(\mathbf{x}) &= \prod_{i=1}^{n-1} \left(\frac{\mathrm{d}}{\mathrm{d}\,t} - \lambda_i \right) x_1 \\ \lambda_1(x_1) &= \Delta_\lambda |x_1| + \lambda_0 \\ \lambda_i(x_1) &= c_i\, \lambda_1(x_1), \quad i \in \{2, 3, \ldots, n-1\} \wedge c_i > 0. \end{aligned} \tag{3.19}$$

Figure 3.4 exemplarily depicts a generic surface for a third order system. By comparing the quasi time-optimal surface depicted in figure 3.2 and the current surface, it is obvious that the successive pole adjustment does not comprise any discontinuity in the resulting surface. It results in a smooth and stable sliding motion approaching the origin.

Generally speaking, the *successive pole adjustment* (SPA) offers an analytic way to define a nonlinear sliding surface of arbitrary order with increased dynamics for small deviations and an attenuated system behavior for larger deviations. In contrast to other approaches, the chosen formulation does not rely on numerical approximation, and its design and parameterization are easy to understand using the linear control theory.

3.4. Lyapunov-based parameter estimation

As outlined in the previous sections, there are several approaches to define either linear or nonlinear siding surfaces for arbitrary systems. However, the parameterization of the sliding surfaces is an important process since upon the parameterization the closed loop dynamics are defined. In general, the manual selection of the parameter values leads to a sub-optimal closed loop performance since a process expert is not able to test every feasible solution. To obtain an optimal parameterization, the Lyapunov-based stability analysis is used to evaluate the stability of discontinuous sliding mode control laws as briefly shown e.g. in section A. As the previously published approach by Krimpmann et al. (2016b) outlines, the Lyapunov-based stability analysis is applicable to arbitrary sliding functions using a notation given in equation (3.6). These are for instance all linear sliding functions and the SPA approach outlined in the previous section.

The primary part of the dynamics in sliding motion is given by the dominant eigenvalue $\lambda_1 = \max(\lambda_i)$, $i \in \{1, 2, \ldots, n\}$ if using a linear surface. When using the SPA method, the dominant dynamics are defined by $\lambda_{1,\max}$; thus, λ_0 can be determined subsequently. For the sake of simplicity, both design parameters are pooled and denoted as λ since the following procedure is identical for the linear and nonlinear surfaces. To deduce an adaption procedure for the dominant design parameter λ, an extended Lyapunov function is proposed:

$$V_\lambda(\mathbf{x}, \lambda) = V(\mathbf{x}) + \frac{1}{2\kappa}(\lambda - \lambda_{\inf})^2, \quad \lambda, \lambda_{\inf} < 0,\ \kappa > 0 \wedge \lambda, \lambda_{\inf}, \kappa \in \mathbb{R}. \tag{3.20}$$

The function $V(\mathbf{x})$ is the Lyapunov function of a SMC law e.g. as shown in section 4.3 or in section A.1. It is expected that $V(\mathbf{x})$ is proven to be finite-time stable. The variable $\kappa > 0$ is an arbitrary but positive factor and $-\infty < \lambda_{\inf}$ is the negative finite infimum of $\lambda \in [\lambda_{\inf}\ 0)$. By assuming stability of the switching control law, the evaluation of $V_\lambda(\mathbf{x}, \lambda)$ only has to show stability of the λ dynamics. For this, the time derivative of equation (3.20) is calculated:

$$\dot{V}_\lambda(\mathbf{x}, \lambda) = \dot{V}(\mathbf{x}) + \frac{1}{\kappa}(\lambda - \lambda_{\inf})\ \dot{\lambda}. \tag{3.21}$$

To simplify the process of showing stability of a dynamic closed-loop system with the aid of equation (3.20), the square root of the additional term of $V_\lambda(\mathbf{x}, \lambda)$ is added to $\dot{V}_\lambda(\mathbf{x}, \lambda)$ as a zero-sum:

$$\dot{V}_\lambda(\mathbf{x}, \lambda) = \dot{V}(\mathbf{x}) + \frac{1}{\sqrt{2\kappa}}|\Delta_\lambda| + \frac{1}{\kappa}\Delta_\lambda\,\dot{\lambda} - \frac{1}{\sqrt{2\kappa}}|\Delta_\lambda|, \quad \Delta_\lambda = \lambda - \lambda_{\inf}. \tag{3.22}$$

Since $V(\mathbf{x})$ is proven finite-time convergent, it is known that

$$\dot{V}(\mathbf{x}) \leq -\eta V^\rho(\mathbf{x}), \quad \rho \in (0 \quad 1) \tag{3.23}$$

is valid (cf. equation (A.4)). Thus, by incorporating this inequality into equation (3.22), one obtains

$$\dot{V}_\lambda(\mathbf{x}, \lambda) \leq -\left(\eta V^{1/2}(\mathbf{x}) + \frac{1}{\sqrt{2\kappa}}|\Delta_\lambda|\right) + \frac{1}{\sqrt{2\kappa}}|\Delta_\lambda| + \frac{1}{\kappa}\Delta_\lambda\,\dot{\lambda} \tag{3.24}$$

with $\rho = 1/2$. Now, the right side of the obtained inequality contains the square roots of the summands of the extended Lyapunov function shown in equation (3.20). This fact can be used for further simplification of inequality (3.24) by applying the triangle inequality

$$\left(\xi_1^2 + \xi_2^2\right)^{1/2} < |\xi_1| + |\xi_2| \,. \tag{3.25}$$

By applying the inequality with $\xi_1 := (2\,\kappa)^{-1/2} |\Delta_\lambda|$ and $\xi_2 := \eta V(\mathbf{x})$, one obtains

$$\dot{V}_\lambda(\mathbf{x},\, \lambda) \leq -\tau V^{1/2}(\mathbf{x},\, \lambda) + \frac{1}{\kappa}\Delta_\lambda\, \dot{\lambda} + \frac{1}{\sqrt{2\,\kappa}} |\Delta_\lambda| \,, \quad \tau = \min(1,\, \eta) \,. \tag{3.26}$$

To achieve finite time convergence of the Lyapunov function $V_\lambda(\mathbf{x},\, \lambda)$, the recently deduced inequality (3.24) has to fulfill the form of inequality (3.23). Hence, the sum of the second and third summand of inequality (3.24) has to be zero. If λ_{inf} is selected sufficiently small, Δ_λ remains positive for arbitrary values of λ. Thus, the $|\cdot|$ operator becomes ineffective and one obtains the following expression:

$$0 = \Delta_\lambda \underbrace{\left(\frac{1}{\sqrt{2\,\kappa}} + \frac{1}{\kappa}\dot{\lambda}\right)}_{=0} . \tag{3.27}$$

The goal of the self-tuning process is to establish an optimal closed loop system behavior. In general, this is the compensation of any control error e or deviation from steady states for the reference control application. Implementing this idea, the desired parameter – in this particular case λ – is adjusted by a given mechanism until the desired control quality is met. Oftentimes, the simple reduction of a deviation from the origin in the state space for a particular state e.g. x_1 is desired (Plestan et al. 2013; Shtessel, Taleb, and Plestan 2012; Taleb, Levant, and Plestan 2013). Such self-tuning procedures in general lead to an appropriate parameter estimation if slowly changing continuously differentiable reference functions such as a sinusoidal signal are commanded. Due to a smooth change in the signal, there are no significant deviations to compensate, and the self-tuning procedure converges after the appropriate system dynamics is established. However, if an abrupt, perhaps discontinuous, change of the reference occurs, the adaption mechanism expects the abrupt state deviation as a mismatch of the closed loop system behavior and continues adjusting the control parameter although the adaption actually has converged. To circumvent the sensitivity of an adaption process against the shape of the reference signal, Krimpmann et al. (2016a,b) propose to use the moving average of the adaption signal. For instance, if the adaption shall lead to a decreased average control error for a sequence of reference steps, the minimization of the moving average signal

$$x_{1,\,av} = \frac{1}{T}\int_0^T |x_1(t-\zeta)|\, \mathrm{d}\,\zeta \tag{3.28}$$

is a feasible solution. The variable T is the length of the filter window of which the mean absolute value of x_1 is calculated. To define a desired closed loop behavior, a threshold δ_x is introduced. If the moving average deviation $x_{1,\,av} \leq \delta_x$ is below the

threshold, the desired system dynamics are established. Otherwise ($x_{1,\,av} > \delta_x$), the adaption process has to increase the dynamics. Now, when combining the convergence condition (3.27) and the moving average of the adaption signal (3.28), one has to consider two different cases.

1. **The desired dynamics is not reached:** In this situation, the sliding surface is not shaped properly to provide the desired convergence into the steady state. Further, the finite time convergence of the Lyapunov function $V_\lambda\,(\mathbf{x},\,\lambda)$ is to be fulfilled. Therefore, in equation (3.27) $\dot{\lambda}$ is isolated and one obtains

$$\dot{\lambda} = -\left(\frac{\kappa}{2}\right)^{1/2}, \quad \forall\, x_{1,\,av} > \delta_x \,\wedge\, \lambda_{\text{inf}} < \lambda. \tag{3.29}$$

   The dominant eigenvalue is decreased to accelerate the system's response.

2. **The desired dynamics is established:** If the current dynamics are sufficiently fast and $x_{1,\,av}$ is lower than the given threshold δ_e, the adaption process has to prevent a breakdown of sliding motion due to an irrationally steep slope of the sliding surface. For this, the adaption rate of (3.29) is negated as shown below:

$$\dot{\lambda} = \left(\frac{\kappa}{2}\right)^{1/2}, \quad \forall\, x_{1,\,av} \leq \delta_x \,\wedge\, \lambda_{\text{inf}} < \lambda. \tag{3.30}$$

   By increasing λ, the system dynamics is reduced to decrease the reaction rate.

The examination of both adaption rates reveals that only equation (3.29) fulfills the zero-sum condition of equation (3.27). For equation (3.30), the condition is not fulfilled and hence, the finite time convergence of $V_\lambda\,(\mathbf{x},\,\lambda)$ is not guaranteed. However, this is not a critical issue. Since the dynamics of the closed loop system is decreased in the given case, the adaption signal $x_{1,\,av}$ increases over the time, and after a period the adaption signal becomes larger than the threshold $\delta_x < x_{1,\,av}$. Thus, the second case becomes inactive, and the adaption rate of the first case is applied which is proven to be stable. As can be seen, independently of the active state the adaption process toggles between the two cases while case 1 maintains the stability of the overall adaption. By combining the adaption rates, the adaption law of the dominant eigenvalue λ can be noted as

$$\dot{\lambda} = -\left(\frac{\kappa}{2}\right)^{1/2} \text{sign}\,(x_{1,\,av} - \delta_x)\,. \tag{3.31}$$

Remark: The stability of the outlined Lyapunov-based adaption strategy only is given if the adaption rate κ is comparably small. The stability analysis rests upon the assumption that the Lyapunov function $V(\mathbf{x})$ is not biased by a variation of λ. However, e.g. considering a second order system with the linear adaptive sliding function $\sigma(\mathbf{x},\,\lambda) = -\lambda\, x_1 + x_2$ with time-depended design parameter λ. The stability of the adaption process rests upon the assumption of finite-time convergence of a first order SMC using $V(\mathbf{x})$ as shown in inequality (3.23). While adapting the sliding function, the Lapunov function (A.2) becomes:

$$V\,(\mathbf{x},\,\lambda) = \frac{1}{2}\,\sigma^2\,(\mathbf{x}) = \frac{1}{2}\,(-\lambda\, x_1 + x_2)^2 \tag{3.32}$$

$$\dot{V}\,(\mathbf{x},\,\lambda) = \left(-\lambda\,\dot{x}_1 - \dot{\lambda}\, x_1 + \dot{x}_2\right)\,(\lambda\, x_1 + x_2)\,. \tag{3.33}$$

Obviously, $\dot{V}(\mathbf{x}, \lambda)$ now comprises an additional dependency of $\dot{\lambda}$, which is not considered originally in the stability analysis of the set law. Nevertheless, the finite time convergence of $V(\mathbf{x}, \lambda)$ shall be maintained practically. A practical approach is to keep the amplitude of $\dot{\lambda}$ rather small such that its influence to $\dot{V}(\mathbf{x}, \lambda)$ becomes negligible in relation to the internal dynamics of the non-adaptive closed loop system respectively the momentum of the Lyapunov function. Within a small local time scale, the variation of λ is negligible. However, the macroscopic change during a long duration defines the closed loop behavior. This assumption also can be taken for higher order sliding modes as outlined in chapter 4. Considering, for instance, the super-twisting algorithm, a different Lyapunov function (D.1) is introduced causing finite time convergence. For this Lyapunov function, the outlined assumption is valid as well.

3.5. Discussion

This chapter investigates the properties of different variants of sliding functions. Initially, the general idea of a sliding function is introduced, and the linear time-invariant sliding functions are discussed. This class of sliding functions is the default and most known one in the literature. Their benefits are their simplicity in design and a good robustness of sliding motion in case of a proper design. However, the resulting linear closed loop dynamics are a limiting factor for practical applications. Due to this, different further variants are investigated.

In case of linear system dynamics, the linear sliding functions can be designed optimally resulting in time-variant linear sliding functions, but due to friction or other nonlinearities of the systems, this approach is not applicable to many devices. By using static nonlinear sliding functions, increased closed loop dynamics can be achieved. By using sliding surfaces comprising a constant jerk or acceleration, quasi time-optimal sliding motions can be obtained. However, these sliding surfaces are data-based and not given in an analytic discretion so that they rely on memory-consuming look-up tables. Additionally, these surfaces comprise a discontinuity at the origin that guarantees a loss of sliding motion.

The novel SPA surface combines the simplicity of linear sliding surfaces with the advantages of nonlinear ones. By continuously adjusting the roots of the sliding function in dependence on the system output or also the state x_1, the convergence rate of the state x_1 is increased for small values and reduced in case of larger deviations. This approach can realize improved closed loop dynamics without a significant increase in complexity. Thus, also non-experts are able to use this method to achieve the desired system behavior. However, the stability of the adaption process bases on an assumption that limits the convergence rate. A complete analytic stability analysis, however, is not easy to perform. The sliding function always depends on the system order and thus, the proof only is valid for a certain class of systems. Therefore, the assumption of a slow variation of the roots provides more flexibility of the design process without increasing the complexity of the stability analysis significantly.

Table 3.1.: Comparison of different sliding functions. The notion of the symbols are neutral ($\circ$), adequate ($+$), moderate ($++$), excellent ($+++$), yes ($\checkmark$) and no ($-$).

	linear	TOS	SPA	optimal
Performance	$\circ$	$++$	$+++$	$+++$
Robustness	$+++$	$\circ$	$++$	$+$
Ease of design	$+++$	$+$	$++$	$\circ$
Self-tuning	$\checkmark$	$-$	$\checkmark$	$-$

Table 3.1 summarizes the four discussed variants of sliding surfaces and scores their properties based on own experiences and prevalence opinions in literature. The comparison reveals the advantages of the default linear sliding function as well as the SPA surface. Both functions are used as the default ones in the latter experimental evaluation. However, the TOS surface also is tested as an additional reference.

4

Chattering Alleviation via Higher Order Sliding Modes

Sliding mode control as depicted in section 1.2 is a powerful tool to control systems under heavy uncertain conditions. In ideal cases, it achieves an accurate system behavior that is robust to any perturbations. However, the practical application of SMC suffers from chattering caused by a discontinuously switching derivative of the sliding function $\sigma(\mathbf{x})$ as well as a limited switching frequency or unconsidered mechanical hysteresis and imperfections of actuators and sensors.

Higher order sliding modes (HOSMs) have been introduced in general by Levantovskii (1985) to overcome the named restrictions. Originally, the theory of HOSM has been developed in Russia in the early 1980s. The first English translated publication for the particular case of second order sliding modes (SOSMs) was presented by Emel'yanov, Korovin, and Levantovsky (1986b). The concept of HOSM increases the degree of smoothness of the sliding variable $\sigma(\mathbf{x})$ by hiding the discontinuous switching in higher derivatives of the sliding function. Thus, the chattering effect can be attenuated efficiently or even canceled out entirely. In contrast to boundary layer solutions that also attenuate the chattering as shown in section 4.1, the HOSMs preserve the robustness properties and accuracy of sliding motion. By keeping the main advantages of the original sliding modes and removing the chattering effect in parallel, the HOSM provides an increased accuracy (Levant 1993).

The main difficulty of designing an r^{th} order sliding controller is the increased complexity because in general the sliding variable $\sigma(\mathbf{x})$ and its $r-1$ derivatives have to be known. There are only few exceptions like the *twisting* controller introduced by Emel'yanov, Korovin, and Levantovsky (1986b), the *super-twisting* controller by Levant (1993) and the *sub-optimal* algorithm introduced by Bartolini, Ferrara, and Usai (1997). All three approaches are in common that they provide second order sliding motion and rely only on the knowledge of $\sigma(\mathbf{x})$ but do not need any derivatives. Thus, they are the most spread algorithms for practical applications.

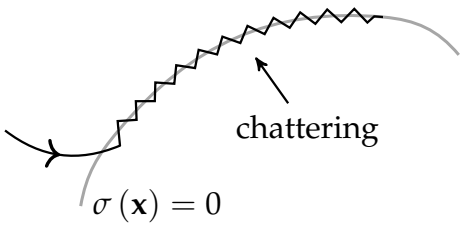

Figure 4.1.: Illustration of chattering.

4.1. Chattering alleviation via boundary layers

The control strategies presented in section 1.2 and in chapter A incorporate discontinuous switching actions and precise system models to establish the desired sliding mode. However, in practical applications, there are model inaccuracies and neglected dynamics that are excited by the high-frequency switching actions while not being taken into account by the plant model. The resulting behavior as illustrated in figure 4.1 is called *chattering*. The system does not follow the sliding function precisely, it rather oscillates around the switching manifold $\sigma(\mathbf{x}) = 0$, and oscillations superimpose the control signal. This is due to a violation of the sliding conditions of infinite switching frequency and the absence of relative degree mismatches. To overcome these harmful issues, practical modifications of the theoretical concepts are discussed in the following. Proceeding analyses of chattering can be found in the contributions of Levant (2010a) and Ventura and Fridman (2016).

In contrast to SMC in the ideal case, the boundary layer control as initially introduced by Slotine and Sastry (1983) and Slotine and Coetsee (1986) does not aim for a precise stabilization of the sliding function on the sliding manifold $\sigma(\mathbf{x}) = 0$ rather than for a stabilization only within a well-defined vicinity

$$\mathcal{S}_B = \left\{ \mathbf{x} \in \mathbb{R}^n \;\middle|\; |\sigma(\mathbf{x})| \leq \epsilon \right\}, \quad \epsilon > 0 \tag{4.1}$$

around the sliding manifold. The resulting behavior often is called *quasi* sliding mode control (qSMC). This approach is very efficient since it directly cancels out the main source of chattering: the discontinuous switching of the control input $u(\mathbf{x})$.

To alleviate the practically occurring chattering caused by high frequent switching actions, the boundary layer control replaces the discontinuous control law by a continuous approximation within a given boundary ϕ. Inside the boundary layer that is defined around the sliding manifold, the controller behaves as a continuous state feedback law. The continuous control input does not excite the neglected plant dynamics as strong as a discontinuous control law does. As a common practical example for a scalar control input, the discontinuous switching law

$$u(\mathbf{x}) = -K \operatorname{sign}(\sigma(\mathbf{x})) \tag{4.2}$$

with the control gain K can be approximated by different functions as shown in figure 4.2. As can be seen in the figure, one possibility of approximating the discontinuity $\operatorname{sign}(\cdot)$ is the use of a piecewise continuous saturation function $\operatorname{sat}(\cdot)$. Within

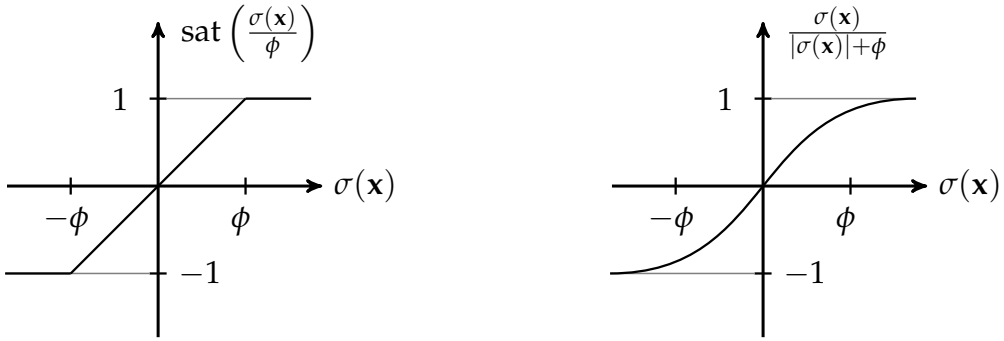

Figure 4.2.: Piecewise linear and continuous nonlinear approximations of a scalar discontinuous signum function.

the boundary with the given width ϕ, the saturation function

$$\text{sat}\left(\frac{\sigma(\mathbf{x})}{\phi}\right) = \begin{cases} \text{sign}\left(\sigma(\mathbf{x})\right) & \text{for } |\sigma(\mathbf{x})| \geq \phi \\ \frac{\sigma(\mathbf{x})}{\phi} & \text{for } |\sigma(\mathbf{x})| < \phi \end{cases} \tag{4.3}$$

behaves as a linear state feedback controller and stabilizes the system within a vicinity $0 < \epsilon \leq \phi$ around the sliding manifold $\mathcal{S}$. A further opportunity of implementing a boundary layer controller is shown in the right part of figure 4.2 using a continuously differentiable approximation

$$u = -K \frac{\sigma(\mathbf{x})}{|\sigma(\mathbf{x})| + \phi} \tag{4.4}$$

of the sign$(\cdot)$ function. Here, a continuous function is utilized to avoid undesired effects caused by an abrupt change between a continuous and a discontinuous control action as given by the sat$(\cdot)$ function. As an alternative, the hyperbolic tangent may also be used as a boundary control function:

$$u(\mathbf{x}) = -K \tanh\left(\frac{\sigma(\mathbf{x})}{\phi}\right). \tag{4.5}$$

Outside of the boundary ϕ, the boundary layer control strategies show a comparable behavior as the discrete switching law (4.2). All controllers can reach the sliding manifold in finite time. However, due to the continuous state feedback, the robustness of a discontinuous switching controller is not preserved. This loss of robustness introduces a design process with two contrary objectives. On the one hand, the controller is supposed to transfer the system into sliding mode as accurate as possible, but this causes chattering in practical applications that deteriorates the control quality. As a second design objective, the chattering is to be attenuated. The attenuation is done by adjusting the width ϕ of the boundary layer. By increasing the width of the boundary layer, the amount of discrete switching of the control input is reduced, and hence, the high-frequent excitation of the real system is reduced which leads to an attenuated chattering.

However, by widening the boundary layer $\mathcal{S}_B$ the robustness and accuracy of the system are decreased (cf. Bessa 2009). The intrinsic robustness against perturbation and

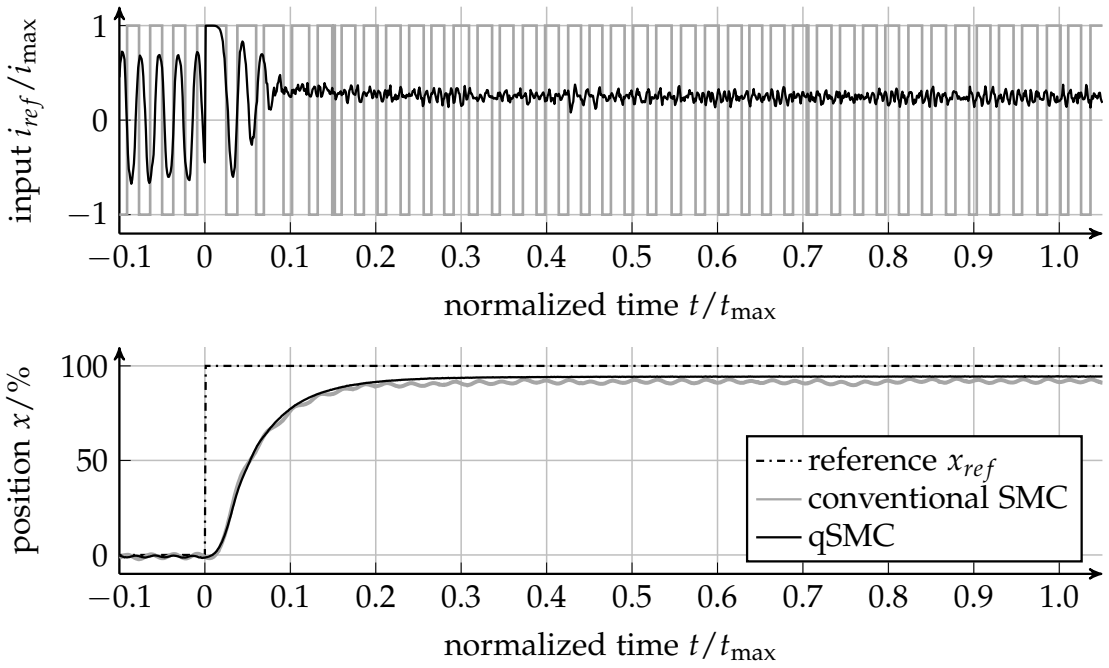

Figure 4.3.: Comparison of conventional SMC and qSMC for a step response of a direct operated directional control valve.

model inaccuracies of a sliding mode controller only is given, if the system is kept in sliding motion respectively if it is stabilized on the sliding manifold $\mathcal{S}$. By introducing the boundary layer, the system is only locked into the vicinity of the manifold $\mathcal{S}$ that does not provide a comparable robustness. This is due to the reduced control input for small deviations of the system from the sliding manifold. While the discontinuous switching law reacts with a constant strong reaction regardless of the magnitude of the deviation, the boundary layer controllers only enforce a small control input that does not offer a comparable strong correction of the system motion. However, these reduced control actions do not cause oscillations in the sense of chattering.

The design of a boundary layer controller can be separated into three steps:

- Selection of a sliding function $\sigma(\mathbf{x})$ that defines the desired closed loop dynamics.
- Adjustment of the control gain K so that the sliding manifold $\mathcal{S}$ is reached in finite time from any point of the state space, even for very large control errors.
- Select a proper value for the boundary width ϕ to attenuate the chattering until a sufficient reduction is achieved without decreasing the tracking performance too much.

A more detailed discussion of the tuning procedure of boundary layer controllers in the context of hydraulic systems is given by Komsta et al. (2010). In figure 4.3, the experimental comparison of conventional SMC and qSMC is shown for the control of a step response of the directional control valve. As can be seen, the qSMC cancels out the oscillations of the position x by providing a continuous input u. However, both approaches do not achieve the desired steady state accuracy in x. As a remark, it has to

be known that the boundary layer control only guarantees motion into the boundary layer, motion within the layer itself is not predefined. Bartolini, Ferrara, and Usani (1998) outlined that the sliding function σ starts to oscillate with unpredictable frequency but finite amplitude. This oscillation can be found in the control input u such that the entire system is superimposed by unknown oscillations. To circumvent the issues caused by unpredictable oscillations and undefined motion within the boundary layer, the HOSMC is a reliable method to obtain continuous control inputs with superior closed loop robustness.

4.2. Sliding order, sliding sets and a general solution

HOSM controllers are characterized by their sliding order. The sliding order r denotes the number of continuous derivatives of the sliding function $\sigma(\mathbf{x})$ including the zero-derivative $\sigma^{(0)}(\mathbf{x})$. The sliding order characterizes the smoothness of the system behavior and is connected to the smoothness degree of the closed loop system. In the following, all system descriptions are considered to be given in CCF as shown in equation (3.2).

The HOSM sliding motion is distinguished by the fact that the $r-1$ derivatives as well as the sliding variable converge to zero in finite time. This property can be formulated by introducing a new type of manifold called sliding set L_r on which a HOSM occurs by definition. The r^{th} order sliding set is defined as follows:

$$\mathcal{L}_r = \left\{ \mathbf{x} \in \mathbb{R}^n \;\middle|\; \sigma(\mathbf{x}) = \dot{\sigma}(\mathbf{x}) = \cdots = \sigma^{(r-1)}(\mathbf{x}) = 0 \right\}. \tag{4.6}$$

The r^{th} order sliding set $\mathcal{L}_r$ evidently is given, if $\sigma(\mathbf{x})$ is a differentiable function of $\mathbf{x}$ and the condition

$$\operatorname{rank}\left\{ \nabla\sigma(\mathbf{x}),\, \nabla\dot{\sigma}(\mathbf{x}), \ldots,\, \nabla\sigma^{(r-1)}(\mathbf{x}) \right\} = r \tag{4.7}$$

is fulfilled (Fridman and Levant 1996). The given condition is called *weak regulatory condition*.

The solution for an r^{th} order sliding mode control problem in general can be obtained e.g. as discussed by Sira-Ramírez (1992, 1993). For this, the r^{th} order dynamic system in control canonical form

$$\begin{aligned} \dot{\varsigma}_i &= \varsigma_{i+1}, \quad i \in \{1, 2, \ldots, r-1\} \\ \dot{\varsigma}_r &= p\left(\mathbf{x}, u, \dot{u}, \ldots, u^{(r-1)}\right) \\ \sigma &= \varsigma_1 \end{aligned} \tag{4.8}$$

is considered, where the generalized state vector $\boldsymbol{\varsigma}$ contains the sliding function $\sigma(\mathbf{x})$ with relative degree of $k = 1$ and its $r-1$ derivatives. To obtain a stable system behavior, a suitable sliding surface as an algebraic function of $\boldsymbol{\varsigma}$ is selected:

$$\Sigma = R_1\varsigma_1 + R_2\varsigma_2 + \cdots + R_{r-1}\varsigma_{r-1} + \varsigma_r, \quad R_i > 0. \tag{4.9}$$

Then, a first order sliding motion is imposed on the linear surface $\Sigma = 0$ by mean of

$$\dot{\Sigma} = -L \ \text{sign}\left(\Sigma\right), \quad L > 0. \tag{4.10}$$

As shown in section A.1, the relay control law causes a finite-time convergence of Σ. By obtaining first order sliding motion of Σ, it is obvious that implicitly an r^{th} order sliding motion is established for $\sigma\left(\mathbf{x}\right) = \varsigma_1\left(\mathbf{x}\right)$ since its $r-1$ derivatives are also stabilized. As a further fact, the discontinuous switching of the control law does not more affect the first derivative $\dot{\sigma}\left(\mathbf{x}\right)$ of the sliding function since now it is hidden in the r^{th} derivative $\sigma^{(r)} = -L\,\text{sign}\left(\Sigma\right)$ of the original sliding function. Thus, the chattering (cf. section 4.1) is eliminated and ideal tracking is established.

4.3. Second order sliding modes

The practical application of SMC suffers from chattering as discussed in section 4.1. Further, many mechatronic systems contain a mechanical hysteresis or backlash caused by gearboxes that do not tolerate an abrupt commutation of the exiting forces. Commuting forces would cause an extensive wear out or immediate destruction of such components. Not considered sensor- and actuator dynamics introduce further undesired system motions if excited by high frequent discontinuous switch inputs. Thus, for practical applications a continuous control input is indispensable.

By using HOSM, the discontinuous switching is hidden in higher derivatives of the sliding function and a continuous control signal is obtained that does not cause an excessive wear out or destruction. However, one practical issue of HOSM is the necessity of knowing the higher derivatives of $\sigma\left(\mathbf{x}\right)$ which in general only is feasible if simulative studies are considered, and process noise or model inaccuracies are not incorporated. However, as e.g. discussed by Bartolini, Ferrara, and Usani (1998), Bartolini et al. (2003), and Levant (2007) the use of SOSMs ($r = 2$) is sufficient to alleviate the chattering phenomenon occurring in mechatronic systems by using a continuous control function which stabilizes $\sigma\left(\mathbf{x}\right)$ as well as $\dot{\sigma}\left(\mathbf{x}\right)$.

One of the first SOSM algorithms published by Emel'yanov, Korovin, and Levantovsky (1986a) is the latterly called terminal SMC (tSMC):

$$\dot{u} = \begin{cases} -u & \text{for } |u| > u_{\max} \\ -\alpha \ \text{sign}\left(\dot{\sigma} - g\left(\sigma\right)\right), \quad \alpha > 0 & \text{for } |u| \leq u_{\max}. \end{cases} \tag{4.11}$$

The parameter $\alpha > 0$ is the control gain and the strictly negatively monotonic function $g\left(\sigma\right)$ is an algebraic expression of the sliding variable. The algorithm establishes a first order sliding motion on the manifold $\Sigma = \dot{\sigma} - g\left(\sigma\right) = 0$. By selecting $g\left(\sigma\right) = -k\,\lfloor\sigma\rceil^{\rho}$ with $k > 0$ and $\rho \in [0.5 \quad 1)$, the sliding function $\sigma\left(\mathbf{x}\right)$ drops to zero on a cubic parabola. The control law (4.11) provides a first order sliding motion on $\Sigma\left(\sigma, \dot{\sigma}\right)$ and thus, a second order sliding motion on $\sigma\left(\mathbf{x}\right)$ as shown in figure 4.4a. Comparing this algorithm to the HOSM approach of Sira-Ramírez (1992, 1993) shown section 4.2 it is obvious that both approaches rest upon the same concept but only the shape of the sliding surface Σ is altered. Hence, the control law (4.11) can be understood as an early special case of a latter published generalized tSMC concept.

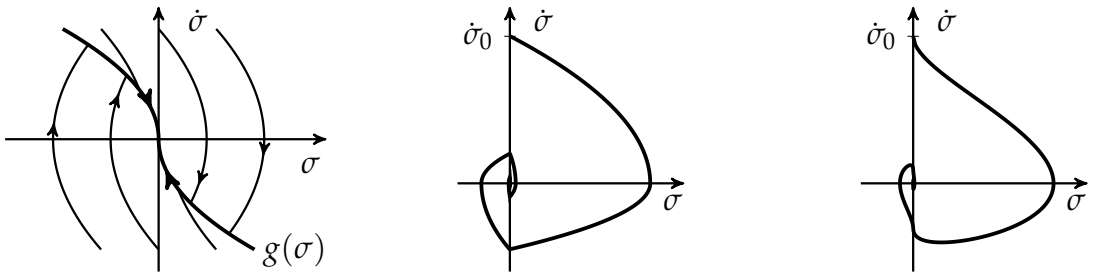

(a) tSMC with $k = 1$ and $\rho = 2/3$.

(b) Twisting algorithm

(c) Super-Twisting algorithm

Figure 4.4.: Generalized state space trajectories of different second order sliding mode controllers for an idealized dynamic system of $\dot{\sigma} = u$.

Since the above-described algorithm requires exact knowledge of $\dot{\sigma}(\mathbf{x})$ and an additional sliding function design of Σ, a different control law called *twisting algorithm* (TA) is wide spread in control applications. The algorithm presented by Emel'yanov, Korovin, and Levantovsky (1986a), Emel'yanov, Korovin, and Levantovsky (1986b), and Levant (1993) only depends on the sign of the derivative of the sliding function $\dot{\sigma}(\mathbf{x})$ and does not prescribe a desired higher order sliding dynamics as shown in figure 4.4b. The twisting algorithm

$$\dot{u} = \begin{cases} -u & \text{for } |u| > u_{\max} \\ -\alpha_0 \operatorname{sign}(\sigma) - \alpha_1 \operatorname{sign}(\dot{\sigma}), \quad \alpha_0, \alpha_1 > 0 & \text{for } |u| \leq u_{\max} \end{cases} \tag{4.12}$$

with the two control gains α_0 and α_1 provides finite time convergence into second order sliding motion of $\sigma(\mathbf{x})$ only if $\alpha_0 > \alpha_1$. It is sufficient to know the sign of $\dot{\sigma}(\mathbf{x})$. Thus, for implementing the TA on discrete time sampling systems at which the value of $\sigma(\mathbf{x})$ is measured at discrete times $t_0, t_1, t_2, \ldots$ where $t_{i+1} - t_i = \Delta t$, $\Delta t = \text{const}$, the TA can be formulated as

$$\begin{aligned} \Delta u_i &= \begin{cases} -u_{i-1} & \text{for } |u_{i-1}| > u_{\max} \\ -\alpha_0 \operatorname{sign}(\sigma_i) - \alpha_1 \operatorname{sign}(\Delta\sigma_i), \quad 0 < \alpha_1 < \alpha_0 & \text{for } |u_{i-1}| \leq u_{\max} \end{cases} \\ u_i &= u_{i-1} + \Delta u_i \, \Delta t. \end{aligned} \tag{4.13}$$

The operator Δ is the finite difference of the given quantity and the subscript $i \in \mathbb{N}_0$ indicates the i^{th} time instance of the signal. According to equation (4.13), the TA can be formulated without the necessity of knowing the explicit derivative of the sliding function $\dot{\sigma}(\mathbf{x})$. However, the resulting discrete-time control law still is sensitive to process noise that is amplified by the finite difference $\Delta\sigma_i$ and corrupts the estimate of $\dot{\sigma}(\mathbf{x})$.

The *super-twisting algorithm* (STA) by Levant (1993) follows a different approach as the algorithms stated above since it provides a formulation that does not rely on any derivatives of the sliding function $\sigma(\mathbf{x})$:

$$\begin{aligned} u &= -\alpha_1 \lfloor \sigma \rceil^{1/2} + u_I, \quad \alpha_0, \alpha_1 > 0 \\ \dot{u}_I &= \begin{cases} -u & \text{for } |u| > u_{\max} \\ -\alpha_0 \lfloor \sigma \rceil^0 & \text{for } |u| \leq u_{\max}. \end{cases} \end{aligned} \tag{4.14}$$

If considering the differential equation

$$\begin{aligned}\dot{\sigma} &= \frac{\partial \sigma}{\partial t} + \frac{\partial \sigma}{\partial \mathbf{x}}\mathbf{f}(t,\, \mathbf{x}) + \frac{\partial \sigma}{\partial \mathbf{x}}\mathbf{g}(t,\, \mathbf{x})\, u \\ &= a\,(t,\, \mathbf{x}) + b\,(\mathbf{x})\;\, u\end{aligned} \tag{4.15}$$

with the bounded perturbation function $a\,(t,\, \mathbf{x})$, the control gains α_1 of the proportional part and α_0 of the integral control u_I are given as

$$\begin{aligned}\alpha_0 &= 1.1\, L \\ \alpha_1 &= 1.5\, \sqrt{L} \\ L &= \frac{A}{K_m}, \quad |\dot{a}\,(t,\, \mathbf{x})| < A, \quad 0 < K_m \leq b\,(\mathbf{x})\,,\end{aligned} \tag{4.16}$$

where A is the Lipschitz bound of $a\,(t,\, \mathbf{x})$ and K_m is the lower bound of the input function $g\,(\mathbf{x})$ and L the fraction of A and K_m.

The STA exhibits a trajectory with a continuous $\dot{\sigma}$ in the $[\sigma,\, \dot{\sigma}]$ state space, as shown in figure 4.4c. In contrast to the STA, cause the other two algorithms abrupt direction changes with discontinuous $\dot{\sigma}$, which can be discovered in the state trajectories of σ. Due to its excellent chattering reduction and the derivative-free formulation, the STA became the standard solution for mechatronic control applications if SOSM with a relative degree of $k = 1$ is considered.

Initially, the stability of the presented SOSM algorithms are proven by using a geometrical discussion of the $[\sigma,\, \dot{\sigma}]$ state-space trajectories (cf. Levant 1993). Nonetheless, Moreno and Osorio (2008, 2012) presented a Lyapunov-based approach of proving a certain class of SOSM algorithms including the STA by introducing a new candidate Lyapunov function

$$V(\mathbf{z}) = 2\,\alpha_0\,|z_1| + \frac{1}{2}\,z_2^2 + \frac{1}{2}\left(\alpha_1\,\lfloor z_1 \rceil^{1/2} - z_2\right)^2, \quad z_1 = \sigma, \quad z_2 = u_I.$$

The detailed proof of the STA is shown in appendix D.1. The application of the Lyapunov's direct method gives additional impetus to develop self-tuning functionality for the STA by further evaluations of adequate candidate functions (see Shtessel, Taleb, and Plestan 2012; Shtessel et al. 2010; Utkin, Poznyak, and Ordaz 2011). A commonly used adaption law for the control gains of the STA is given as follows (Shtessel, Taleb, and Plestan 2012):

$$\begin{aligned}\dot{\alpha}_1 &= \begin{cases}\omega_1 \sqrt{\frac{\gamma_1}{2}}\,\mathrm{sign}\,(|\sigma| - \delta_\sigma) & \text{for } \alpha_1 > \alpha_{1,\,\min} \\ \eta & \text{for } \alpha_1 \leq \alpha_{1,\,\min}\end{cases} \\ \alpha_0 &= 2\,\beta\,\alpha_1.\end{aligned} \tag{4.17}$$

By properly selecting suitable values for the adaption gains $\omega_1 > 0$ and $\gamma_1 > 0$ as well as the proportionality factor $\beta > 0$, the adaption rate of α_1 and thus, the convergence of $\sigma \to 0$ is adjusted. As recapitulated in section 3.4 and by Krimpmann et al. (2016a), the adaption of the average value of $\sigma\,(\mathbf{x})$ is more reasonable for the practical application than using non-smooth reference signals.

Comparably to the parameter adaption process of the STA, parameter estimation techniques have been introduced for the TA (Taleb, Levant, and Plestan 2013) that have been deduced experimentally or also based on a Lyapunov-design for the conventional SMC (Plestan et al. 2013; Polyakov and Poznyak 2009).

As a remark, the tSMC algorithm (4.11) and the TA (4.12) are equipped with an additional integrator for the control input u since the algorithms provide a definition of $\dot{u}$ in case of a relative degree of $k = 1$. If considering the direct output feedback control of a second order system ($n = 2$), the tSMC and the TA can directly be applied to control the system output x_1 without a particular design of a sliding function $\sigma(\mathbf{x})$. In this case, the sliding function is given as $\sigma(\mathbf{x}) = x_1$. Thus, the tSMC and the TA can be applied directly to a system with a relative degree of $k = 2$ by omitting the additional integrator of the control input u. However, in this case, the control input becomes discontinuous, but the system output $y = x_1$ is finite-time convergent. Summing up, the tSMC and TA can be used to control either systems of relative degree $k = 2$ or to alleviate the chattering for $k = 1$-systems by providing a continuous non-smooth control input u. In contrast to this, the STA only is applicable for systems with a relative degree of $k = 1$ offering a continuous and smooth control input u.

4.4. Arbitrary order sliding modes

While the SOSM control was introduced to alleviate the chattering caused by first order sliding motions via hiding the switching in the second derivative of $\sigma(\mathbf{x})$, the general concept of HOSM offers a further control design opportunity. As initially discussed, the approach by Sira-Ramírez (1992, 1993) provides r^{th} order sliding motion for the system output y but it still is not finite-time convergent. Among others (see e.g. Harmouche, Laghrouche, and Chitour 2012; Yiguang Hong, Jiankui Wang, and Zairong Xi 2005), Levant (2001, 2003, 2005a,b) provided finite-time convergence of the system output y by building an arbitrary order sliding controller. For this, the sliding function design is neglected and a direct output feedback takes place ($\sigma(\mathbf{x}) = x_1 = y$).

For a first order system, the sliding motion is obtained by using a relay control $u = -\alpha \operatorname{sign}(\sigma(y))$ and for a second order system by using the tSMC with $u = -\alpha \operatorname{sign}\left(\dot{\sigma}(y) + \lfloor \sigma(y) \rceil^{1/2}\right)$ (cf. equation (4.11)). In general, finite time convergence of the system's output y is achieved by following arbitrary order sliding mode (AOSM) recursive controller:

$$u = -\alpha \, \Psi_{r-1,r} \left(\sigma(y), \dot{\sigma}(y), \ldots, \sigma^{(r-1)}(y) \right) \tag{4.18}$$

with

$$\begin{aligned}
&\Psi_{i,r} = \frac{\varphi_{i,r}}{N_{i,r}}, \quad \varphi_{0,r} = \sigma(y), \quad N_{0,r} = |\sigma(y)|, \quad i \in \{0, 1, 2, \ldots, r-1\} \\
&\varphi_{i,r} = \sigma^{(i)}(y) + \beta_i \, N_{i-1,r}^{(r-i)/(r-i+1)} \, \Psi_{i-1,r}, \quad \beta_i > 0 \\
&N_{i,r} = |\sigma^{(i)}(y)| + \beta_i \, N_{i-1,r}^{(r-i)/(r-i+1)}
\end{aligned}$$

if the control gains $\alpha > 0$ and $\beta_i > 0$ are selected properly. The AOSM controller can be interpreted as a controller that recursively stacks a variant of the tSMC algorithm with a sliding order of $r_{\text{tSMC}} = 2$ and the conventional SMC ($r_{\text{SMC}} = 1$) until the desired order r is achieved.

However, the main drawbacks that prevent the algorithm (4.18) from being widespread in practical applications is the necessity of knowing all $r - 1$ derivatives of $\sigma(y)$ and its recursive structure. The algorithm is not rather intuitive for parameterization compared to the STA that, e.g., can be interpreted as a nonlinear PI controller. Thus, the aforementioned neglected sliding function design is dearly bought by a controller that is difficult to interpret and to design. Since in general the derivatives of the output are unknown, they have to be estimated using adequate filtering and estimation techniques as shown in chapter 5.

4.5. Quasi higher order sliding modes

Higher order sliding mode strategies alleviate the chattering caused by model imperfections and discontinuous switching by hiding the switching action in higher derivatives of σ. Even though, the switching action still is present. One approach to achieve a further alleviation is the use of disturbance observers (cf. Levant 1998; Utkin, Guldner, and Shi 2009) but for the application of those, assumptions for certain model structures have to be taken.

Shtessel, Shkolnikov, and Brown (2003), however, follow a different approach. By using the nonlinear PI controller

$$\begin{aligned} u &= -\alpha_1 \lfloor \sigma \rceil^{1/2} + u_I, \quad \alpha_0,\, \alpha_1 > 0 \\ \dot{u}_I &= \begin{cases} -u & \text{for } |u| > u_{\max} \\ -\alpha_0 \lfloor \sigma \rceil^{1/3} & \text{for } |u| \leq u_{\max} \end{cases} \end{aligned} \tag{4.19}$$

with the control gains α_0 and α_1, an asymptotic second order sliding motion is established in case of the absence of disturbances. The Lyapunov-based stability proof is outlined in section D.2. Compared to the conventional STA, this controller does not contain a discontinuity within the integral part since the formerly binary integrand is scaled with $\sqrt[3]{|\sigma|}$. However, due to the structural similarity, in the following this controller is called *quasi* STA or briefly qSTA. In contrast to the default definition of a higher order sliding mode, this controller rests upon a weakened one. Shtessel, Shkolnikov, and Brown (2003) declare a second order sliding mode to be only given in case of $\{\sigma(\mathbf{x}),\, \dot{\sigma}(\mathbf{x})\} \to \mathbf{0}$. A discontinuity of $\ddot{\sigma}$ is omitted and thus, the finite time convergence is lost.

The qSTA offers high potential for the practical applications to systems with relative degree mismatches, e.g., caused by neglected higher dynamics. Due to the smoothness of the control signal, these dynamics are less excited such that less chattering is caused. Nevertheless, the qSTA only should be applied if the conventional STA does not achieve the desired attenuation since the qSTA alters the robustness properties.

Levant (2005a) introduces a so called homogeneity approach for the design of HOSM control design. The homogeneity approach describes a modification of the AOSM controller shown in equation (4.18) that replaces the sign functions by sat functions for all derivatives of σ. Thus, the amount of discontinuous switching of the control input u is reduced to a minimum and increased smoothness of σ as well as its derivatives is obtained while the convergence properties remain nearly unattached.

Quasi SM controllers are valuable tools for the practical control of real world systems. However, their use shall be well reasoned since these controllers rest upon a changed conception of sliding modes as highlighted for the qSTA. Additionally, the robustness properties of the system within the sliding mode are different from conventional sliding modes. Thus, if using qHOSM control the comparison with HOSMC shall be taken.

4.6. Comparison of sliding mode algorithms

In many practical applications of SMC, chattering due to unmodeled dynamics and limited switching frequencies may pose a critical issue. While the equivalent control u_{eq} (cf. section A.2) directly cancels out the chattering caused by limited switching frequencies, it is not able to cope with neglected dynamics since it follows a model-based control design. Boundary layer solutions as shown in section 4.1 may deal with both reasons for chattering but once the system is locked into the boundary layer $\mathcal{B}$ around the sliding manifold $\mathcal{S}$, the system behavior becomes unpredictable with oscillations of unknown frequencies.

Effective chattering alleviation is provided using HOSM techniques as shown before. By hiding the switching action of the control input in the second derivative of $\sigma(\mathbf{x})$, the SOSM provides a good trade-off between complexity and control quality, e.g. for the control of mechatronic systems. All presented algorithms are in common to have a continuous input function u with a smoothness degree of at least one. While the tSMC rests upon the principle of stacked sliding modes, the TA and the STA are variants of nonlinear PD- and PI-controllers that are comparable easy to parameterize. The AOSM generalizes the SMC concept by recursively stacking sliding modes until the desired order is met. Thus, the sliding surface design is no longer necessary. However, the resulting controller is not as intuitive to parameterize as the other ones, and the system output dynamics is no longer predefined. Nevertheless, the AOSM provides superior robustness properties compared to SOSM or conventional SMC since it is invariant against relative degree mismatches meaning not considered dynamics (see Levant 2005a,b, 2010b). For detailed discussions and comparison of chattering effects and its alleviations, the reader is pleased to refer to Brandtstädter (2009), Levant (2010a), Utkin (2016), and Ventura and Fridman (2016).

Table 4.1 summarizes the relevant properties of the SMC algorithms and gives a ranking on their quality based on own experiences and prevalence opinions in literature. The comparison reveals that ultimate robustness against chattering cannot be obtained by a controller that is as easy to design as a conventional SMC algorithm. The process expert has to determine the sensitivity of the system against discontinuous

Table 4.1.: Comparison of different sliding mode control algorithms. The notion of the symbols are neutral ($\circ$), adequate ($+$), moderate ($++$) and excellent ($+++$).

	SMC	u_{eq}	qSMC	tSMC	TA	STA	AOSM
Chattering Reduction	$\circ$	$+++$	$++$	$++$	$++$	$+++$	$+++$
Robustness	$+++$	$\circ$	$+$	$+++$	$++$	$++$	$++$
Ease of Design	$+++$	$+$	$++$	$+$	$++$	$++$	$\circ$

switching inputs and to estimate the degree of uncertainty of the model assumptions. Based on these evaluations, the STA reveals as the most suitable controller for the electro-hydraulic systems that are introduced in sections 2.2, B.2 and B.1 due to its good trade-off between chattering alleviation and robustness.

5

Model-free State Estimation for Electro-Hydraulic Systems

In order to design high-performance state feedback controllers e.g. basing on SM concepts, precise knowledge about the systems states is mandatory. In practical applications like the control of electro-hydraulic systems as shown in sections 2.2, B.1 and B.2, oftentimes only the output information are known. For example, for the directional control valve, only the piston position measurement x is known while the remaining states v and a are unknown since they are not measurable. To apply state feedback concepts, the states v and a have to be estimated by using a feasible method fulfilling high demands as reliability or noise amplification for the estimates $\hat{v}$ and $\hat{a}$.

Principally, state estimation techniques can be separated into two major classes, the *model-based* observers and *model-less* methods meaning numerical output differentiation[1]. In practice, the difficulty of applying model-based observers is the determination of an accurate plant model (refer to section 2.2). While simple linear observers likely fail in the presence of model inaccuracies, observers using a nonlinear system description suffer from their complexity. As shown in section B.1, the description of the solenoid force F_{sol} rests upon experimentally determined lookup tables. To apply model-based nonlinear observers e.g. as introduced by Luenberger (1966) or summarized by Adamy (2014), these lookup tables need to be differentiated as investigated by Abel (June 2016). For this, the measurements have to be approximated by differentiable functions leading to increased complexity. Additionally, at each time instance, the partial derivatives of the system state equation are determined such that a pole placement for the observer feedback can be performed. This real time observer parameterization is computationally intensive and thus, difficult to implement, and its application is restricted to slowly sampling systems. In contrast to this, SMC approaches are supposed to be sampled as fast as possible, and the computational effort is small.

As a solution to the issues arising from the application of model-based observers, the model-free state estimation is a valuable method to determine unknown state information if the system is given in CCF. Under ideal conditions and in the absence of measurement noise, the unknown derivatives of the i^{th} state are obtained by applying

[1]The term *model* refers to a dynamic plant model.

the finite differences

$$\hat{x}_{i,j} = \frac{x_{i,j} - x_{i,j-1}}{\Delta t}, \quad i \in \{0, 1, \ldots, n\} \tag{5.1}$$

$$\hat{\hat{x}}_{i,j} = \frac{\hat{x}_{i,j} - \hat{x}_{i,j-1}}{\Delta t} \tag{5.2}$$

where $j \in \mathbb{N}_0$ is the index of the current sample of the signal x with the sampling interval of Δt. There are two drawbacks for the practical application of finite differences. Equation (5.1) causes a time shift of $0.5\,\Delta t$ and the second derivative (5.2) causes a delay of Δt. However, the major drawback is the noise amplification without bandwidth-limitations that deteriorates the estimation quality. To circumvent the spurious noise gain, two different approaches are discussed.

5.1. Polynomial filters

To cope with the differentiation of noise-affected signals, an ordinary approach is to perform a moving average filtering before applying the finite differences. However, a moving average filter causes a time delay depending on the filter length and the weighting coefficients. A more sophisticated smoothing filter is achieved by a local polynomial least-squares approximation (see e.g. Heiss 1989; Schafer 2011; Zehetner, Reger, and Horn 2007a,b). The resulting intermediate analytic function can be evaluated at any point of the filtering interval.

To obtain an analytic description for an interval of $2\,M + 1$ samples with a temporal resolution of Δt centered around the m^{th} sample, one has to obtain the coefficients a_k of the N^{th} order polynomial

$$p(m) = \sum_{k=0}^{N} a_k\, m^k \tag{5.3}$$

that minimizes the least-squares approximation

$$\epsilon_N = \sum_{m=-M}^{M} \left(p\,(m) - x\,(m)\right)^2 = \sum_{m=-M}^{M} \left(\sum_{k=0}^{N} a_k\, m^k - x\,(m) \right)^2 . \tag{5.4}$$

For the sake of simplicity, the center sample of $m \in \{\mathbb{Z} \mid -M \leq m \leq M\}$ is chosen to be zero ($m = 0$) such that the point $m = 0$ is the ordinate-intercept of the symmetrically windowed polynomial. Thus, the filter output of the center sample is

$$\hat{x}(m = 0) = p(m = 0) = a_0 \tag{5.5}$$

that is identical to the 0^{th} coefficient of the polynomial $p(m)$. To determine the next output value, the filtering interval is shifted right for one sample and the polynomial fitting is repeated. Hence, the coefficients a_k are updated so that a new output value is generated.

Savitzky and Golay (1964) show that the signal smoothing based on polynomial fitting can be implemented as a finite input response (FIR) filter with fixed weighting

coefficients. Due to this, the computational effort for the polynomial smoothing is significantly reduced because the least-squares problem does not need to be solved repeatedly and online. To show that there is a unique solution for a FIR filter, first the least-squares problem (5.4) is to be solved to determine a_k:

$$\frac{\partial \epsilon_N}{\partial a_i} = \sum_{m=-M}^{M} 2\, m^i \left(\sum_{k=0}^{N} a_k\, m^k - x(m) \right) = 0, \quad i \in \{0,\, 1, \ldots,\, N\}\,. \tag{5.6}$$

By interchanging the order of the summations, one obtains a set of $N+1$ equations with $N+1$ unknown parameters a_k:

$$\sum_{k=0}^{N} \left(\sum_{m=-M}^{M} m^{i+k} \right) a_k = \sum_{m=-M}^{M} m^i\, x(m), \quad i \in \{0,\, 1, \ldots,\, N\}\,. \tag{5.7}$$

The equations above are known as the normal equations of a least-squares problem. To obtain a unique solution for equations (5.7), the number of data points needs to be larger or equal than the number of parameters ($N \leq 2\,M$). For more convenience, equation (5.7) can be written in matrix notation. For this, the $(2\,M+1) \times (N+1)$-dimensional matrix $\mathbf{A} = \{a_{m,\,i}\}$ is defined with

$$a_{m,\,i} = m^i, \quad -M \leq m \leq M, \quad i \in \{0,\, 1, \ldots,\, N\}\,. \tag{5.8}$$

Let the $(N+1) \times (N+1)$-dimensional matrix $\mathbf{B} = \mathbf{A}^{\mathrm{T}}\mathbf{A}$ with the elements

$$b_{i,\,k} = \sum_{m=-M}^{M} a_{m,\,i}\, a_{m,\,k} = \sum_{m=-M}^{M} m^{i+k} \tag{5.9}$$

be symmetrical for $i \in \{0,\, 1, \ldots,\, N\}$ and $k \in \{0,\, 1, \ldots,\, N\}$. As can be figured out by comparing the matrix elements $a_{m,\,i}$ and $b_{i,\,k}$ with the equation (5.7), the equation can be expressed as

$$\mathbf{B}\,\mathbf{a} = \mathbf{A}^{\mathrm{T}}\mathbf{A}\,\mathbf{a} = \mathbf{A}^{\mathrm{T}}\,\mathbf{x}. \tag{5.10}$$

The vector $\mathbf{x} = [x(-M),\, x(-M+1), \ldots,\, x(0),\, x(1), \ldots,\, x(M-1),\, x(M)]^{\mathrm{T}}$ collects the symmetrically windowed values of the signal to be smoothed. By solving equation (5.10) for $\mathbf{a}$, one obtains

$$\mathbf{a} = \left(\mathbf{A}^{\mathrm{T}}\mathbf{A}\right)^{-1} \mathbf{A}^{\mathrm{T}}\,\mathbf{x} = \mathbf{M}\,\mathbf{x}. \tag{5.11}$$

As shown, the matrix $\mathbf{M}$ only depends on the half-sided window length M and the polynomial order N but the matrix is not state-dependent. Now recall that the output of the smoothed signal $\hat{x}$ is identical to a_0 meaning the first element of $\mathbf{a}$. Thus, for application purpose it is sufficient to implement the scalar product $a_0 = \mathbf{m}_1\,\mathbf{x}$, where $\mathbf{m}_1$ is the first row vector of $\mathbf{M}$ and therefore the weighting coefficients of the resulting smoothing FIR filter.

By taking the assumption that the current sample is taken for $m = 0$, the estimates of the first and second derivatives of $x(m)$ are given as follows:

$$\frac{\mathrm{d}\,x(t)}{\mathrm{d}\,t} \approx \frac{\mathrm{d}\,\hat{x}(m)}{\mathrm{d}\,m} = \left.\frac{\mathrm{d}\,p(m)}{\mathrm{d}\,m}\right|_{m=0} = a_1 \tag{5.12}$$

$$\frac{\mathrm{d}^2\,\hat{x}(m)}{\mathrm{d}\,m^2} = \left.\frac{\mathrm{d}^2\,p(m)}{\mathrm{d}\,m^2}\right|_{m=0} = 2\,a_2. \tag{5.13}$$

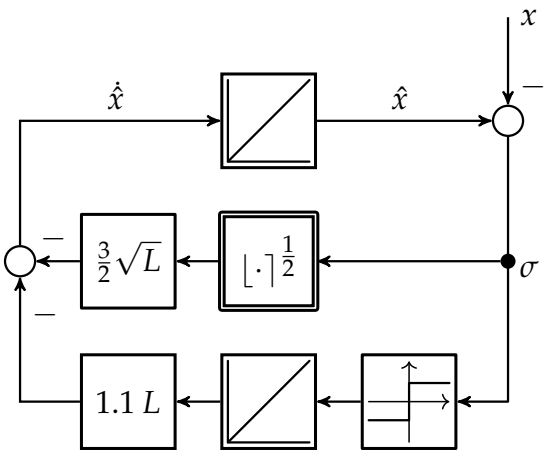

Figure 5.1.: Robust first order differentiator based on the STA.

It is obvious that the calculation of the i^{th} derivative $\hat{x}^{(i)}$ again can be implemented as the scaled scalar product of the $(i+1)^{\text{th}}$ row of $\mathbf{M}$ and $\mathbf{x}$.

At this point, the polynomial filters are acausal systems because the vector $\mathbf{x}$ contains future values for $m > 0$, $x(m = 0)$ is considered to be the current sample. By shifting the smoothing window back so that $x(m = 0)$ is delayed for M values, the FIR filter comprises a delay of M values since still the polynomial is evaluated at its center position. To compensate for the delay, the polynomial is to be evaluated at the right edge of the smoothing window.

5.2. Sliding mode differentiation techniques

The estimation of derivatives also can be understood as an artificial tracking control problem at which a generic first order integrator is controlled such that its output value $\hat{x}$ is identical to the value x that is supposed to be differentiated. In case of a sufficiently fast controller providing a continuous input function u, the derivative $\dot{\hat{x}} = u$ is a valid approximation of the derivative of x. For this control task, the STA as introduced in section 4.3 can be used as shown by Levant (1998). The resulting so-called *robust exact differentiator* (RED) is depicted in figure 5.1. The only requirement for its application is that the true derivative $\dot{x}$ is Lipschitz-bounded by a constant L meaning $|\ddot{x}| \leq L$.

By recursively applying the first order differentiator, an arbitrary order differentiator (AO-RED) is defined as shown by Levant (2003, 2005a). This differentiator can be used to estimate not only one but also all states of a system in CCF. Again, it is required that the highest derivative of the output signal $y^{(n-1)} = x_n$ is Lipschitz-bounded by L.

By applying the algorithm

$$\begin{aligned}
\dot{z}_0 &= -\lambda_r\, L^{1/r}\, |z_0 - y|^{(r-1)/r}\, \operatorname{sign}(z_0 - y) + \hat{z}_1 \\
\dot{z}_k &= -\lambda_{r-k}\, L^{1/(r-k)}\, |z_k - z_{k-1}|^{(r-k-1)/(r-k)}\, \operatorname{sign}(z_k - z_{k-1}) + z_{k+1} \\
\dot{z}_{r-1} &= -\lambda_1\, L\, \operatorname{sign}(z_{r-1} - z_{r-2}), \quad k \in \{1, 2, \ldots, r-2\}
\end{aligned} \tag{5.14}$$

$(r-1)$ derivatives of the output signal y are precisely approximated in finite time

where $z_i = \hat{y}^{(i)} = \hat{x}_{i+1}$ with $i \in \{0, 1, \ldots, r-1\}$. In case of $r = n - 1$ all unknown states are estimated. As Levant (2003) showed, the differentiator gains λ_i can be predefined for $r \leq 5$. Thus, the values are givens as $\boldsymbol{\lambda} = [1.1, 1.5, 2, 3, 5, 8]^{\mathrm{T}}$.

Especially in the context of hydraulic systems, the output feedback differentiation is frequently applied as discussed by Koch and Reichhartinger (2016), Komsta, Adamy, and Antoszkiewicz (2010), Komsta (2013), Komsta, van Oijen, and Antoszkiewicz (2013), Krimpmann et al. (2016a), Reichhartinger and Horn (2009), and Yan, Primot, and Plestan (2016). However, as outlined by Chalanga et al. (2016) its application in conjunction with SOSM controllers comprises a significant issue as outlined in the following example.

Consider the sliding function

$$\sigma = r_1\, x + \dot{x} \tag{5.15}$$

with the factor $r_1 > 0$ and the state x as well as its derivative $\dot{x}$. Now, consider that the derivative is estimated on-line by using a RED based on the STA as illustrated in figure 5.1 with

$$\begin{aligned} \dot{\hat{x}} &= \omega - \frac{3}{2}\, L^{1/2} \lfloor \hat{x} - x \rceil^{\frac{1}{2}} \\ \dot{\omega} &= -1.1\, L \operatorname{sign}(\hat{x} - x)\,. \end{aligned} \tag{5.16}$$

For SOSM control, the general behavior is given by the sliding set $\mathcal{L}_2$. As a consequence, the second derivative of σ is the first discontinuous one. To investigate whether SOSM is given in case of the application of the RED, the derivatives of σ are considered:

$$\sigma = r_1\, x + \dot{\hat{x}} \tag{5.17}$$

$$\Leftrightarrow \sigma = r_1\, x + \omega - \frac{3}{2}\, L^{\frac{1}{2}} \lfloor \hat{x} - x \rceil^{\frac{1}{2}} \tag{5.18}$$

$$\dot{\sigma} = r_1\, \dot{x} - 1.1\, L \operatorname{sign}(\hat{x} - x) - \frac{3}{2}\, L^{\frac{1}{2}}\, \frac{\mathrm{d}\, \lfloor \hat{x} - x \rceil^{\frac{1}{2}}}{\mathrm{d}\, t} + u. \tag{5.19}$$

In case of using the STA (cf. equation (4.14)), it is obvious that the control law is not able to compensate the discrete switching component $-1.1\, L \operatorname{sign}(\hat{x} - x)$ out of $\dot{\sigma}$. Thus, the sliding set $\mathcal{L}_2$ is empty since already the first derivative of the sliding function σ is discontinuous. For the practical application, however, the sliding order reduction can be omitted because the discontinuity's contribution is small compared to the other influence factors of $\dot{\sigma}$. Further, the main source of chattering still is the discontinuous control input u caused by a relay set law while the STA provides a continuous low-frequent signal.

5.3. Experimental validations of differentiation techniques

For the practical application of various differentiation techniques, a sophisticated parameter selection is mandatory. In case of a less accurate parameterization, the calculated estimates $\hat{\mathbf{x}}$ are of poor quality and do not reflect the actual system states. Thus, the controller utilizing the estimated system states is not able to perform at its desired

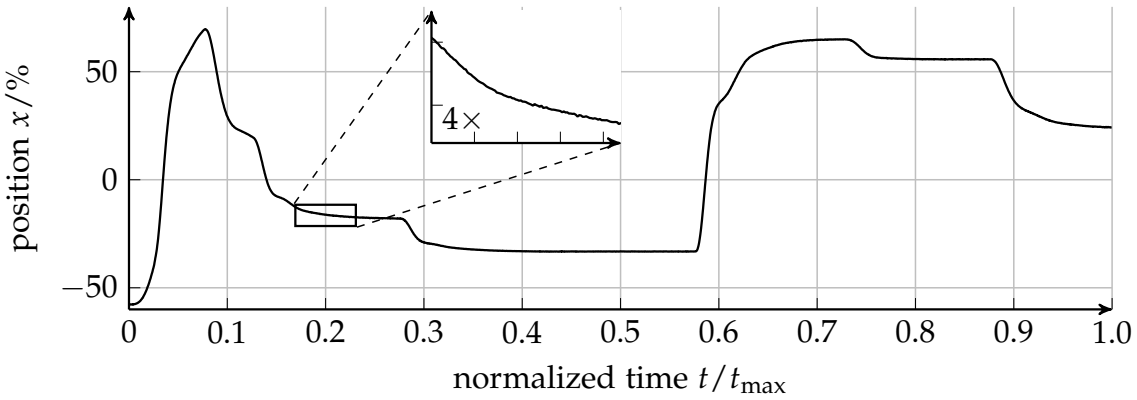

Figure 5.2.: Measured position response of a directional control valve.

quality. Furthermore, the differentiators comprise own dynamics. In case of maladjustments, these dynamics do not correspond correctly to provide the sufficient values of $\hat{\mathbf{x}}$. Too fast dynamics may cause a significant noise amplification due to insufficient attenuation, and rather slow dynamics virtually decrease the overall plant behavior. In the worst case, this leads to severe damage to the system since the controller is not able to compensate harmful movements because it does not get sufficient information about the plant's movement at the right time.

To circumvent the named issues, the separation principle of independent dynamics of observers and closed loop systems needs to be fulfilled. For the case of conventional model based observers, this is, e.g., achieved by correctly placing the eigenvalues of the observer thus providing a faster convergence of the estimation error than of the closed loop system. The procedure for output differentiators, however, is more application-driven and will be depicted in the following. In the first case, the velocity $\hat{v}$ and acceleration $\hat{a}$ estimation for the directional control valve as introduced in section 2.2 is considered. The induction-based position sensor of a directional control valve typically is of high accuracy and does not cause significant measurement noise so that a special noise-treatment is not necessary. A captured open-loop response of the valve is depicted in figure 5.2. Even though inspecting a four-time magnification of the signal, no significant noise is visible.

The direct application of the finite differences (5.1) and (5.2) to the position signal is depicted in figure 5.3. Despite the good signal quality of the measured position, the velocity estimate $\hat{v}_{FD}$ indicates a high noise level. Compared to the expected signal shape, the qualitative progress of $\hat{v}_{FD}$ does not give accurate information of the true piston velocity v. Furthermore, the estimate $\hat{a}_{FD}$ is noise corrupted so that no valid estimation is provided. Using finite differences estimations for a state feedback controller causes even for rather low noise-affected output signals tremendous control actions due to the noise amplification. In case of conventional SM controllers, the localization of the system in the state space becomes infeasible, and thus, the evaluation on which side of the surface the system is located is not possible. For higher order SMC the overall stability may be kept however the control quality will be decreased significantly.

The parameterization of the polynomial filters can be understood as an iterative

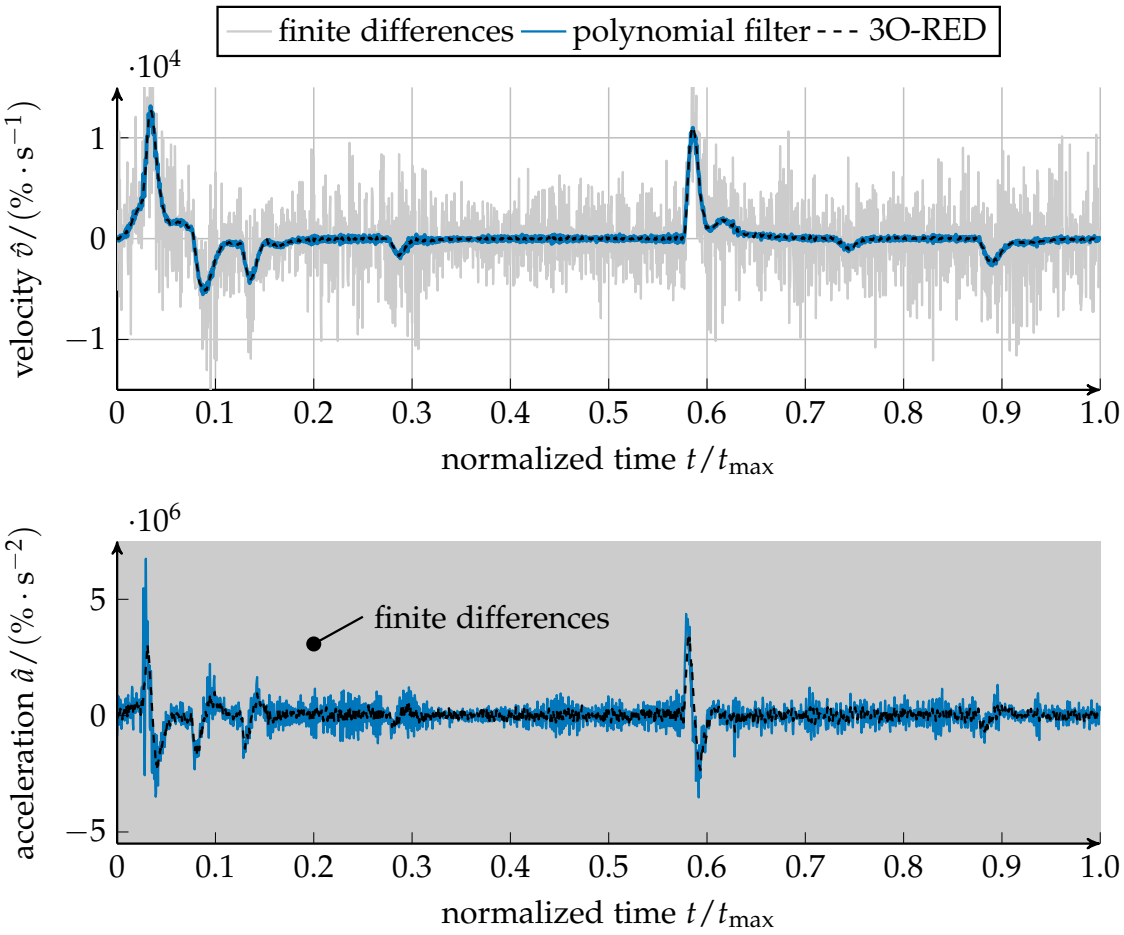

Figure 5.3.: Estimated velocity and acceleration signals using different differentiation methods for the position sequence shown in figure 5.2. The estimated acceleration $\hat{a}$ provided by finite differences is cropped to that the other signals are sufficiently depicted.

discrete optimization process as shown in the following. The evaluation of the estimation quality of the velocity $\hat{v}$ and the acceleration $\hat{a}$ is not as straight forward because the actual signals v and a are not known. Because of this, the direct analysis of the estimation errors $e_v = v - \hat{v}$ and $e_a = a - \hat{a}$ are not feasible. As an alternative measure, the deviation between the true position x and the integral of the velocity estimate $\hat{v}$ is considered for minimization:

$$J_v = \int \left(x - \int \hat{v}_{PF} \, \mathrm{d}\, t \right)^2 \mathrm{d}\, t. \tag{5.20}$$

Obviously, the objective function J_v is zero if the estimate $\hat{v}$ is identical to the true velocity v. Due to the smoothing properties of the polynomial filters, this is not given. However, the optimal velocity estimate of the polynomial filter $\hat{v}^*_{PF}$ is obtained by solving the discrete problem

$$[M_v^*, \, N_v^*] = \arg\min J_v. \tag{5.21}$$

For this, suitable intervals of polynomial orders N and half-sided window lengths M are defined and for every tuple, the value of J_v is determined. Thus, the solution

space is discrete and limited, resulting in a finite number of parameter combinations. By selecting the tuple with the smallest deviation, the optimal parameterization for a polynomial filter calculating the first derivative of the position is obtained. The polynomial order is kept low ($N \leq 5$) to prevent local overfitting and to provide sufficient smoothing properties. The window length is limited to $M \leq 20$. The resulting velocity estimate $\hat{v}_{PF}$ shown in figure 5.3 is obtained for an order of $N = 2$ and a window of $M = 16$.

Now in awareness of $\hat{v}^*_{PF}$ the same parameterization procedure is carried out for the acceleration estimate. For this, the objective function

$$J_a = \int \left(\hat{v}^*_{PF} - \int \hat{a}_{PF} \, \mathrm{d}\, t \right)^2 \mathrm{d}\, t \tag{5.22}$$

is utilized. Here, the deviation from the optimized velocity estimate $\hat{v}^*_{PF}$ for the integral of the acceleration $\hat{a}_{PF}$ is judged. By performing the illustrated discrete optimization one obtains values of $N = 3$ and $M = 43$ for the position signal as depicted. This bootstrapping process can be understood as the solution for the chicken-or-the-egg dilemma regarding the availability of proper reference signals. However, it is obvious that by repeatedly applying the design process, an error propagation takes place and the quality of higher order derivatives is reduced.

The parameterization of a RED though is not comparable to the one of the polynomial filters since it cannot be carried out as a bootstrapping process. The RED computes all derivatives of the signal x at once in dependence on a given Lipschitz-constant L. A stacked first order RED (1O-RED) may be feasible by applying the same procedure as before. However, this is not the original intention of REDs. An expedient process to design a third order RED (3O-RED) to estimate the first and second derivative in common is illustrated in the following. For this, please refer to figure 5.4. This figure illustrates the estimated velocities and accelerations of a 3O-RED for the given position trajectory in dependence on two different Lipschitz-constants. The estimated position signal $z_0 \approx x$ is not able to follow the measured position response and causes strong overshoots. This behavior is reflected in the velocity estimate $z_1 = \hat{v}$. The estimated signal again oscillates and is of slow dynamics. Now, by inspecting the acceleration signal obtained by a small Lipschitz-bound L, it is evident that the Lipschitz-bound is chosen too small as indicated by a triangular-shaped acceleration signal z_2. As denoted in equation (5.14), the derivative of z_2 consists of only two possible states. Thus, in case of small Lipschitz-constants, the adjustment of the state is too slow. By increasing L, an adequate estimation of $z_2 = \hat{a}$ is achieved as shown in figure 5.3. The resulting estimate is comparable to the one obtained by a polynomial filter. However, the noise attenuation is slightly improved using the 3O-RED. A further increase of the Lipschitz-constant again deteriorates the signal quality as seen in figure 5.4. The signals obtained by a high value of L are affected by noise. The quality of the acceleration signal is entirely decreased. Compared to a small value of L the amplitude is ten times higher, and no qualitative shape is identifiable. The velocity signal, however, is of better quality. Nevertheless, the velocity estimate $\hat{v}$ contains a significant amount of noise, but the signal is comparable to the ones obtained by properly adjusted differentiators as shown in figure 5.3. As expected, the high-L-RED

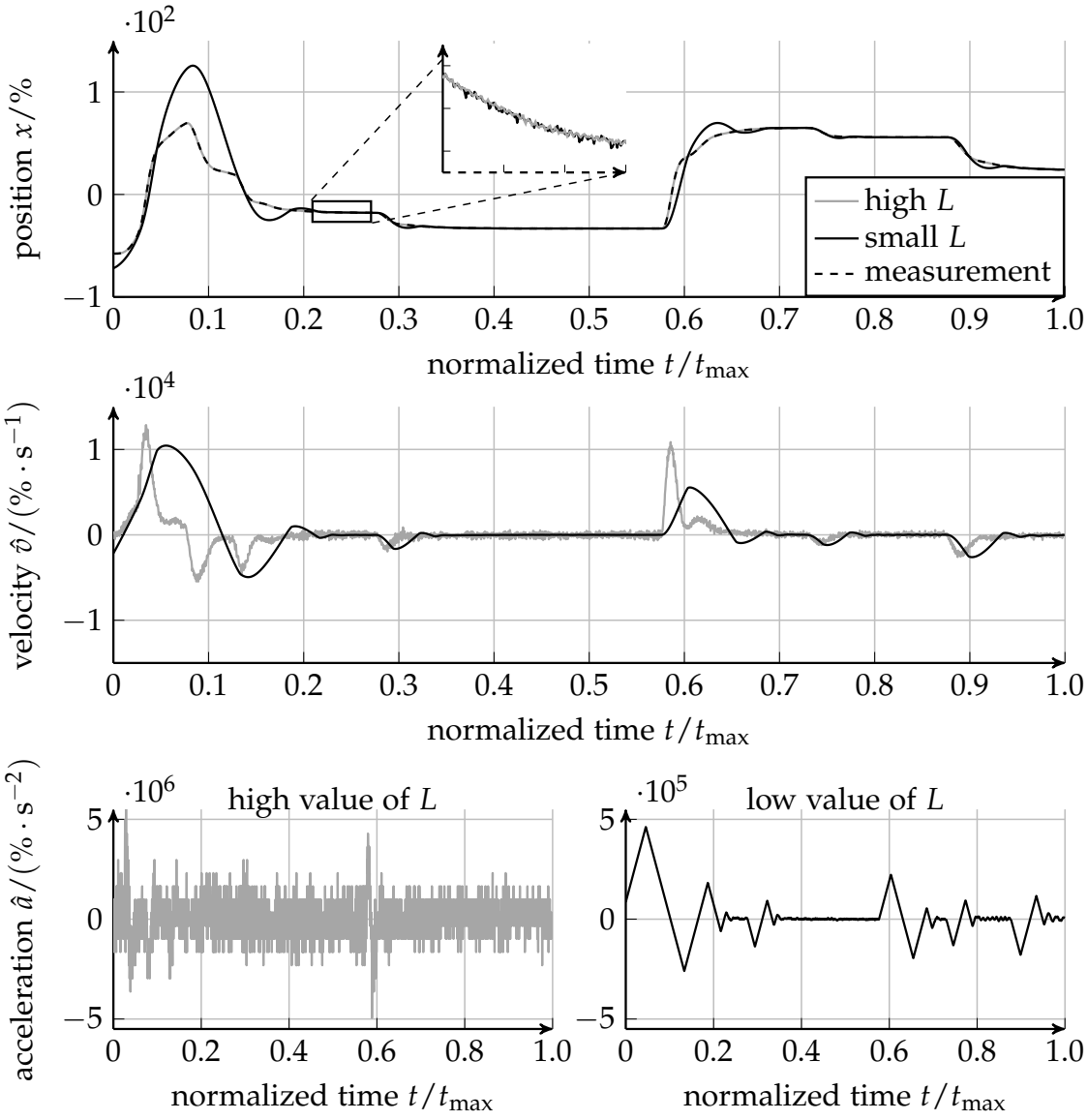

Figure 5.4.: Comparison of the influence of different Lipschitz constants for a 3O-RED.

reconstructs the position signal x without any deviation. As a general approach, the Lipschitz-constant is to be selected small initially. By continuous increasing L and inspection of the highest derivative, the adequate value of L is obtained at the point, at which the state z_{r-1} is not triangular-shaped, and the noise suppression is high. As shown in figure 5.3, both differentiation approaches, the polynomial filters and the RED, compute comparable estimations of the system's velocity $\hat{v}$ and the acceleration $\hat{a}$. To evaluate the correctness of the estimated signals, they are integrated again. The integration of the velocity signals $\hat{v}_{PF}$ and $\hat{v}_{RED}$ are depicted in figure 5.5. As can be seen, the integrated polynomial filter signal $\int \hat{v}_{PF}\,\mathrm{d}\,t$ is identical to the measured position signal x. The RED signal $\int \hat{v}_{RED}\,\mathrm{d}\,t$ comprises a slight positive drift. From approximately $t = 0.15\,t_{\max}$, the signal starts to drift away from the measurement. The drift is caused by small estimation errors that are integrated over time. In contrast to the polynomial filter, that does not incorporate integrating elements; the RED is a

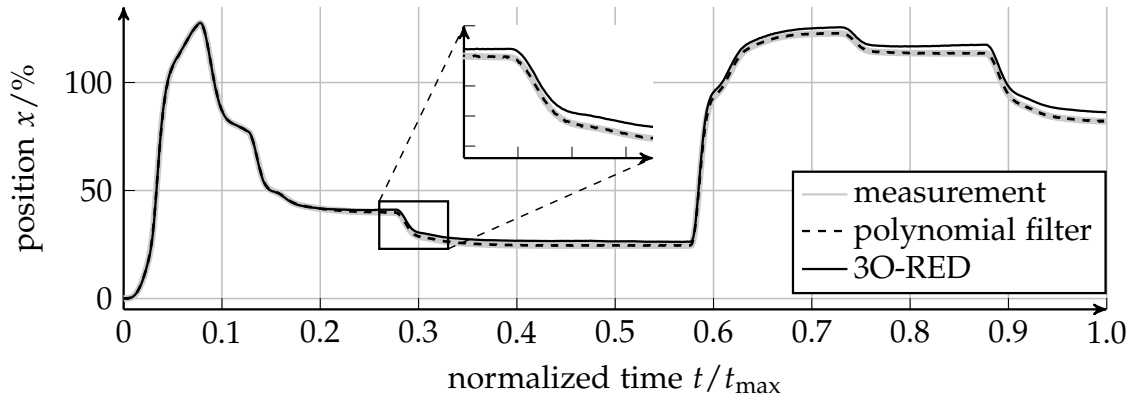

Figure 5.5.: Integration of estimated velocity signals $\hat{v}$ obtained by different differentiation methods. For evaluation purpose, the measured position signal x is offset-adjusted to start initially at $x(t = 0) = 0$.

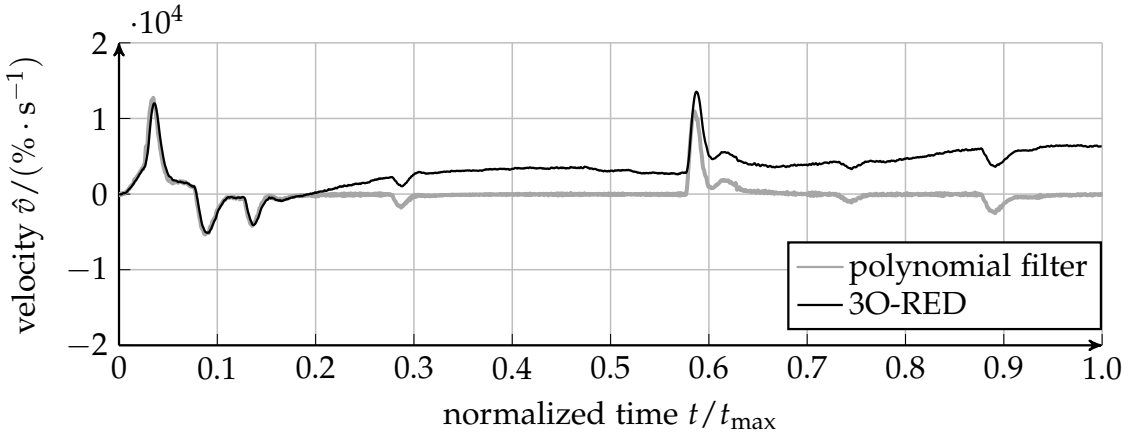

Figure 5.6.: Integration of estimated acceleration signals $\hat{a}_{PF}$ and $\hat{a}_{RED}$ obtained by different differentiation methods.

nonlinear dynamic system with integrating properties. This especially is observed in figure 5.6 depicting the integrated acceleration signals. Again, the signal $\hat{a}_{PF}$ is not bias-affected while the RED signal $\int \hat{a}_{RED}\,\mathrm{d}\,t$ comprises a strong drift. The drift indicates a locally incorrect estimation of the signal. Thus, the signal quality of the polynomial filter is understood to be better in contrast to a RED. Despite the unbiased estimation, polynomial filters are not preferred in general. The subsequent filter arrays of such filters are memory consuming and computational intensive compared to the RED. For industrial control units, the amount of memory and the power the processing units are severely limited either due to the availability of special microchips that are allowed to be used for industrial applications or the general aim to decrease the overall costs of the control units. Thus, the offset affected estimations provided by a RED may be favorable if low-cost control units are supposed to be used.

6

Robust Controller Parameterization using Evolutionary Optimization

The computer-aided optimization and in particular the evolutionary algorithms (EA) are valuable tools in engineering tasks to solve complex design problems. They are inspired by the concept of evolution or rather rest upon the strategy "*the survival of the fittest*" as formulated by Darwin (1859). These methods, however, do not constitute a replacement of the work of an engineer but offer him a well-equipped toolbox to solve commonly occurring engineering problems. As a consequence, the role of the executing engineer changes from a practical work in which the design parameter of a system, e.g., are obtained in manually executed experiments based on a trial and error process towards an architectural and conceptual work. Based on the experience and knowledge, the engineer is responsible for determining critical design parameters and those of negligible influence. To achieve an optimal or rather optimized system behavior, the engineer also needs to formulate precise mathematical objective functions of the subjective, often weakly defined, design requirements. Thus, the work of the engineer likely is successful if he has in-depth knowledge of the subordinate process and the working principles.

Over the last decades, various numbers of different computer-aided optimization techniques emerged. For the application to technical systems, the evolutionary optimization as a member of heuristic methods became renown due to its sampling based derivative-free algorithms. In contrast to Gauss-Newton methods, evolutionary optimization does not rely on Jacobian matrices and, thus, the system does not need to be differentiable or given in an analytic form. Additionally, the evolutionary optimization can optimize not only scalar valued objective functions but also multi-objective vectorized optimization problems consisting of several conflicting design aspects. A general introduction into evolutionary optimization e.g. is given by Kruse et al. (2015) and further fundamentals of multi-objective optimization is provided by Deb (2001). In the following, the focus is set on derandomized evolutionary strategies as one of the major optimization techniques used in industrial applications.

6.1. Derandomized evolution strategies

Due to its ability to solve arbitrary scalar objective functions, the covariance matrix adaption evolutionary strategy (CMA-ES) as initially introduced by Hansen and Ostermeier (1996) emerged as the state of the art heuristic optimizer. In the following, this section introduces the $(1+\lambda)$-CMA-ES and its derivate, the active-CMA-ES developed by Jastrebski et al. (2006).

All strategies are in common that they utilize a comparable representation $\mathbf{a}$ consisting at least of the five-tuple $\mathbf{a} = [\boldsymbol{\theta}, \mathbf{C}, s, \mathbf{p}_c, \overline{p}_{succ}]$ where $\boldsymbol{\theta} \subset \Omega \in \mathbb{R}^n$ is the candidate solution for the n-dimensional objective function $J : \mathbb{R}^n \mapsto \mathbb{R}$. The matrix $\mathbf{C} \in \mathbb{R}^{n \times n}$ is the covariance of the candidate solution and $s \in \mathbb{R}$ the step size respectively the mutation strength, $\mathbf{p}_c \in \mathbb{R}^n$ the evolution path and $\overline{p}_{succ} \in \mathbb{R}^n$ the average success rate of a mutation. Further, $\lambda_{succ} = \left\{ i = 1, 2, \ldots, \lambda \middle| J(\boldsymbol{\theta}_i) \leq J\left(\boldsymbol{\theta}_{parent}\right) \right\}$ is the number of successful offspring solutions obtained by mutating the parental solution $\boldsymbol{\theta}_{parent}$. The covariance matrix $\mathbf{C}$ can be decomposed into the matrix $\mathbf{B} \in \mathbb{R}^{n \times n}$ containing the normalized eigenvectors and the diagonal matrix $\mathbf{D} \in \mathbb{R}^{n \times n}$ being a diagonal matrix of the square roots of the eigenvalues. Thus, it is $\mathbf{C} = \mathbf{B}\,\mathbf{D}\,(\mathbf{B}\,\mathbf{D})^{\mathrm{T}}$. The variable $\mathbf{z} \sim \mathcal{N}(\mathbf{0}, \mathbf{I})$ denotes a mutation vector drawn from a normal distribution $\mathcal{N}$ with the mean $\mathbf{0} \in \mathbb{R}^n$ and the covariance $\mathbf{I} \in \mathbb{R}^{n \times n}$. The CMA-ES algorithms adapt the outlined parameters in every iteration. Please refer to Krimpmann et al. (2013a,b) for a detailed evaluation of the presented algorithms.

The $(1+\lambda)$-CMA-ES

Igel, Hansen, and Roth (2007) present a basic algorithm to realize a derandomized evolution strategy that constitutes the basis for several variants of the CMA-ES. Each iteration g of the algorithm consists of four operations as outlined in the following:

1. Initially, the best individual of the prior generation is selected as the current parental solution $\mathbf{a}_i^{g+1}$. For this solution, the eigendecomoposition of $\mathbf{C}$ is calculated and mutation vectors $\mathbf{z}_i$ with $i \in \{1, 2, \ldots, \lambda\}$ are generated. By performing random mutations of the parent as outlined in equation (6.1), the offspring solutions are obtained.

$$\begin{aligned} \mathbf{a}_i^{g+1} &\leftarrow \mathbf{a}_{parent}^{g} \\ \boldsymbol{\theta}_i^{g+1} &= \boldsymbol{\theta}_{parent}^{g} + s^2 \mathbf{B}\,\mathbf{D}\,\mathbf{z}_i \end{aligned} \tag{6.1}$$

2. The fitness values $f(\boldsymbol{\theta}_i)$ are determined and the average success rate according to the improvements accomplished by individuals are updated.

$$\overline{p}_{succ} \leftarrow (1 - c_p)\overline{p}_{succ} + c_p \frac{\lambda_{succ}}{\lambda} \tag{6.2}$$

where $c_p = \frac{p_{succ}^{target} \lambda}{2 + p_{succ}^{target} \lambda}$.

3. The step size is updated according to

$$s \leftarrow s \exp\left(\frac{1}{d}\frac{\overline{p}_{succ} - p_{succ}^{target}}{1 - p_{succ}^{target}}\right) \tag{6.3}$$

with $d = 1 + \frac{n}{2\lambda}$ and $p_{succ}^{target} = \frac{1}{5+\sqrt{\lambda}/2}$.

4. The evolution path $\mathbf{p}_c$ and the covariance matrix $\mathbf{C}$ are updated with respect to the average success rate $\overline{p}_{succ}$. In case of $\overline{p}_{succ} < p_{thresh}$ the update is given by:

$$\mathbf{p}_c \leftarrow (1 - c_c)\,\mathbf{p}_c + \sqrt{c_c\,(2 - c_c)}\boldsymbol{\theta}_{step}, \tag{6.4}$$

$$\mathbf{C} \leftarrow (1 - c_{cov})\,\mathbf{C} + c_{cov}\mathbf{p}_c\mathbf{p}_c^{\mathrm{T}} \tag{6.5}$$

with

$$\boldsymbol{\theta}_{step} = \frac{\boldsymbol{\theta}_{parent}^{g+1} - \boldsymbol{\theta}_{parent}^{g}}{s_{parent}^{g}}.$$

If the average success rate is larger than the threshold ($\overline{p}_{succ} \geq p_{thresh}$), the modified update is applied:

$$\mathbf{p}_c \leftarrow (1 - c_c)\,\mathbf{p}_c, \tag{6.6}$$

$$\mathbf{C} \leftarrow (1 - c_{cov})\,\mathbf{C} + c_{cov}\left(\mathbf{p}_c\mathbf{p}_c^{\mathrm{T}} + c_c\,(2 - c_c)\,\mathbf{C}\right) \tag{6.7}$$

with $c_c = 2/(n+2)$, $c_{cov} = 2/\left(n^2 + 6\right)$ and $p_{thresh} = 0.44$.

By repeating the four steps consecutively, a scalar objective function is optimized heuristically for arbitrary initial populations.

active-CMA-ES

Since the first appearance of the CMA-ES in 1996 until now, several variations of the original algorithm have been developed. A comparative overview of some variants and benchmark results are given by Bäck, Foussette, and Krause (2012). The outlined results indicate a superior optimization performance on most benchmark problems for the active-CMA-ES by Jastrebski et al. (2006). The principal advantage of this algorithm is that it not only relies on successful mutation for the covariance update. It also incorporates explicitly the information obtained by unsuccessful mutations to decrease the variance in directions of inferior mutations. This behavior causes a faster adaption to the given optimization problem, and thus, the process is accelerated.

The solution update consists of seven steps:

1. The normalized eigenvectors $\mathbf{B}$ and the diagonal matrix $\mathbf{D}$ are computed.

2. A number of λ offspring individuals are determined.

$$\boldsymbol{\theta}_i = \boldsymbol{\theta}_{parent} + s\,\mathbf{B}\,\mathbf{D}\,\mathbf{z}_i \tag{6.8}$$

3. The objective function values $f(\boldsymbol{\theta}_i)$ are evaluated and the population is sorted in ascending order so that $k \in \{1, 2, \ldots, \lambda\}$ refers to the k^{th} best individual. Then, the average mutation vector

$$\mathbf{z}^{avg} = \frac{1}{\mu} \sum_{k=1}^{\mu} \mathbf{z}_k \tag{6.9}$$

of the μ best individuals is determined.

4. The parents solution vector $\boldsymbol{\theta}_{parent}$ is updated as following:

$$\boldsymbol{\theta}_{parent} \leftarrow \boldsymbol{\theta}_{parent} + s\, \mathbf{B}\, \mathbf{D}\, \mathbf{z}^{avg}. \tag{6.10}$$

5. In contrast to the $(1+\lambda)$-CMA-ES the active-CMA-ES uses two evolution paths $\mathbf{p}_c$ and $\mathbf{p}_s$.

$$\mathbf{p}_c \leftarrow (1 - c_c)\, \mathbf{p}_c + \sqrt{\mu c_c\, (2 - c_c)}\, \mathbf{B}\mathbf{D}\mathbf{z}^{avg}, \tag{6.11}$$

$$\mathbf{p}_s \leftarrow (1 - c_s)\, \mathbf{p}_\sigma + \sqrt{\mu c_s\, (2 - c_s)}\, \mathbf{B}\mathbf{z}^{avg}, \tag{6.12}$$

where $c_c = c_s = 4/\,(n + 4)$.

6. The covariance matrix update uses not only the successful mutations but also the mutations that are inferior to its parent. This strategy accelerates the convergence compared to an update that only comprises successful mutations:

$$\mathbf{C} \leftarrow (1 - c_{cov})\, \mathbf{C} + c_{cov} \mathbf{p}_c \mathbf{p}_c^{\mathrm{T}} + \beta \mathbf{Z} \tag{6.13}$$

with $c_{cov} = 2/\left(n + \sqrt{2}\right)^2$,

$$\beta = \frac{4\mu - 2}{(n + 12)^2 + 4\mu} \quad \text{and}$$

$$\mathbf{Z} = \mathbf{B}\mathbf{D} \left(\frac{1}{\mu} \sum_{k=1}^{\mu} \mathbf{z}_k \mathbf{z}_k^{\mathrm{T}} - \frac{1}{\mu} \sum_{k=\lambda-\mu+1}^{\lambda} \mathbf{z}_k \mathbf{z}_k^{\mathrm{T}} \right) (\mathbf{B}\, \mathbf{D})^{\mathrm{T}}.$$

7. The step size is updated according to

$$s \leftarrow s \exp\left(\frac{\|\mathbf{p}_s\|_2 - \mathcal{X}_n}{d_s\, \mathcal{X}_n} \right), \tag{6.14}$$

where $\mathcal{X}_n \approx E\left(\|\mathcal{N}(\mathbf{0}, \mathbf{I})\|_2\right)$ (cf. Kern et al. 2004) and $d = 1 + c_s^{-1}$.

The outlined optimization strategies are well studied and frequently used for solving scalar optimization problems. However, it is also feasible to extend the outlined approaches to solve multi-objective optimization problems that handle several conflicting objectives at the same time as outlined in the following section.

6.2. Multi-objective optimization

The optimization problems formulated for engineering purposes incorporate different design aspects and demands. Thus, they are constituted of several independent and conflicting objective functions. In particular, optimization of technical systems, in general, incorporates the minimization of production costs, which in its nature is conflicting with high-performance demands of the system to design. A simple example for this is the design of a car providing high comfort, e.g., by advanced entertainment systems and a powerful engine while the selling price is minimized. The solutions to this conflicting problems can be diverse. A low-budget car with only essential comfort features is a solution that fulfills the optimization problem as good as an expensive premium car. From the perspective of an optimization algorithm, a proceeding distinction is not possible while a customer decides on behalf of his personal preferences.

To investigate the question "*Which solution is better?*" from an algorithmic perspective, the concept of *Pareto*-dominance is introduced. For this, two candidate solutions $\boldsymbol{\theta}_1 = [\theta_{1,1},\, \theta_{1,2}, \ldots,\, \theta_{1,n}]^{\mathrm{T}}$ and $\boldsymbol{\theta}_2 = [\theta_{2,1},\, \theta_{2,2}, \ldots,\, \theta_{2,n}]^{\mathrm{T}}$ of the $n \times q$-dimensional objective function

$$\boldsymbol{J}(\boldsymbol{\theta}) = \left[J_1(\boldsymbol{\theta}),\, J_2(\boldsymbol{\theta}), \ldots,\, J_q(\boldsymbol{\theta})\right]^{\mathrm{T}}, \quad \boldsymbol{J} : \mathbb{R}^n \mapsto \mathbb{R}^q \tag{6.15}$$

are compared. It is said that solution $\boldsymbol{\theta}_1$ dominates $\boldsymbol{\theta}_2$, denoted as $\boldsymbol{\theta}_1 \prec \boldsymbol{\theta}_2$, if

$$\forall i \in \{1,\, 2, \ldots,\, q\} : J_i(\boldsymbol{\theta}_1) \leq J_i(\boldsymbol{\theta}_2) \;\wedge\; \exists i \in \{1,\, 2, \ldots,\, q\} : J_i(\boldsymbol{\theta}_1) < J_i(\boldsymbol{\theta}_2). \tag{6.16}$$

Illustratively speaking, solution $\boldsymbol{\theta}_1$ has to be better in at least one objective $J_i(\boldsymbol{\theta})$ while the remaining objectives are of the same value as achieved by $\boldsymbol{\theta}_2$. Due to this, an optimizer cannot distinguish between a low budget and a premium car if only the costs and the comfort are regarded. The resulting solutions do not dominate each other. In general, solutions are *not distinguishable* if none of the solutions dominate another one. A set of solutions $\mathcal{L}_s$ within the feasible solution space Ω constitutes a Pareto-optimal set if

$$\mathcal{L}_s = \left\{ \boldsymbol{\theta} \in \Omega \;\middle|\; \neg \exists \boldsymbol{\theta}^* \in \Omega : \boldsymbol{\theta}^* \prec \boldsymbol{\theta} \right\} \tag{6.17}$$

meaning that there is no other solution $\boldsymbol{\theta}^*$ that dominates any member $\boldsymbol{\theta}$ of $\mathcal{L}_s$.

Evolutionary algorithms commonly operate on a fixed number of solutions in each generation. Each set of solutions is called population. To classify the candidate solutions within a population a pure determination of the dominance is not sufficient because this only separates the population into not dominated solutions and dominated ones. However, by iteratively calculating the dominance of individuals of a population, the *non-dominated sorting* is achieved. For this, initially the non-dominated solutions are determined, and they are said to be rank 1 individuals. The reduced set of remaining solutions again is evaluated and the rank 2 is assigned to the non-dominated individuals of the reduced subset. This process is repeated until every individual **a** is labeled. The non-dominated sorting is used in several multi-objective algorithms e.g. as presented by Deb (2001) and Deb et al. (2002) or Igel, Hansen, and Roth (2007).

A second criterion is mandatory to sort the solutions within a set of equally ranked individuals since by now they are not distinguishable. This criterion is important

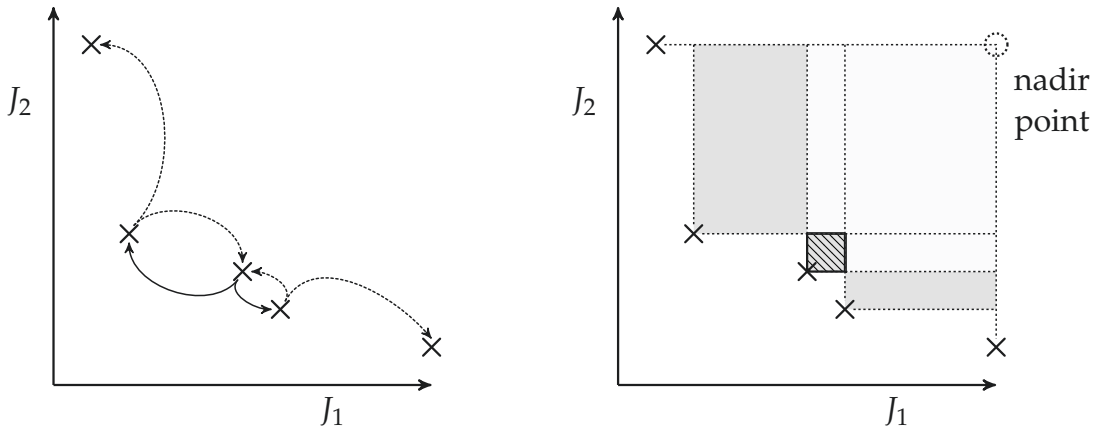

Figure 6.1.: Illustration of Crowding-distance (left) and contributing hypervolume (right) metrics for a two-dimensional optimization problem.

because at the end of every iteration the evolutionary algorithms select a specified number of good solutions to create offspring individuals. Since the number of non-dominated solutions is not predictable, lower ranked solutions also need to be chosen to fill the parental population. Therefore, the quality of the individuals within their sets has to be determined. Deb et al. (2002) introduced the *crowding-distance* measure as a secondary objective. The crowding-distance measures the sum of Euclidean distances to the closest neighbors of a solution. The crowding-distance quantifies how much an individual solution contributes to the diversity (or the spread) of the set of objective values having the same rank. One aim of any multi-objective evolutionary algorithm (MOEA) is to cover a broad range of the solution space to obtain a heterogeneous and versatile set of different solutions that cover different aspects in the sense of Pareto-optimality. A crowding-distance based selection prefers individuals that contribute to a higher overall diversity of the solutions and those with a low contribution, e.g., caused by being rather close to other solutions are rejected in case of doubt.

Another frequently used secondary measure is the *contributing hypervolume* purposed by Zitzler et al. (2003) and Zitzler and Thiele (1998). The hypervolume itself equals the volume covered by the entire population and the nadir point given by the boundary points of the population. As illustrated in figure 6.1 the hypervolume is provided by the filled area. The contributed hypervolume quantifies the contribution of each candidate solution to the overall hypervolume, illustrated as independent gray areas. If the contribution is high, the individual solution is preferable compared to an individual of low contribution (hatched area). One disadvantage of the contribution hypervolume measure is its computational cost. With increasing number of objective functions the effort to calculate the volumes increases exponentially and thus, its practical application is limited to optimization problems of low order, e.g., second or third order.

As investigated by Igel, Hansen, and Roth (2007) and Krimpmann et al. (2013a,b), a scalar-objective CMA-ES can be transferred into a MOEA by applying the non-dominated sorting and a secondary measure instead of the min-operation to determine the quality of individuals. The benchmark results shown by Krimpmann et al. (2013a,b)

indicate an improved performance of the newly presented active-$(\mu + \lambda)$-MO-CMA-ES compared to other MOEA on a set of generic benchmarks. The active-$(\mu + \lambda)$-MO-CMA-ES is the multi-objective counterpart of the active-CMA-ES being executed in parallel for μ times. Especially, the short-term performance of MOEA is of interest if real world optimization problems are supposed to be solved. The objective functions of such problems often perform long-lasting experiments or simulations, and since the solution of a problem is expected to be obtained in a limited time interval, the number of fitness evaluations is restricted.

6.3. Hardware-in-the-loop optimization of valve controllers

The parameterization of controllers applied to hydraulic valves often rests upon a manual parameter selection performed by process experts. As briefly sketched in section B.3, this process can be automated by evolutionary optimization. Due to the no-free-lunch theorem (see Wolpert and Macready 1996 and e.g. Auger and Doerr 2011), the choice of an EA is entirely arbitrary since there are numerous optimization algorithms available that solve optimization problems with comparable quality if the optimization time is not constrained, see e.g. the NSGA-II by Deb et al. (2000a,b) or the SMS-MOEA by Beume, Naujoks, and Rudolph (2008) as alternatives to the sketched CMA-ES approaches. Nevertheless, in HiL optimizations containing long-lasting experiments, the optimal solution set shall be found in limited time, and thus, an algorithm with high convergence rates is reasonable to use. Krimpmann et al. (2013a,b) showed empirically that the active-$(\mu + \lambda)$-MO-CMA-ES outperforms other algorithms for short term optimizations.

The primary challenge in achieving the desired control quality utilizing HiL optimization of hydraulic valve controllers is the mapping of the process experts' preferences into crisp analytical objectives. Krettek (2013), Krettek et al. (2009), and Krimpmann et al. (2014) presented different interactive approaches to incorporate the expert's preferences into the optimization process at runtime to optimize the nonlinear PID controller as introduced in section B.3. A further approach by Krimpmann et al. (2012) separates the overall optimization process into several subsequently optimized smaller problems whose combined solution constitutes the solution to the overall more complex design task. However, the complexity handling within the optimization process only is necessary because of a large number of free design parameters of the nonlinear PID controller. By replacing this controller with an SMC strategy, the number of free parameters is significantly reduced and additionally, the closed loop dynamics is predefined by the sliding function. Thus, by selecting the type of sliding function the process expert's demands are priorly defined and do not need to be integrated into the optimization process. Therefore, only conventional objective functions are mandatory to form a suitable optimization problem for SMC controllers.

The HiL optimization of valve controllers typically optimizes the tracking behavior concerning reference step responses. To quantify the step responses, there are innumerable variants of applicable objectives. Nevertheless, there are commonly used objectives e.g. as discussed in Krimpmann et al. (2014) and Krimpmann et al. (2015a,b, 2016c).

One frequently used measure is the rise time $T_{r,90}$ that directly maps process expert's demands into a crisp objective. The rise time quantifies the time delay between the time at which the reference step takes place and the time when the system reaches 90 % of the set value for the first time. By minimizing this time delay, the system's response is accelerated. Aside from a fast response, the steady state accuracy is to be optimized to maintain high precision. For this, the measure MSE_{ss} measures the mean square value of the control error after the system remains within a given tolerance band around the set value. In case of PID controllers, the system causes strong overshoots if the rise time is decreased and, thus, the overshoot should be minimized. But due to the sliding function with only real valued eigenvalues, an SM controller does not cause significant overshoots. Therefore, this objective is not useful. However, it has to be guaranteed that the sliding motion is established by minimizing the system's deviation from the surface $\sigma(\mathbf{x}) = 0$. The minimization is achieved by the criterion MSE_σ measuring the mean square value of the sliding function. In a conventional parameterization process, the reaching condition has explicitly to be considered. However, by minimizing MSE_σ, this is implicitly fulfilled. In equation (6.18), the mathematical description of the relevant objectives is given for a discrete sampling system that captures N samples for a step response.

$$T_{r,90} = t_{90\,\%} - t_0 \qquad MSE_{ss} = \frac{2}{N} \sum_{j=\lfloor 0.5\,N \rceil}^{N} e_j^2 \qquad MSE_\sigma = \frac{1}{N} \sum_{j=1}^{N} \sigma_j^2 \tag{6.18}$$

Depending on the effective system order and the selected sliding mode strategy, the resulting number of optimization parameters is variable. Depending on the system's order, either two or three states are aggregated. Thus, the number of coefficients r_i of a linear sliding function varies. For the main stage valve, the output of the STA controller is limited such that $|u| \leq u_{\max}$. In contrast to the other valves, this saturation is not known a priori since in this case, the saturation is not related to a maximum solenoid current as it is for the pilot valve or the pressure valve. In this particular case, $u_{\max}$ reflects the maximum opening of the pilot valve, which is a design parameter instead of a protective limitation.

7

Experimental Evaluation of Robust Valve Control

The following two chapters investigate the properties of the theoretically discussed sliding mode concepts regarding practical applications. The current chapter deals with the *robust control* of different hydraulic valves. For this, a controller parameterization based on HiL optimization techniques is taken and during the experiments, the control parameters are fixed. In contrast to this, chapter 8 deals with the *adaptive control* of hydraulic valves at which the control gains are estimated at runtime. The evaluation is designed to be compliant with industrial requirements, e.g. defined by a certain closed loop performance or shortness in optimization as outlined in chapter 1 and section 2.2.

7.1. Hardware setup and design of experimental investigations

To investigate the properties of the outlined control strategies, a tripartite setup as illustrated in figure 7.1 is utilized. In the given illustration, the sketch exemplary depicts the setup for the control of a pressure relief valve. The left part of the diagram contains the supervisory and management functions that are implemented in MATLAB and are used for the optimization of the control parameters. The setup control handles the experiment execution. It is responsible for predefining the reference trajectory for the valve controller and additionally for the flow control valve if needed. Further, it sets up the data acquisition such that the number of samples to capture contains a predefined number step responses. Typically, four responses are captured with a resolution of $\Delta t = 0.1\,\text{ms}$ within an experiment duration of $T_{exp} = 1\,\text{s}$ plus an additional pretriggering time of 100 ms to observe the valve's behavior prior to the first reference step. Additionally, the setup control handles which particular control strategy is carried out. By sending control flags, the system can alter the control law and the sliding function to investigate different strategies without hardware-dependent reconfiguration.

The evaluation block handles the judgment of the captured step responses based on the traced signals and system's states. For this, the data stream is split up into single

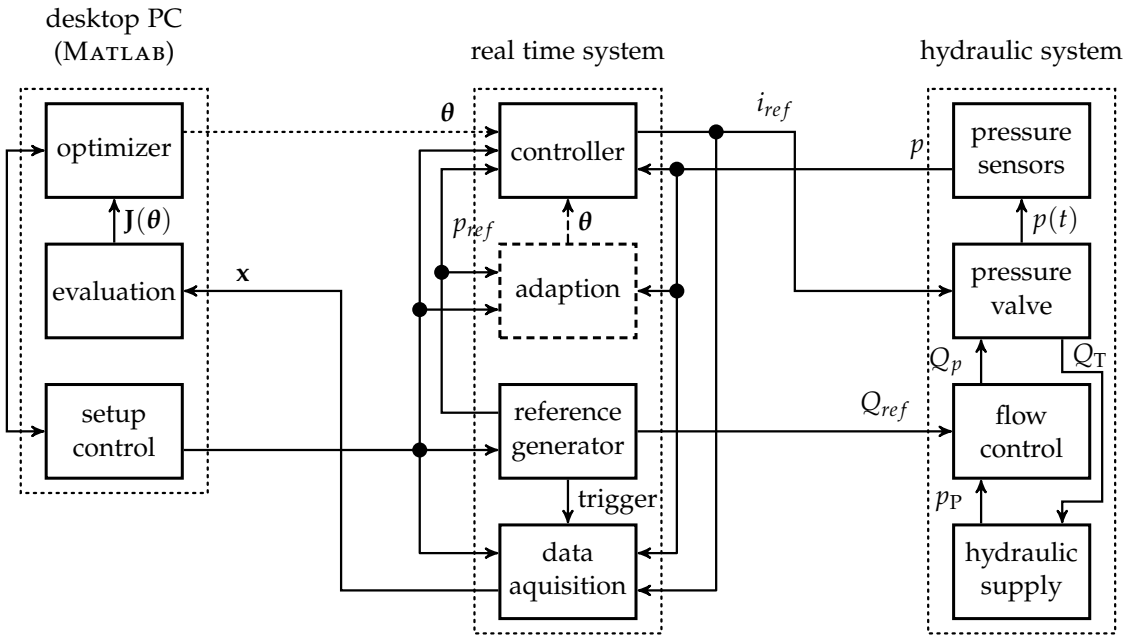

Figure 7.1.: Experimental setup of the HiL optimization of a pressure relief valve consisting of a desktop PC being used for management purpose, a real time system executing the controller and data acquisition and the hydraulic system comprised of the hydraulic power supply, a flow control valve and the pressure control valve.

step responses and for each response, all objectives are calculated as outlined in section 6.3. Due to the nonlinear properties of the hydraulic valves, the step responses of the valves vary depending on the direction at which the reference step is performed. Thus, it is not sufficient to optimize solely one step response in one direction but therefore various steps in different directions. However, optimizing all steps in parallel with an individual set of objectives for each step comprises an optimization problem of too high dimensionality. To cope with the curse of dimensionality (cf. Bellman 1972) the objectives are not optimized for all responses. Instead, the maximum value of each criterion over all steps is determined and minimized. Thus, it is obvious that the optimized controller performs step responses with, e.g., higher accuracy MSE_{ss} as achieved as objective value during the optimization process.

The optimizer executes the evolutionary strategy. In particular, an active-$(10+50)$-MO-CMA-ES with contributing hypervolume selection as outlined in section 6.2 is utilized. This means, the ES operates on a parental population of 10 individuals while each individual generates 5 offsprings. The evolutionary loop is repeated 50 times such that 2500 individuals are investigated during the optimization. For each candidate solution, the parameter vector $\boldsymbol{\theta}$ is applied to the controller at the real time system. After parameter application, the setup control initiates the experiment and the evaluation determines the objective values $\mathbf{J}(\boldsymbol{\theta})$. During the optimization, a set of at most 100 non-dominated solutions – the so-called elitist set – is collected for the latter evaluation of the achieved optimization results.

The real time system consisting of an ordinary PC with the MATLAB Simulink Real Time Target operating system and a multi-functional input-output-board executes the

control and the signal recording with a frequency of $f_s = 50\,\text{kHz}$. As discussed in section B.1, the input nonlinearity of the pressure relief valve is known such that the controller directly applies a current signal i_{ref} to the hydraulic valve. The attached sensor measures the pressure p in front of the valve; the low side pressure p_T is not traced since it is not relevant for the control application. Because of the inertia of the gear type flow meter that is assembled in the hydraulic setup, a fast measurement of the flow Q_T through the valve is not feasible so that a real time flow evaluation is not possible. Thus, it has to be assumed that the flow Q_{ref} set by the flow control valve is valid.

In contrast to Krimpmann et al. (2012) emphasizing a multi-staged optimization process for nonlinear PID controllers, the optimization process of SM controllers uses only large-scale reference steps. This is sufficient to achieve the desired closed loop performance since the complexity concerning the number of design parameters is significantly reduced. Table 7.1 displays the sequence of reference values for all considered valves. Here, the value p_max is the maximum pressure – a constructive property. For the particular valve, the value is $p_\text{max} = 100\,\text{bar}$. The maximum openings $x_{p,\,\text{max}}$ of the direct operated control valve and $x_{ms,\,\text{max}}$ of the main stage valve are normalized to a value of 100 %.

Table 7.1.: Reference trajectories for different valves used in the optimization process.

Valve Type	Reference trajectory
pressure valve	$0.5\,p_\text{max} \rightarrow 0.1\,p_\text{max} \rightarrow 0.5\,p_\text{max} \rightarrow 0.9\,p_\text{max} \rightarrow 0.5\,p_\text{max}$
directional valve	$0 \rightarrow x_{p,\,\text{max}} \rightarrow 0 \rightarrow x_{p,\,\text{min}} \rightarrow 0$
main stage valve	$0 \rightarrow x_{ms,\,\text{max}} \rightarrow 0 \rightarrow x_{ms,\,\text{min}} \rightarrow 0$

7.2. Hardware-in-the-loop optimization of a pressure relief valve

In the given section, the results obtained by HiL optimization of a SOSM controller for the pressure relief valve are discussed. For this, a controller consisting of the STA set law, and a first order linear sliding function is used. By applying the optimization algorithm, a set of elitist individuals is obtained as shown in figure 7.2. The diagrams depict all feasible projections of the resulting objective space that contains 59 non-distinguishable solutions. From the algorithm's perspective, all solutions are of the same quality, but as can be seen, the resulting behaviors are widely scattered. There are solutions comprising a fast response of small rise time $T_{r,\,90}$ but dearly bought by a comparable high steady state error MSE_{ss}. In contrast to this, slow realizations tend to an increased accuracy being almost twice as good as for fast responses.

In figure 7.2 three selected solutions are highlighted either by the symbol △, ◇ or by ☆. The solutions are selected to illustrate the different system behaviors obtained by a multi-objective optimization. Since the pure evaluation of the objective space is only little insightful for the resulting system dynamics, the step responses and the progress of the sliding variables $\sigma(p,\,\dot{p}) = r_0\,p + \dot{p}$ are depicted in figure 7.3. Basically, the

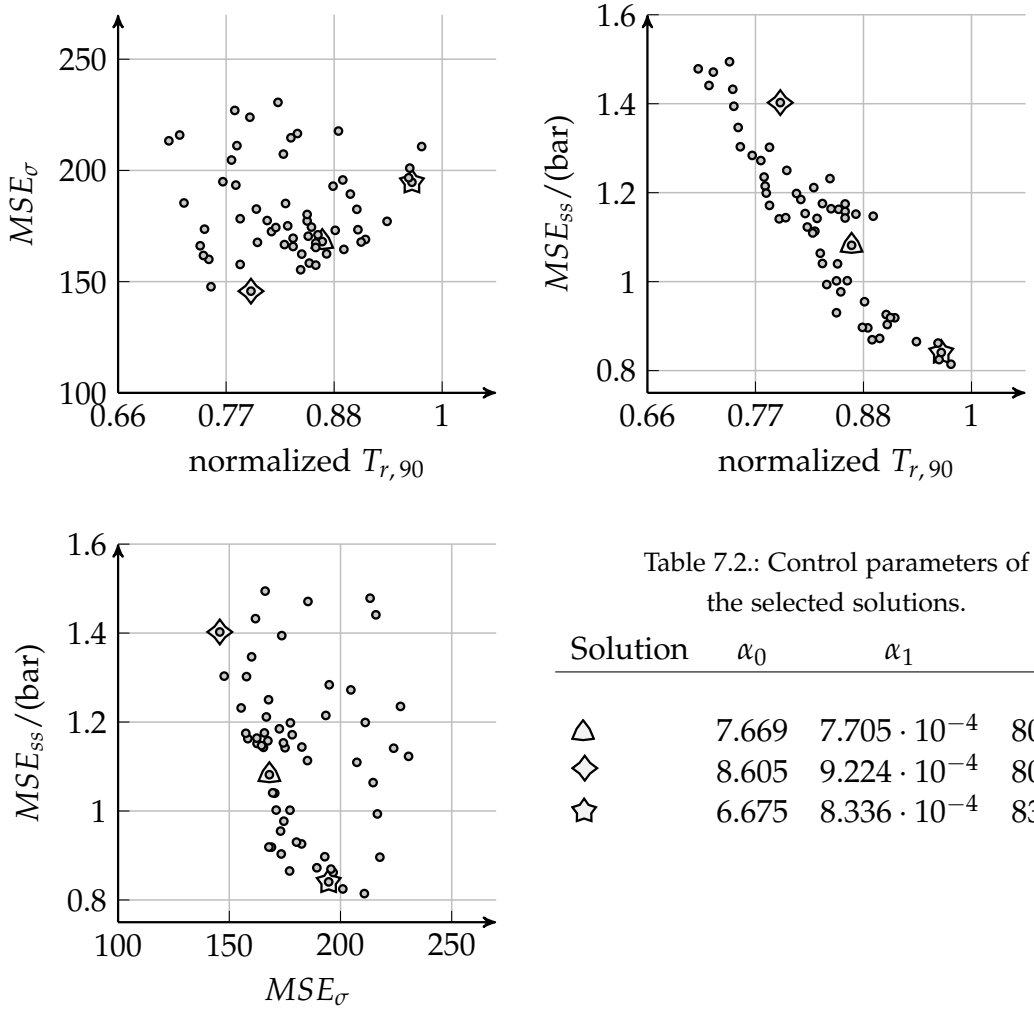

Table 7.2.: Control parameters of the selected solutions.

Solution	α_0	α_1	r_0
△	7.669	$7.705 \cdot 10^{-4}$	80.430
◇	8.605	$9.224 \cdot 10^{-4}$	80.228
☆	6.675	$8.336 \cdot 10^{-4}$	83.436

Figure 7.2.: Projections of the resulting elitist set obtained after 50 generations of a HiL optimization process. Three solutions △, ◇ and ☆ are highlighted to locate their positions for the latter discussion.

selected solutions fulfill the requirement to stay in a steady state region within a $\pm 4\,\%$ vicinity of the set value p_{ref} after the system is converged. Although the responses are comparable from a macroscopic view, the precise behavior is different. The solution ☆ provides an almost oscillation-free response that only is slightly slower than the other ones. In contrast to this, the parameterization ◇ causes the fastest response and most accurate tracking of the sliding function among the selected solutions. As a side effect, the aggressiveness of controller caused by increased control gains α_0 and α_1 leads to chattering around the set value for the center and the upper reference pressure. This particular behavior can be examined in the close-up views of figure 7.3. At this point, it is recalled that the power electronics of the pressure relief valve contains a dither that is superimposed to the control input i_{ref}. The strength and frequency of the dither depend on i_{ref} such that the cone's movement is more oscillating for large control inputs causing a high pressure. Due to this, the valve tends to stronger oscillations for higher pressure values. This fact also motivates the varying steady state tolerance region being defined in dependence on the desired pressure. The influence of the

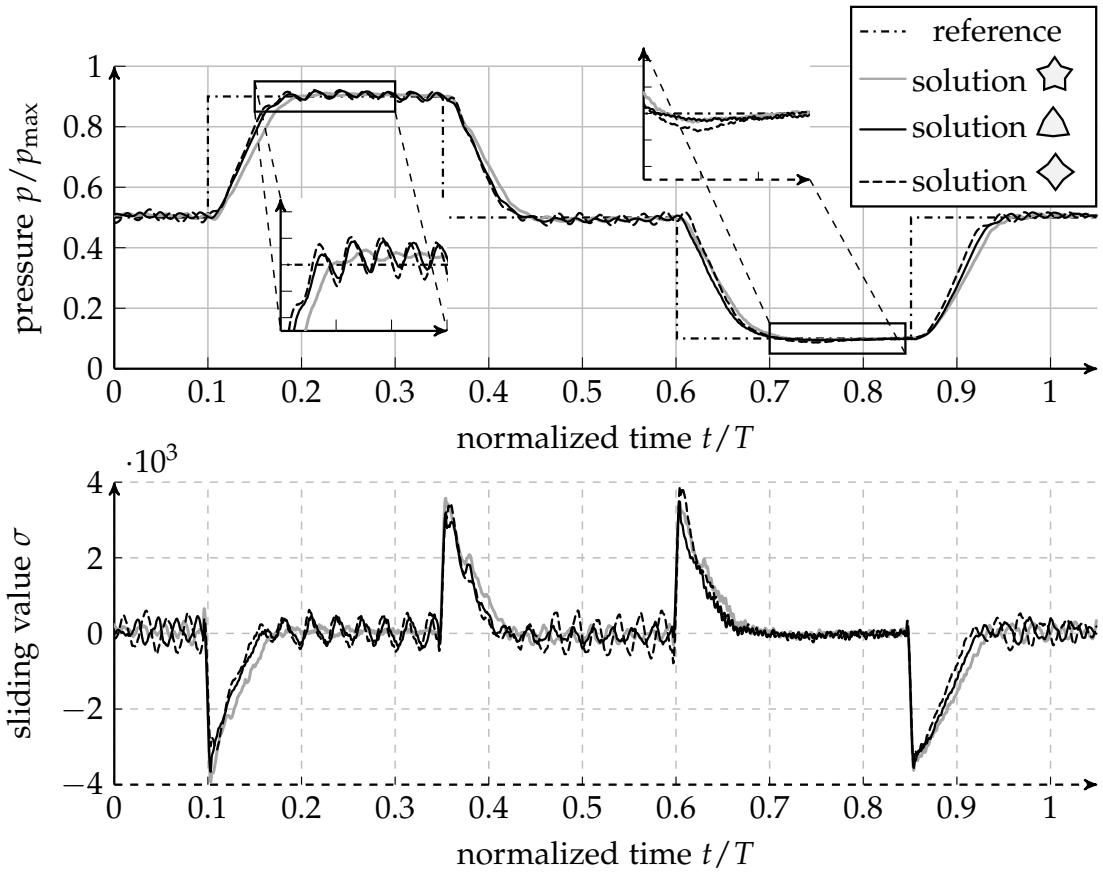

Figure 7.3.: Step responses of selected candidate solutions that are highlighted in objective space shown in figure 7.2. Additionally to the pressure response, the progress of the sliding variable σ is depicted. The evaluation is carried out for $Q_{ref} = 1\ \mathrm{dm}^3 \cdot \mathrm{min}^{-1}$.

dither also is remarkable in the progress of the sliding functions. While the signal for approaching $p_{ref} = 10\,\mathrm{bar}$ hardly shows any oscillations, they are obvious for the other steps. The controller $\triangle$ however generates an interesting behavior. For large pressure values, it is not able to compensate the oscillations caused by the dither, but for the center position and the lower one, the oscillations are attenuated. Apparently, by decreasing the control gains α_0 and α_1 (cf. table 7.2) the occurred chattering can be attenuated.

As the outlined results indicate, the minimization of MSE_σ constitutes a control-theoretical dilemma. The optimization of the given objective is intended to establish a real sliding motion such that the controller stabilizes the system as good as possible. The observable results, however, indicate a non-intended behavior. Since for each occurring reference step the sliding motion is interrupted, a new reaching phase is entered as can be seen in figure 7.3. Further, can be seen that the controller only achieves a stabilization of the sliding motion at the steady state part of the response meaning the transient behavior does not precisely follow the predefined dynamics of the sliding function σ. The emphasized issue that is characterized by a chattering-affected closed loop performance can be ascribed to the structural assumptions taken for the pressure relief valve. As outlined in section C.2, originally the pressure relief

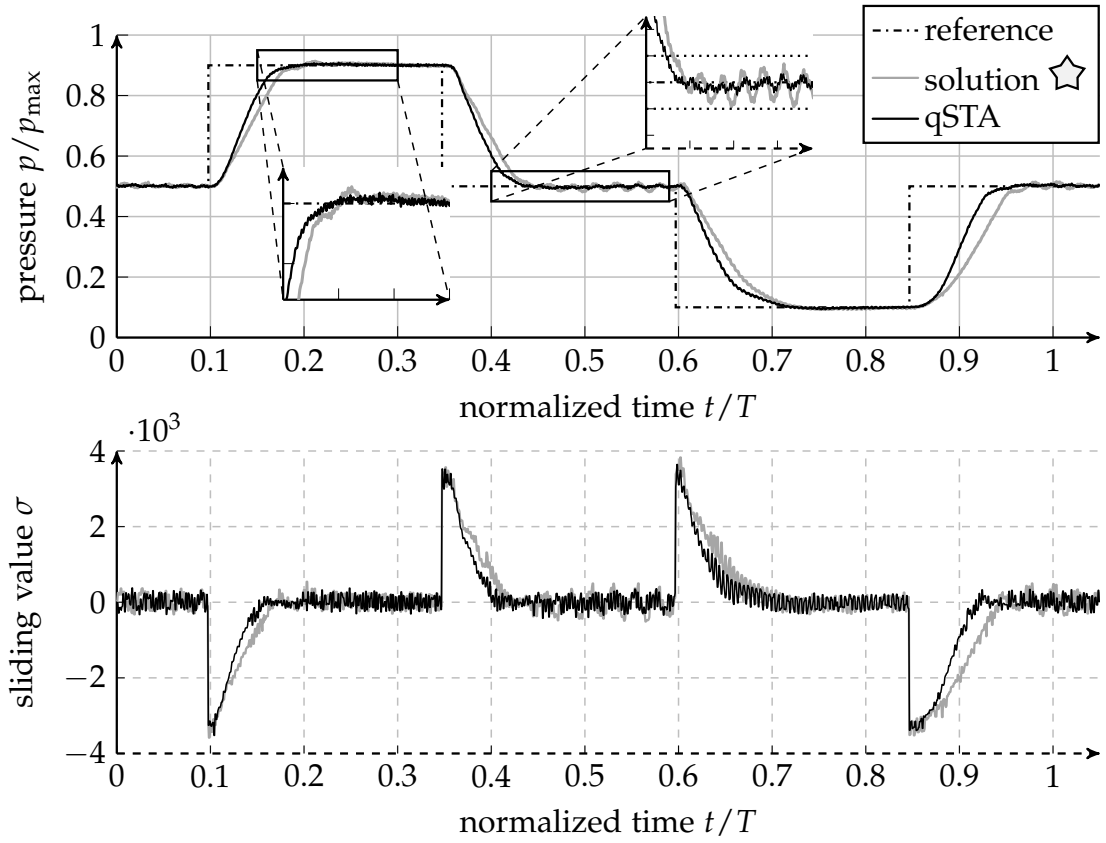

Figure 7.4.: Comparison of step responses obtained by a STA and a quasi STA controller while using equally parameterized sliding functions.

valve comprises four states. However, the structural evaluation of the deduced model indicates that two states are sufficient to approximate the dynamic behavior and thus fewer states need to be estimated. Nevertheless, this simplification leads to neglected higher order dynamics that also affect the system's motion and subsequently cause chattering.

The outlined chattering-attenuation approaches based on HOSMs can cope with the influence of neglected states; however, they are not able to compensate their influence entirely. The STA shifts the control-input switching from the first derivative $\dot{\sigma}$ into the second derivative $\ddot{\sigma}$ as described in section 4.3. Nevertheless, the switching still is present and excites the system. Recapitulating section 4.5, the ultimate step to compensate the chattering is to utilize a quasi HOSM algorithm, e.g. the qSTA (4.19). However, this influences the theoretical robustness properties of the system due to the abandoned switching of the controller. The practical results however are depicted in figure 7.4. The figure illustrates the resulting step responses of the pressure relief valve for the same sliding function with $r_0 = 83$ either being controlled by the STA or the qSTA. As the practical examination reveals, the use of quasi sliding modes can attenuate the occurred chattering significantly, and the stabilization of the sliding mode is improved. The qSTA achieves a second order stabilization within the transient part of the step response while the STA only achieves a sufficient stabilization when the system already has reached the desired set value. Due to the precise stabilization

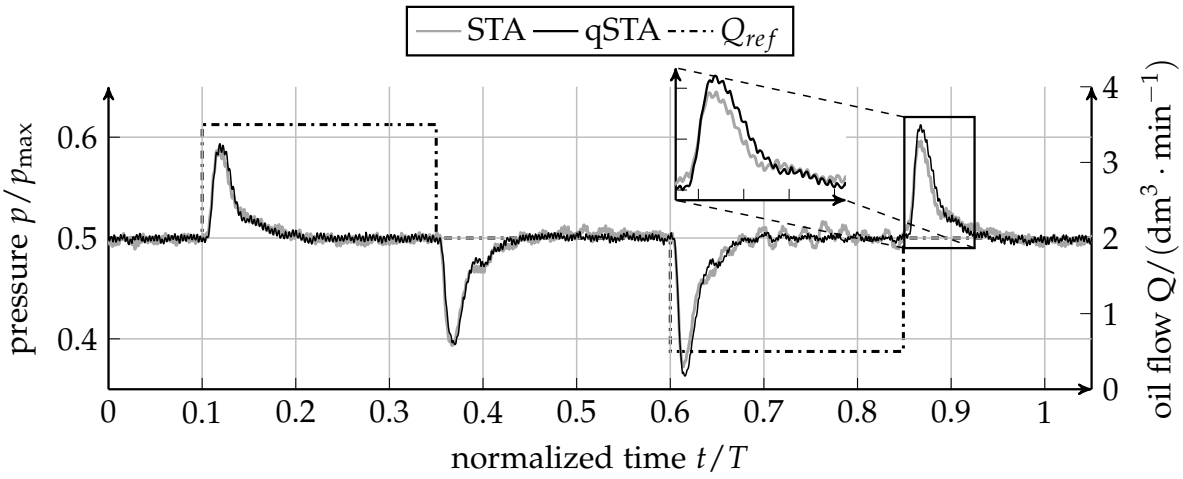

Figure 7.5.: Comparison of pressure responses for a step sequence of reference flows Q_{ref} obtained by the STA controller (solution ☆) and the quasi STA controller for the same sliding function.

of the qSTA, the step responses are practically asymptotically converging, and the chattering of the STA is canceled out, and now, the predefined dynamics of the sliding motion are prevalent.

As mentioned beforehand, the changed robustness properties of the qSTA may cause a disadvantage in case of occurring disturbances. To investigate this issue, the controllers are exposed to varying boundary conditions. Since the step responses are investigated for a constant flow rate of $Q_{ref} = 1\,\mathrm{dm}^3 \cdot \mathrm{min}^{-1}$ the variation of Q_{ref} is to be understood as a distortion from the desired behavior. In figure 7.5, the disturbance rejection of the two different algorithms are illustrated. For a constant reference pressure $p_{ref} = 0.5\,p_{\max}$ the oil flow is varied step-like in $Q_{ref} \in \{0.5,\, 2,\, 3.5\}\ \mathrm{dm}^3 \cdot \mathrm{min}^{-1}$. The variation of the oil flow causes an increase or decrease of the pressure p. In case of an increased flow, the ram pressure in front of the valve's cone is increased since the valve cannot relief the flow at a time. For a reduced flow, the controller has to close the valve's orifice to stow the fluid. As can be seen in the figure, the pressure rises or falls for approximately $\Delta p \approx \pm 0.1\,p_{\max}$ for a flow step. Both algorithms can compensate the distortion within the same amount of time due to the equally parameterized sliding function.

However, the qSTA does not cause the intense low-frequent oscillations of large amplitudes and only produces small high-frequent oscillations. In contrast, the STA comprises significant low-frequent fluctuations around the steady state value. For the second two flow steps, the qSTA sustains slightly higher deviations as the STA. On the one hand, this effect can be ascribed to the changed robustness properties of the qSTA compared to the STA. On the contrary, however, the occurring deviations are comparably small, and thus, they also may be attributed to process noise or repeatability of the experiment. A precise separation of these effects is not feasible, and thus, it can be stated that the qSTA provides the same or even improved closed loop performance for the pressure control of the relief valve compared to the conventional STA.

As a completing analysis (cf. Krimpmann et al. 2016a), the system's responses

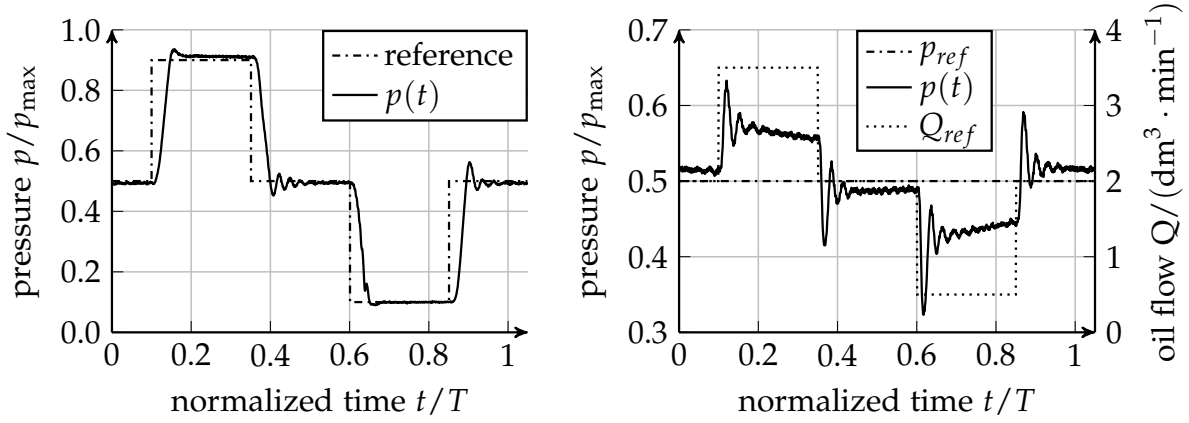

Figure 7.6.: Reference step responses and disturbance rejection of the pressure relief valve being controlled with a linear PI controller and a feed forward control.

obtained by a simple linear PI controller and a feed forward controller are investigated. This kind of controller is of particular interest since it can be understood as the state of the art controller for pressure relief valves and additionally, it consists of the same number of parameters as the STA with a linear sliding function. The parameters of this controller are determined in a comparable optimization-based design process as described before this by Schlattmann (October 2015). As depicted in the left part of figure 7.6, the linear controller, however, generates a 40 % faster response in average but steady state errors remain after all oscillations are decayed. The response also is not asymptotically converging, and substantial overshoots are present for the steps towards medium and high reference values. The disturbance rejection depicted in the right part of figure 7.6 exposes the significant drawbacks of the linear PI controller. Since the disturbance rejection is evaluated for an average oil flow of $Q_{ref} = 2\,\mathrm{dm}^3 \cdot \mathrm{min}^{-1}$ instead of $Q_{ref} = 1\,\mathrm{dm}^3 \cdot \mathrm{min}^{-1}$ for the reference step responses, stronger steady state errors are apparent. Due to the utilized feed forward element that is used to provide an educated guess for the input signal i_{ref} for a constant and known flow rate Q_{ref}, the gains of the PI controller are comparably small. Thus, the pressure stabilization for different flows is not sufficient and characterized by strong pressure peaks followed by oscillations. Within the given time, the controller is not able to compensate the distortions.

A nonlinear PI controller is considered as a second benchmark. The controller consists of a gain-scheduled P-branch with independent small-signal and large-signal gains with adjustable break points and a conventional linear I part with an anti-windup mechanism. Thus, the gain-scheduled PI (gsPI) controller comprises four design parameters and therefore, one parameter more than the qSTA with linear sliding function. Again, the controller is parameterized via HiL optimization for a symmetrical step sequence and a representative solution is depicted in figure 7.7. Additionally, the qSTA solution is shown as a reference. The gsPI controller achieves superior rise times and comparable steady state accuracy compared to the qSTA. The ratio of performance

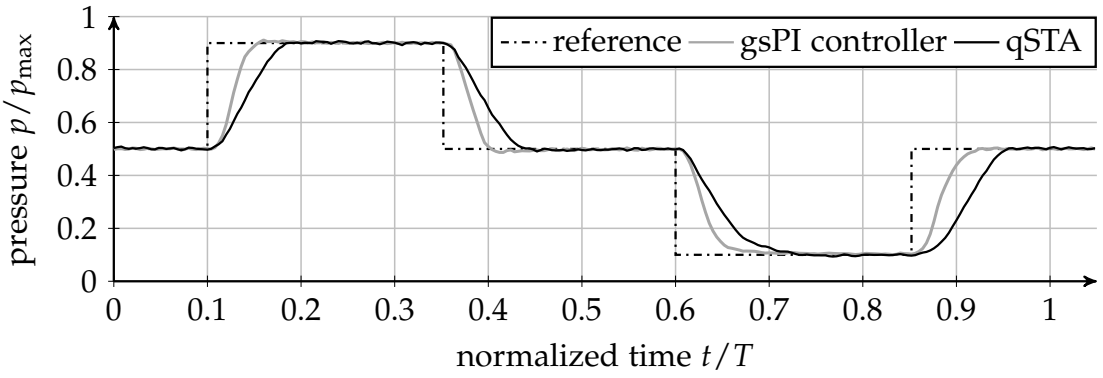

Figure 7.7.: Comparison of step responses obtained by a qSTA and a gain scheduling PI controller.

indices are as follows:

$$T_{r,\,\mathrm{gsPI}}/T_{r,\,\mathrm{qSTA}} \in [0.608 \quad 0.625]\,, \quad T_{s,\,\mathrm{gsPI}}/T_{s,\,\mathrm{qSTA}} \in [0.600 \quad 0.631]\,.$$

As can be seen, the gsPI controller performs better on the demanded stimulus due to its nonlinear gain characteristics that are fitted to this particular stimulus. The generalization properties of the qSTA and the gsPI controller are evaluated for an unknown sequence of steps as illustrated in figure 7.8. The top diagram shows the responses for the same conditions (unchanged flow rate of $Q_p = 1\,\mathrm{dm}^3 \cdot \mathrm{min}^{-1}$) as applied in the experiment of figure 7.7. The second and third diagrams reveal the robustness of the qSTA and the gsPI controller for different flow rates. The flow rates are spread as wide as feasible to obtain the strongest variations in the test conditions ($Q_p \in [0.3 \quad 3.5]\ \mathrm{dm}^3 \cdot \mathrm{min}^{-1}$). The responses for small reference steps are very robust and do not vary significantly in dependence on a changed oil flow. Also, the differences between the gsPI and the qSTA controller are negligible. Both controllers achieve comparable settling times without overshoots. However, for larger steps than the ones being used during the optimization, the results are different. The gsPI controller produces faster rise times. However, it also causes significant overshoots, and the step responses settle at approximately the same point at which the qSTA is converged. As it is depicted, the overshoots strongly depend upon the applied test conditions and are attenuated for higher flow rates. Because of the optimization process, the gain curve of the gsPI controller is tailored to the former stimulus. Larger steps are not considered during optimization such that the extrapolation behavior for the controller is not sufficient. In contrast to this, the qSTA controller always follows the predefined dynamics of the sliding function. Thus, there can be small variations in the desired behavior, but in general, the desired motion is maintained such that the qSTA controller reproduces the same dynamics for any oil flow Q_p without causing overshoots. Because of this, it can be reasoned that the qSTA provides a superior robustness to changed use cases compared to conventional linear or nonlinear PI controllers.

Summarizing the results, it is obvious that use of SOSM algorithms is a valuable approach to achieve high quality control of a pressure relief valve. The comparison with structurally different linear or nonlinear PI controller of the same number of

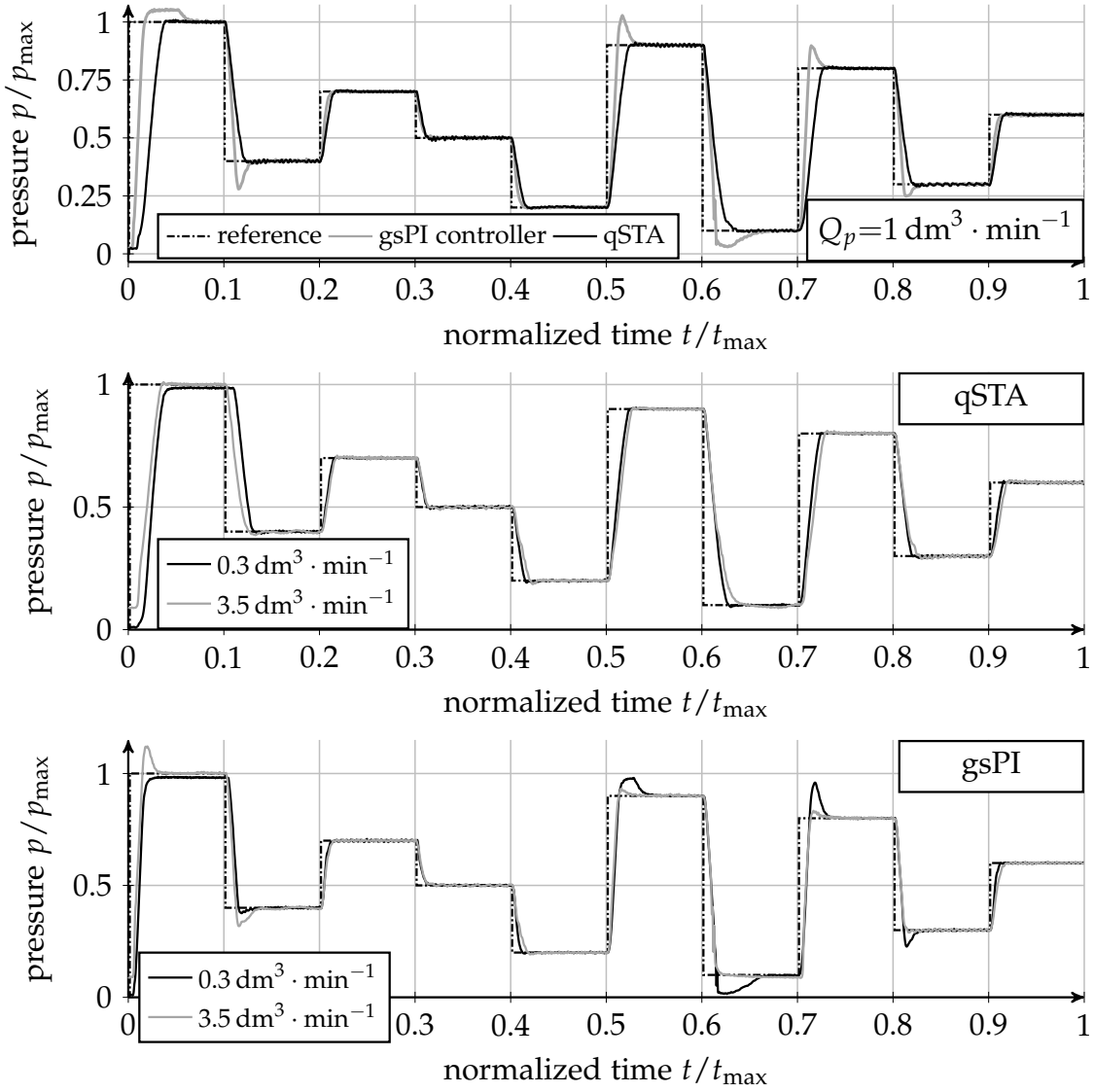

Figure 7.8.: Comparison of a nonlinear gain-scheduled PI controller and the qSTA applied to the pressure relief valve.

parameters underlines the control quality of sliding motions in contrast to pure output feedback control.

7.3. Evaluation of nonlinear sliding surfaces on the control of a directional valve

The given section is focused on the evaluation of performance influences obtained by different nonlinear sliding functions as introduced in section 3. As an application example, the piston position control of the direct operated directional valve being introduced in section 2.2 as an example for a mechatronic system is discussed.

The experimental setup used for this evaluation is rather identical to the one outlined in figure 7.1. However, the flow control valve is omitted because the flow through the

directional control valve only depends on the piston's position and the pressure across the control edges (see section B.2). For the control design, the application ports A and B of the valve are closed such that no oil flow is present. This setup coincides with the industrial testing setups. Thus, no additional pressure sensors are mandatory, and the only relevant signal is the piston position provided by the inbuilt position transducer. Hence, the hydraulic part of the experimental setup only consists of the HPU and the valve itself. By applying the same optimization process as used for the pressure relief valve (cf. sections 6.3 and 7.2), the optimal set of parameterized controllers is obtained. However, a detailed examination of the resulting Pareto-optimal solution space is omitted. The optimization only is used to determine a set of feasible solution from which an adequate parameterization for the STA and the three different sliding functions are selected. The Pareto-solution spaces of the obtained elitist sets are shown in figure E.1.

The following performance evaluation is carried out in two logical parts. While the second part deals with the responsiveness of the closed loop motion, initially the sliding properties are investigated. As illustrated for the pressure relief valve using a linear sliding function, the entrance of real sliding motion occurs rather late. The controller reaches the sliding mode only within the last third or only in the vicinity of the set value that exposes a comparable long reaching phase. A related result can be seen in figure 7.9. In the given figure, the step responses and belonging state trajectories obtained by two different controllers are depicted. One controller consists of a linear sliding function and the STA to stabilize the sliding motion. The other one uses the nonlinear sliding surface SPA (cf. section 3.3) and the STA. Obviously, the achieved step responses are almost identical offering the same rise time and accuracy. However, the major difference can be observed in the sliding motion. As already mentioned, the reaching phase of the system is rather long for the linear sliding function. The controller has to accelerate the system such that the state point reaches a desired height in the phase plane. From that point, it converges in sliding motion along a straight line into the steady state. The convergence of the system rests upon the slope of the sliding surface. By increasing the slope, the reaching phase is extended until the slope is such steep that a successful establishment of sliding motion becomes unfeasible.

The depicted result of the controller with linear sliding function causes a sliding entrance after approximately 50 % of the settling time. The entrance point is marked with the symbol ■ either for the positive step as well as for the negative step. The entry of the SPA controller is marked with ○. The evaluation of the negative working rage is omitted at this point since the valve has symmetrical behavior due to the two identical counteracting solenoids. Obviously, the linear sliding function can only be reached if the further motion remains in a straight line within the two-dimensional projection of the three-dimensional state space. This is illustrated in figure 7.9 in the bottom left part. From the system theoretical perspective, the reaching motion of the system with linear sliding motion is prone to external disturbances, e.g., occurring flow forces in latter applications not being investigated during the control design process. To maximize the sliding phase without decreasing the system's responsiveness, the SPA sliding function can be utilized. As depicted, the system that is controlled with the SPA enters the sliding mode after one fourth of the settling time or at approximately

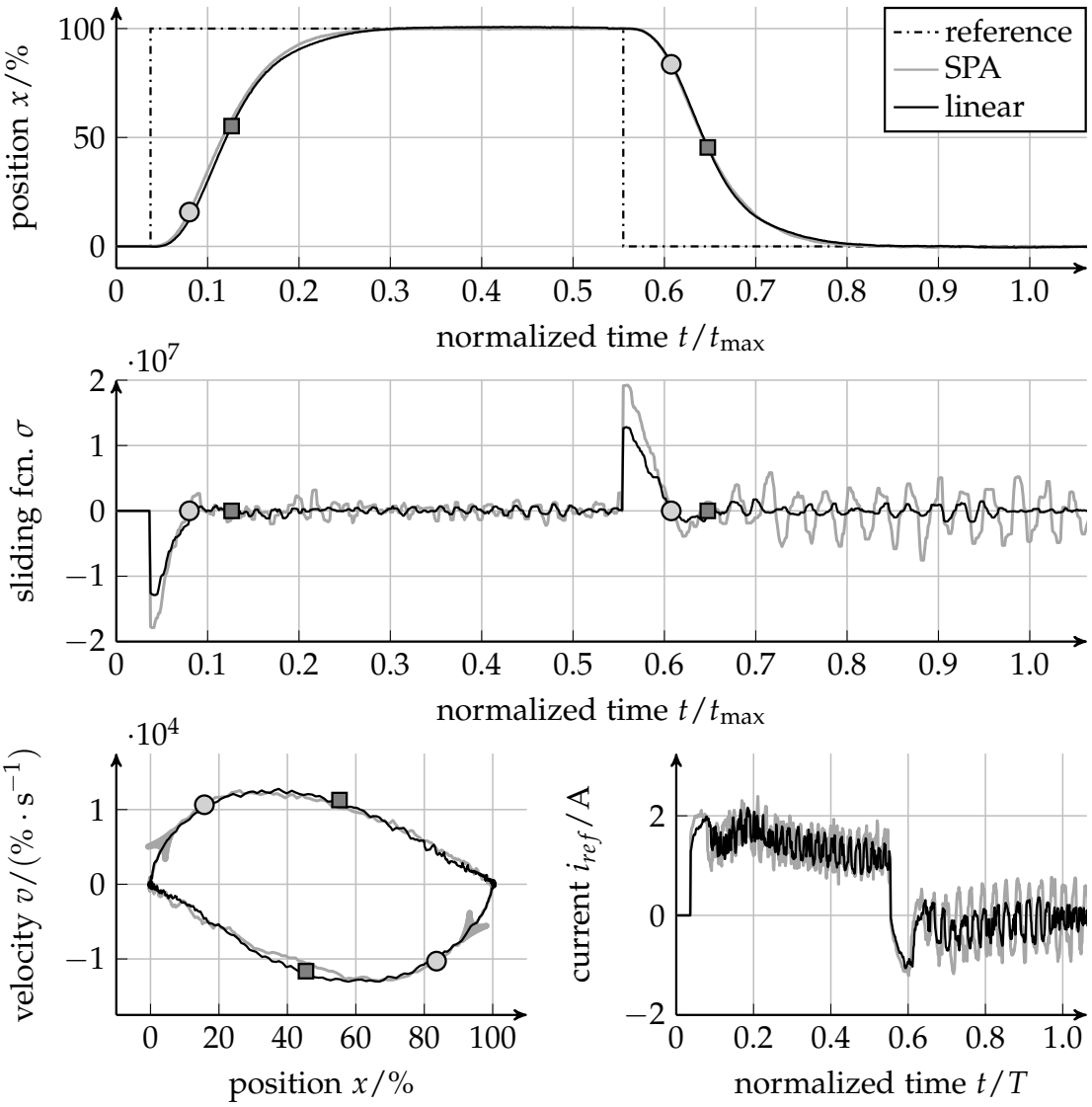

Figure 7.9.: Comparison of sliding modes obtained by a controller using linear sliding function and a controller using the SPA function. The controllers are selected to have the same dynamics to illustrate the different properties of sliding motion.

$e = 85\,\%$ remaining control error. From this point, sliding motion is established, and the system becomes invariant against the perturbations. The early sliding entrance is achieved by the nonlinear shape of the surface. Due to the nonlinearity, the surface is bent such that the system reaches the surface as fast as possible. While the linear ones only decelerate the system's motion in the direction of the steady state, the nonlinear SPA surface also accelerates the system until the maximum of the surface is reached from that the system is decelerated in the direction of the origin $\mathbf{e} = \mathbf{0}$.

As a side effect of the SPA surface, the control input i_{ref} of the valve comprises stronger oscillations as seen in figure 7.9. This is due to the comparable steep surface for $|e| \to 0$. However, the steady state accuracy of the piston's position x is as good as of the controller with a linear surface. Nevertheless, the power consumption of the valve is slightly increased.

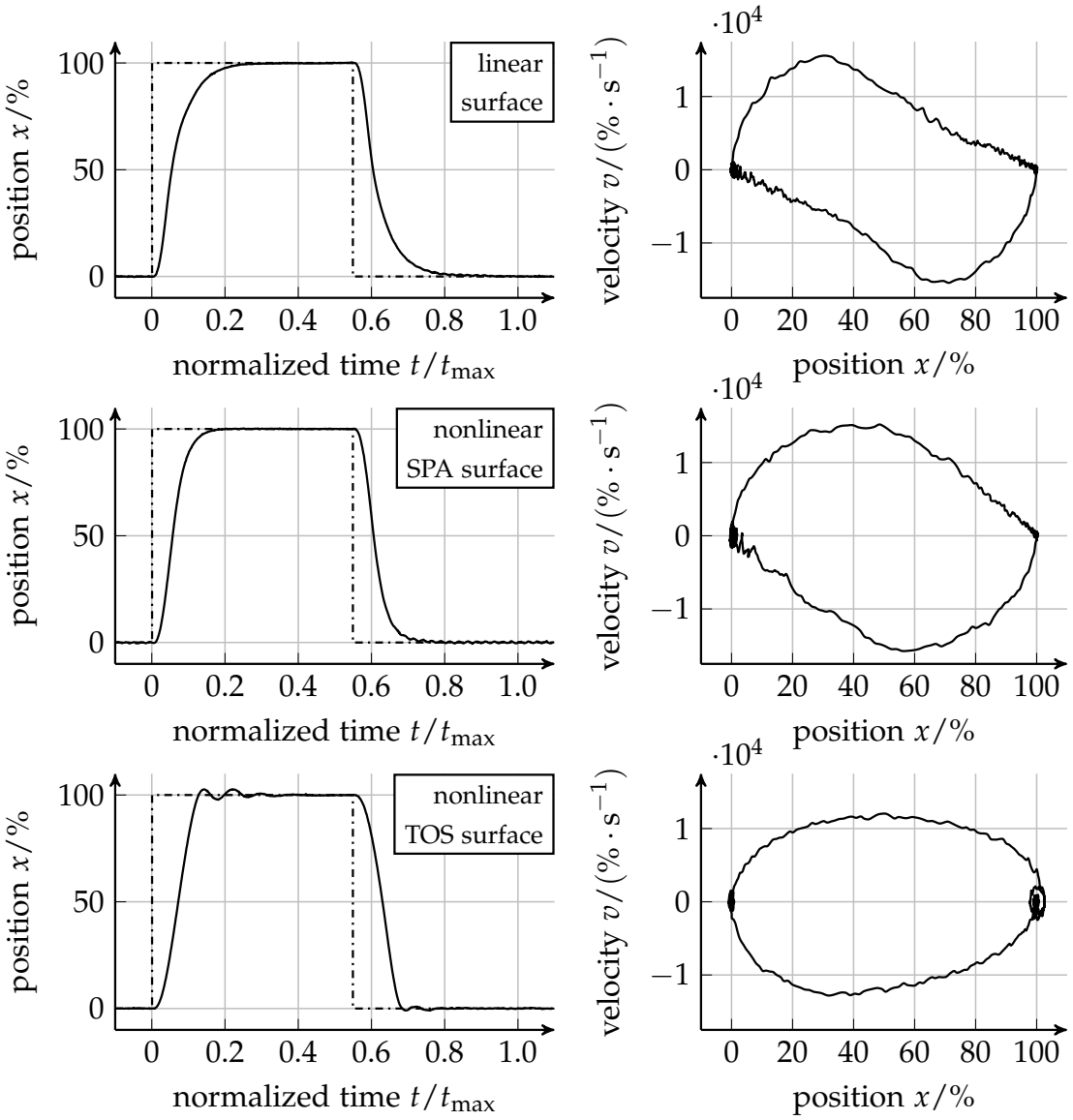

Figure 7.10.: Comparison of step responses obtained by different sliding function while using the same parameterization of the STA.

If the robustness of the sliding motion is not the major design factor, nonlinear sliding functions can accelerate the system's dynamics. As just outlined, the use of the nonlinearity increases the duration of the sliding mode significantly. By spending the obtained margin for a belated sliding mode entry, the responses are accelerated as depicted in figure 7.10. The figure contains three different step responses and reduced phase trajectories obtained by a linear sliding function, a SPA sliding function and a TOS sliding function. The parameters of the given functions are summed up in table 7.3. The sliding functions parameters are obtained by evolutionary optimizations (see section E.1 for the resulting solution sets). However, for stabilizing the sliding functions, all controllers utilize the same parameterization of the STA such that the resulting differences are only related to the differently shaped sliding surfaces.

All solutions are in common that they reach the sliding surface at approximately

Table 7.3.: Control parameters of the selected solutions.

	parameter 1	parameter 2
STA	$\alpha_0 = 183.18$	$\alpha_1 = 0.0015$
linear	$r_0 = 662114$	$r_1 = 3210$
SPA	$\lambda_0 = -438.16$	$\Delta\lambda = 29.98$
TOS	$j_c = 10^{8.4}$	–

$|e| = 50\,\%$ for the first time. As can be seen for the system with a linear surface in the top of the figure, the system heads directly in the direction of the origin after entering the sliding mode. This is a comparable behavior as discussed before. The system with SPA surface, however, provides a faster response since now; the sliding margin is spent to accelerate the system instead of maximizing the sliding phase. The sliding surface is shaped such that the system is accelerated further instead of guiding the state point directly to the steady state position. The result is an accelerated asymptotic response without any oscillations. In contrast to this, the third response obtained by the TOS surface is as fast as the one achieved by the SPA surface. Nevertheless, this solution does not provide a sufficient sliding mode as indicated by the oscillating convergence. These oscillations are caused by the geometrical properties of the TOS surface. As illustrated in section 3.2, the surface comprises an infinitely steep slope at the origin $\mathbf{e} = \mathbf{0}$ which cannot be followed by any physical system. Thus, the sliding motion is lost in the vicinity of the steady state position being induced by the slope. Consequently, the system responds with undesired overshoots. This disadvantageous behavior also cannot be attenuated by decreasing the surface's jerk j_c since the slope at the origin is not changed. In contrast to this, the SPA surface comprises a limited slope at the origin. Due to this, the sliding motion can be maintained even for high demanded convergence rates. Gamble (1992) proposes a smoothing of the TOS surface, however, this does not circumvent the property that the TOS surface only can be implemented as a data based lookup table instead of an analytic equation as the other sliding surfaces are.

As shown, the use of nonlinear sliding surfaces offers a valuable influence factor for the design of SM controllers. On the one hand, the nonlinearity can be used to extend the sliding motion within transient responses to increase the robustness of the system. On the other hand, the nonlinear sliding surfaces can increase the convergence rate of the closed loop system. While comparably small errors are compensated with high dynamics, the response for large deviations is attenuated to guarantee a motion no being comprised with chattering after reaching the surface. Nonetheless, increasing the slope to its extent as done by the TOS surface also offers the drawback of losing sliding mode in the vicinity of the steady state which causes oscillations around the set value instead of a smooth response.

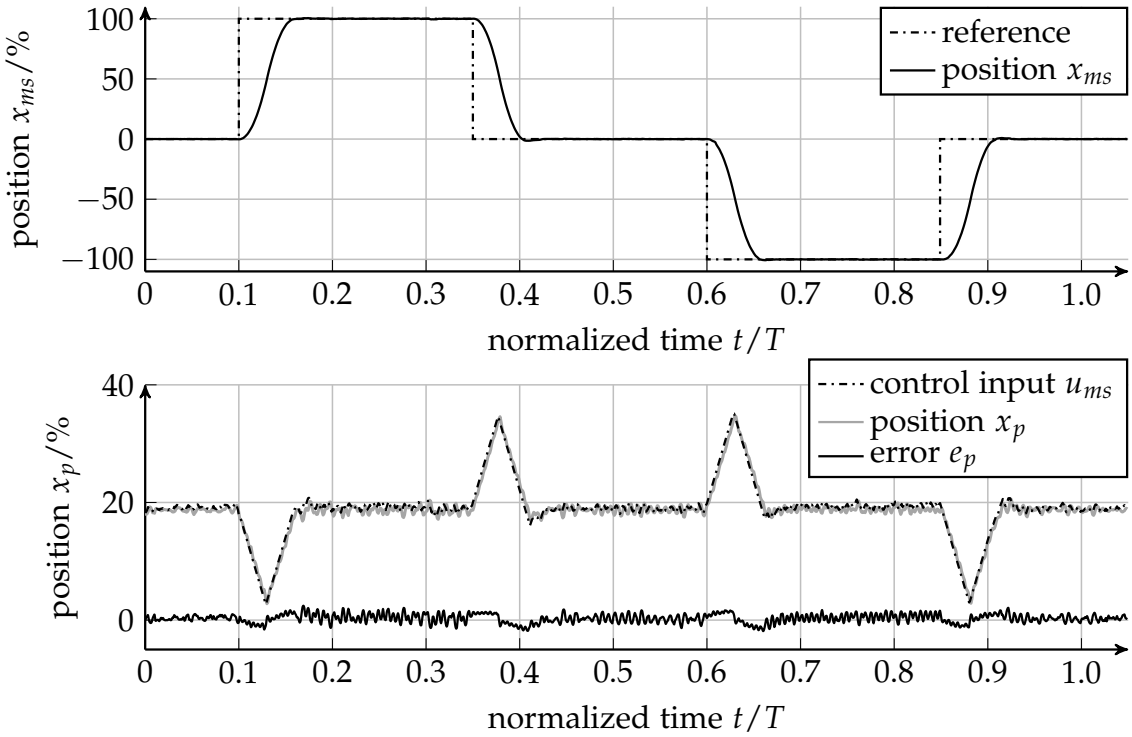

Figure 7.11.: Step responses of a cascaded main stage valve. Top: response of the main stage valve, bottom: reference and response of the pilot valve not being hydraulically neutral for $x_p = 0\,\%$.

7.4. Cascaded sliding mode control of a main stage valve

As outlined in section B.2, main stage valves are passively actuated hydraulic amplifiers that are used to handle large hydraulic loads. For this, the pressure chambers $\mathcal{A}$ and $\mathcal{B}$ are pressurized according to the pilot valve's piston position. To obtain an accurate positioning of the main stage valve, the pilot valve's dynamics are supposed to be sufficiently fast and accurate for small signal ranges to achieve a precise pressurization of the control chambers.

Due to comparable small control chamber volumes, the main stage valve is approximated as a second order system (cf. section B.2) and thus, the main stage sliding function σ_{ms} defines a first order differential equation that is stabilized by an outer STA loop while the inner pilot controller remains unmodified. Therefore, only the main stage control parameters are optimized by the evolutionary optimization process. A representative individual of the Pareto-optimal solution set is depicted in figure 7.11.

From the control theoretical perspective, the relative degree of the plant is formed by the system order of the main stage sliding function and the order of the inner control loop, ergo a first order and a second order system. However, the STA demands a relative degree of one between the control input and output $\sigma_{ms} = r_{0,\,ms}\, e_{ms} + \dot{e}_{ms}$. Because of this, the pilot valve's dynamics are understood as a relative degree mismatch probably being a source of chattering. To prevent the deterioration of the system's dynamics, the main stage controller providing the reference position $u_{ms} \equiv x_{p,\,ref}$ of

the pilot valve has to generate continuous and smooth trajectories such that there are no high-frequent input signals such that the pilot controller compensates any tracking error as fast as possible. For this, the SPA sliding surface is predestined as it offers high convergence rates for small errors.

As figure 7.11 indicates, the tracking error of the pilot valve e_p is sufficiently small due to the continuous reference position $x_{p,ref}$ such that there is no obvious delay of the inner control loop. Thus, it is constituted that the relative degree mismatch of the main stage controller is negligible and is excluded as a source of chattering. This results in a smooth and asymptotic response of the main stage valve. A further characteristic system behavior can also be investigated in figure 7.11. To achieve proper step responses of x_{ms}, the pilot valve follows a triangular profile outgoing from a hydraulically neutral position. The triangular shape is lead back to an I-dominance of the main stage controller. This means that the integral part is responsible for defining the pilot valve's large-scale behavior while the proportional part only is used for the steady-state accuracy after reaching the set value. The pilot valve reaches its full opening at precisely 50 % of the response. The first side of the triangular trajectory is supposed to accelerate the main stage while the second part decreases the response such that it settles without any overshoots. A contrary opening of the pilot valve is not necessary to stop the main valve's motion since the main stage control spring acts as a counterpart. To keep the main stage piston at a constant position, the pilot valve has to take a hydraulically neutral position meaning that the pressure p is distributed equally into both chambers $\mathcal{A}$ and $\mathcal{B}$. Obviously, the pilot valve used for the experiment depicted in figure 7.11 is not hydraulically centered which means that the hydraulic center is not at the center position $x_p = 0\,\%$. Nonetheless, the integral part of the main stage STA controller compensates for the missing balancing such that even for an unbalanced valve a proper response is obtained. A symmetrical limitation of the pilot valve's position around the hydraulically neutral center may be used to constrain the velocity v_{ms} of the main stage piston. However, such a constraint is adverse in terms of achieving a fast stabilization of the sliding motion since this limitation artificially extends the reaching phase after a step-like change of the reference signal $x_{ms,ref}$.

The tracking behavior of the cascaded SM controller is depicted in figure 7.12 showing the Bode diagrams of the system for different excitation amplitudes to indicate the nonlinear properties. The gain progress $|A(f,\, \hat{x}_{ms,ref})|$ shows a constant damping of $|A(f,\, \hat{x}_{ms,ref})| \approx 0$ dB for frequencies f up to 10 Hz followed by a decrease of approximately 37 dB/dec if a reference amplitude of $\hat{x}_{ref} = 100\,\%$ is investigated. For decreased amplitudes, the gain $|A(f,\, \hat{x}_{ms,ref})|$ is kept constant for higher frequencies until the decrease in the amplitude is apparent. Due to the sampled magnitude, the closed loop system may be characterized as a second order system with variable cutoff frequency. The progress of the phase shift $\angle A(f,\, \hat{x}_{ms,ref})$, however, reveals an interesting behavior. While the amplitude progress intentionally indicates a continuous decrease of the closed loop gain probably followed by a continuous phase shift, the given progress of $\angle A(f,\, \hat{x}_{ms,ref})$ outlines an entirely different result. Obviously, the system does not comprise any phase shift, thus $\angle A(f,\, \hat{x}_{ms,ref}) \approx 0^\circ$, as long as $|A(f,\, \hat{x}_{ms,ref})| \approx 0\,\text{dB}$. This means that the system is able to follow any continuous reference signal without any phase shift and any damping or in other words, the control

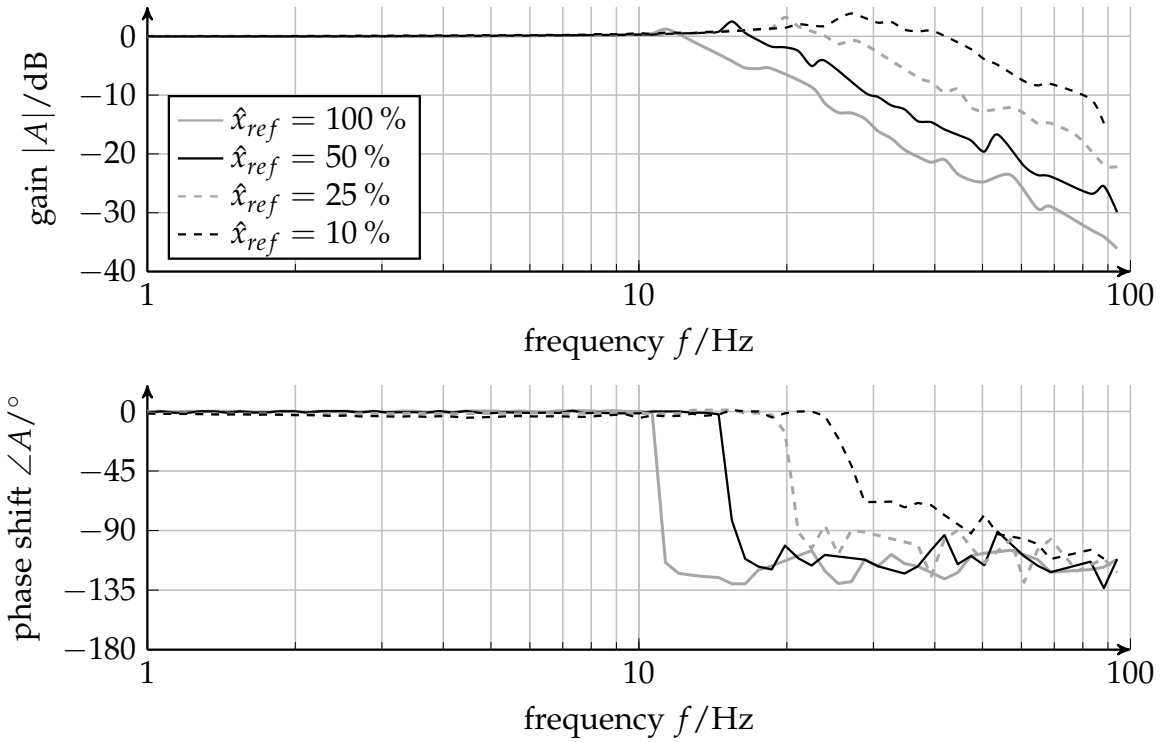

Figure 7.12.: Measured Bode diagram of the main stage valve for different reference amplitudes $\hat{x}_{ms,ref}$, $x_{ms,ref}(t) = \hat{x}_{ms,ref} \sin(2\,\pi\,f\,t)$.

error e always remains infinitesimal. However, if the signal frequency exceeds a certain value, the control collapses and the system oscillates with an attenuated amplitude of arbitrary phase shift. The abrupt breakdown of the main stage control quality is caused by the I-dominance of the main stage controller. Due to the binary integrand of the STA (cf. equation (4.14)), the control input $u_{I,ms}$ only has a constant rate of change as already indicated in figure 7.11. Once the cutoff frequency is exceeded, the main stage controller is not able to generate a pilot valve's trajectory to distribute the oil flow into the control chambers properly such that no reasonable response is generated. Thus, it can be reasoned that the cutoff frequency of the cascaded system only rests upon the parameterization of the main stage controller and the system does not comprise any significant tracking error as long as the cutoff frequency is not exceeded.

The fastest possible response of a cascaded SM controller for a main stage valve is achieved if the following conditions are fulfilled:

- the pilot valve is excited by a continuous signal u_{ms},
- the pilot valve remains in sliding motion for arbitrary signals of u_{ms},
- a sliding mode breakdown of the main stage valve does not cause a sliding breakdown of the pilot valve.

The first two points are directly addressable by the parameterization of the main stage controller and thus, limiting the dynamics of u_{ms}. It has to be guaranteed that the inner loop does not sustain a breakdown because in that case, the outer loop sustains a breakdown as well since no proper adjustment of the oil flows is feasible and the overall control collapses.

7.5. Discussion

This chapter investigates the sliding mode control of different hydraulic valves experimentally. To determine the optimal control parameters, multi-objective HiL optimizations of the system's responses are carried out for predefined reference steps. Different properties of the multi-objective HiL optimization, as well as the properties of relative degree mismatches, are investigated on the control of a pressure relief valve. For this, specific solutions of a broad Pareto solution set are compared to each other to inquire into the different influences of the objectives being used for the optimization of the control gains. From the algorithm's perspective, there are several different realizations obtained that are all equivalent to each other. However, as outlined, some of them are oscillation-affected such that they are not compliant with the process expert's requirements. Additionally, it is shown that an estimation of the system's order can lead to chattering since a relative degree mismatch between structural assumption and the real system is given. The use of *quasi* SOSM control proves to alleviate this chattering even if a conventional STA is not able to attenuate the chattering sufficiently. The benefits and properties of nonlinear sliding surfaces are investigated on the control of a directional control pilot valve. A control using a linear sliding function is affected by long reaching phases compared to the sliding phase. This exposes the system to disturbances for a comparably long time and the robustness properties of SM controllers are not given. To maximize the sliding phase and to increase the robustness without decreasing the convergence time, the nonlinear SPA surface has proven to be a valuable method. In addition, the SPA approach also outlines its properties to accelerate the closed loop system since it adjusts the convergence rates at runtime. Compared to the nonlinear TOS surface that rests upon the time optimal motion planning, the SPA shows improved system motions since it does not comprise oscillations at the steady-state position due to limited slopes on the sliding surface.

The cascaded control of a main stage directional valve being actuated by the previously discussed pilot valve examines two facts. On the one hand, the precise control of the main stage valve requires an accurate and fast small range response of the pilot valve. As illustrated, the pilot valve using the STA and SPA method also performs very accurately under real conditions so that a precise position of the main stage's piston is possible. On the other hand, it is explained that the cutoff frequency of a main stage valve with cascaded SM controller only is defined by the pilot controller's gains. As long as the excitation frequency remains below the cutoff frequency, the valve does not comprise any phase shift or tracking error.

8

Experimental Evaluation of Adaptive Valve Control

While the previous chapter 7 investigates the robust SM control of hydraulic valves, the given chapter focuses on the adaptive self-tuning possibilities of advanced sliding mode controllers. As outlined, the parameterization of the robust controllers is carried out by evolutionary HiL-optimizations. Since a multitude of system responses have to be measured in physical experiments, this approach is time-consuming but, though, leads to an optimal solution for the given setup. To accelerate the parameterization process, several approaches are applicable. One possibility is to estimate the control gains of the STA beforehand by approximating the system's Lipschitz bound L. Thus, the gains α_0 and α_1 are immediately known as shown in equation (4.16). This relation, however, only reduces the optimization problem by one dimension and since the Lipschitz bound L cannot be approximated if no precise model is deduced; this possibility only comprises minor advantages to accelerate the parameterization. A different process is investigated by Krimpmann et al. (2016c). Based on a highly accurate model of the desired valve, the entire parameter optimization process is carried out in simulations. The simulative experiments can be performed in parallel, or their execution is much faster compared to real measurements. Therefore, the optimization is far more quickly than using physical experiments. As a positive side effect, the application of unstable controller settings does not cause the risk of damaging real valves that may only be available as cost-intensive prototypes in early development stages. To obtain these advantages, an accurate system model needs to be known. For this, a complex modeling process or in case of known model structures, parameter optimizations are mandatory, but certainly, this does not simplify the parameterization process.

In contrast to the HiL-optimization of a robust controller, the self-tuning of an adaptive controller leads to optimal gains within a fraction of time and the ability to adapt to different application tasks. The use of such adaptation strategies not only accelerates the development process of industrial devices but also enables new marketing strategies. More and more customers demand an individual configuration of their devices for specific applications and the possibilities to adjust the properties of the controller. By using adaption techniques, the customers can set up the bought devices to their specific needs and use cases such that they can use their own configuration instead of the delivered one being designed for a most general use case. The use of adaptive

systems enables such possibilities since they always guarantee stable system dynamics. The direct variation of control gains may lead to unstable or harmful results, and thus, the customer is not desired to vary the gains directly.

The setup that is used to investigate the properties of adaptive SOSM controllers is comparable to the one shown in figure 7.1. Now, the *optimizer* block is omitted and the control parameters $\boldsymbol{\theta}$ are determined by the *adaption* block. The investigations are carried out for periodic reference signals of constant frequency, and the absolute values of all initial parameters $\boldsymbol{\theta}(t = 0)$ are selected arbitrarily small. Initially, the adaption of the linear and nonlinear sliding surfaces are investigated while the set law gains are selected constant. In a second step, the adaption of the set law is studied regarding finite-time and asymptotic convergence, and in a final step, the combined self-tuning of the sliding surface with a conjoined adaption of the set law is outlined.

8.1. Lyapunov-based self-tuning of sliding surfaces

The given section focuses on the practical evaluation of the self-tuning functionality of sliding surfaces. In literature, dominantly the well-known tuning of the sliding mode set law is discussed in excess while the sliding function is not considered except by single approaches for specialized applications (cf. section 1.2). The newly introduced Lyapunov-based self-tuning is a general solution to the given problem and in the following; it is investigated for the application to the directional control pilot valve (cf. section 2.2).

To investigate the properties of the sliding surface adaption solely, the control gains of the STA set law remain unchanged during the experiment. Since the valve has already been evaluated for HiL-optimizations, an optimal parameterization of the STA (cf. table 7.3) is known and reused for the following experiments. To maintain the comparability of the results, again the valve is supposed to perform a sequence of constant symmetrical steps. Figure 8.1 depicts the self-tuning process of a linear sliding surface as discussed in section 3.1. The top diagram shows the reference piston position x_{ref}, the valve's response x and the mean square control error e_{av}. The lower diagram shows the rise times $T_{r,90}$ for each step of the sequence and additionally, the progress of the design parameter λ is depicted. Following equation (3.6), λ is identical to λ_1 being the dominant pole of the sliding dynamics. Since the sliding function is of second order, λ_2 needs to be determined. It is intended to define the dynamics by adjusting $\lambda \equiv \lambda_1$. Thus, the influence of the second pole λ_2 is reduced by shifting its position far left by $\lambda_2 = c_1\,\lambda_1$, $c_1 = 15$.

For the initial step, the system does not show any responses since the adaption process is not enabled yet and the initial value of the design parameter is chosen as $\lambda(0) = 0$. After the first step, the adaption is enabled as can be seen in the progress of λ. From now, the valve shows reactions. Within the first two steps, the responses seem like a drift since it is opposed to the reference. This can be traced back to the comparable small values of the sliding function's parameters only causing a marginal control input u. However, from the second period on the design parameter λ is suffi-

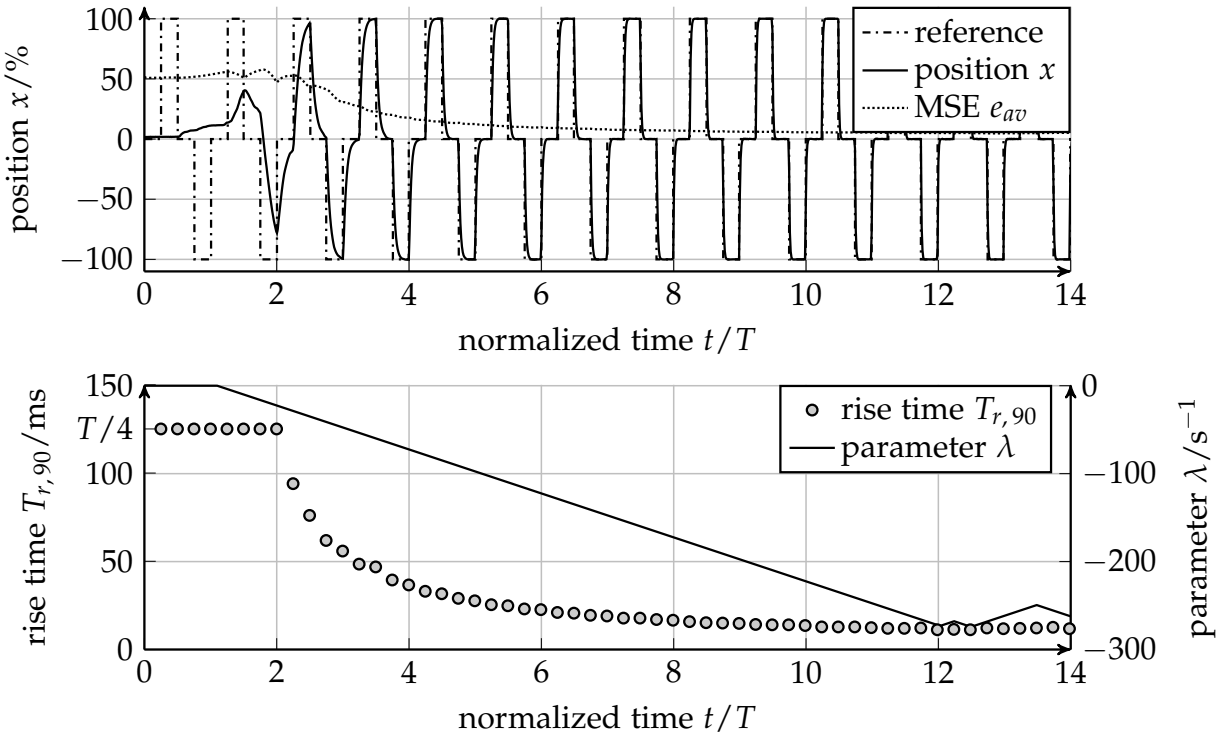

Figure 8.1.: Adaption progress for a linear sliding surface.

ciently large to enforce a movement into the correct direction, but the convergence is still too slow to settle within the given time interval. The progress of the rise time $T_{r,90}$ indicates that the adaption achieves the first proper response after little more than two reference signal periods. From this point, the rise times decrease continuously until they converge after a short time. This also reduces the moving average of the control error e_{av} that is chosen as the adaption signal. As long as $e_{av} > \delta_e$, the design parameter λ is decreased and the system's response is accelerated. Due to the moving average filter, the adaption acts slightly delayed such that the adaption does not change or stop instantaneously at the desired control quality. Since the average filter incorporates the past performance, λ still is decreased while actually a switching action should have taken place. This causes a limit cycle around the desired value of $\lambda(t \to \infty)$. This limit cycle continuously adjusts the closed loop dynamics. The influence, however, can be reasoned as insignificant as the rise times $T_{r,90}$ indicate. The variation of rise times within the last two periods of the progress is of approximately 5.36 % around the mean rise time.

Figure 8.2 depicts the adaption process of the nonlinear SPA surface. For the SPA surface, the design parameter λ represents the maximum dominant eigenvalue $\lambda \equiv \lambda_{1,\max}$ (cf. equation 3.17) that is equal to the smallest possible value of the dominant root. The scaling factor $c_1 = 15$ is chosen equal to the prior experiment and the adaption rate κ is selected identical. The prevalent difference in the given system response for an equally initiated controller ($\lambda(0) = 0$) is that the controller can reach the reference from the first step. This is traced back to the control error depended adjustment of the sliding function parameters of the SPA surface. While initially, the response is rather slow, the

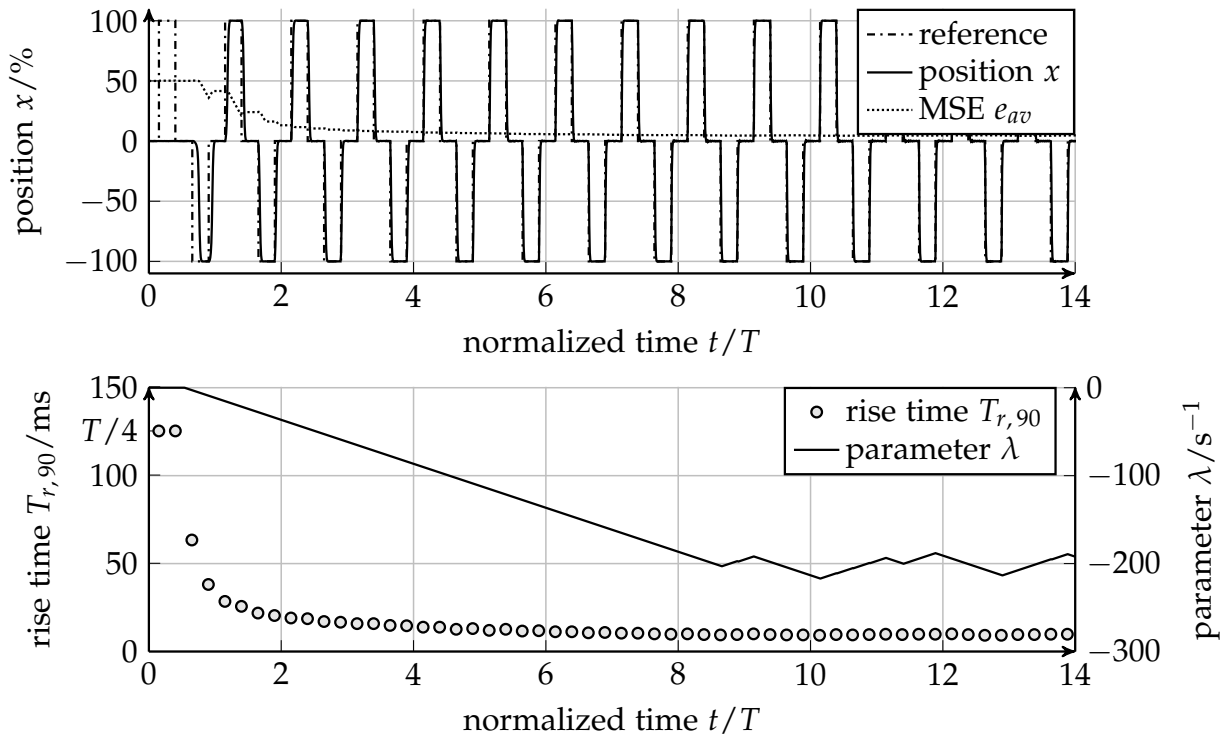

Figure 8.2.: Adaption progress for a SPA sliding surface.

piston position does not drift unexpectedly. The progress of the rise time values $T_{r,90}$ indicates a rapid acceleration of the system's dynamics since the values remain rather constant after three periods of the reference signal x_{ref}. Nevertheless, the value of the design parameter λ still is increased since the desired control quality defined by δ_e not jet is reached. After some periods, the average control error e_{av} is minimized such that $e_{av} \leq \delta_e$ and hence, the design parameter λ enters a limit cycle. Within this limit cycle, the rise times vary in a range of at maximum 5.26 % around the mean value. As outlined in section 7.3, an optimized nonlinear SPA surface leads to higher system dynamics compared to a linear sliding function. Therefore, the predefined adaption threshold δ_e can be lowered since the system enters the steady state earlier. For this example, the value of δ_e for the SPA surface is reduced by 10 % in relation to the value of δ_e used for the linear surface.

As the presented results show, Lyapunov-based adaption methods can be used for self-tuning of sliding functions. For a predefined desired control quality – in this case, quantified by a moving average control error e_{av} – the adaption law leads to an optimal parameterization of the sliding function within a fraction of the time that is used for an evolutionary optimization as outlined in section 6.3.

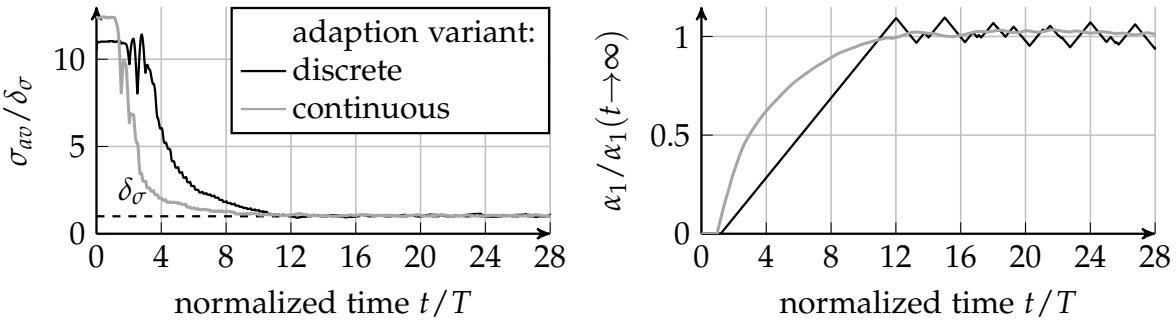

Figure 8.3.: Comparison of different adaption processes using continuous and discrete parameter adjustments for a sequence of reference steps. Left: deviation, right: parameter.

8.2. Lyapunov-based self-tuning of the SOSM controller

In the following, the self-tuning of the STA algorithm is investigated. For general investigations on adaptive SMC and adaptive SOSMC, the reader e.g. is referred to section 4.3 or Plestan et al. (2010) and Shtessel, Taleb, and Plestan (2012). In literature, dominantly the discrete finite-time parameter adjustment is discussed that utilizes binary derivatives of the control parameters as shown in equation (4.17) where the derivative of the control gain $\dot{\alpha}_1 \propto \omega_1$ is proportional to a given rate factor ω_1. In general, this adaption is goal leading in case of being the only adaption process that is carried out at a time. Comparable to the adaption of the sliding surfaces outlined in the previous section, this adaption process finally results in a limit cycle of the control gain α_1 around the terminal value $\alpha_1(t \to \infty)$. The described limit cycle is depicted in figure 8.3 that presents the progress of the adaption signals σ_{av} and control gains α_1 of self-tuning processes for a sequence of reference steps of the directional control pilot valve (cf. section 2.2). By increasing the control gain α_1, the average sliding accuracy σ_{av} is increased such that the value approaches the threshold δ_σ after approximately 11 periods. From this point, the discrete adaption remains in a limit cycle causing the zigzag-shaped progress of the control gain. Due to this jitter, the system behavior also varies slightly.

However, considering a multi-staged adaption process to obtain not only optimal sliding motion but also optimal closed loop dynamics there are at least two cascaded adaption processes. While the inner faster one preserves optimal sliding motion, the outer slower one establishes optimal closed loop dynamics. Thus, the inner one does not need finite-time convergence if the outer one is finite-time convergent. Consequently, a continuous adjustment of the STA control gain α_1 as also shown in figure 8.3 is reasonable. In the given example, the adaption law $\dot{\alpha}_1 = \omega_1 \left|\sigma_{av} - \delta_\sigma\right| \sqrt{0.5\,\gamma_1}\,\mathrm{sign}\left(\sigma_{av} - \delta_\sigma\right)$ is applied. While having practically the same convergence time, the convergence itself is not guaranteed since the derivative of the subordinate Lyapunov function is only negative semi-definite (cf. section 3.4). For the practical application, nevertheless, the adaption is smoother than the discrete one and does not cause a jittering behavior. Further, the finite-time convergence often only is a theoretical concern because the real processes are noise-affected and the control design rests upon simplified assumptions for the sake of a simplified control design.

8.3. Combined adaption of sliding surfaces and second order sliding mode controllers

As the previously discussed adaption laws reveal, the self-tuning of control parameters only focuses on single aspects of the control quality. For SMC, the control quality not only is given by the closed loop dynamics, e.g., characterized by rise times and steady state deviations but also by the sliding accuracy. The sole adaption either of the sliding surface or the STA gains, thus, does not lead to an overall optimal behavior. Compared to the multi-objective HiL optimization, the adaption methods accelerate the parameterization. However, they do not result in an overall optimized behavior. Hence, the consequential step is to combine both – the sliding surface and the control gain – adaptations.

Obviously, the set law, e.g., the STA, shall realize the desired sliding accuracy for any given but plausible sliding function. To do so, the adaption of the control gains as outlined in section 8.2 should be converged or rapidly compensate deviations from the desired sliding accuracy defined by δ_σ. In case of varying sliding function parameters; the system should not sustain a breakdown of sliding motion that leads to a loss of robustness. Thus, the adjustment of the sliding function has to be comparable slow with regard to the adjustment of the control gains. Otherwise, an adequate tracking of the predefined dynamics is not feasible. Consequentially, the combination of the sliding function self-tuning and the control gain adaption is understood as a cascaded adaption process at which the inner cascade is the control gain adaption, and the outer loop adjusts the sliding function.

As illustrated before, both adaptations result in discrete limit cycles if finite time convergence is considered. In case of asymptotic convergence as shown in section 8.2, the limit cycles are attenuated. The finite time convergence of the outer adaption loop is reasonable to obtain an optimal closed loop behavior within a dedicated time interval. Due to the rather low adaption rate, the resulting limit cycle's amplitude of the sliding function parameter $\lambda(t)$ remains low, and thus, the jitter in the control quality also is small. However, the control gain adaption utilizes higher convergence rates and stays in a quasi-converged state. Thus, the parameter $\alpha_1(t)$ remains in a strong limit cycle in case of finite time convergence that is reflected in a jittering sliding accuracy as well as a slightly varying closed loop dynamics. However, the finite time convergence is not necessary for the inner adaption since it only shall realize the desired accuracy. Due to the quasi-convergence of the adaption, the convergence time is negligible. In the following experiments, these properties are investigated in detail. The combined adaption initially is evaluated for the self-tuning process of linear sliding function and the STA being applied to the directional control pilot valve. Initially, the sliding function gain is selected as $\lambda(0) = 0$ and the control gain is chosen as $\alpha_1(0) = 5 \cdot 10^{-5}$; the ratio between the eigenvalues λ_1 and λ_2 is $c = 15$. Reference signal x_{ref} is identical to the signal shown in figures 8.1 and 8.2. During the following experiments, the adaption thresholds δ_σ and δ_e are constant to achieve the best comparability.

Figure 8.4 presents the obtained results for a finite time convergent adaption of the sliding function using discrete adaption rates of $\dot{\lambda} = \pm\kappa$. On the left part (figure 8.4a),

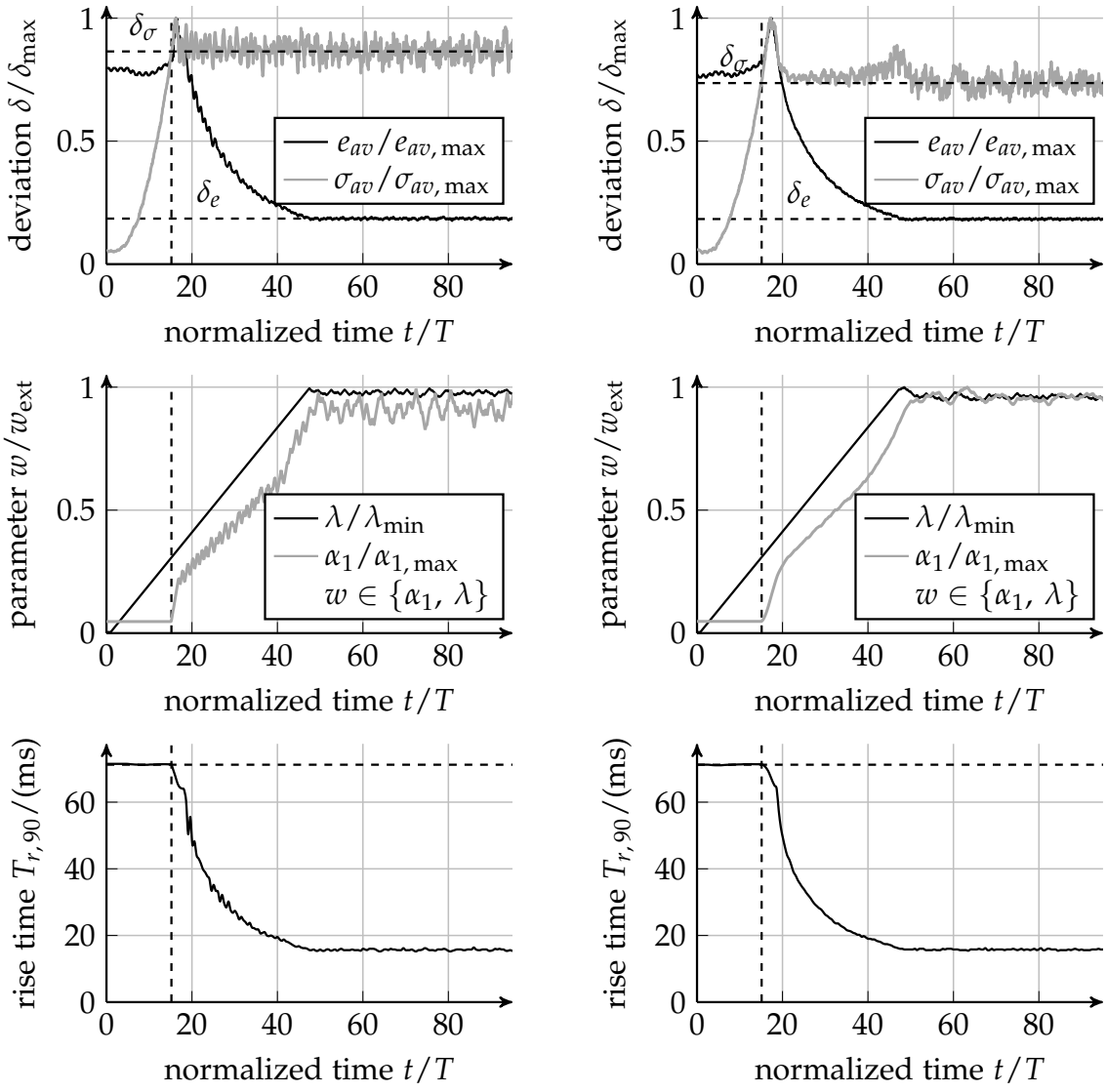

(a) $\dot{\lambda}$ discrete, $\dot{\alpha}_1$ discrete (b) $\dot{\lambda}$ discrete, $\dot{\alpha}_1$ continuous

Figure 8.4.: Progress of combined adaptations of sliding functions and STA controllers for different adaption strategies.

a finite time convergent self-tuning of the STA is applied that uses a discrete derivative $\dot{\alpha}_1 \in \{\dot{\alpha}_1^-, \dot{\alpha}_1^+\}$; on the right half (figure 8.4b), an asymptotically convergent adaption with continuous $\dot{\alpha}_1 \in \mathbb{R}$ as described in section 8.2 is applied.

Initially, both experiments have large average control errors e_{av} but only small average deviations from the sliding mode σ_{av}. This is due to the small initial values of the controller not causing a sufficient control input i_{ref} for the valve. Because of the large value of $e_{av} > \delta_e$, λ is increased constantly in both cases, however, α_1 remains unchanged because the average sliding accuracy is smaller than the threshold ($\sigma_{av} < \delta_\sigma$). Obviously, there is hardly any reaction, and thus, no real sliding motion is evident. After approximately 16 periods, the slope of the sliding surface is sufficiently increased such that the average sliding accuracy is below the desired one ($\sigma_{av} > \delta_\sigma$) and α_1 is increased. The discrete STA tuning as shown on the left immediately remains at the

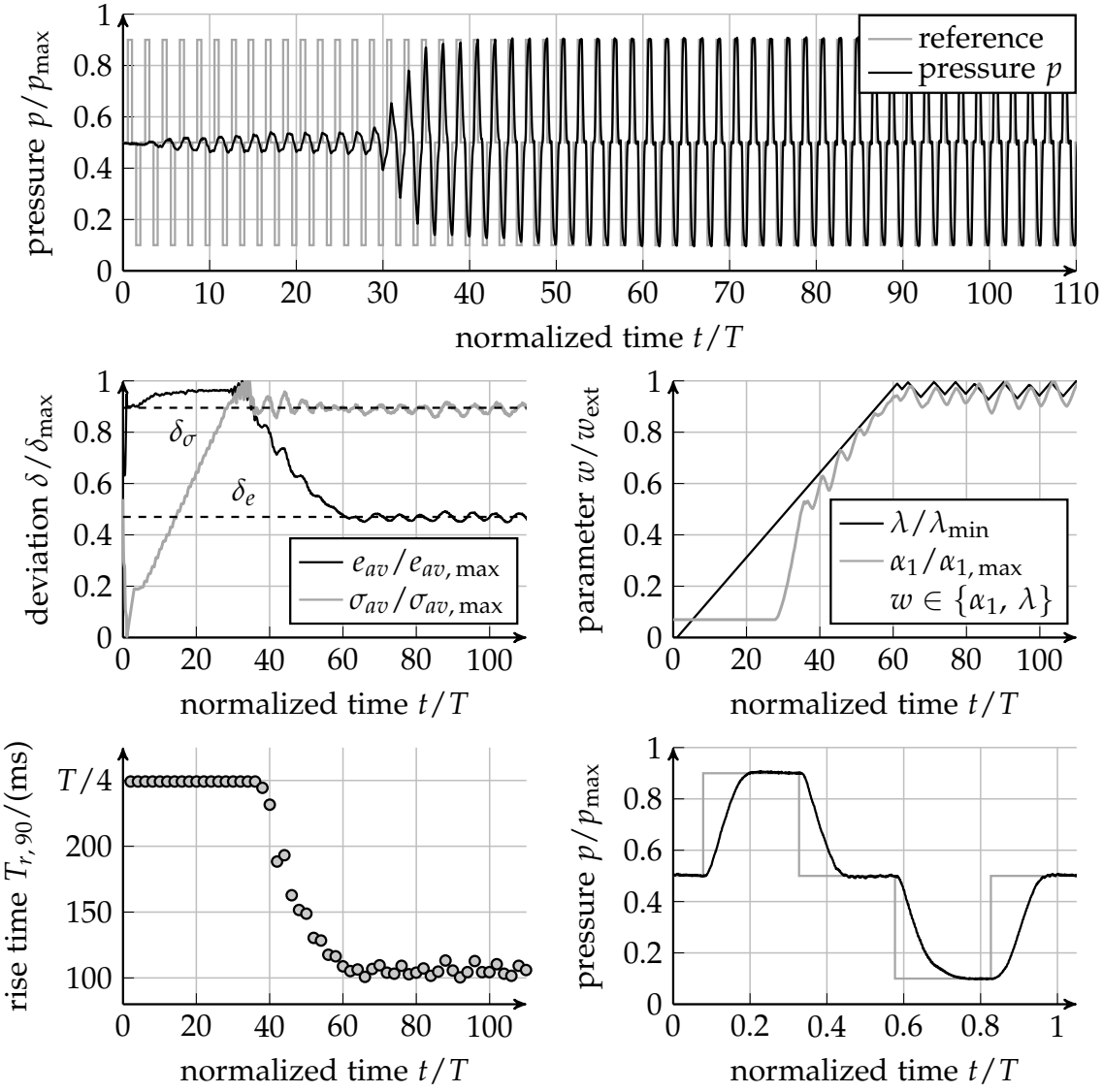

Figure 8.5.: Adaption progress for a combined sliding surface and qSTA controller.

desired accuracy since σ_{av} oscillates around δ_σ. To maintain the sliding accuracy, the control gain α_1 shows a non-smooth progress ending in a strong limit cycle. As the non-smooth descend of e_{av} and the rise time $T_{r,90}$ indicate, causes the limit cycle of α_1 a variation in the closed loop dynamics. This effect is adverse regarding an optimal closed loop behavior. Contrarily to the discrete modification causes the continuous adaption of α_1 an increased behavior as shown in figure 8.4b. The continuous adaption of α_1, however, does not lead to a sliding accuracy that is as accurate as before. However, the limit cycles of α_1 and subsequently of λ are attenuated and thus, the closed loop dynamics are not comprised by a jitter which is a remarkable improvement of the control quality.

Figure E.3 shows the adaption processes for a continuous adjustment of $\dot{\lambda}$. While the behavior of the control gain adaption is rather identical, the continuous adjustment of the sliding function initially leads to a rapid acceleration of the system's dynamics. However, due to the small deviation from the desired average control error δ_e, the latter

change in dynamics is rather slow such that the adaption results in creep processes. The continuous adaption of λ may lead to a further reduction of the dynamics jitter; however, the missing finite time convergence is a drawback for the design process.

A stronger influence of the jitter can be outlined in the application of the adaption process to the pressure relief valve that is controlled as described in section 7.2. The adaption process is identical to the already discussed one with discrete adjustment of the sliding surface and continuous adjustment of the qSTA controller. Due to the reduced system dynamics, the adaption is carried out with reduced adaption gains; thus, the convergence rate is reduced. Nevertheless, strong limit cycles are given after either the inner control gain adaption or the outer slower sliding surface adaption have converged. Now, the jitter is significantly visible in the variation of the rise times $T_{r,90}$ as shown in the lower left diagram of figure 8.5. The limit cycles cause variations of up to $\pm 6.45\,\%$ in the values of $T_{r,90}$ resulting in an inhomogeneous closed loop dynamics.

Nevertheless, the application of self-tuning strategies leads to an optimized closed loop behavior within a fraction of time compared to the evolutionary HiL-optimizations. As shown at the top of figure 8.5, the adaption process leads to proper step responses within less than 100 periods whereby one period lasts less than one second. Initially, the response is arbitrarily small due to the idle control gain adaption, but once the sliding surface is parameterized sufficiently, the responses grow significantly, and the desired behavior is reached rapidly.

8.4. Discussion

This chapter experimentally investigates the Lyapunov-based self-tuning strategies of a sliding mode controller. The objective of the adaption strategies is to replace long lasting manual design processes or time-consuming HiL optimizations by methods that estimate suitable control gains for a certain control quality measure within a short time. To enforce sufficient excitation to realize a well-performing self-tuning process, a repeating sequence of different amplitudes is used as the reference signal.

Initially, the adaption of the sliding surfaces is investigated. The sliding surface defines the closed loop dynamics of the set law is parameterized adequately. By adjusting the surface parameters, the system's response to the given reference is adjusted, and hence, the average control error e_{av} is varied. By defining a certain threshold for the average control error, the desired closed loop dynamics are defined. The illustrated experiments evidently indicate the possibilities of the outlined self-tuning process. While the adaption of the linear sliding surface leads to a converged behavior within a longer time interval, the adaption of the SPA surface, however, leads to converging step responses from the initial step while only the responses are still accelerated. In a second evaluation, the known adaption of the STA is evaluated briefly regarding finite time and asymptotic convergence. While finite time convergence leads to limit cycles of the control gains, the asymptotic convergence into sliding mode practically settles within the same time interval and does not comprise significant limit cycles. Thus, the ongoing parameter variations are rather small and do not cause a jittering system behavior.

The Lyapunov-based adaption of the sliding surface and the STA only consider the parameterization of one disjunct part of the sliding mode controller. To solve the bootstrapping dilemma of a fully parameterized controller, both adaption methods are combined into a cascaded adaption scheme that adjusts the STA in an inner fast adaption loop to realize sufficient sliding accuracy for arbitrary sliding functions while the sliding function is adjusted in an outer slow adaption process. As the experimental investigations reveal, achieves this combined approach system responses with desired closed loop dynamics and sliding accuracy. For this, only the adaption thresholds need to be defined instead of a further parameterization.

Nevertheless, the adaption process is limited by some properties. A loss of sliding motion due to a variation of the sliding surface caused by the adaption has to be prevented since this causes an undesired system behavior. Thus, for a change of the sliding surface, the system has to remain in sliding motion. Obviously, this only is realized if the subordinate STA adaption is much faster than the surface adaption so that the STA tuning is converged. The adaption process demands a certain minimum excitation such that the average control error e_{av} and the average sliding function σ_{av} are not arbitrary small. In case of smooth, slow or even static reference signals, there is not enough excitation, and the adaption does not lead to the desired behavior. Thus, a sufficient excitation is necessary. The outlined adaption processes shall be understood as a powerful tool to obtain high control quality within the manufacturing or commissioning of the hydraulic devices. Once the desired behavior is established, the control gains are supposed to be fixed for the latter application. Due to the robustness properties of the SMC or SOSMC, the closed loop behavior remains unaffected to outer perturbations or changing use cases.

9

Summary, Conclusion and Outlook

Nonlinear effects like friction or flow forces as well as unknown or time-varying system parameters are often discussed as undesired effects for control design. The driving force behind this thesis is to deduce control strategies to cope with these nonlinear effects and uncertainties as well as to provide methods for a fast and easy parameterization of the utilized controllers. For this, control strategies and observers for electro-hydraulic valves as dedicated examples of mechatronic systems are designed based on the sliding mode principle. The presentation, as well as the evaluation of these controllers particularly, focuses on the practical examination on real world experimental test benches to demonstrate the high practical relevance of these approaches and their ease of applicability.

Summary and concluding remarks

This thesis contributes new theoretical concepts of defining the closed loop dynamics for increased system dynamics compared to state-of-the-art approaches as well as procedures to extend these concepts originally being designed for robust controllers to be equipped with adaptive self-tuning features to replace time-consuming parameterization processes by automated procedures. Additional to the extensive practical evaluation of the presented concepts, the combined adaptive sliding mode controller is discussed for the first time while previously in literature only single parts of the control structure have been designed adaptive. The chosen methodology and major results of this thesis can be summarized as follows.

Experimental setup and valve dynamics

Considering the prevalent opinion on precise modeling of hydraulic valves, the use of CFD and finite elements models is the only way to obtain precise simulation models. However, these models are disadvantageous in case of control theoretical investigations. Thus, for the SMC design, the directional control and pressure relief valves are investigated based on first principle approaches to deduce rough approximating models to describe the system behavior. For the directional control valves, the system orders are determined by measuring the frequency response while the pressure relief valve is modeled more accurately with a subsequent model based order reduction.

Robust control using sliding modes

To obtain highly accurate and robust control of the different valves being approximated by coarse system models with inaccurate or unknown parameters, the sliding mode control principle is followed. By using discontinuous switching actions, these controllers stabilize the systems on predefined manifolds within the state space and realize invariance against perturbations like load or flow changes. However, these discontinuous high frequent switching actions also excite unmodeled or neglected higher order dynamics like actuator or sensor dynamics. The excitation of these dynamics causes a relative degree mismatch and leads to oscillations that are known as chattering. To compensate the chattering effects, the properties of higher order sliding modes are outlined which hide the discontinuous switching action in higher derivatives of the sliding functions and thus, provide effective cancellation of harmful oscillations.

Nonlinear sliding functions and Lyapunov-based self tuning

In case of SMC design for mechatronic systems, conventionally the switching manifold leads to linear closed loop dynamics, e.g., a linear first or second order differential equation of the control error. To increase the closed loop dynamics the use of time-varying sliding surfaces is a well-known approach. This approach, however, demands precise and linear system descriptions such that these approaches are not robust against model inaccuracies or are applicable for nonlinear systems. The approach outlined in this thesis follows a successive adjustment of the roots of the characteristic polynomial of the closed loop system in dependence on the control error. In case of significant errors, the convergence rate of the system is reduced to prevent a loss of sliding motion and maintain stability while the convergence rate is increased for small control errors to compensate them faster, and thus to accelerate the system. The novel approach rests upon an analytic formulation and does not need any numerical inversions or memory-consuming look up table implementations.

While the theoretical evaluation of SMC concepts is straight forward, the parameterization of those concepts for practical applications is a crucial task. By using Lyapunov's direct method, the stability properties of sliding functions are investigated and an intuitive adaption rule is deduced such that either the linear or the novel SPA surface become adaptive. The aim of the adaption process is the minimization of the average control error. By using certain convergence properties, the optimal closed loop performance is obtained within a finite time interval.

Experimental evaluation of robust and adaptive control

The extensive practical evaluation of the SMC for the electro-hydraulic valve control is separated into two major parts. Firstly, the non-adaptive robust control of reference steps is investigated. By using hardware-in-the-loop optimizations, the control gains are determined in practical experiments, and the system behavior for different sliding functions is compared. Theses evaluations clearly indicate the superior performance

obtained by the nonlinear SPA sliding surface. The second major investigation focuses on the adaptive self-tuning methods. The ease of parameterization by using the Lyapunov-based self-tuning is highlighted. The time-consuming HiL-optimizations or complex manual design processes can be replaced entirely by the adaption process that leads to optimal parameterization within a fraction of time. Either the adaption of the sliding surface or the self-tuning of the set law converge within short time intervals. As an additional novelty, the combined self-tuning of the sliding function with a subordinate adaption of the set law is presented and constitutes the first combined adaptive sliding mode controller. Using the SMC methods in conjunction with adaption techniques instead of manual selection or HiL-optimization converts the parameterization problem into a selection of performance indices that can be interpreted easily by any control engineer.

Outlook

Further investigations of the sliding mode control concept, which is presented in this work, may build on the promising experimental results. They outline the applicability to a wide range of different hydraulic systems and, thus, it is reasoned that the concepts are also applicable to entirely different settings. One particular example may be the joint angle control in lightweight and flexible robotics as discussed e.g. by Malzahn (2014). The joint dynamics strongly depend on the joint angle configuration of the robot. Therefore, the dynamics can vary in a wide range. Often, conventional PI controllers are used for controlling the joint angles and the control gains are tuned empirically by applying well-known heuristics like the Ziegler-Nichols approach. Especially in lightweight and flexible robotics, the axis controllers are supposed to be accurate and asymptotically convergent such that overshoots induce no further oscillations in the robot's body. However, in case of configuration-dependent joint dynamics, the PI controllers are not able to provide comparable closed loop dynamics for the joint positioning. As a solution to the variant dynamics, the SMC can be an attractive possibility to reduce the amount of self-induced oscillations and to maintain constant closed loop dynamics instead of using bandwidth-limiting sinusoidal reference trajectories for a linear PI controller.

A

Design of First Order Sliding Mode Control

This chapter provides additional mathematical relations for conventional first order SMC as supplementary fundamentals for the interested reader. For detailed introductions to the general principles of SMC, is referred to DeCarlo, Zak, and Matthews (1988), Slotine and Li (1991), Utkin, Guldner, and Shi (2009), Edwards and Spurgeon (1998) as well as Young, Utkin, and Ozguner (1996) for a introduction to the practical application of first order methods.

A.1. Reaching conditions and control design

To ensure that a system remains in sliding mode $\sigma(\mathbf{x}) = 0$ after it has reached the sliding manifold, the existence condition has to be fulfilled:

$$\lim_{\sigma(\mathbf{x})\to 0^+} \dot{\sigma}(\mathbf{x}) < 0 \quad \text{and} \quad \lim_{\sigma(\mathbf{x})\to 0^-} \dot{\sigma}(\mathbf{x}) > 0. \tag{A.1}$$

This condition is fulfilled if a control law can be found that lets the system head towards the sliding manifold independent of the initial condition $\mathbf{x}(t = 0)$. In terms of Lyapunov's direct method, the existence condition can be expressed as a Lyapunov function

$$V(\sigma) = \frac{1}{2}\sigma^2(\mathbf{x}) \tag{A.2}$$

that exhibits the following properties:

$$V(\sigma) \in \mathbb{R} : \begin{cases} V(\sigma) = 0 & \text{for } \sigma(\mathbf{x}) = 0 \\ V(\sigma) > 0 & \text{for } \sigma(\mathbf{x}) \neq 0. \end{cases}$$

In sliding mode, $\dot{\sigma}(\mathbf{x})$ depends on the control and if the switched feedback gains can be selected so that

$$\dot{V}(\sigma) = \sigma(\mathbf{x}) \frac{\mathrm{d}\,\sigma(\mathbf{x})}{\mathrm{d}\,t} = \sigma(\mathbf{x})\,\dot{\sigma}(\mathbf{x}) < 0, \tag{A.3}$$

the sliding mode exists on $\sigma(\mathbf{x}) = 0$. It is reached after starting from any initial state and is restricted to the manifold for the further time. However, condition (A.3) only

provides asymptotic convergence into sliding mode. This is necessary but not sufficient for a functioning sliding mode control. Thus, the stronger so-called η-reachability condition (cf. e.g. Bhat and Bernstein 2000; Utkin 1992)

$$\dot{V}(\sigma) \leq -\eta\, V^{\rho}(\sigma), \quad \eta > 0 \tag{A.4}$$

$$T(\sigma) \leq \frac{1}{\eta\,(1-\alpha)} V^{1-\rho}(\sigma), \quad \rho \in (0 \quad 1) \tag{A.5}$$

is applied with $\alpha = 1/2$ that enforces finite time convergence into sliding mode in at least a time interval $T(\sigma)$. This condition provides a design rule to deduce a switching control law to obtain finite time convergence into sliding mode. One widespread implementation of such a control law is deduced by Gao and Hung (1993). Here, a continuous decrease of $\dot{\sigma}(\mathbf{x})$ along the trajectories of $\mathbf{x}(t)$ is demanded. Consider

$$\dot{\sigma}(\mathbf{x}) = -q\ \mathrm{sign}(\sigma(\mathbf{x})) - k\,\sigma(\mathbf{x}) \tag{A.6}$$

with positive values for the constants q and k. As one can see, the equation (A.6) fulfills the necessary condition

$$\sigma(\mathbf{x})\,\dot{\sigma}(\mathbf{x}) = -q\,|\sigma(\mathbf{x})| - k\,\sigma^2(\mathbf{x}) < 0. \tag{A.7}$$

Due to the selection of $\dot{\sigma}(\mathbf{x})$, the sliding function $\sigma(\mathbf{x})$ exhibits a constant increase of $\dot{\sigma}(\mathbf{x}) > q$ respectively a decrease of $\dot{\sigma}(\mathbf{x}) < -q$ even for rather small values of $|\sigma(\mathbf{x})|$. These constant adjustments lead to a finite time convergence into sliding mode as demanded by inequality (A.4).

By considering

$$\dot{\sigma}(\mathbf{x}) = \nabla\sigma(\mathbf{x})\ \dot{\mathbf{x}} = \mathcal{L}_f\sigma(\mathbf{x}) + \mathcal{L}_g\sigma(\mathbf{x})\ u, \tag{A.8}$$

in awareness of equations (1.1) and (3.1) one obtains the control law

$$u(\mathbf{x}) = -\frac{\mathcal{L}_f\sigma(\mathbf{x}) + q\ \mathrm{sign}(\sigma(\mathbf{x})) - k\,\sigma(\mathbf{x})}{\mathcal{L}_g\sigma(\mathbf{x})} \tag{A.9}$$

if equation (A.6) is incorporated and the control input u is isolated. By applying the derived control law, a given system is transferred into sliding mode within a finite time interval since the η-reachability condition is fulfilled. Due to the parameters q and k that can be selected arbitrarily, the control quality can be adjusted advantageously.

A.2. Equivalent control approach

The equivalent control introduced by Utkin (1971, 1972) is a method to describe the system dynamics in sliding mode by deriving a continuous control input u_{eq} that causes identical system motion as the discontinuous control input (1.2) so that a conventional solution for the differential equation (1.1) exists. It is assumed that for the initial condition $\mathbf{x}(t=0)$, the system lies on the sliding manifold $\sigma(\mathbf{x}) = 0$ and again, the uncertainty $\boldsymbol{\zeta}(t, \mathbf{x})$ is omitted. For any time, the system shall remain in sliding mode $\sigma(\mathbf{x}) = 0$ and hence, the condition

$$\dot{\sigma}(\mathbf{x}) = 0 \tag{A.10}$$

is true. The continuous control input u_{eq} is supposed to describe the sliding motion along the switching manifold. Thus, it can be derived by applying standard techniques. The approach by Utkin and Chang (2002)

$$\dot{\sigma}(\mathbf{x}) = \nabla\sigma(\mathbf{x})\ \dot{\mathbf{x}} \tag{A.11}$$
$$= \nabla\sigma(\mathbf{x})\ \mathbf{f}(t,\ \mathbf{x}) + \nabla\sigma(\mathbf{x})\ g(t,\ \mathbf{x})\ u_{eq} \tag{A.12}$$
$$= \mathcal{L}_f\sigma(\mathbf{x}) + \mathcal{L}_\mathbf{g}\sigma(\mathbf{x})\ u_{eq} = 0 \tag{A.13}$$

leads to

$$u_{eq}(\mathbf{x}) = -\frac{\mathcal{L}_f\sigma(\mathbf{x})}{\mathcal{L}_g\sigma(\mathbf{x})}. \tag{A.14}$$

Hence, the equivalent closed loop sliding motion is given by

$$\dot{\mathbf{x}} = \mathbf{f}(t,\ \mathbf{x}) + \mathbf{g}(t,\ \mathbf{x})\ u_{eq}(\mathbf{x}). \tag{A.15}$$

However, the resulting closed loop behavior is not a sliding motion in the original sense, since the control law does not comprise a discontinuity that separates two different control actions. Additionally, u_{eq} is the solution for an ODE instead of the differential inclusion $\dot{\mathbf{x}} \in \mathbf{F}(t,\ \mathbf{x})$.

A.3. Resume

The illustrated methods describe how the sliding mode can be reached and maintained for arbitrary initial conditions. All methods incorporate the same properties:

- The model of the system that is supposed to be controlled has to be known in detail and needs to be given in analytic form.
- The switching frequency of the control input is not limited and reactions of the control law can be applied without any delay.

However, both properties cannot be fulfilled for real applications. A system's model always is a simplified description of the real world system in which assumptions and simplifications have to be incorporated to achieve a manageable complexity. Oftentimes high-frequent sensor- and actuator dynamics are neglected or nonlinear friction effects are implemented as linear damping factors. These and further more simplifications prevent a highly accurate analytical model. The second property also cannot be fulfilled. Since digital control systems with fixed sampling rates emerged continuously and now are the default industrial solution, the control input only can be changed at given time instances. By using analog controllers consisting of operational amplifiers even though their reaction is not limited to a fixed frequency, the reaction delay still is present due to parasitic effects within the electrical devices.

In order to cope with the displayed limitations, chapter 4 introduces concepts to circumvent the limited switching frequency and to handle the absence of precise system models.

B

Additional Examples of hydraulic Valves

B.1. Pressure relief valve

Hydraulic pressure relief valves are electro-hydraulic devices that are used to limit the pressure within a hydraulic system e.g. as illustrated in figure 2.3. The cross sectional drawing in figure B.1 depicts the typical assembly of such a valve. As one can see, the pressure relief valve consists of an electrically actuated solenoid that generates a force on the armature plunger in dependence on the electrical current provided by the power electronics. By adjusting the force, the position of the valve cone that is attached to the armature plunger is regulated to achieve the desired opening. The resulting connection between the connecting pressure port P and the tank connection port T constitutes a bypass to the hydraulic system as shown in figure 2.3 and reliefs an oil flow from the hydraulic power supply back to the tank so that the overall system pressure is lowered. Thus, by regulating the electrical current, the pressure loss across the valve is adjusted in dependence on the provided oil flow and the volume of oil in the overall system.

Keeping the hydraulic pressure at a constant level is an essential criterion to obtain optimal performance of the hydraulic system on the application side. However, due to random load perturbations in the form of force or torque feedbacks on the actuators, there are unknown changes in the oil flow and the pressure provided by the hydraulic power unit. These influences lead to a varying pressure loss across the relief valve. From a conservative industrial perspective, the variations are tolerated. Traditionally, the hydraulic systems are designed rather robust with sufficient performance and robustness margins. Thus, the pressure relief valves commonly are operated in open loop control scenarios without any pressure feedback. However, the continuously increasing performance demands in conjunction with tightened financial budgets of the customers force the OEMs to reduce the design margins of their hydraulic systems and to improve the performance by incorporating advanced control techniques. As a consequence, the pressure relief valves have to be controlled to achieve a constant system pressure and thus, to provide optimal performance for the subsequent hydraulic actuators irregardless of occurring perturbations. While conventional and advanced PID control strategies emerged as state-of-the-art for directional control valves (see section 2.2), the pressure relief valves of the depicted type remain only feed forward

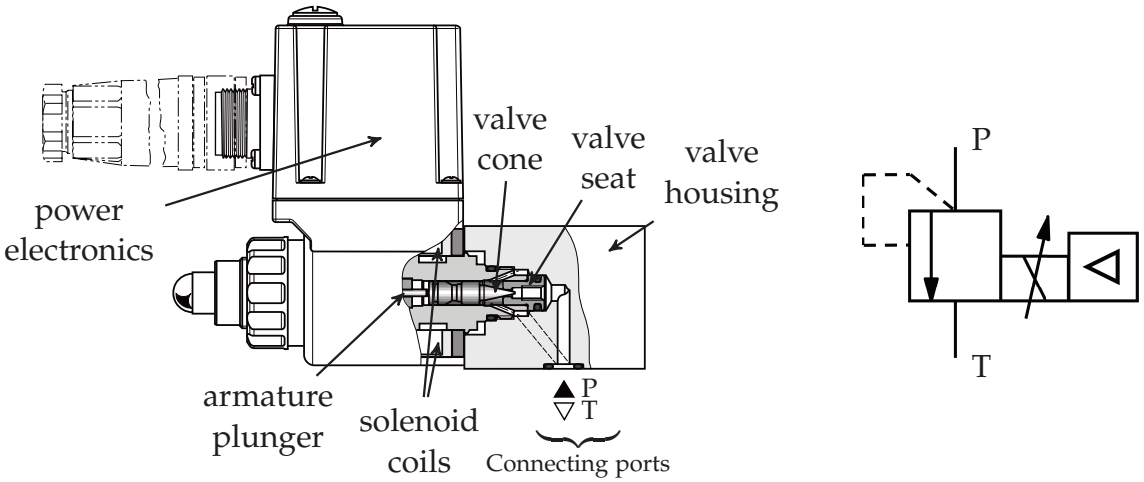

Figure B.1.: Cross sectional view and hydraulic symbol of a directly operated pressure relief valve (Bosch Rexroth AG 2013).

controlled. As a remark, there are position-controlled pressure relief valves using PID controllers while again, the pressure is adjusted by feed forward control. Those valves rest upon directional valve technology with a changed valve housing and from a purely technical perspective, the actuators are not comparable with the one shown in figure B.1. Krimpmann et al. (2016a) introduced a conventional PI controller in conjunction with a feed forward for the pressure control of a relief valve. However, this controller is taken as a benchmark for sliding mode based control concepts and does not intend to be a state-of-the-art controller.

In contrast to conventional PID controllers, the design of advanced state feedback control strategies, e.g., sliding mode controllers need in-depth knowledge of the inner working principles and dynamics of the system to be controlled. The relative degree of the plant or the perturbation bounds need to be known. Due to this, a physically inspired modeling and structural evaluation is reasonable to carry out before the control design. The model structure originally was developed by Abel (June 2016) during his master thesis.

Model of a pressure relief valve

The structure of a pressure relief valve can be partitioned as depicted in figure B.2 showing a structural diagram and working principles. The input voltage u_p is propor-

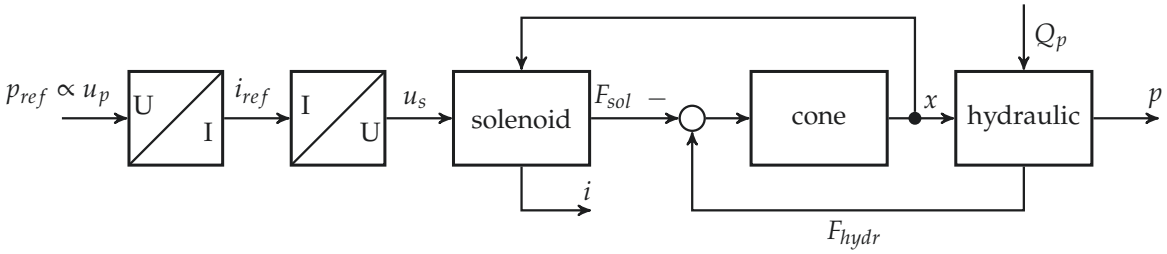

Figure B.2.: Working principle of a directly operated pressure relief valve.

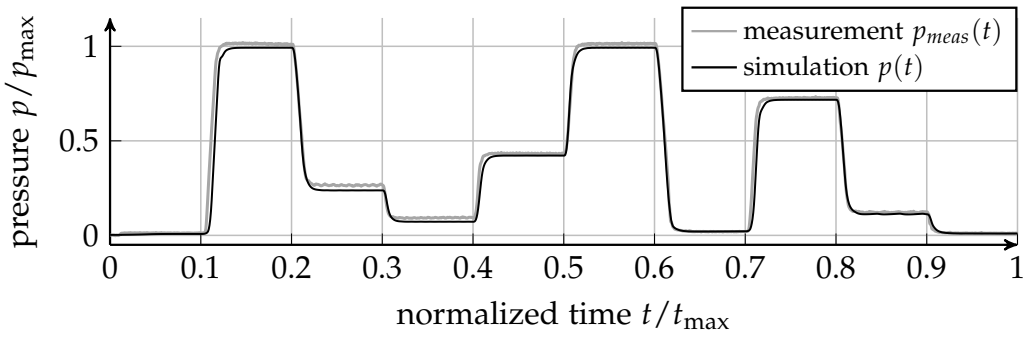

Figure B.3.: Comparison of measurement and simulation with optimized model parameters of a pressure relief valve for a sequence of reference current i_{ref} steps.

tional to a desired pressure p_{ref} for a predefined oil flow Q_p. The power electronics converts the input voltage into a desired electrical current i_{ref} by using a nonlinear characteristic curve. By using predefined duty cycles for certain values of i_{ref} the power electronics drives the solenoid current i by a pulse width modulated voltage u_s. Since the current i is measurable, the nonlinear dependence between u_p and i_{ref} is identifiable. Thus by inverting this relation, the reference current i_{ref} also can be understood as an input variable. The solenoid current i is superimposed by an additional dither signal to compensate stick slip friction effects of the mechanical parts. However, since the friction effects are omitted in the model, the dither also can be neglected.

In dependence on the current i and the cone's position x, the solenoid generates a pushing force F_{sol}. The force acts against the hydraulic force F_{hydr} caused by the oil flowing against the cone. Additionally, two control springs act against the solenoid and open the valve entirely if no current i is applied. Depending on the sum of forces, the cone is positioned with the velocity v and opens or closes the valve's orifice. If the orifice is small or closed, the oil is impounded, and the pressure p across the valve raises. By opening the orifice, the oil flows back to the tank and the pressure p is lowered.

Due to brevity, the complete deduction of the system model is shown in appendix C. By combining the differential equations of the separate sub-models, the complete model as depicted in figure B.5 is given in form of an analytic system with linear input (ALS):

$$\begin{aligned} \dot{\mathbf{x}} &= \mathbf{a}(\mathbf{x}) + \mathbf{B}\,\mathbf{u}, \quad \mathbf{x}(t=0) = \mathbf{x}_0 \\ p &= \mathbf{c}^{\mathrm{T}}\,\mathbf{x} \end{aligned} \tag{B.1}$$

with

$$\mathbf{x} = \begin{bmatrix} i \\ v \\ x \\ p \end{bmatrix}, \; \mathbf{a}(\mathbf{x}) = \begin{bmatrix} -\frac{L}{R}\,i \\ \frac{A_p}{m}\,p - \frac{d}{m}\,v + \frac{F_s(x)}{m} - \frac{F_{sol}(x,i)}{m} \\ v \\ -\frac{K}{V_d}\gamma\,C_d\,x\sqrt{\frac{2}{\rho}\,p} \end{bmatrix}, \; \mathbf{B} = \begin{bmatrix} 1/T_i & 0 \\ 0 & 0 \\ 0 & 0 \\ 0 & K/V_d \end{bmatrix}, \; \mathbf{c} = \begin{bmatrix} 0 \\ 0 \\ 0 \\ 1 \end{bmatrix}, \; \mathbf{u} = \begin{bmatrix} i_{ref} \\ Q_p \end{bmatrix}. \tag{B.2}$$

The unknown model parameters are determined by a genetic algorithm that minimizes the quadratic error between the model output p of an open loop simulation

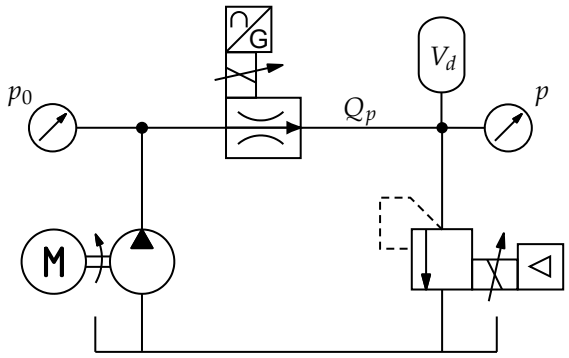

Figure B.4.: Simplified schematic diagram of the hydraulic setup.

and the measured pressure p_{meas} for a sequence of reference current steps i_{ref}. The optimized simulation result is shown in figure B.3. As can be seen, the simulation has a comparable transient behavior to the real system but partially shows inaccuracies for the steady state values. This effect is caused by the not optimized solenoid force $F_{sol}\,(i,\,x)$. Since this function directly implements the measured look-up table as shown in figure C.1 there remain solenoid force inaccuracies. The quantitative accuracy of the model is given by a fit value of 88.16 %. A model with a value of 100 % does not have any deviation while a model of 0 % only explains the mean value of the output.

As the evaluation of the structural properties of the system (B.2) indicates as shown in section C.2 that the pressure relief valve can be described sufficiently by a nonlinear second order system for the control design. Since the pressure p is measurable, this model simplification reveals that only one further state $\dot{p} = Q_d$ needs to be estimated by an observer instead of three unknown states of model (B.2).

To evaluate the properties and deduced controller of the pressure relief valve, the hydraulic setup as shown in figure B.4 is used. The setup consists of an axial piston pump providing a nominal pressure p_0. The oil flow Q_p is regulated by a pressure compensated flow control valve such that the pressure relief valve can be exposed to different flow rated. Between the flow control valve and the pressure relief valve, a chamber with a dead volume V_d is mounted to vary the system's stiffness. Right in front of the pressure relief valve, the pressure p is measured. Since the valve is directly connected to the tank, the pressure p is the pressure loss across the relief valve and thus, to be controlled the different SMC strategies.

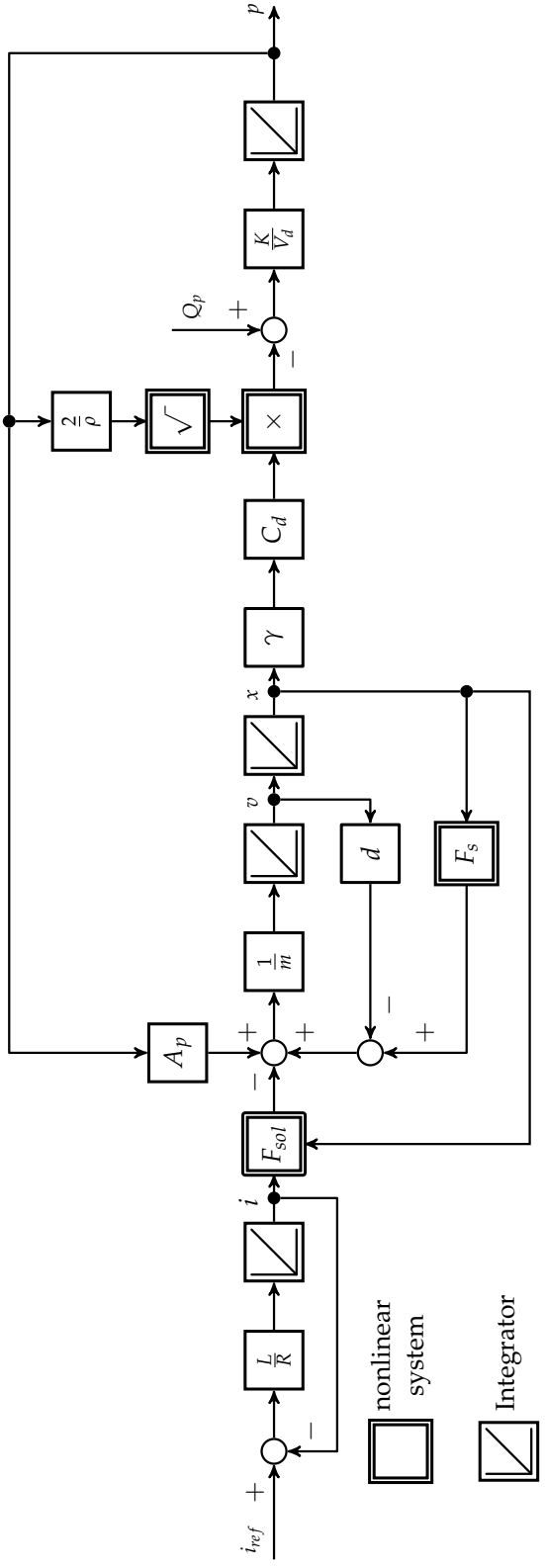

Figure B.5.: Block set diagram of a pressure relief valve.

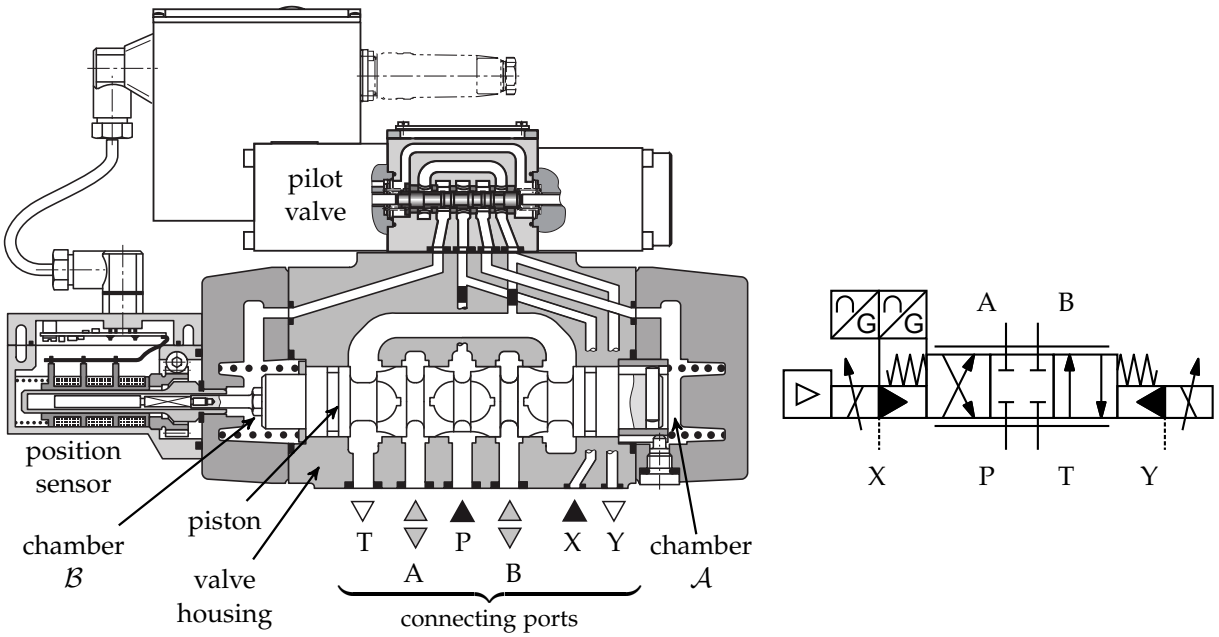

Figure B.6.: Cross sectional view and hydraulic symbol of a directional control main stage valve with attached pilot valve.

B.2. Directional main stage valve

Direct operated control valves as introduced in section 2.2 in general do not provide the capabilities to handle the hydraulic power as demanded in industrial applications. Their main benefits are given in a high dynamical bandwidth and good control quality. To handle higher hydraulic flows and thus a larger hydraulic power, these valves offer a too small throughput. To manage these loads, e.g., caused by large industrial presses, so-called directional main stage valves are used. A typical main stage valve is depicted in figure B.6 consisting of the passively actuated main stage valve shown in gray and a directly operated pilot valve. The main stage valve can be understood as a hydraulic amplifier that controls high hydraulic loads in dependence on a small hydraulic power that is regulated by a pilot valve. The pilot valve is supplied with a control pressure at the connecting port X while the main pressure supply is connected at port P. By adjusting the pilot valve's piston at the position x_p, the port X is connected to one of the two control chambers $\mathcal{A}$ or $\mathcal{B}$ of the main stage valve. Thus, for $x_p > 0$ the oil flows into chamber $\mathcal{A}$ while chamber $\mathcal{B}$ is relieved to the control outlet port Y. As a consequence, the pressure in $\mathcal{A}$ raises and causes a pushing force $F_{\mathcal{A}}$ which acts on the main stage piston head area A_h. In case of $x_p < 0$, $\mathcal{A}$ is relieved and in chamber $\mathcal{B}$, a counteracting pushing force $F_{\mathcal{B}}$ acts on the main stage piston. Thus, the main stage piston is adjusted at the position x_{ms} by mutual pressurization of the two control chambers depending on the pilot valve's piston position x_p.

The resulting working principle of a main stage valve is depicted in figure B.7 and indicates a fourth order system with two parallel acting nonlinear first order

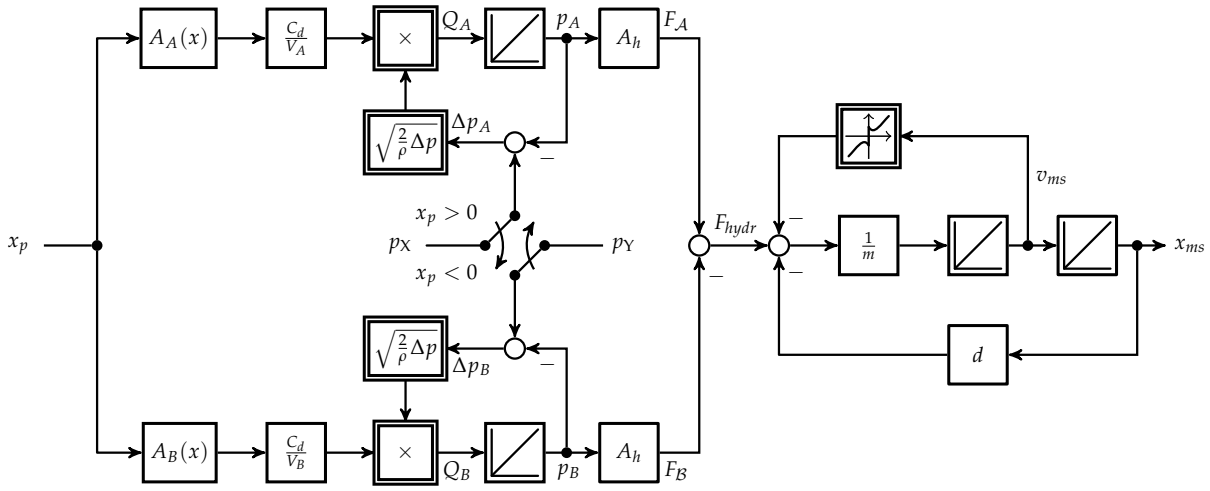

Figure B.7.: Block set diagram of a main stage valve.

differential equations describing the pressure p in the two chambers:

$$\dot{p}_i = A_i(x)\frac{C_d}{V_i}\sqrt{\frac{2}{\rho}\Delta p_i}, \quad i \in \{A,\, B\}\,. \tag{B.3}$$

The piston's movement is described by an second order differential equation that incorporates nonlinear friction and a linear damping d to center the piston if no control pressure p_X is provided:

$$a_{ms} = \frac{1}{m}\left(F_A - F_B - d\, x_{ms} - F_{fric}\left(v_{ms}\right)\right). \tag{B.4}$$

The model structure is comparable to the one of a differential cylinder and thus, there are several comparable design approaches being applicable to the given valve's structure. For them, it can be referred e.g. to El-Araby, El-Kafrawy, and Fahmy (2011), Khoshzaban Zavarehi, Lawrence, and Sassani (1999), Köckemann (1989), Lausch (1990), and Lin and Akers (1991).

The volumes V_A and V_B are crucial design parameters of the main stage valve. As apparent in the block set diagram, large chamber volumes cause a reduction of dynamics of the acting forces F_A and F_B, respectively. To accelerate the system's behavior, the mechanical construction of the main stage valve is carried out such that the chambers comprise a minimum volume and the force dynamics are as high as possible. Thus, comparing the force dynamics to the motion dynamics of the main stage piston, the force $F_{hydr} \propto x_p$ can be assumed to be proportional to the pilot stage's piston position x_p because the chambers are pressurized before a movement of the main stage piston is given. Consequentially, the dominant system dynamics are reduced to the motion equation describing the movement x_{ms} being a nonlinear second order system. One advantage of this structural assumption is that only the velocity v_{ms} has to be determined for control purpose and the pressure within the control chambers V_A and V_B is negligible.

The hydraulic setup being used to evaluate the directional control main stage valve with an attached pilot valve is shown in figure B.8. The axial piston pump provides

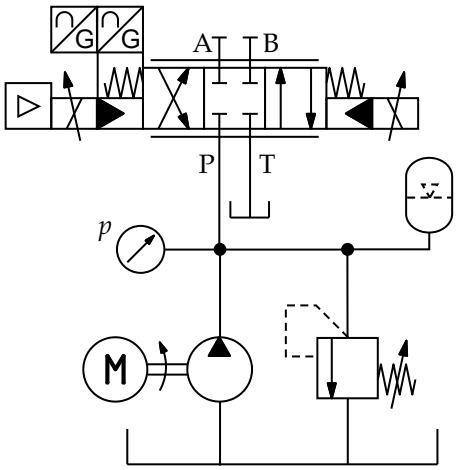

Figure B.8.: Simplified schematic diagram of the hydraulic setup.

a pressure p, and a passively actuated pressure relief valve protects the setup from over pressures that may harm the setup. The main stage valve is directly attached to the pump; the pilot valve is supplied by the same pressure supply, thus, there is no additional control pressure and the connecting ports X and Y are neglected. To compensate small variations in the pressure p, a pressure accumulator is attached directly in front of the valve.

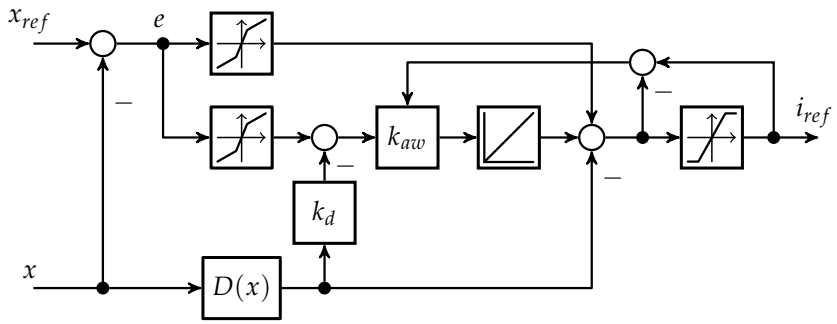

Figure B.9.: PI controller with nonlinear gain curves and an additional state feedback element.

B.3. Industrial control of hydraulic valves

As previously introduced, for the industrial application of hydraulic valves often structures based on the PID control are used. One major advantage of such controllers is that this simple control concept is not only known to control experts but also to technicians only having a practical education. The simplicity and design rules, e.g., as published by Ziegler, Nichols, and Rochester (1942) and Ziegler and Nichols (1993) lead to a widespread acceptance of these controllers. However, due to the given simplicity, the control performance is not acceptable for nonlinear systems like directional valves since different behaviors are demanded for varying use-cases. This cannot be achieved by a simple PID controller. To compensate this drawback, the PID controller initially has been equipped with a single nonlinear gain curve for the proportional controller branch while the integral and differential part remained linear (cf. Gamble and Vaughan 1996). Since the performance demands are continuously increased, this configuration is not sufficient and the integral branch is equipped with an individual nonlinear gain curve. In a further step, the differential branch is replaced by a state feedback element $D(x)$ providing an additional velocity and acceleration impact. The resulting controller is depicted in figure B.9.

The so-called *nonlinear PID controller* can be understood as an industrial standard. However, this controller suffers from its complexity. Due to the parameterizable gain curves, the state feedback, and the adjustable anti-windup mechanism, the controller comprises approximately 25 to 40 independent parameters, dependent on the intended application purpose. The values of the control parameters often are determined manually by a process expert. For this, the expert varies the parameter values and inspects the step responses of the system for different signal ranges until the desired behavior is established. This cumbersome and long lasting process offers the opportunity of automation. Blumendeller et al. (2000), Nicolaus et al. (2001) or Krettek et al. (2007, 2009) and Krimpmann et al. (2014) published different approaches that base on evolutionary parameter optimization in hardware-in-the-loop (HiL) experimental setups. Despite the automation, these design processes again increase the complexity of the design process so that only optimization experts can tune this nonlinear PID controller.

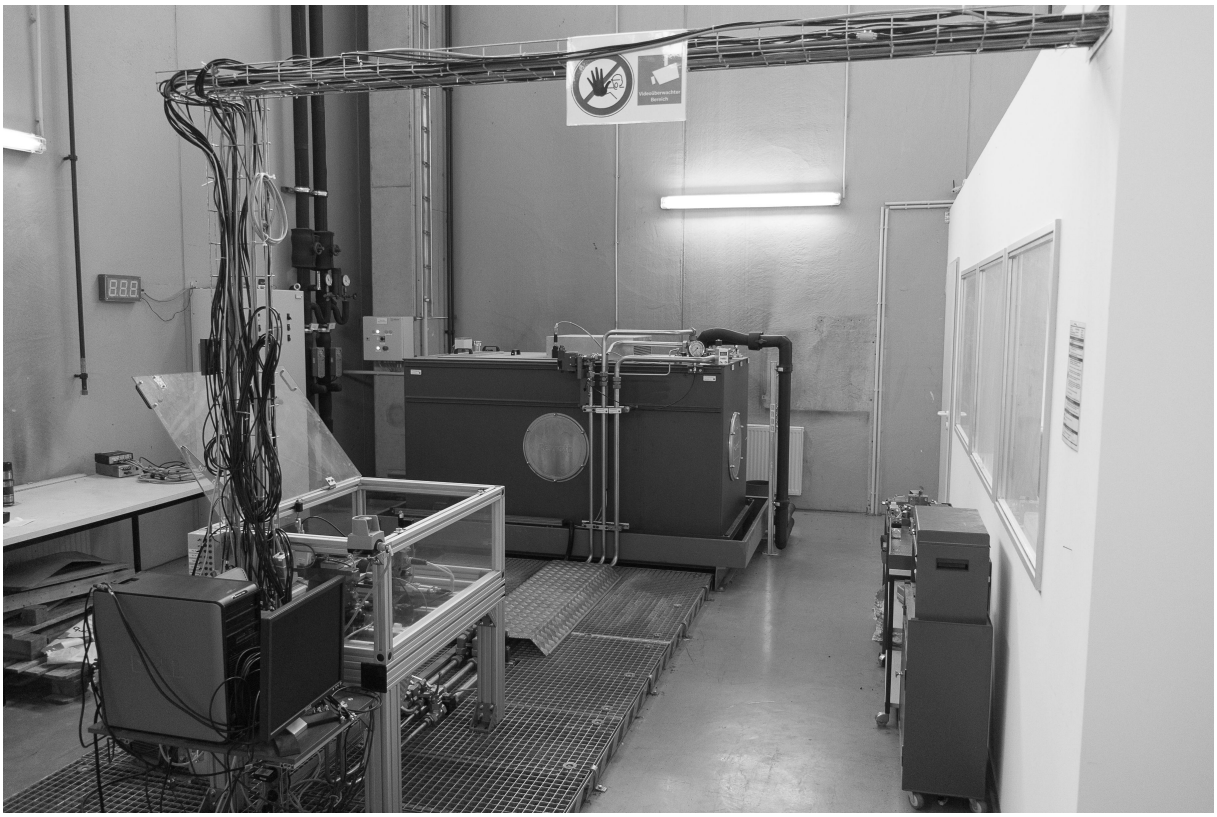

Figure B.10.: Picture of the hydraulic test laboratory.

B.4. Hydraulic test bench

The hydraulic laboratory of the Institute of Control Theory and Systems Engineering at the TU Dortmund University consists of a hydraulic setup and a noise-protected operator station. The hydraulic setup that is shown in figure B.10 comprises a *ABFAG-0630S-2 / A10VSO 71/225M-4-B1/WTM*-type HPU shown in the back of the picture and the test bench in the front of the picture. The HPU is controlled by the cabinet on the left. To provide sufficient cooling, the HPU is directly attached to the central cooling infrastructure of the TU Dortmund University via the thick black pipes in the left back. The test bench and the HPU are mounted in a tank that is sufficiently large to contain the total hydraulic liquid. Thus, in case of leakages, the impairment of the environment is minimized. A PC with DAQ board is directly attached to the test bench (see table B.1 for hardware specifications). It acts as a real time system executing the control algorithms and traces the relevant signals. Additionally, further signals can be captured via a second real time system in the operator station. For this, the supplementary signals are transferred via the cable tree that connects the test bench and the station (top front of the picture). The test bench is covered by shock-resistant acrylic glass to protect the operator in case of damages or abrupt leakages.

As shown in figure B.11, the test bench comprises two independent hydraulic setups. Basically, both setups provide a size 16 outlet for directional control valves. Via adapters, either connection ports for size 10 or size 6 directional valves are provided. Additionally, a pressure relief valve setup is provided by an individual connection

block. The picture in figure B.11 shows two different mounted setups. In the back, a size 10 main stage valve with size 6 pilot valve is connected to the test bench. This is the setup explained in section B.2. The pressure relief valve setup as discussed in section B.1 is shown in the front of the photograph, where the pressure relief valve is mounted on the left side of the connection block above the two cigar-shaped pressure sensors. The flow control valve is mounted on the right side of the front connection block. For further measurements, a Kracht *VC* 0,04 flow sensor can be integrated into the setup; however, due to its inertia, it can only be used for steady state measurements. The directional valves' transducers and the pressure sensors, as well as the control output signals, are connected to a patch field at the test bench that fits into the DAQ board of the real time PC. The flow control valve and the flow sensor are controlled from the operator station.

Table B.1.: Specifications of utilized PCs

Parameter	Unit	**Operator PC**	**Real time PC**
Type	-	Fujitsu Esprimo P910 E90+	Dell Optiplex 755
CPU type	-	Intel Core i5-35370K	Intel Core2Duo E6650
CPU clock	GHz	3.40	2.33
RAM	MB	8192	2048
DAQ		-	NI PCI-6259

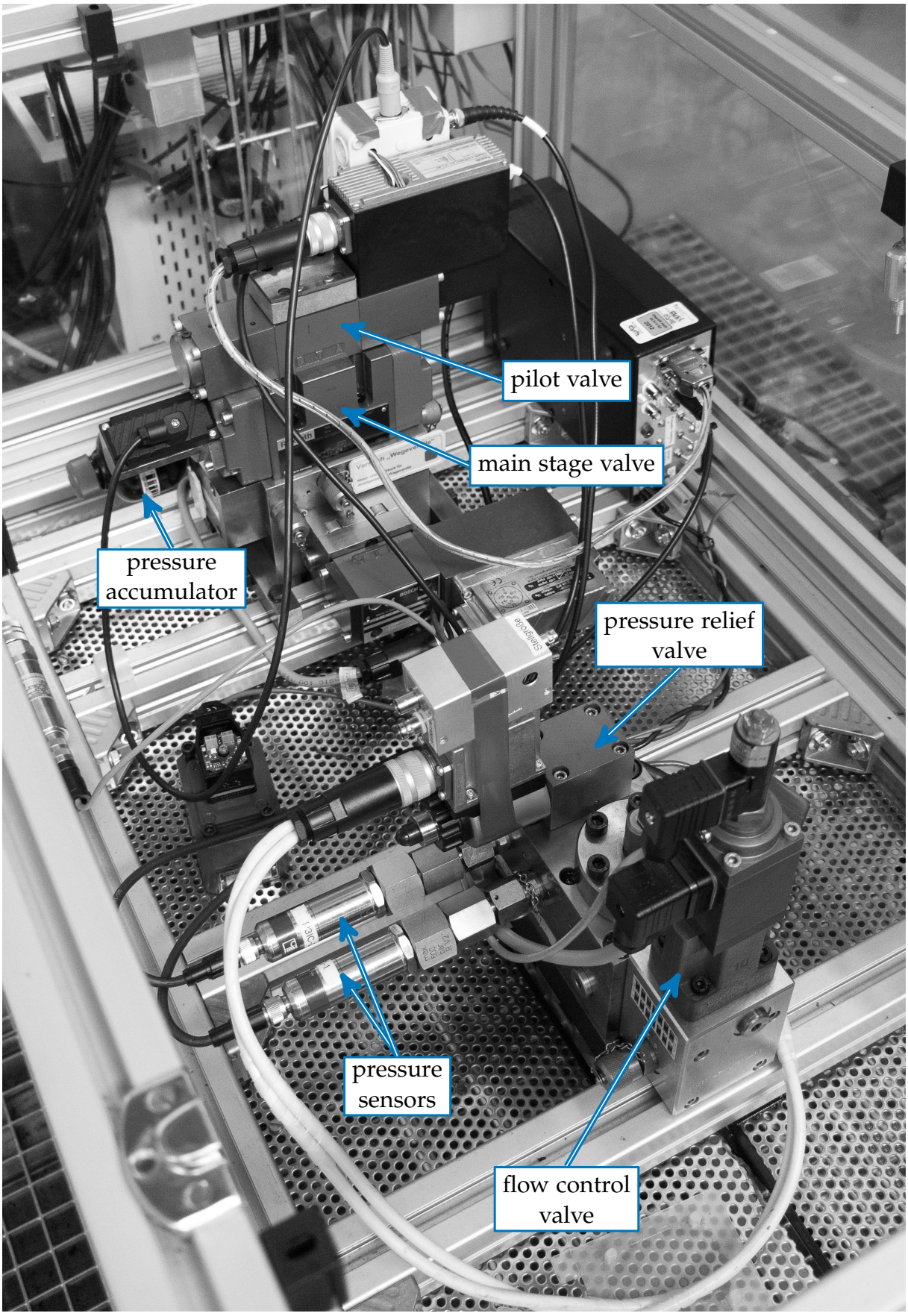

Figure B.11.: Picture of the hydraulic test bench with two independent test assemblies.

C

Modeling and Structural Analysis of a Pressure Relief Valve

This chapter outlines the detailed modeling process of the pressure relief valve. Due to brevity, the detailed modeling process is separated from the general introduction of the valve given in section B.1.

C.1. Model of a pressure relief valve

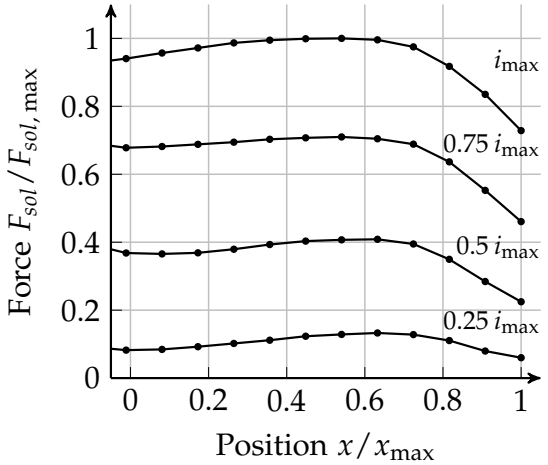

Figure C.1.: Measured relationship between the solenoid force F_{sol} and the position x as well as the current i

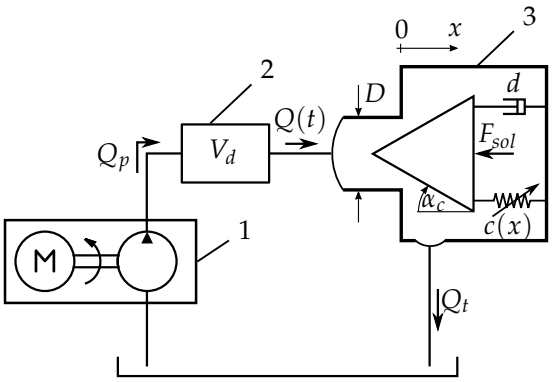

Figure C.2.: Simplified schematic diagram of the hydraulic setup used for system modeling purposes. Hydraulic power unit (1), artificial chamber (2), pressure relief valve (3)

Electro-Magnetic Model

The dynamics of the hydraulic pressure relief valve is composed of an electro-magnetic and a hydro-mechanic part. The electro-magnetic part meaning the solenoid can be decomposed into a simple first order differential equation describing the current $i(t)$

in dependence on the coil resistance R and its inductance L as well as the reference current $i_{ref}(t)$:

$$\frac{\mathrm{d}\, i}{\mathrm{d}\, t} = \frac{1}{T_i}\left(i_{ref} - i\right). \tag{C.1}$$

For sake of simplicity, the resistance R and the inductance L are combined to a single time constant $T_i = \frac{L}{R}$. The desired current $i_{ref}(t)$ can be understood as the control input. A modeling of the magnetic characteristics is not intended since the flux $\Psi(t)$ generated by the solenoid effectively is proportional to the current $i(t)$. There are more detailed solenoid models that consider a variable inductance (see e.g. Elmer and Gentle 2001). However, those models describe the relation between the voltage at the clamps of the solenoid and F_{sol}. This also requires a model of the power electronics that increases the model complexity significantly.

The pushing force $F_{sol}(i,\, x)$ that is generated by the solenoid depends on the current i as well as on the position of the cone $x(t)$. The relationship between F_{sol} and i along to x is nonlinear and is not straightforward to model analytically. Hence, the relation is determined by measurements for a set of constant values of i and x resulting into a lookup table as shown in figure C.1.

By combining (C.1) and the measured force $F_{sol}(i,\, x)$, the valve's actuator can be described in a simple but accurate way.

Hydraulic Model

The hydro-mechanical part of the model follows the mass balance approach as discussed in Ferreira, Almeida, and Quintas (2002), Kasai (1968), and Licskó, Champneys, and Hõs (2009). The dynamics of the pressure relief valve are directly related to the surrounding system as shown in figure C.2. The system consists of a hydraulic power unit that provides a pressure $p(t)$ and a constant flow rate $Q_p(t)$. However, based on the compressibility of the oil and the elasticity of the tubes, the flow rate $Q(t)$ at the valve's connecting port P can be different from Q_p. To describe this compressibility, the artificial chamber V_d sums up the overall dead volume of the system.

The mass balance equation of the chamber is given by

$$\frac{\mathrm{d}(\rho\, V_d)}{\mathrm{d}\, t} = \rho\left(Q_p - Q(x,\, p)\right) \tag{C.2}$$

where V_d denoted the cumulative dead volume of the system, ρ is the density of the hydraulic fluid and $Q(x,\, p)$ is the flow rate through the valve. The flow rate $Q(x,\, p)$ is a function of the valve cone's position, the system pressure p and the discharge coefficient C_d:

$$Q(x,\, p) = A(x)\, C_d \sqrt{\frac{2\, p}{\rho}}. \tag{C.3}$$

The flow through area $A(x)$ is a nonlinear function of the cone's position. The valve's cone is assumed to be radially symmetrically. Hence, $A(x)$ is calculated around the symmetry axis of the cone times the minimum normal distance between the cone and

the seat. As shown by Licskó, Champneys, and Hõs (2009), $A(x)$ is given by

$$A(x) = \left(1 - \frac{x}{D}\sin(\alpha)\,\cos(\alpha)\right)\, D\,\pi\sin(\alpha)\,x, \tag{C.4}$$

where D denotes the diameter of the seat and α is the angle of the cone as shown in figure C.2. However, since this complex expression of $A(x)$ shows almost a linear dependency within the desired working range of x, $A(x)$ is approximated by a linear equation

$$\tilde{A}(x) = \gamma\, x. \tag{C.5}$$

Further, it is assumed that the used fluid is barotropic. Hence, the fluid density $\rho = \rho(p)$ only depends on the pressure p. By using this assumption, the left hand side of (C.2) is reformulated as follows (Licskó, Champneys, and Hõs 2009):

$$\frac{\mathrm{d}}{\mathrm{d}\,t}\left(\rho\, V_d\right) = V_d\frac{\mathrm{d}\,\rho}{\mathrm{d}\,t} + \rho\frac{\mathrm{d}\,V_d}{\mathrm{d}\,t}. \tag{C.6}$$

Since the volume V_d of the chamber is constant, the second part of the total derivative is omitted and by multiplying the first addend with $\mathrm{d}\,p/\,\mathrm{d}\,p$, one obtains

$$\frac{\mathrm{d}}{\mathrm{d}\,t}\left(\rho\, V_d\right) = V_d\frac{\mathrm{d}\,\rho}{\mathrm{d}\,p}\frac{\mathrm{d}\,p}{\mathrm{d}\,t} = V_d\frac{1}{c_{fluid}^2}\frac{\mathrm{d}\,p}{\mathrm{d}\,t}. \tag{C.7}$$

As one can see, (C.7) is a function of the sonic velocity $c_{fluid} = \sqrt{K/\rho}$, where K is the bulk modulus of the fluid. Hence, the left hand side of (C.2) can be rewritten as follows:

$$\frac{\mathrm{d}}{\mathrm{d}\,t}\left(\rho\, V_d\right) = V_d\frac{\rho}{K}\frac{\mathrm{d}\,p}{\mathrm{d}\,t}. \tag{C.8}$$

Despite its comparably small influence due to the cone's geometry (cf. Backé, Wobben, and Wassenberg 1979), the static flow reaction force is incorporated into the model for the sake of completeness. In general, the flow reaction force is determined by defining a control volume around the valve's cone so that a momentum equation as the line integral around this volume is calculated. By solving this integral, the flow reaction force is determined (cf. e.g. Shin 1991; Stone 1960). In Shin (1991), parametric flow force equations are deduced for a two-stage relief valve. The pilot valve's geometry is comparable to the given one. Thus, the static flow reaction force $F_r(x,\,p)$ is determined as:

$$F_r(x,\,p) = -8\,\pi\,C_d^2\,\sin^2(\alpha)\;p\,x^2 + 2\,C_d^2\,\pi\,D\,\sin(\alpha)\,\cos(\alpha)\;p\,x. \tag{C.9}$$

Mechanical Sub-Model

The movement of the cone is described by Newton's second law in conjunction with nonlinear control spring characteristics as shown in following differential equations:

$$\begin{aligned}\frac{\mathrm{d}\,v}{\mathrm{d}\,t} &= \frac{1}{m}\Big(A_p\,p\,(t) - F_{sol}\,(i,\,x) - d\,v + F_s\,(x) + F_r(x,\,p)\Big)\\ \frac{\mathrm{d}\,x}{\mathrm{d}\,t} &= v.\end{aligned} \tag{C.10}$$

The states x and v are the displacement and velocity of the valve's cone in dependence on the sum of acting forces. The gain A_p is the area of the cone on which the pressure acts, d is a damping factor, m the mass of the cone and $F_s(x)$ denotes the force, generated by the control spring package. Two in series connected springs counteract against the solenoid force and open the valve if no pressure p and no current i are applied. The spring package is pre-stressed so that the opening of the cone reduces the spring force $F_s(x)$. Since one spring loses contact within the working range of x, the combined spring stiffness $c(x)$ is a function of the cone's position. Due to this, $F_s(x)$ is understood as a piecewise defined Hooke's law, where $F_{s,0}$ denotes the pre-stress force for $x = 0$ mm and $F_{s,1}$ is the resulting force when the first control spring becomes ineffective at position x_1. The second control spring gets ineffective at position x_2. The coefficients c_1 and c_2 are the different degrees of spring stiffness of the position intervals:

$$F_s(x) = \begin{cases} F_{s,0} - c_1\, x & \text{if } 0 \leq x < x_1 \\ F_{s,1} - c_2\, x & \text{if } x_1 \leq x < x_2 \\ 0 & \text{else.} \end{cases} \tag{C.11}$$

For a physically correct movement of the cone, the mechanical dead ends of the valve need to be considered as well. For this, the simple impact law

$$v^+ = -\beta\, v^- \tag{C.12}$$

is used where $v^-(t)$ is the velocity before the impact and $v^+(t)$ denotes the velocity immediately after the impact. The parameter $\beta > 0$ is a repelling factor.

By combining the equations (C.1), (C.2), (C.8), (C.9) and (C.10), one obtains the overall nonlinear pressure relief valve model as shown in (C.13). The system is of fourth order ($n = 4$) and can be described in general as a multi-input single-output system

$$\mathbf{z} = \begin{bmatrix} i \\ v \\ x \\ p \end{bmatrix}, \quad \mathbf{a}(\mathbf{z}) = \begin{bmatrix} -\frac{1}{T_i}\, i \\ \frac{A_p}{m}\, p - \frac{d}{m}\, v + \frac{F_s(x)}{m} - \frac{F_{sol}(x,i)}{m} + \frac{F_r(x,p)}{m} \\ v \\ -\frac{K}{V_d}\gamma\, C_d\, x \sqrt{\frac{2}{\rho}\, p} \end{bmatrix}, \quad \mathbf{b} = \begin{bmatrix} 1/T_i & 0 \\ 0 & 0 \\ 0 & 0 \\ 0 & K/V_d \end{bmatrix}, \quad \mathbf{c} = \begin{bmatrix} 0 \\ 0 \\ 0 \\ 1 \end{bmatrix} \tag{C.13}$$

where $\mathbf{z} = [i,\, v,\, x,\, p]^{\mathrm{T}}$ is the state vector and $\mathbf{u} = \left[i_{ref},\, Q_p\right]^{\mathrm{T}}$ is the input vector. The vectors $\mathbf{b}$ and $\mathbf{c}$ are the input respectively the output gains and the system dynamics are given by the nonlinear state function $\mathbf{a} : \mathbb{R}^n \mapsto \mathbb{R}^n$.

C.2. Structural analysis of a pressure relief valve

In case of linear system dynamics ($\mathbf{a}(\mathbf{z}) = \mathbf{A}\,\mathbf{z},\ \mathbf{A} \in \mathbb{R}^{n \times n}$), an analysis of the dynamic system behavior is independent of the input sequence $\mathbf{u}(t)$. It is done by evaluating the eigenvalues $\lambda_j,\ j \in \mathcal{J} = \{1, 2, \ldots, n\}$ of the system matrix $\mathbf{A}$. Hence, by comparing the eigenvalues λ_j one gets insight of damping and oscillation characteristics. Moreover, the relative position of the eigenvalues reveals whether a structural simplification

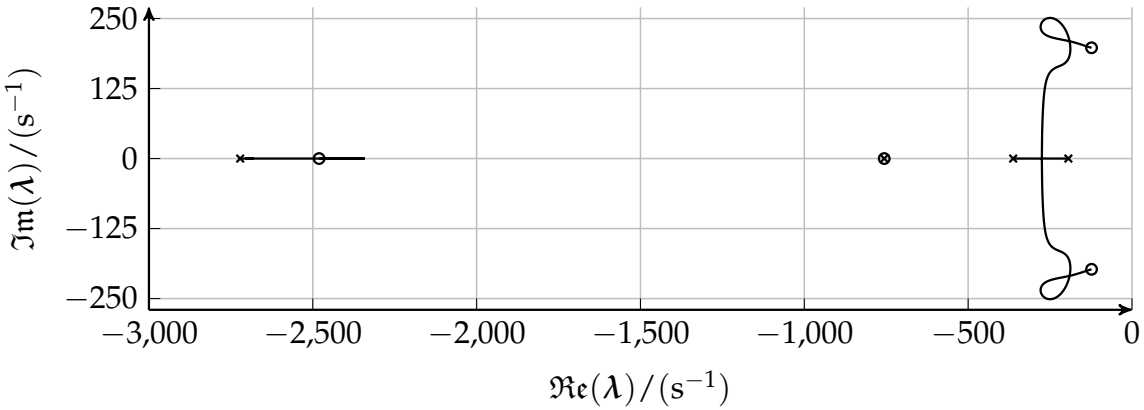

Figure C.3.: Variation of eigenvalues $\boldsymbol{\lambda}(\mathbf{z})$ for $x \in [0 \quad x_{\max}]$, $p = 0.1\, p_{\max}$ and $i = 0.5\, i_{\max}$. The symbol $\circ$ denotes $x = 0\,\mathrm{mm}$ and $\times$ stands for $x = x_{\max}$.

of the system is possible or not. A reduction of the system order for instance is feasible if one eigenvalue $\lambda_k \leq 5\,\lambda_i,\ i \in \mathcal{J}\backslash\{k\}$ is approximately five times faster than all the other eigenvalues. Thus, a first order differential equation $\dot{z}_k - \lambda_k\, z_k = K_k\, u_k,\ \lambda_k < 0$ can be replaced by a static gain $z_k \approx -(K_k/\lambda_k)\, u_k$. This heuristic rests upon the assumption that the transient processes of the faster transfer element have approximately converged while the transient motion of the slower element still is rather close to the initial position.

However, in case of a nonlinear system like (1.1) such an analysis is not straight forward since a state matrix $\mathbf{A}$ is not given and has to be calculated in dependence on the current state variables $\mathbf{z}$ by partially differentiating the state function $\mathbf{a}\,(\mathbf{z})$:

$$\mathbf{A}\,(\mathbf{z}) = \frac{\partial \mathbf{a}(\mathbf{z})}{\partial \mathbf{z}}. \tag{C.14}$$

As one can see, the system matrix becomes state dependent and hence, its eigenvalues $\boldsymbol{\lambda}(\mathbf{z})$ are also state dependent.

For this application, the system matrix $\mathbf{A}\,(\mathbf{z})$ consists of three variable eigenvalues and one fixed eigenvalue. The fixed eigenvalue λ_2 is given by the first order differential equation of the current i. However, the mechanical part provides a pair of conjugate complex poles for the states x and v. The dynamics between the position x and the pressure p is modeled based on a first order differential equation with nonlinear feedback gain.

To obtain information for a possible order reduction, the system is evaluated for a set of state trajectories where the pressure p and the current i are kept constant while the position x is varied through the whole working range $x \in [0 \quad x_{\max}]$. The resulting movement of the eigenvalues for different working points is shown in figure C.3 and figure C.4. The symbol $\circ$ denotes the position of the eigenvalue for $x = 0\,\mathrm{mm}$ and $\times$ is the location for $x = x_{\max}$. While Fig. C.4 shows the pressure dependency of the conjugate complex eigenvalues $\boldsymbol{\lambda}_{3,4}(\mathbf{z})$, the fast state dependent eigenvalue $\lambda_1(\mathbf{z})$ does not have a significant dependency.

The obtained eigenvalue configurations lead to the assumption that the dynamics can be described sufficiently by a nonlinear second order system with parametric

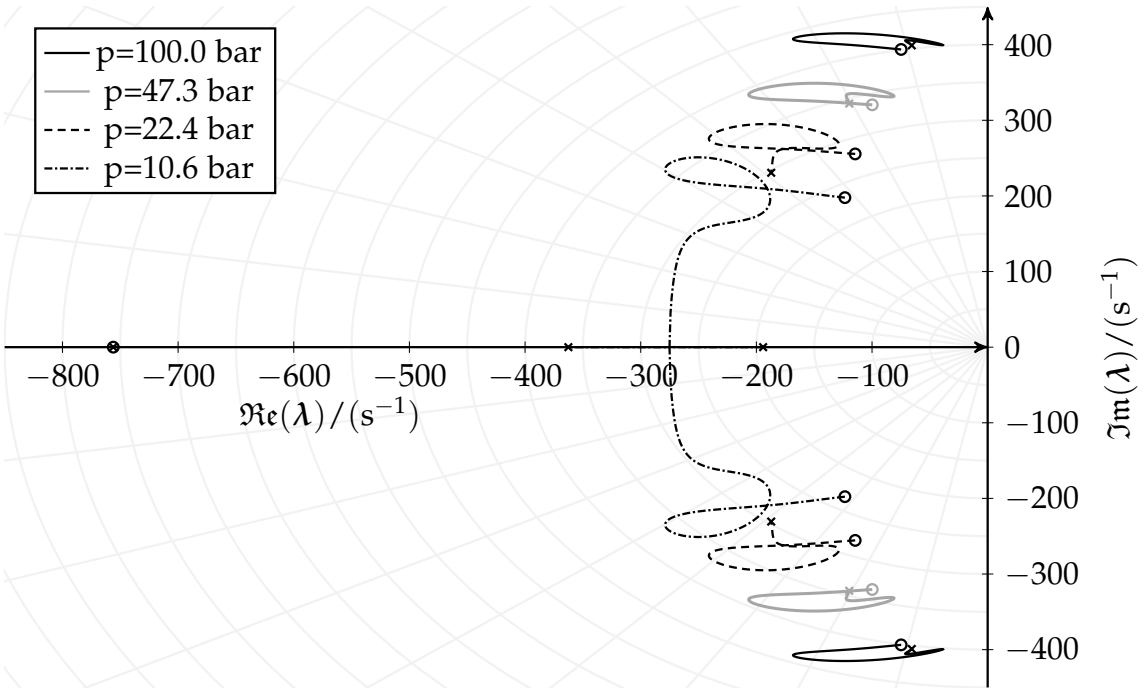

Figure C.4.: Variation of the conjugate complex eigenvalues $\boldsymbol{\lambda}_{3,4}(\mathbf{z})$ of $\mathbf{A}(\mathbf{z})$ for $x \in [0 \quad x_{\max}]$ with different constant pressure values p and constant current $i = 0.5\, i_{\max}$.

perturbations because of the dominating position of $\boldsymbol{\lambda}_{3,4}(\mathbf{z})$. Thus, for the control design the reduced model structure (C.15) in control canonical form is sufficient, where $\tilde{\mathbf{a}} : \mathbb{R}^{\tilde{n}} \mapsto \mathbb{R}^{\tilde{n}}$ and $\tilde{\mathbf{b}} : \mathbb{R}^{\tilde{n}} \mapsto \mathbb{R}^{\tilde{n}}$ are the reduced state and input functions for the reduced order control vector $\tilde{\mathbf{z}} = [\tilde{z}_1, \tilde{z}_2]^{\mathrm{T}} = [p, Q_d]^{\mathrm{T}}$ and $i_{ref} \propto u$ is the control input. The flow rate Q_d denotes the volume that flows into the dead volume V_d. The perturbation function $\boldsymbol{\zeta}(t)$ summarizes all structural and parameter errors while $\tilde{n} = 2$ is the reduced system order:

$$\begin{aligned} \dot{\tilde{\mathbf{z}}} &= \tilde{\mathbf{a}}(\tilde{\mathbf{z}}) + \tilde{\mathbf{b}}(\tilde{\mathbf{z}})\; u + \boldsymbol{\zeta}, \quad \tilde{\mathbf{z}}(0) = \tilde{\mathbf{z}}_0 \\ p &= \tilde{\mathbf{c}}^{\mathrm{T}}\, \tilde{\mathbf{z}}\,. \end{aligned} \tag{C.15}$$

The major advantage of using the reduced order system (C.15) instead of using the system as shown in (C.13) is the reduced number of states that need to be measured or estimated for applying a state feedback controller. To obtain the oil flow Q_d, a robust differentiation of p can easily be carried out with sliding mode techniques as e.g. discussed in chapter 5.

D

Stability Analysis of the Super-Twisting Algorithm

D.1. Lyapunov-based stability of the super-twisting algorithm

As initially shown by Moreno and Osorio (2008), the stability of the STA can be shown by the use of quadratic Lyapunov functions. For the particular set law (4.14) and for unperturbed sliding dynamics ($\dot{\sigma} = u$), the Lyapunov function is given as follows (Moreno and Osorio 2008). At this, (4.14) is understood as a two-state nonlinear system with the states $z_1 = \sigma$ and $z_2 = v$:

$$V(\mathbf{z}) = 2\,\alpha_0\,|z_1| + \frac{1}{2}\,z_2^2 + \frac{1}{2}\left(\alpha_1\,\lfloor z_1 \rceil^{1/2} - z_2\right)^2 \tag{D.1}$$

To show stability of the STA, the Lyapunov function can be transformed into a quadratic form $V(\mathbf{z}) = \boldsymbol{\zeta}^{\mathrm{T}}\,\mathbf{P}\,\boldsymbol{\zeta}$ with $\boldsymbol{\zeta} = \left[\lfloor z_1 \rceil^{1/2},\ z_2\right]^{\mathrm{T}}$.

$$\mathbf{P} = \begin{bmatrix} 4\,\alpha_0 + \alpha_1^2 & -\alpha_1 \\ -\alpha_1 & 2 \end{bmatrix} \tag{D.2}$$

To ensure positive definiteness of the Lyapunov function and hence, positive definiteness of $\mathbf{P}$ the control gain $\alpha_0 > 0$ has to be positive. The time derivative of (D.1) is given as $\dot{V}\,(\mathbf{z}) = -|z_1|^{-1/2}\,\boldsymbol{\zeta}^{\mathrm{T}}\,\mathbf{Q}\,\boldsymbol{\zeta}$ with

$$\mathbf{Q} = \frac{\alpha_1}{2}\begin{bmatrix} 2\alpha_0 + \alpha_1^2 & -\alpha_1 \\ -\alpha_1 & 1 \end{bmatrix}.$$

Note that the STA is stable, if the matrices $\mathbf{P}$ and $\mathbf{Q}$ are positive definite. For the case of unperturbed sliding dynamics, this is achieved if $\alpha_0,\ \alpha_1 > 0$. Further discussions and the proof for perturbed dynamics can be found in Moreno and Osorio 2008.

D.2. Lyapunov-based stability of the *quasi* super-twisting algorithm

The quasi STA (cf. section 4.5) presented by Shtessel, Shkolnikov, and Brown (2003) is considered since it provides an increased smoothness of the control variable u, resulting in an increased chattering attenuation if the gains α_0 and α_1 are chosen properly. The control law consists of a proportional part u_p and an integral part u_i.

$$\begin{aligned} u &= u_p + u_i \\ u_p &= -\alpha_1 \left|\sigma\right|^{1/2} \operatorname{sign}(\sigma) \\ \dot{u}_i &= -\alpha_0 \left|\sigma\right|^{1/3} \operatorname{sign}(\sigma) \end{aligned} \tag{D.3}$$

Theorem: If the relative degree of σ is equal to 1 ($\dot{\sigma} \leftarrow u$) and $\alpha_i \in \mathbb{R}_+$, $i \in \{0, 1\}$ are given, control law (D.3) provides asymptotic convergence of the dynamic system (4.15) into 2-sliding mode $[\sigma, \dot{\sigma}] \to \mathbf{0}$ if perturbations are omitted.

Proof: The system (4.15) can be converted to the input-output dynamics $\dot{\sigma} = a(\mathbf{x}) + b(\mathbf{x})\, u$. If a and b are assumed unknown, it follows that $\dot{\sigma} = u$. By incorporating (D.3), a system of two first order differential equations of the states $z_1 = \sigma$ and $z_2 = -\alpha_0 \int \left|\sigma\right|^{1/3} \operatorname{sign}(\sigma)\, \mathrm{d}\, t$, $\mathbf{z} = [z_1,\, z_2]^{\mathrm{T}}$ is obtained.

$$\begin{aligned} \dot{z}_1 &= -\alpha_1 \left|z_1\right|^{1/2} \operatorname{sign}(z_1) + z_2 \\ \dot{z}_2 &= -\alpha_0 \left|z_1\right|^{1/3} \operatorname{sign}(z_1) \end{aligned} \tag{D.4}$$

Let a suitable candidate for a Lyapunov function be given by

$$V_0(\mathbf{z}) = \frac{z_2^2}{2} + \int_0^{z_1} \alpha_0 \left|\epsilon\right|^{1/3} \operatorname{sign}(\epsilon)\, \mathrm{d}\, \epsilon \tag{D.5}$$

with $V_0(\mathbf{z}) > 0$, if $\mathbf{z} \in \mathbb{R}^2 \backslash \{\mathbf{0}\}$ as shown by Shtessel, Shkolnikov, and Brown (2003). As a consequence, the derivative of the Lyapunov function is given as

$$\dot{V}_0(\mathbf{z}) = \left(\nabla_{\mathbf{z}} V_0(\mathbf{z})\right)^{\mathrm{T}} \dot{\mathbf{z}} = -\alpha_0\, \alpha_1 \left|z_1\right|^{5/6}, \tag{D.6}$$

if $\mathbf{z} \in \mathbb{R}^2 \backslash \{\mathbf{0}\}$. By application of Lyapunov's direct method, it can be shown that $\mathbf{z} \to \mathbf{0}$ and thus, asymptotic stability of σ is given.

Remark: The qSTA does not contain a discontinuous switching term. Thus, it is not a sliding mode controller in the original sense. Yet, it establishes second order sliding motion, however, it does not provide the identical robustness properties. One has to be aware that Shtessel, Shkolnikov, and Brown (2003) use a weakened definition of sliding motion.

E

Supplementary Experimental Results

In addition to the experimental results provided in chapter 7 and chapter 8, this appendix complements the evaluations with further results. Due to brevity, in chapter 7 not all obtained solution sets are displayed as Pareto-space projections; they are delivered in the following. In addition, further variants of the combined adaptive parameter estimation as outlined in section 8.3 are illustrated.

E.1. Performance evaluation of SM controllers for the directional valves

This section provides supplementary Pareto-space projections of the solution sets that are discussed in chapter 7. While the solution set obtained for the HiL optimization of the STA controller of the pressure relief valve are discussed in section 7.2, the further ones are omitted due to brevity.

Performance evaluation of different sliding surfaces

To obtain a competitive evaluation, the STA controller in conjunction with three different sliding functions, the linear one, the SPA surface and the TOS surface, are optimized for the directional control pilot valve. The space projections resulting solution sets are shown in figure E.1. The comparison of the surfaces properties can be found in section 7.3, particularly in figure 7.10. All three variants achieve a high diversity of solutions. However, they are all in a comparable range. One obvious correlation can be found in the top left diagram of figure E.1 showing the projections of MSE_σ against $T_{r,90}$. All three sliding functions comprise a negative linear correlation of the shown objectives. This can be traced back to the point that for fast step responses, the system enters sliding mode rather late or yet in steady state position since the sliding functions act as virtual bandwidth limitations. To accelerate the system, the objective of sliding motion is neglected. However, one has to be aware that the ranges of the objective MSE_σ are not directly comparable between the different populations since the values rest upon different sliding surface geometries. Thus, the values are only comparable to the same population.

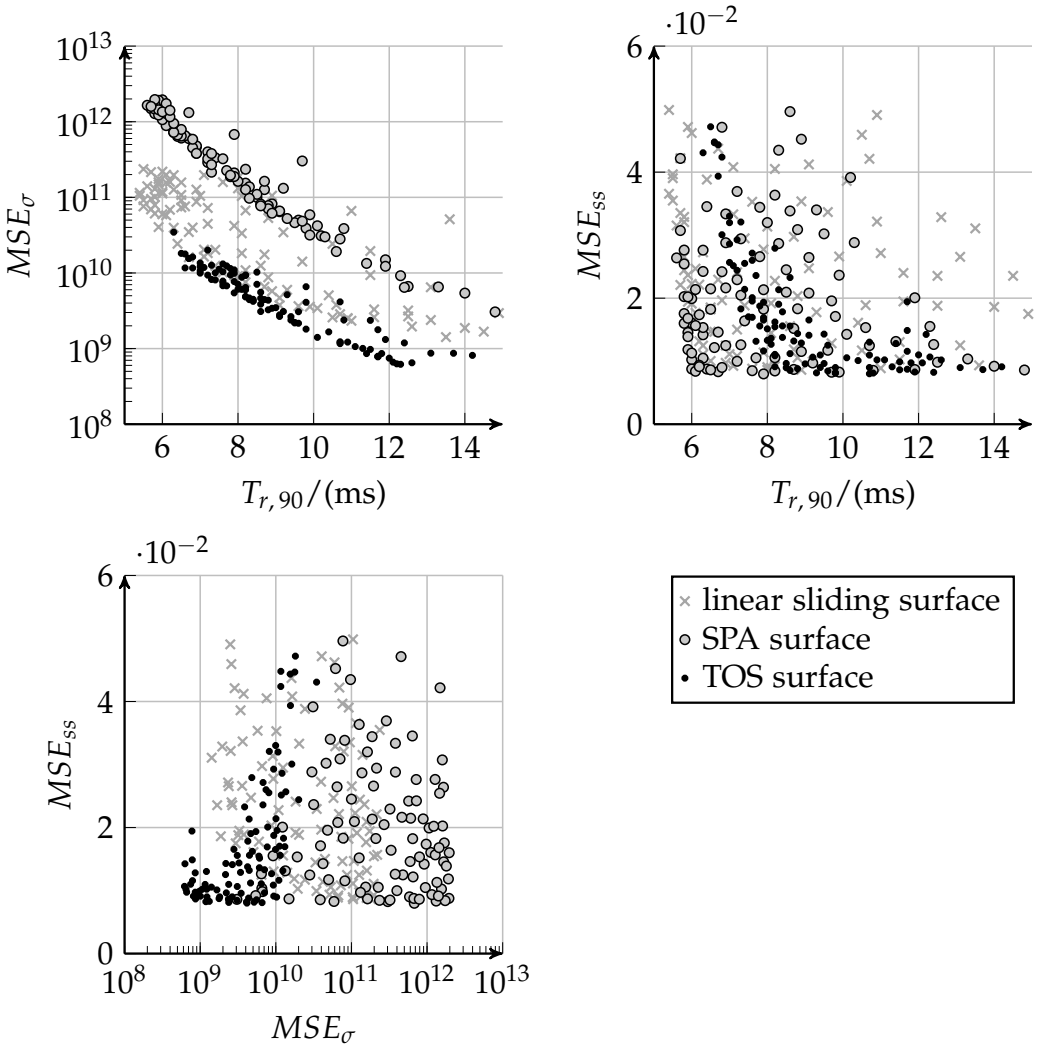

Figure E.1.: Projections of the resulting elitist set obtained after 50 generations of HiL optimization processes. The different markers indicate elitist sets of different sliding functions that are optimized and compared.

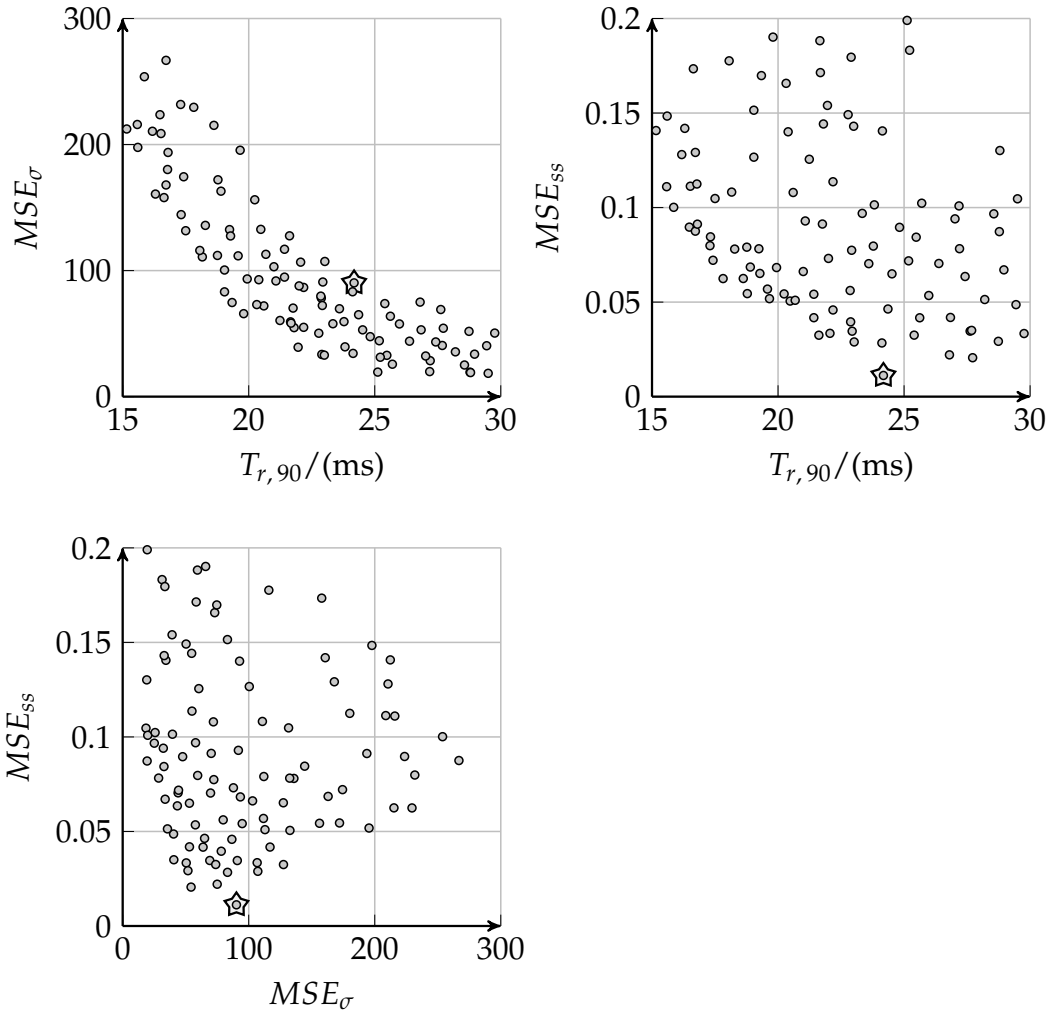

Figure E.2.: Projections of the resulting elitist set obtained after 50 generations of HiL optimization processes. The marker indicates the solution being discussed in section 7.4.

Optimization of the main stage directional valve

Figure E.2 displays the solution set obtained by an optimization of the STA controller with linear sliding surface and fixed pilot stage controller of the main stage directional valve as introduced in section B.2. In the diagrams, a selected solution is highlighted with a ✩ symbol. This solution is discussed in particular in section 7.4. As already discussed before this, there is a strong negative correlation between the MSE_σ and $T_{r,90}$ objectives displaying the trade off between sliding accuracy and fast system responses. For the detailed discussion of the control quality, an individual solution with very good steady state accuracy and average rise times is selected. This individual is of comparable performance as the solution obtained by the industrially equipped main stage PD controller (cf. section B.3).

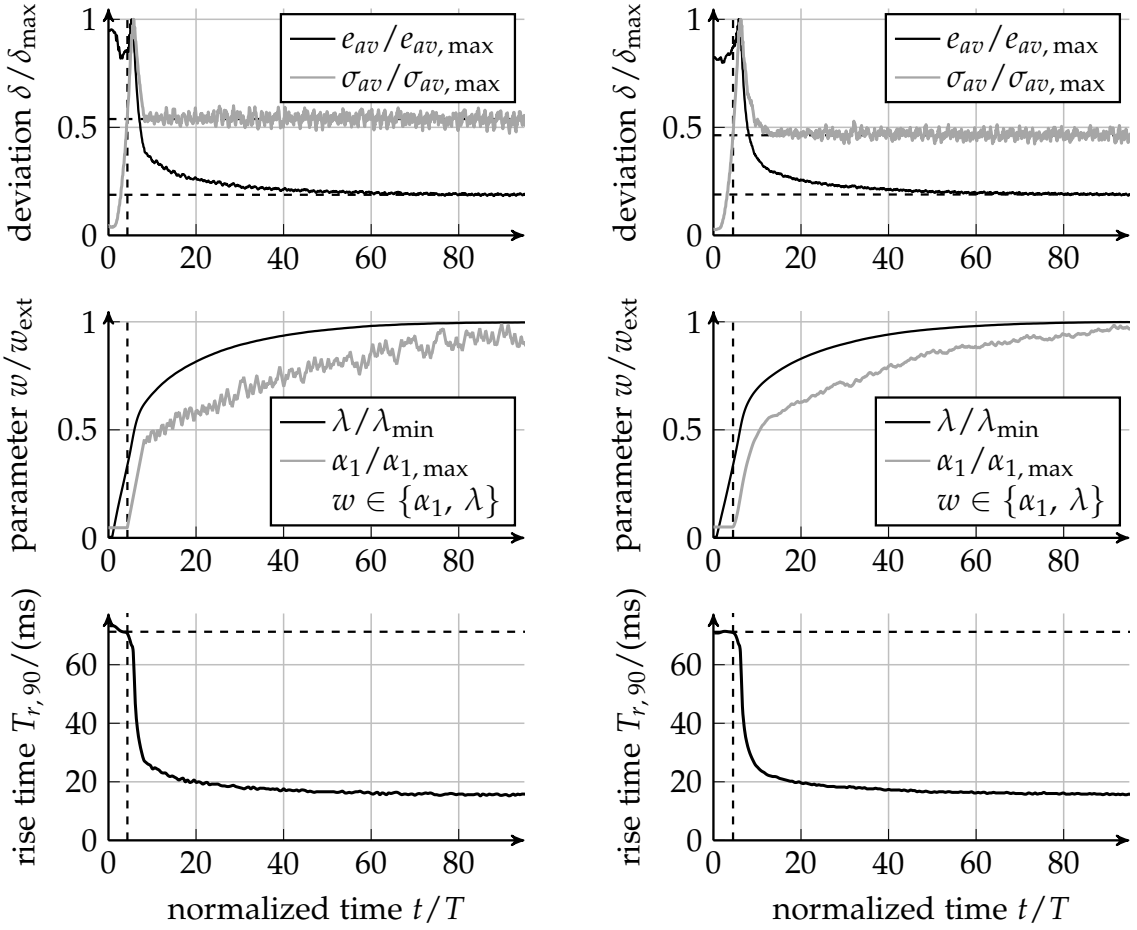

(a) $\dot{\lambda}$ continuous, $\dot{\alpha}_1$ discrete (b) $\dot{\lambda}$ continuous, $\dot{\alpha}_1$ continuous

Figure E.3.: Progress of combined adaptations of sliding functions and STA controllers for different adaption strategies.

E.2. Further variants of Lyapunov-based self-tuning of SMC

Figure E.3 provides supplementary diagrams for the discussion of adaptive sliding mode controllers in section 8.3. While the discrete adaption of λ is displayed in section 8.3, the continuous modification of λ is displayed here for the sake of brevity. As can be seen in figure E.3, the continuous adaption of λ, $\dot{\lambda} \in \mathbb{R}$, provides asymptotic convergence into the desired control quality. In contrast to this, the discrete variation $\dot{\lambda} \in \pm\kappa$ causes a finite time convergence. However, from a practical point of view, both variants reach the desired closed loop performance within the same time interval. In addition, the different realizations of the subordinate STA self-tuning do not cause sharp differences. Nevertheless, the combined continuous adaption shown in figure E.3b shows the smoothest adaption of all variants. For further discussions, please refer to section 8.3.

Bibliography

References

Parts of the material presented in this work has been originally published in conferences and journals. These publications as well as the resources by other researchers are summarized in the following list:

Adamy, J. (1991): *Strukturvariable Regelungen mittels impliziter Ljapunov-Funktionen*. Vol. 271. Fortschrittberichte VDI : Reihe 8, Meß-, Steuerungs- und Regelungstechnik. Düsseldorf: VDI Verlag (cit. on p. 7).

Adamy, J. (2014): *Nichtlineare Systeme und Regelungen*. 2. bearbeitete und erweiterte Auflage 2014. Berlin: Springer Berlin (cit. on p. 49).

Albadawi, A. (2010): "Ein Beitrag zur Steuerung und Regelung des hydraulisch angetriebenen Schwerlastroboters ALDURO". PhD thesis. Duisburg: Universität Duisburg-Essen (cit. on p. 7).

Armstrong-Hélouvry, B. (1991): *Control of machines with friction*. Vol. SECS 128. The Kluwer international series in engineering and computer science Robotics. Boston: Kluwer Academic Publishers (cit. on p. 17).

Auger, A. and B. Doerr (2011): *Theory of randomized search heuristics: Foundations and recent developments*. Vol. 1. Series on theoretical computer science. Singapore and Hackensack, NJ: World Scientific (cit. on p. 65).

Bäck, T., C. Foussette, and P. Krause (2012): "Eine Übersicht moderner Evolutionsstrategien und empirische Analyse ihrer Effizienz". In: *Proceedings 22. Workshop Computational Intelligence*. Ed. by F. Hoffmann. Karlsruhe: KIT Scientific Publishing, pp. 273–305 (cit. on p. 61).

Backé, W., G.-D. Wobben, and E. Wassenberg (1979): *Investigations of stationary and dynamic behaviors of mechanical and electrically actuated pressure relief valves (in German)*. Vol. 2811. Proceedings of the State North Rhine-Westphalia (cit. on p. 117).

Barth, A., M. Reichhartinger, J. Reger, M. Horn, and K. Wulff (2015): "Lyapunov-design for a super-twisting sliding-mode controller using the certainty-equivalence principle". In: *1st IFAC Conference on Modelling, Identification and Control of Nonlinear Systems MICNON 2015*, pp. 860–865 (cit. on p. 4).

Bartolini, G., A. Ferrara, and E. Usai (1997): "Applications of a sub-optimal discontinuous control algorithm for uncertain second order systems". In: *International Journal of Robust and Nonlinear Control* 7.4, pp. 299–319 (cit. on p. 37).

Bartolini, G., A. Ferrara, and E. Usani (1998): "Chattering avoidance by second-order sliding mode control". In: *IEEE Transactions on Automatic Control* 43.2, pp. 241–246 (cit. on pp. 7, 41, 42).

Bartolini, G., A. Pisano, E. Punta, and E. Usai (2003): "A survey of applications of second-order sliding mode control to mechanical systems". In: *International Journal of Control* 76.9-10, pp. 875–892 (cit. on pp. 7, 42).

Bartoszewicz, A. and A. Nowacka (2006): "Optimal design of the shifted switching planes for VSC of a third-order system". In: *Transactions of the Institute of Measurement and Control* 28.4, pp. 335–352 (cit. on p. 24).

Bartoszewicz, A. and A. Nowacka-Leverton (2010): "ITAE Optimal Sliding Modes for Third-Order Systems With Input Signal and State Constraints". In: *IEEE Transactions on Automatic Control* 55.8, pp. 1928–1932 (cit. on p. 24).

Bartoszewicz, A. (1995): "A comment on 'A time-varying sliding surface for fast and robust tracking control of second-order uncertain systems'". In: *Automatica* 31.12, pp. 1893–1895 (cit. on p. 24).

Bellman, R. (1972): *Dynamic programming*. 6th ed. Princeton: Princeton University Press (cit. on p. 68).

Bessa, W. M. (2009): "Some remarks on the boundedness and convergence properties of smooth sliding mode controllers". In: *International Journal of Automation and Computing* 6.2, pp. 154–158 (cit. on pp. 4, 39).

Beume, N., B. Naujoks, and G. Rudolph (2008): "SMS-EMOA – Effektive evolutionäre Mehrzieloptimierung". In: *at - Automatisierungstechnik* 56.7, pp. 357–364 (cit. on p. 65).

Bhat, S. P. and D. S. Bernstein (2000): "Finite-Time Stability of Continuous Autonomous Systems". In: *SIAM Journal on Control and Optimization* 38.3, pp. 751–766 (cit. on p. 100).

Blackburn, J. F., G. Reethof, and J. L. Shearer (1960): *Fluid power control*. New York and London: Technology Press of M.I.T. and Wiley (cit. on p. 3).

Blumendeller, W., V. Leutner, U. Schwane, and H. Kiendl (2000): "Regleroptimierung mit evolutionaren Algorithmen". In: *Internationales Fluidtechnisches Kolloquium*. Vol. 2, pp. 437–452 (cit. on pp. 6, 8, 111).

Bonchis, A., P. I. Corke, D. C. Rye, and Q. P. Ha (2001): "Variable structure methods in hydraulic servo systems control". In: *Automatica* 37.4, pp. 589–595 (cit. on p. 7).

Bosch Rexroth AG (2013): *Proportional-Druckbegrenzungsventil direktgesteuert, ohne/mit integrierter Elektronik (OBE): Typ DBET und DBETE: Technisches Datenblatt RD 29162* (cit. on p. 104).

Brandtstädter, H. (2009): "Sliding mode control of electromechanical systems". PhD thesis. TU München (cit. on p. 47).

Braun, J., J. Krettek, F. Hoffmann, and T. Bertram (2011a): "Structure and parameter identification of nonlinear systems with an evolution strategy". In: *IEEE Congress on Evolutionary Computation (CEC)*, pp. 2444–2451 (cit. on p. 8).

Braun, J., J. Krettek, F. Hoffmann, T. Bertram, H. Lausch, and G. Schoppel (2011b): "Struktur- und Parameteridentifikation mit Evolutionären Algorithmen". In: *at - Automatisierungstechnik* 59.6, pp. 340–352 (cit. on p. 8).

Braun, J., C. Krimpmann, F. Hoffmann, and T. Bertram (2014): "Evolutionäre Strukturoptimierung für LOLIMOT". In: *Proceedings. 24. Workshop Computational Intelligence*. Ed. by E. Hüllermeier and F. Hoffmann. Schriftenreihe des Instituts für Angewandte Informatik - Automatisierungstechnik, Karlsruher Institut für Technologie. Karlsruhe, Baden: KIT Scientific Publishing, pp. 113–129.

Braun, T., J. Reuter, and J. Rudolph (2017): "Sensorlose Positionsregelung eines hydraulischen Proportional-Wegeventils mittels Signalinjektion". In: *at - Automatisierungstechnik* 65.4, pp. 260–269 (cit. on p. 7).

Bröhl, A. P. and W. Dröschel (1995): *Das V-Modell: Der Standard für die Softwareentwicklung mit Praxisleitfaden*. 2. Auflage. Software - Anwendungsentwicklung - Informationssysteme. München and Wien: Oldenbourg (cit. on p. 12).

Chalanga, A., S. Kamal, L. Fridman, B. Bandyopadhyay, and J. Moreno (2016): "Implementation of Super-Twisting Control: Super-Twisting and Higher Order Sliding Mode Observer Based Approaches". In: *IEEE Transactions on Industrial Electronics* 63.6, pp. 3677–3685 (cit. on p. 53).

Chen, H.-M., J.-C. Renn, and J.-P. Su (2005): "Sliding mode control with varying boundary layers for an electro-hydraulic position servo system". In: *The International Journal of Advanced Manufacturing Technology* 26.1-2, pp. 117–123 (cit. on p. 7).

Choi, S.-B., D.-W. Park, and S. Jayasuriya (1994): "A time-varying sliding surface for fast and robust tracking control of second-order uncertain systems". In: *Automatica* 30.5, pp. 899–904 (cit. on p. 23).

Darwin, C. (1859): *The origin of species by means of natural selection*. London: John Murray (cit. on p. 59).

Davila, J., L. Fridman, and A. Levant (2005): "Second-order sliding-mode observer for mechanical systems". In: *IEEE Transactions on Automatic Control* 50.11, pp. 1785–1789 (cit. on p. 4).

Deb, K. (2001): *Multi-objective optimization using evolutionary algorithms*. 1st ed. Chichester and New York: John Wiley & Sons (cit. on pp. 59, 63).

Deb, K., A. Pratap, S. Agarwal, and T. Meyarivan (2000a): *A Fast and Elitist Multi-Objective Genetic Algorithm: NSGA-II*. Kanpur, India (cit. on p. 65).

Deb, K., S. Agrawal, A. Pratap, and T. Meyarivan (2000b): "A Fast Elitist Non-dominated Sorting Genetic Algorithm for Multi-objective Optimization: NSGA-II". In: *Parallel Problem Solving from Nature PPSN VI*. Ed. by G. Goos, J. Hartmanis, J. van Leeuwen, M. Schoenauer, K. Deb, G. Rudolph, X. Yao, E. Lutton, J. J. Merelo, and H.-P. Schwefel. Vol. 1917. Lecture Notes in Computer Science. Berlin, Heidelberg: Springer Berlin Heidelberg, pp. 849–858 (cit. on p. 65).

Deb, K., A. Pratap, S. Agarwal, and T. Meyarivan (2002): "A fast and elitist multiobjective genetic algorithm: NSGA-II". In: *IEEE Transactions on Evolutionary Computation* 6.2, pp. 182–197 (cit. on pp. 8, 63, 64).

DeCarlo, R. A., S. H. Zak, and G. P. Matthews (1988): "Variable structure control of nonlinear multivariable systems: A tutorial". In: *Proceedings of the IEEE* 76.3, pp. 212–232 (cit. on p. 99).

Do, H. T. and K. K. Ahn (2013): "Velocity control of a secondary controlled closed-loop hydrostatic transmission system using an adaptive fuzzy sliding mode controller". In: *Journal of Mechanical Science and Technology* 27.3, pp. 875–884 (cit. on p. 8).

Draženović, B. (1969): "The invariance conditions in variable structure systems". In: *Automatica* 5.3, pp. 287–295 (cit. on p. 22).

Edwards, C. and S. K. Spurgeon (1998): *Sliding mode control: Theory and applications*. Systems and control book series. London: Taylor & Francis (cit. on p. 99).

El-Araby, M., A. El-Kafrawy, and A. Fahmy (2011): "Dynamic performance of a non-linear non-dimensional two stage electrohydraulic servovalve model". In: *International Journal of Mechanics and Materials in Design* 7.2, pp. 99–110 (cit. on p. 109).

Elmer, K. F. and C. R. Gentle (2001): "A parsimonious model for the proportional control valve". In: *Proceedings of the Institution of Mechanical Engineers, Part C: Journal of Mechanical Engineering Science* 215.11, pp. 1357–1363 (cit. on p. 116).

Emel'yanov, S. V. (2007): "Theory of variable-structure control systems: Inception and initial development". In: *Computational Mathematics and Modeling* 18.4, pp. 321–331 (cit. on p. 4).

Emel'yanov, S. V., S. K. Korovin, and L. V. Levantovsky (1986a): "Higher-order sliding modes in binary control systems". In: *Soviet Physics Doklady* 31.4, pp. 291–293 (cit. on pp. 42, 43).

Emel'yanov, S. V., S. K. Korovin, and L. V. Levantovsky (1986b): "Second order sliding modes in controlling uncertain systems". In: *Soviet Journal of Computer and System Science* 24.4, pp. 63–68 (cit. on pp. 37, 43).

Emel'yanov, S. V. and V. A. Taran (1962): "On a class of variable structure control systems". In: *Proceedings of USSR Academy of Sciences, Energy and Automation* 3 (cit. on p. 4).

Emel'yanov, S. V., V. I. Utkin, V. A. Taran, N. E. Kostyleva, A. M. Shubladze, and V. B. Ezerov (1970): "Theory of variable structure systems". In: *Moscow: Nauka* (cit. on p. 4).

Ferreira, J. A., F. G. de Almeida, and M. R. Quintas (2002): "Semi-empirical model for a hydraulic servo-solenoid valve". In: *Proceedings of the Institution of Mechanical Engineers, Part I: Journal of Systems and Control Engineering* 216.3, pp. 237–248 (cit. on p. 116).

Filippov, A. F. and F. M. Arscott (1988): *Differential equations with discontinuous right-hand sides*. Mathematics and its applications (Soviet series). Dordrecht, Boston: Kluwer Academic Publishers (cit. on p. 5).

Föllinger, O. (1985): *Optimierung dynamischer Systeme: Eine Einführung für Ingenieure*. München and Wien: Oldenbourg (cit. on pp. 24, 25).

Fridman, L. (2012): "Sliding Mode Enforcement after 1990: Main Results and Some Open Problems". In: *Sliding modes after the first decade of the 21st century*. Ed. by L. Fridman, J. Moreno, and R. Iriarte. Vol. 412. Lecture notes in control and information sciences. Berlin: Springer Berlin Heidelberg, pp. 3–57 (cit. on p. 4).

Fridman, L. and A. Levant (1996): "Higher order sliding modes as a natural phenomenon in control theory". In: *Robust Control via Variable Structure and Lyapunov Techniques*. Ed. by F. Garofalo and L. Glielmo. Vol. 217. London: Springer-Verlag, pp. 107–133 (cit. on p. 41).

Fuller, A. T. (1973): "Proof of the time-optimality of a predictive control strategy for systems of higher order". In: *International Journal of Control* 18.6, pp. 1121–1127 (cit. on p. 25).

Gamble, J. B. and N. D. Vaughan (1996): "Comparison of Sliding Mode Control With State Feedback and PID Control Applied to a Proportional Solenoid Valve". In: *Journal of Dynamic Systems, Measurement, and Control* 118, pp. 434–438 (cit. on pp. 3, 6, 7, 17, 111).

Gamble, J. B. (1992): "Sliding mode control of a proportional solenoid valve". PhD thesis. University of Bath (cit. on pp. 7, 80).

Gao, W. and J. C. Hung (1993): "Variable structure control of nonlinear systems: A new approach". In: *IEEE Transactions on Industrial Electronics* 40.1, pp. 45–55 (cit. on pp. 22, 100).

Gulko, F. B. and B. Y. Kogan (1963): "A method of optimal control prediction". In: *Proceedings of the 2nd IFAC Congress*, pp. 63–68 (cit. on p. 25).

Hansen, N. and A. Ostermeier (1996): "Adapting arbitrary normal mutation distributions in evolution strategies: the covariance matrix adaptation". In: *Proceedings of the IEEE International Conference eon Evolutionary Computation*, pp. 312–317 (cit. on p. 60).

Harashima, F., H. Hashimoto, and S. Kondo (1985): "MOSFET Converter-Fed Position Servo System with Sliding Mode Control". In: *IEEE Transactions on Industrial Electronics* 32.3, pp. 238–244 (cit. on p. 23).

Harashima, F., M. Tomizuka, and T. Fukuda (1996): "Mechatronics - What Is It, Why, and How? An editorial". In: *IEEE/ASME Transactions on Mechatronics* 1.1, pp. 1–4 (cit. on p. 12).

Harmouche, M., S. Laghrouche, and Y. Chitour (2012): "Robust and adaptive Higher Order Sliding mode controllers". In: *51th IEEE Conference on Decision and Control (CDC)*, pp. 6436–6441 (cit. on p. 45).

Heiss, M. (1989): "Regressionsparabelfilter und -Differenzierer". In: *at - Automatisierungstechnik* 37.12, pp. 468–470 (cit. on p. 50).

Igel, C., N. Hansen, and S. Roth (2007): "Covariance Matrix Adaptation for Multi-objective Optimization". In: *Evolutionary computation* 15.1, pp. 1–28 (cit. on pp. 60, 63, 64).

Isermann, R. (2008): "Mechatronic systems—Innovative products with embedded control". In: *Control Engineering Practice* 16.1, pp. 14–29 (cit. on p. 14).

Itkis, U. (1976): *Control systems of variable structure*. New York: John Wiley & Sons (cit. on p. 4).

Jastrebski, G. A., D. V. Arnold, G. Jastrebski, and D. Arnold (2006): "Improving Evolution Strategies through Active Covariance Matrix Adaptation". In: *IEEE Congress on Evolutionary Computation (CEC)*, pp. 2814–2821 (cit. on pp. 60, 61).

Jelali, M. and A. Kroll (2003): *Hydraulic Servo-systems: Modelling, Identification and Control*. Advances in Industrial Control. London: Springer London (cit. on pp. 8, 16, 17).

Kallenbach, E. (2012): *Elektromagnete: Grundlagen, Berechnung, Entwurf und Anwendung*. 4., überarbeitete und erweiterte Auflage. Wiesbaden: Vieweg+Teubner Verlag (cit. on p. 16).

Kasai, K. (1968): "On the Stability of a Poppet Valve with an Elastic Support: 1st Report, Considering the Effect of the Inlet Piping System". In: *Bulletin of JSME* 11.48, pp. 1068–1083 (cit. on p. 116).

Kaynak, O. (2017): "Guest Editorial: A Look Into the Past and a Perspective on the Future". In: *IEEE/ASME Transactions on Mechatronics* 22.1, pp. 1–2 (cit. on p. 12).

Kern, S., S. D. Müller, N. Hansen, D. Büche, J. Ocenasek, and P. Koumoutsakos (2004): "Learning probability distributions in continuous evolutionary algorithms – a comparative review". In: *Natural computing* 3.1, pp. 77–112 (cit. on p. 62).

Khoshzaban Zavarehi, M., P. D. Lawrence, and F. Sassani (1999): "Nonlinear modeling and validation of solenoid-controlled pilot-operated servovalves". In: *IEEE/ASME Transactions on Mechatronics* 4.3, pp. 324–334 (cit. on p. 109).

Kiendl, H. (2012): "Computational Intelligence: Muster ihrer Entstehung". In: *at - Automatisierungstechnik* 60.10, pp. 589–599 (cit. on p. 8).

Koch, S. and M. Reichhartinger (2016): "Observer-based sliding mode control of hydraulic cylinders in the presence of unknown load forces". In: *e & i Elektrotechnik und Informationstechnik* 133.6 (cit. on p. 53).

Köckemann, A. (1989): *Zur adaptiven Regelung elektro-hydraulischer Antriebe*. Vol. 174. Fortschritt-Berichte VDI Reihe 8. Düsseldorf: VDI-Verl. (cit. on pp. 7, 109).

Koh, K. C., H. S. Aum, and H. S. Cho (1999): "A minimum-time motion planning method based on phase space analysis". In: *Proceedings of the 1999 IEEE International Conference on Control Applications* 1, pp. 273–278 (cit. on pp. 25, 26).

Komsta, J., J. Adamy, and P. Antoszkiewicz (2010): "Input-output linearization and integral sliding mode disturbance compensation for electro-hydraulic drives". In: *11th International Workshop on Variable Structure Systems*, pp. 446–451 (cit. on pp. 7, 53).

Komsta, J., P. Antoszkiewicz, T. Heeg, and J. Adamy (2010): "New Nonlinear Robust Control Concept for Electro-Hydraulic Drives". In: *7th International Fluid Power Conference*, pp. 1–12 (cit. on p. 40).

Komsta, J. (2013): *Nonlinear robust control of electrohydraulic systems*. Als Ms. gedr. Vol. 1224. Berichte aus dem Institut für Automatisierungstechnik und Mechatronik der TU Darmstadt. Düsseldorf: VDI-Verlag (cit. on pp. 7, 53).

Komsta, J., N. van Oijen, and P. Antoszkiewicz (2013): "Integral sliding mode compensator for load pressure control of die-cushion cylinder drive". In: *Control Engineering Practice* 21.5, pp. 708–718 (cit. on p. 53).

Krettek, J. (2013): *Ein multikriterieller evolutionärer Algorithmus mit interaktiver Präferenzintegration - angewendet zur Optimierung von Hydraulikventilreglern*. Vol. Nr. 1221. Fortschritt-Berichte VDI. Reihe 8, Mess-, Steuerungs- und Regelungstechnik. Düsseldorf: VDI Verlag (cit. on pp. 8, 65).

Krettek, J., D. Schauten, F. Hoffmann, and T. Bertram (2007): "Evolutionary hardware-in-the-loop optimization of a controller for cascaded hydraulic valves". In: *IEEE/ASME International Conference on Advanced Intelligent Mechatronics*, pp. 1–6 (cit. on pp. 8, 17, 111).

Krettek, J., J. Braun, F. Hoffmann, T. Bertram, T. Ewald, H.-G. Schubert, and H. Lausch (2009): "Interactive evolutionary multiobjective optimization for hydraulic valve controller parameters". In: *IEEE/ASME International Conference on Advanced Intelligent Mechatronics*, pp. 816–821 (cit. on pp. 3, 8, 65, 111).

Krimpmann, C., J. Braun, T. Bertram, I. Glowatzky, T. Ewald, and H. Lausch (2014): "Intuitive Objective Definition for the automated Optimization of Hydraulic Valves". In: *9th International Fluid Power Conference*, pp. 68–78 (cit. on pp. 65, 111).

Krimpmann, C., J. Braun, J. Krettek, F. Hoffmann, and T. Bertram (2012): "Optimierung komplexer Systeme durch Identifikation inhärenter Teilprobleme und Fusion ihrer Lösungen". In: *Proceedings 22. Workshop Computational Intelligence*. Ed. by F. Hoffmann. Karlsruhe: KIT Scientific Publishing, pp. 307–325 (cit. on pp. 65, 69).

Krimpmann, C., J. Braun, F. Hoffmann, and T. Bertram (2013a): "Active covariance matrix adaptation for multi-objective CMA-ES". In: *IEEE Sixth International Conference on Advanced Computational Intelligence*, pp. 189–194 (cit. on pp. 60, 64, 65).

Krimpmann, C., J. Braun, F. Hoffmann, and T. Bertram (2013b): "Modifikation der Adaptionsstrategie für derandomisierte, multikriterielle Evolutionsstrategien". In: *Proceedings 23. Workshop Computational Intelligence*. Ed. by F. Hoffmann. Karlsruhe: KIT Scientific Publishing, pp. 75–93 (cit. on pp. 60, 64, 65).

Krimpmann, C., G. Schoppel, I. Glowatzky, and T. Bertram (2015a): "Performance evaluation of nonlinear surfaces for sliding mode control of a hydraulic valve". In: *IEEE Multi-Conference on Systems and Control*, pp. 822–827 (cit. on pp. 21, 26, 29, 65).

Krimpmann, C., T. Bertram, G. Schoppel, and I. Glowatzky (2015b): "Vergleich nichtlinearer Schaltfunktionen für Gleitzustandsregler am Beispiel hydraulischer Wegeventile". In: *First IFToMM D-A-CH Conference* (cit. on pp. 21, 29, 65).

Krimpmann, C., T. Bertram, G. Schoppel, and I. Glowatzky (2016a): "Adaptive sliding mode control of a pressure relief valve". In: *e & i Elektrotechnik und Informationstechnik* 133.6, pp. 261–265 (cit. on pp. 32, 44, 53, 73, 104).

Krimpmann, C., G. Schoppel, I. Glowatzky, and T. Bertram (2016b): "Lyapunov-based self-tuning of sliding surfaces — methodology and application to hydraulic valves". In: *IEEE International Conference on Advanced Intelligent Mechatronics (AIM)*, pp. 457–462 (cit. on pp. 21, 31, 32).

Krimpmann, C., A. Makarow, T. Bertram, I. Glowatzky, G. Schoppel, and H. Lausch (2016c): "Simulationsgestützte Optimierung von Gleitzustandsreglern für hydraulische Wegeventile". In: *at - Automatisierungstechnik* 64.6, pp. 443–456 (cit. on pp. 29, 65, 85).

Kroll, A. and H. Schulte (2014): "Benchmark problems for nonlinear system identification and control using Soft Computing methods: Need and overview". In: *Applied Soft Computing* 25, pp. 496–513 (cit. on p. 8).

Kruse, R., C. Borgelt, C. Braune, F. Klawonn, C. Moewes, and M. Steinbrecher (2015): *Computational Intelligence: Eine methodische Einführung in Künstliche Neuronale Netze, Evolutionäre Algorithmen, Fuzzy-Systeme und Bayes-Netze*. 2., überarb. und erw. Aufl. 2015. Computational Intelligence. Wiesbaden: Springer Fachmedien Wiesbaden (cit. on pp. 8, 59).

Kyura, N. and H. Oho (1996): "Mechatronics - an industrial perspective". In: *IEEE/ASME Transactions on Mechatronics* 1.1, pp. 10–15 (cit. on p. 11).

Lausch, H. (1990): *Digitale Regelung hydraulischer Antriebe mittels pulsbreitenmoduliert angesteuerter Proportionalventile*. Vol. 213. Fortschrittberichte VDI : Reihe 8, Meß-, Steuerungs- und Regelungstechnik. Düsseldorf: VDI-Verlag (cit. on pp. 7, 109).

Levant, A. (1993): "Sliding order and sliding accuracy in sliding mode control". In: *International Journal of Control* 58.6, pp. 1247–1263 (cit. on pp. 4, 37, 43, 44).

Levant, A. (1997): "Higher order sliding: Collection of design tools". In: *European Control Conference (ECC)*, pp. 3043–3048 (cit. on p. 4).

Levant, A. (1998): "Robust exact differentiation via sliding mode technique". In: *Automatica* 34.3, pp. 379–384 (cit. on pp. 4, 46, 52).

Levant, A. (2001): "Universal single-input-single-output (SISO) sliding-mode controllers with finite-time convergence". In: *IEEE Transactions on Automatic Control* 46.9, pp. 1447–1451 (cit. on pp. 4, 45).

Levant, A. (2002): "Universal output-feedback SISO controller". In: *15th Triennial IFAC World Congress*, pp. 1106–1111 (cit. on p. 4).

Levant, A. (2003): "Higher-order sliding modes, differentiation and output-feedback control". In: *International Journal of Control* 76.9-10, pp. 924–941 (cit. on pp. 4, 45, 52, 53).

Levant, A. (2005a): "Homogeneity approach to high-order sliding mode design". In: *Automatica* 41.5, pp. 823–830 (cit. on pp. 4, 45, 47, 52).

Levant, A. (2005b): "Quasi-continuous high-order sliding-mode controllers". In: *IEEE Transactions on Automatic Control* 50.11, pp. 1812–1816 (cit. on pp. 45, 47).

Levant, A. (2007): "Principles of 2-sliding mode design". In: *Automatica* 43.4, pp. 576–586 (cit. on p. 42).

Levant, A. (2010a): "Chattering Analysis". In: *IEEE Transactions on Automatic Control* 55.6, pp. 1380–1389 (cit. on pp. 38, 47).

Levant, A. (2010b): "Ultimate robustness of homogeneous sliding modes". In: *11th International Workshop on Variable Structure Systems (VSS)*, pp. 26–31 (cit. on p. 47).

Levantovskii, L. V. (1985): "Second-order sliding algorithms and their realization (in Russian)". In: *Dynamics of nonhomogeneous systems: Proceedings of seminar* (cit. on pp. 4, 37).

Li, Y., K. C. Ng, D. J. Murray-Smith, G. J. Gray, and K. C. Sharman (1996): "Genetic algorithm automated approach to the design of sliding mode control systems". In: *International Journal of Control* 63.4, pp. 721–739 (cit. on p. 8).

Licskó, G., A. Champneys, and C. Hõs (2009): "Nonlinear Analysis of a Single Stage Pressure Relief Valve". In: *International Journal of Applied Mathematics* 39.4, pp. 286–299 (cit. on pp. 116, 117).

Lin, S. J. and A. Akers (1991): "Dynamic Analysis of a Flapper-Nozzle Valve". In: *Journal of Dynamic Systems, Measurement, and Control* 113.1, pp. 163–167 (cit. on p. 109).

Luenberger, D. (1966): "Observers for multivariable systems". In: *IEEE Transactions on Automatic Control* 11.2, pp. 190–197 (cit. on p. 49).

Makarow, A., J. Braun, C. Krimpmann, G. Schoppel, and I. Glowatzky (2015a): "Regelungstechnische Modellierung eines hydraulischen Wegeventils". In: *VDI/VDE Mechatronik*, pp. 215–220 (cit. on p. 18).

Makarow, A., J. Braun, C. Krimpmann, T. Bertram, G. Schoppel, and I. Glowatzky (2015b): "System Model of a Directional Control Valve for Control Applications". In: *Proceedings of the Fourteenth Scandinavian International Conference on Fluid Power (SICFP15)*. Tampere, Finnland, pp. 542–553 (cit. on p. 18).

Malzahn, J. (2014): *Modeling and control of multi-elastic-link robots under gravity: From oscillation damping and position control to physical interaction*. Als Ms. gedr. Vol. Nr. 1237. Fortschrittberichte VDI : Reihe 8, Meß-, Steuerungs- und Regelungstechnik. Düsseldorf: VDI-Verlag (cit. on p. 97).

Moreno, J. A. and M. Osorio (2008): "A Lyapunov approach to second-order sliding mode controllers and observers". In: *47th IEEE Conference on Decision and Control (CDC 2008)*, pp. 2856–2861 (cit. on pp. 4, 44, 121).

Moreno, J. A. and M. Osorio (2012): "Strict Lyapunov Functions for the Super-Twisting Algorithm". In: *IEEE Transactions on Automatic Control* 57.4, pp. 1035–1040 (cit. on pp. 4, 44).

Nicolaus, B., H. Kiendl, W. Blumendeller, and U. Schwane (2001): "Evolutionary optimization of an industrial hydraulic valve with the help of a fuzzy performance-index". In: *10th IEEE International Conference on Fuzzy Systems*, pp. 139–142 (cit. on pp. 8, 111).

Niewels, F. (2002): *Mehrdeutige Ljapunov-Funktionen und ihre Verwendung zum Entwurf strukturvariabler Regelungssysteme*. Vol. 959. Fortschrittberichte VDI : Reihe 8, Meß-, Steuerungs- und Regelungstechnik. Düsseldorf: VDI-Verlag (cit. on p. 7).

Oleson, J. P. (1984): *Greek and Roman mechanical water-lifting devices: The history of a technology*. Vol. 16. Phoenix: journal of the Classical association of Canada, Supplementary volume. Dordrecht, Boston, and Lancaster: D. Reidel (cit. on p. 3).

Plestan, F., Y. Shtessel, V. Brégeault, and A. Poznyak (2010): "New methodologies for adaptive sliding mode control". In: *International Journal of Control* 83.9, pp. 1907–1919 (cit. on pp. 4, 89).

Plestan, F., Y. Shtessel, V. Brégeault, and A. Poznyak (2013): "Sliding mode control with gain adaptation—Application to an electropneumatic actuator". In: *Control Engineering Practice* 21.5, pp. 679–688 (cit. on pp. 4, 7, 32, 45).

Polyakov, A. and A. Poznyak (2009): "Lyapunov function design for finite-time convergence analysis: "Twisting" controller for second-order sliding mode realization". In: *Automatica* 45.2, pp. 444–448 (cit. on p. 45).

Reichhartinger, M. and M. Horn (2009): "Application of Higher Order Sliding-Mode Concepts to a Throttle Actuator for Gasoline Engines". In: *IEEE Transactions on Industrial Electronics* 56.9, pp. 3322–3329 (cit. on pp. 7, 28, 53).

Ritelli, G. F. and A. Vacca (2014): "Experimental-Auto-Tuning Method for Active Vibration Damping Controller. The Case Study of a Hydraulic Crane". In: *9th International Fluid Power Conference*, pp. 212–223 (cit. on p. 3).

Ruderman, M. (2012): *Zur Modellierung und Kompensation dynamischer Reibung in Aktuatorsystemen*. Technische Universität Dortmund (cit. on p. 17).

Sanchez, T. and J. A. Moreno (2014): "A constructive Lyapunov function design method for a class of homogeneous systems". In: *IEEE 53rd Annual Conference on Decision and Control (CDC)*, pp. 5500–5505 (cit. on p. 4).

Savitzky, A. and M. J. E. Golay (1964): "Smoothing and Differentiation of Data by Simplified Least Squares Procedures". In: *Analytical Chemistry* 36.8, pp. 1627–1639 (cit. on p. 50).

Schafer, R. (2011): "What Is a Savitzky-Golay Filter? [Lecture Notes]". In: *IEEE Signal Processing Magazine* 28.4, pp. 111–117 (cit. on p. 50).

Schauten, D. (2008): *Evolutionäre Merkmalsselektion und Suchraumpartitionierung für die datenbasierte Fuzzy-Modellierung hochkomplexer Systeme*. Technische Universität Dortmund (cit. on p. 8).

Schulte, H. and H. Hahn (2004): "Fuzzy state feedback gain scheduling control of servo-pneumatic actuators". In: *Control Engineering Practice* 12.5, pp. 639–650 (cit. on p. 8).

Schulte, H. (2007): "Control-Oriented Modeling of Hydrostatic Transmissions using Takagi-Sugeno Fuzzy Systems". In: *IEEE International Fuzzy Systems Converence*, pp. 1–6 (cit. on p. 8).

Shin, Y. C. (1991): "Static and Dynamic Characteristics of a Two Stage Pilot Relief Valve". In: *Journal of Dynamic Systems, Measurement, and Control* 113.2, p. 280 (cit. on p. 117).

Shtessel, Y., M. Taleb, and F. Plestan (2012): "A novel adaptive-gain supertwisting sliding mode controller: Methodology and application". In: *Automatica* 48.5, pp. 759–769 (cit. on pp. 4, 7, 32, 44, 89).

Shtessel, Y. B., I. A. Shkolnikov, and M. D. Brown (2003): "An Asymptotic Second-Order Smooth Sliding Mode Control". In: *Asian Journal of Control* 5.4, pp. 498–504 (cit. on pp. 46, 122).

Shtessel, Y. B., J. A. Moreno, F. Plestan, L. M. Fridman, and A. S. Poznyak (2010): "Super-twisting adaptive sliding mode control: A Lyapunov design". In: *49th IEEE Conference on Decision and Control (CDC)*, pp. 5109–5113 (cit. on pp. 4, 44).

Sira-Ramírez, H. (1992): "On the sliding mode control of nonlinear systems". In: *Systems & Control Letters* 19.4, pp. 303–312 (cit. on pp. 41, 42, 45).

Sira-Ramírez, H. (1993): "On the dynamical sliding mode control of nonlinear systems". In: *International Journal of Control* 57.5, pp. 1039–1061 (cit. on pp. 41, 42, 45).

Slotine, J. J. and J. A. Coetsee (1986): "Adaptive sliding controller synthesis for non-linear systems". In: *International Journal of Control* 43.6, pp. 1631–1651 (cit. on pp. 4, 38).

Slotine, J. J. and S. S. Sastry (1983): "Tracking control of non-linear systems using sliding surfaces, with application to robot manipulators". In: *International Journal of Control* 38.2, pp. 465–492 (cit. on pp. 4, 38).

Slotine, J.-J. E. and W. Li (1991): *Applied nonlinear control*. Englewood Cliffs, N.J: Prentice Hall (cit. on pp. 3, 4, 99).

Stone, J. A. (1960): "Discharge Coefficients and Steady-State Flow Forces for Hydraulic Poppet Valves". In: *Journal of Basic Engineering* 82.1, p. 144 (cit. on p. 117).

Takagi, T. and M. Sugeno (1985): "Fuzzy identification of systems and its applications to modeling and control". In: *Systems, Man and Cybernetics, IEEE Transactions on* SMC-15.1, pp. 116–132 (cit. on p. 8).

Taleb, M., A. Levant, and F. Plestan (2013): "Pneumatic actuator control: Solution based on adaptive twisting and experimentation". In: *Control Engineering Practice* 21.5, pp. 727–736 (cit. on pp. 4, 7, 32, 45).

Tomizuka, M. (2002): "Mechatronics: from the 20th to 21st century". In: *Control Engineering Practice* 10.8, pp. 877–886 (cit. on p. 12).

Utkin, V. I. (1971): "Equations of Slipping Regime in Discontinuous Systems. 1". In: *Automation and Remote Control* 32.12, pp. 1897–1907 (cit. on p. 100).

Utkin, V. I. (1972): "Equations of Slipping Regime in Discontinuous Systems. 2". In: *Automation and Remote Control* 33.2, pp. 211–219 (cit. on p. 100).

Utkin, V. (1977): "Variable structure systems with sliding modes". In: *IEEE Transactions on Automatic Control* 22.2, pp. 212–222 (cit. on p. 4).

Utkin, V. (2016): "Discussion Aspects of High-Order Sliding Mode Control". In: *IEEE Transactions on Automatic Control* 61.3, pp. 829–833 (cit. on p. 47).

Utkin, V. I. and H.-C. Chang (2002): "Sliding mode control on electro-mechanical systems". In: *Mathematical Problems in Engineering* 8.4-5, pp. 451–473 (cit. on p. 101).

Utkin, V. I., A. S. Poznyak, and P. Ordaz (2011): "Adaptive super-twist control with minimal chattering effect". In: *50th IEEE Conference on Decision and Control and European Control Conference (CDC-ECC)*, pp. 7009–7014 (cit. on p. 44).

Utkin, V. I. (1992): *Sliding modes in control and optimization*. Communication and control engineering series. Berlin and New York: Springer-Verlag (cit. on p. 100).

Utkin, V. I., J. Guldner, and J. Shi (2009): *Sliding mode control in electromechanical systems*. 2nd ed. Boca Raton, FL and London: CRC Press and Taylor & Francis (cit. on pp. 2, 46, 99).

Ventura, U. P. and L. Fridman (2016): "Chattering measurement in SMC and HOSMC". In: *IEEE 14th International Workshop on Variable Structure Systems (VSS)*, pp. 108–113 (cit. on pp. 38, 47).

Verein Deutscher Ingenieure (2004): *Richtlinie VDI 2206: Entwicklungsmethodik für mechatronische Systeme*. Berlin (cit. on pp. 12–14).

Wolpert, D. H. and W. G. Macready (1996): *No Free Lunch Theorems for Search*. Ed. by The Sante Fe Institute. Santa Fe (cit. on p. 65).

Yan, X., M. Primot, and F. Plestan (2016): "Electropneumatic actuator position control using second order sliding mode". In: *e & i Elektrotechnik und Informationstechnik* 133.6 (cit. on p. 53).

Yiguang Hong, Jiankui Wang, and Zairong Xi (2005): "Stabilization of uncertain chained form systems within finite settling time". In: *IEEE Transactions on Automatic Control* 50.9, pp. 1379–1384 (cit. on p. 45).

Young, K. D., V. I. Utkin, and U. Ozguner (1996): "A control engineer's guide to sliding mode control". In: *IEEE Workshop on Variable Structure Systems*, pp. 1–14 (cit. on p. 99).

Zehetner, J., J. Reger, and M. Horn (2007a): "A Derivative Estimation Toolbox based on Algebraic Methods - Theory and Practice". In: *IEEE International Conference on Control Applications (CCA)*, pp. 331–336 (cit. on p. 50).

Zehetner, J., J. Reger, and M. Horn (2007b): "Echtzeit-Implementierung eines algebraischen Ableitungsschätzverfahrens". In: *at - Automatisierungstechnik* 55.11, pp. 553–560 (cit. on p. 50).

Ziegler, J. G. and N. B. Nichols (1993): "Optimum Settings for Automatic Controllers". In: *Journal of Dynamic Systems, Measurement, and Control* 115.2B, pp. 220–222 (cit. on p. 111).

Ziegler, J. G., N. B. Nichols, and N. Y. Rochester (1942): "Optimum Settings for Automatic Controllers". In: *Transactions of the A.S.M.E*, pp. 759–765 (cit. on p. 111).

Zitzler, E., L. Thiele, M. Laumanns, C. M. Fonseca, and V. G. da Fonseca (2003): "Performance assessment of multiobjective optimizers: An analysis and review". In: *IEEE Transactions on Evolutionary Computation* 7.2, pp. 117–132 (cit. on p. 64).

Zitzler, E. and L. Thiele (1998): "Multiobjective optimization using evolutionary algorithms — A comparative case study". In: *Parallel Problem Solving from Nature - PPSN V*. Ed. by A. E. Eiben, T. Bäck, M. Schoenauer, and H.-P. Schwefel. Vol. 1498. Springer-Verlag, pp. 292–301 (cit. on p. 64).

Supervised theses

A number of ideas grown during this work emerged from discussions in the context of following supervised theses:

Abel, O. (June 2016): "Modellierung und adaptive Regelung eines Druckbegrenzungsventils". Masterthesis. Dortmund: Technische Universität Dortmund (cit. on pp. 49, 104).

Cagdas, M. (July 2013): "Identification of Friction and Backlash of a Hydraulic Servo Valve with Neuro and Fuzzy Models". Masterthesis. Dortmund: Technische Universität Dortmund.

Eggers, T. (March 2014): "Untersuchung der Parallelisierung für die automatisierte Optimierung digitaler Ventilregler". Masterthesis. Dortmund: Technische Universität Dortmund.

Krause, C. (October 2016): "Entwurf und Validierung einer Festwertregelung zur Stabilisierung des Lichtstroms bei LED-Beleuchtungssystemen". Bachelorthesis. Dortmund: Technische Universität Dortmund.

Makarow, A. (October 2014): "Systematische Modellbildung eines hydraulischen Wegeventils". Masterthesis. Dortmund: Technische Universität Dortmund (cit. on p. 18).

Möllenbeck, B. (October 2015): "Untersuchung von Operatoren evolutionärer Algorithmen in Hinblick auf die Optimierung diskreter Lageregler-Parameter hydraulischer Wegeventile". Bachelorthesis. Dortmund: Technische Universität Dortmund.

Peters, F. (October 2014): "Entwicklung eines Regelungskonzeptes für hydraulische Wegeventile". Masterthesis. Dortmund: Technische Universität Dortmund.

Schlattmann, D. (October 2015): "Entwurf von Konzepten zur Regelung hydraulischer Druckbegrenzungsventile". Masterthesis. Dortmund: Technische Universität Dortmund (cit. on p. 74).

Tabassum, F. (April 2016): "Untersuchung der Diskretisierung elektrischer Bauteile in Hinblick auf die Güte analoger Lageregler für hydraulische Wegeventile". Bachelorthesis. Dortmund: Technische Universität Dortmund.

Tabassum, F. and C. Hebbeker (September 2015): "Recherche und Implementierung von Konzepten zur Regelung von Portalkränen am Beispiel eines Linearpendel-Experimentalsystems". Scientific research project. Dortmund: Technische Universität Dortmund.

Wolf, C. (September 2016): "Auslegung und Evaluation eines modellprädiktiven Reglers für ein mechatronisches Antriebssystem". Bachelorthesis. Dortmund: Technische Universität Dortmund.

Own publications

A dedicated list of own contributions is given in the following. Parts of the material presented in this work have been originally published in conferences and journals.

Braun, J., C. Krimpmann, F. Hoffmann, and T. Bertram (2014): "Evolutionäre Strukturoptimierung für LOLIMOT". In: *Proceedings. 24. Workshop Computational Intelligence*. Ed. by E. Hüllermeier and F. Hoffmann. Schriftenreihe des Instituts für Angewandte Informatik - Automatisierungstechnik, Karlsruher Institut für Technologie. Karlsruhe, Baden: KIT Scientific Publishing, pp. 113–129.

Krimpmann, C., J. Braun, T. Bertram, I. Glowatzky, T. Ewald, and H. Lausch (2014): "Intuitive Objective Definition for the automated Optimization of Hydraulic Valves". In: *9th International Fluid Power Conference*, pp. 68–78 (cit. on pp. 65, 111).

Krimpmann, C., J. Braun, J. Krettek, F. Hoffmann, and T. Bertram (2012): "Optimierung komplexer Systeme durch Identifikation inhärenter Teilprobleme und Fusion ihrer Lösungen". In: *Proceedings 22. Workshop Computational Intelligence*. Ed. by F. Hoffmann. Karlsruhe: KIT Scientific Publishing, pp. 307–325 (cit. on pp. 65, 69).

Krimpmann, C., J. Braun, F. Hoffmann, and T. Bertram (2013a): "Active covariance matrix adaptation for multi-objective CMA-ES". In: *IEEE Sixth International Conference on Advanced Computational Intelligence*, pp. 189–194 (cit. on pp. 60, 64, 65).

Krimpmann, C., J. Braun, F. Hoffmann, and T. Bertram (2013b): "Modifikation der Adaptionsstrategie für derandomisierte, multikriterielle Evolutionsstrategien". In: *Proceedings 23. Workshop Computational Intelligence*. Ed. by F. Hoffmann. Karlsruhe: KIT Scientific Publishing, pp. 75–93 (cit. on pp. 60, 64, 65).

Krimpmann, C., G. Schoppel, I. Glowatzky, and T. Bertram (2015a): "Performance evaluation of nonlinear surfaces for sliding mode control of a hydraulic valve". In: *IEEE Multi-Conference on Systems and Control*, pp. 822–827 (cit. on pp. 21, 26, 29, 65).

Krimpmann, C., T. Bertram, G. Schoppel, and I. Glowatzky (2015b): "Vergleich nichtlinearer Schaltfunktionen für Gleitzustandsregler am Beispiel hydraulischer Wegeventile". In: *First IFToMM D-A-CH Conference* (cit. on pp. 21, 29, 65).

Krimpmann, C., T. Bertram, G. Schoppel, and I. Glowatzky (2016a): "Adaptive sliding mode control of a pressure relief valve". In: *e & i Elektrotechnik und Informationstechnik* 133.6, pp. 261–265 (cit. on pp. 32, 44, 53, 73, 104).

Krimpmann, C., G. Schoppel, I. Glowatzky, and T. Bertram (2016b): "Lyapunov-based self-tuning of sliding surfaces — methodology and application to hydraulic valves". In: *IEEE International Conference on Advanced Intelligent Mechatronics (AIM)*, pp. 457–462 (cit. on pp. 21, 31, 32).

Krimpmann, C., A. Makarow, T. Bertram, I. Glowatzky, G. Schoppel, and H. Lausch (2016c): "Simulationsgestützte Optimierung von Gleitzustandsreglern für hydraulische Wegeventile". In: *at - Automatisierungstechnik* 64.6, pp. 443–456 (cit. on pp. 29, 65, 85).

Makarow, A., J. Braun, C. Krimpmann, G. Schoppel, and I. Glowatzky (2015a): "Regelungstechnische Modellierung eines hydraulischen Wegeventils". In: *VDI/VDE Mechatronik*, pp. 215–220 (cit. on p. 18).

Makarow, A., J. Braun, C. Krimpmann, T. Bertram, G. Schoppel, and I. Glowatzky (2015b): "System Model of a Directional Control Valve for Control Applications". In: *Proceedings of the Fourteenth Scandinavian International Conference on Fluid Power (SICFP15)*. Tampere, Finnland, pp. 542–553 (cit. on p. 18).